AWARD NUMBER: W81XWH-15-2-0087

TITLE: Pathomechanics of Post-Traumatic OA Development in the Military Following Articular Fracture

PRINCIPAL INVESTIGATOR: Donald D. Anderson, PhD

CONTRACTING ORGANIZATION: University of Iowa, The
Iowa City, IA 52242-1316

REPORT DATE: Dec-2019

TYPE OF REPORT: Final

PREPARED FOR: U.S. Army Medical Research and Materiel Command
Fort Detrick, Maryland 21702-5012

DISTRIBUTION STATEMENT: Approved for Public Release;
Distribution Unlimited

REPORT DOCUMENTATION PAGE

Form Approved OMB No. 0704-0188

1. REPORT DATE
Dec-2019

2. REPORT TYPE
Final

3. DATES COVERED
30 Sep 2015 – 29 Sep 2019

4. TITLE AND SUBTITLE
Pathomechanics of Post-Traumatic OA Development in the Military Following Articular Fracture

5a. CONTRACT NUMBER

5b. GRANT NUMBER
W81XWH-15-2-0087

5c. PROGRAM ELEMENT NUMBER

6. AUTHOR(S)

Donald D. Anderson, PhD

E-Mail: don-anderson@uiowa.edu

5d. PROJECT NUMBER

5e. TASK NUMBER

5f. WORK UNIT NUMBER

7. PERFORMING ORGANIZATION NAME(S) AND ADDRESS(ES)

University of Iowa, The
105 Jessup Hall
Iowa City, IA 52242-1316

8. PERFORMING ORGANIZATION REPORT NUMBER

9. SPONSORING / MONITORING AGENCY NAME(S) AND ADDRESS(ES)

U.S. Army Medical Research and Materiel Command
Fort Detrick, Maryland 21702-5012

10. SPONSOR/MONITOR'S ACRONYM(S)

11. SPONSOR/MONITOR'S REPORT NUMBER(S)

12. DISTRIBUTION / AVAILABILITY STATEMENT

Approved for Public Release; Distribution Unlimited

13. SUPPLEMENTARY NOTES

14. ABSTRACT

The objective of this research was to develop new models for predicting the risk of post-traumatic osteoarthritis (PTOA) following intra-articular fracture (IAF). New methods were developed to expedite the computation of acute fracture severity and chronic contact stress elevation after IAF. Using these new methods, pre- and post-treatment CT data from patients with IAFs were analyzed to measure fracture severity and post-reduction contact stress exposure. Imaging data for 70 subjects with collectively 112 fractures were received, and we completed fracture severity analysis of 82 IAFs. This is in addition to fracture energies having now been computed for 394 civilian IAFs. We found a strong positive correlation (explaining ~97% of the variance) between fracture energy per unit contact area and PTOA rates across 5 different joints, without controlling for any operative factors, whatsoever. Analyses of contact stress elevation after IAF of the distal tibial pilon, acetabulum, or calcaneus also demonstrated an exposure threshold above which cases predictably progress to PTOA. The best combined predictive models had excellent agreement with PTOA outcome after IAF of the distal tibial pilon (100%), acetabulum (91%), or calcaneus (88%).

15. SUBJECT TERMS

post-traumatic osteoarthritis, CT-based analysis, intra-articular fractures

16. SECURITY CLASSIFICATION OF: a. REPORT	b. ABSTRACT	c. THIS PAGE	17. LIMITATION OF ABSTRACT	18. NUMBER OF PAGES	19a. NAME OF RESPONSIBLE PERSON
Unclassified	Unclassified	Unclassified	Unclassified	181	USAMRMC
					19b. TELEPHONE NUMBER *(include area code)*

Table of Contents

Page

1. Introduction

The objective of this research project was to develop new models for predicting the risk of post-traumatic osteoarthritis (PTOA) following intra-articular fracture (IAF). We had previously developed capabilities to predict PTOA risk from acute fracture severity (measured from pre-op CT) and chronic elevated contact stress (post-op CT) associated with IAFs, but more patient data were needed to build clinically useful risk models. Prospective studies of PTOA development following IAFs face many challenges. Severe IAFs are not frequently seen in civilian practice, making it difficult to accrue sufficient numbers for clinical study. An added challenge is that to determine if a patient develops PTOA, they may need to be followed for years into the future, threatening subject retention. One of the attractive features of the CT-based measures of mechanical factors pioneered by the Initiating PI is that retrospective studies can include patients who were injured years in the past. Recent military conflicts, which unfortunately produced a substantial number of IAFs (as reported by the Partnering PI), provided a unique opportunity to overcome these challenges and to honor the military personnel who suffered combat-related IAFs. Given their prevalence and severity, and the degree to which these injuries impact long-term function of injured service members, better methods to predict PTOA risk would benefit our current generation of new veterans, as well as future service members at risk for IAF.

2. Keywords

post-traumatic osteoarthritis, CT analysis, intra-articular fractures, clinical outcome

3. Accomplishments

What were the major goals of the project?

Below is the original SOW (completion dates indicated in text following the SOW):

Specific Aim 1: Evaluate pre- and post-treatment CT data from patients with combat-related IAFs to measure fracture severity and post-reduction contact stress exposure	
Major Task 1: Regulatory Approval	Months
Subtask 1.1: Obtain local IRB	1-3
Subtask 1.2: Obtain HRPO approval	4-6
Milestone #1: Regulatory approval received	5-6
Major Task 2: Adapt CT Analysis Methods	Months
Subtask 2.1: Obtain representative CT studies	3
Subtask 2.2: Trial analysis methods with CT studies	1-3
Subtask 2.3: Modify analysis methods as needed	3-9
Milestone #2: Co-author manuscript on methods to analyze combat-related IAFs	9-12
Major Task 3: Subject Identification	Months
Subtask 3.1: Obtain potential subject list with demographic and injury data from DoDTR	7
Subtask 3.2: Screen available CT scans for requisite images for inclusion	8-12
Milestone #3: Subject list finalized	12
Major Task 4: CT Calculations	Months
Subtask 4.1: De-identified CDs compiled and express mailed from Site 2 to Site 1	9-13
Subtask 4.2: CT calculations for injury severity and post-reduction contact stresses	10-18
Milestone #4: Co-author manuscript on fracture severity and post-reduction contact stress measures in patients with combat-related IAFs	18-24

Specific Aim 2: Measure the occurrence of PTOA up to ten years following fracture reduction surgery	
Major Task 5: PTOA radiographic frequency	Months
Subtask 5.1: Identify radiographs for KL grading; multiple investigators do KL grading	9-14
Milestone #5: Co-author paper detailing PTOA incidence and grading for patients with combat-related IAFs	16-20

Specific Aim 3: Quantify the extent to which fracture severity and post-reduction contact stress predict PTOA	
Major Task 6: PTOA symptoms and quality of life	Months
Subtask 6.1: Identify subjects' contact information through DoD and/or VA sources	12-16
Subtask 6.2: Conduct prospective contacting of subjects for outcomes questionnaires	12-28
Milestone #6: Co-author manuscript detailing symptoms and treatment timelines for patients with combat-related IAFs	25-32
Subtask 6.3: Correlate CT-based analysis results with KL grade/PTOA status, questionnaire outcomes, and various radiographic results	28-32
Milestone #7: Co-author manuscript detailing relationships between CT-based results and PTOA outcomes – PTOA risk model	32-36

What was accomplished under these goals?

Major Task 1 (regulatory approval) completed 23-Oct-2015 (HRPO Log Number A-18855)

Major Task 2 (adapt CT analysis methods) was completed in late 2016, and a manuscript detailing the new methods (see Appendix) has been submitted. The new methods were first detailed in our revised 2016 Annual Report that was submitted on 01-Mar-2017.

Detailed report of Major Task 2 accomplishments

New fracture severity assessment methods based on pre-op CT

In our work prior to this research project, we had developed objective techniques to measure fracture severity from CT scan data. Fracture severity was assessed primarily based on the energy released in fracture, which is directly related to the amount of inter-fragmentary bone surface liberated. These techniques, as originally developed, were dependent upon a CT scan of the intact contralateral bone, which is rarely available for the military fractures now being studied. Furthermore, fracture energy had previously been analyzed only in a single joint (the ankle), and we now needed to evaluate fractures in other joints.

To expand the clinical utility of fracture energy as an objective metric of severity, we developed new methods to implement fracture energy as a universal tool in any fracture with pre-operatively available CT-scans. CT images are first segmented, identifying all bone fragments, to generate a 3D model of the fracture. Surfaces are then smoothed to remove voxellation effects and to prepare the data for use in a surface classification algorithm. An automated classifier then identifies fractured surfaces on the fragments, with a graph cut method used to create a clear boundary between the intact and fractured bone surfaces. Manual adjustment of this boundary is performed to finalize the fractured surface identification. The CT Hounsfield Unit intensities are then sampled along the fractured surface for use in obtaining a bone density distribution over the surface. The fractured areas are then scaled by these location specific densities and multiplied by a density-dependent energy release rate to obtain the fracture energy. Articular comminution is quantified by measuring the fracture edge length along the articular surface from the fractured surface boundaries, a parameter chosen based on prior in vitro work establishing a high degree of chondrocyte death along fracture edges.

We validated the new methods by showing that the fracture energies obtained for a series of 20 tibial pilon fractures using the new methods agreed with values obtained using our original methods. We then utilized the new methods to measure fracture severity (Figure 1) in 394 patients with IAFs of the calcaneus (n=48), tibial pilon (n=118), tibial plateau (n=129), acetabulum (n=79), and distal radius (n=20). Fracture energies varied between joints with higher/lower levels for some and wider/narrower ranges for some. These unique features partly explain differences in PTOA propensity among these different joints (see Major Task 5 section).

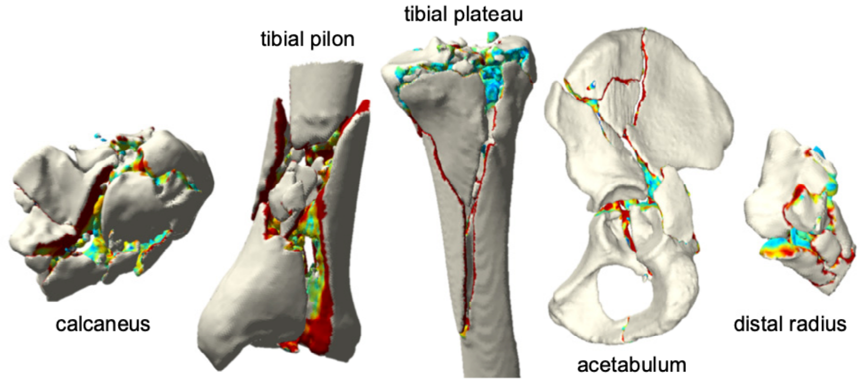

Figure 1. These renderings show the segmented fracture fragments, with inter-fragmentary surfaces colored according to their local bone density. High energy fractures have similar characteristics across joints with many fragments, significant comminution, and disruption of the articular surface.

New contact stress assessment methods based on post-op joint models

We had originally developed techniques to index chronic contact stress elevations by patient-specific finite element analysis (FEA), using models derived from post-reduction CT scans. The prohibitive costs and inherent challenges of performing 3D contact FEA on a subject- or patient-specific basis makes FEA of questionable utility for study of the role of aberrant levels of articular contact stress in PTOA risk, at least for larger patient series needed to show statistically robust causality. We adopted an alternative numerical approach to modeling articular contact called discrete element analysis (DEA). DEA involves treating bones as rigid bodies, and the cartilage as an array of compressive-only springs distributed over the articulating bony surfaces. We first established the equivalence of DEA and FEA results for the post-op contact stress exposures in 11 patients with tibial pilon fractures as predictors of PTOA risk. We then extended our DEA methods for application (Figure 2) in the hip joint (IAF of the acetabulum) and subtalar joint (IAF of the calcaneus). The results of these analyses are detailed in Major Task 5 section.

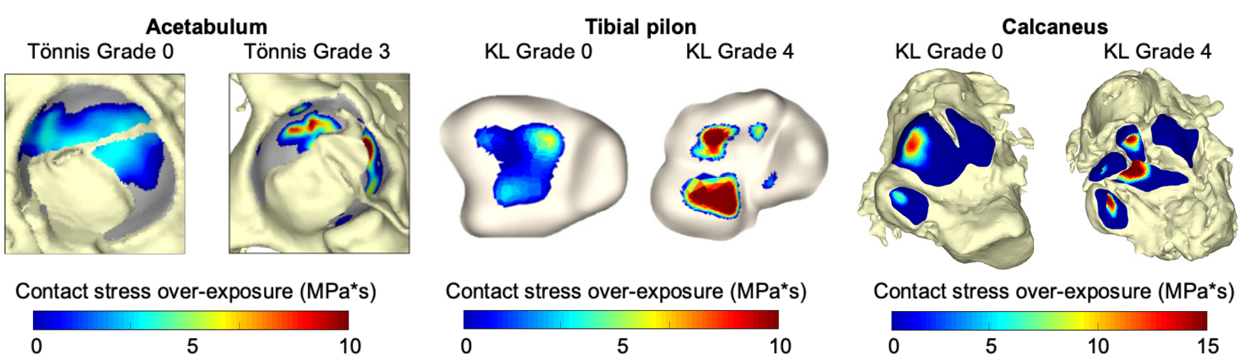

Figure 2. These renderings show fractured articular surfaces of the acetabulum, distal tibial pilon, and the calcaneus with contact stress over-exposures plotted on them. For each joint, one case (left) is shown where PTOA was not found and one case (right) where PTOA was found.

We have shown this approach can be highly automated (Figure 3), an advance initially predicated on the availability of a post-op CT scan. Unfortunately,

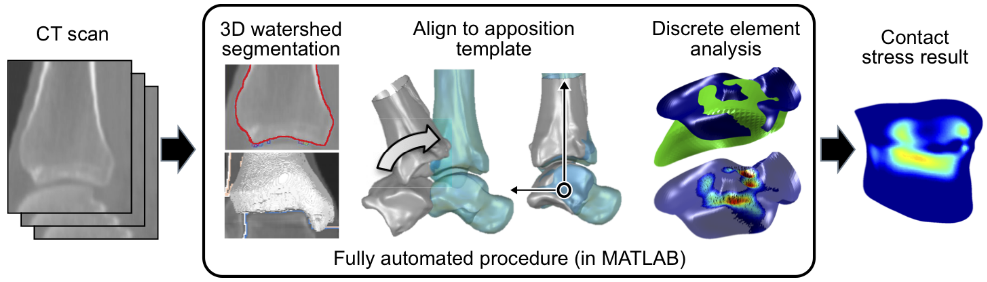

Figure 3. Schematic of fully automated procedure for determining habitual contact stress exposure in a given articular fracture reduction, with geometry extracted from CT scan data.

changing clinical practice patterns have recently led to much less routine acquisition of these CT scans. To move away from a reliance upon post-op CTs, we developed methods to deduce bone fragment poses from post-op plain radiographs. This approach (Figure 4) involves aligning 3D bone fragment models (a byproduct of the fracture severity assessments) to match their projective pose captured on intra-op 2D fluoroscopic images. The output from these methods is the pose of the assembled fragments, which together constitute the surgically reduced joint surface. DEA simulations can then be run to provide a cumulative contact stress exposure estimate to be further considered as a predictor of PTOA risk.

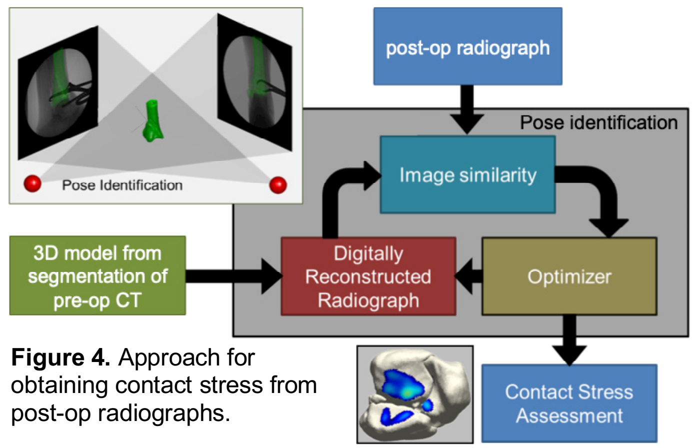

Figure 4. Approach for obtaining contact stress from post-op radiographs.

Major Task 3 (subject identification) was completed August 2018. Seventy subjects with collectively 112 fractures were identified/enrolled.

Major Task 4 (CT calculations) has been completed, with all CDs containing de-identified CT data having been sent from Site 2 (BAMC) to Site 1 (Iowa). We performed calculations of fracture severity and post-reduction contact stress as cases arrived in Iowa. The imaging data for 70 subjects with collectively 112 IAFs (see Table 1 for details) were forwarded to Iowa for analysis. We completed fracture severity analysis of 82 of the IAFs, with the remaining 30 either having significant metal artifact or antibiotic beads placed that precluded reliable segmentation (Figure 5) or including fractures not protocoled for study (cuboid, patella, etc.).

Table 1. Assortment of fractures and CT data collected for the study.

Fracture location	Pre-op	Post-op
Calcaneus	40	8
Distal tibia	38	8
Proximal tibia	11	6
Talus	12	0
Distal femur	10	3
Acetabulum	1	0

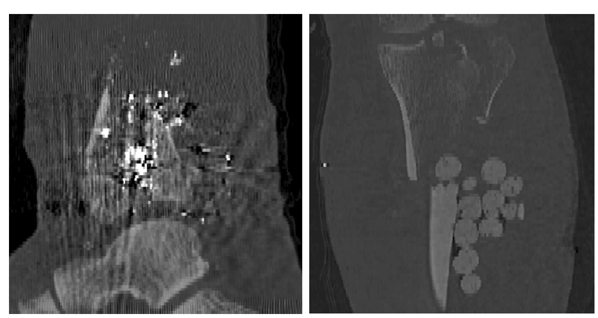

Figure 5. Two CT slices reflecting issues that preclude reliable segmentation, with the one to the left having substantial metal artifact from shrapnel and to the right having antibiotic beads placed.

Detailed report of progress on Major Task 4

Acute fracture severity assessment

In addition to the military cases, we have continued to analyze civilian IAF cases, with fracture energies having now been computed for 295 comparable IAFs, as well as for 99 additional IAFs at joints for which we have limited comparable military cases (Table 2). We were interested to see how the fracture energies vary between military and civilian cases, as well as between isolated and multiple fracture scenarios in a single limb. Intuitively, cases involving multiple fractures in a single limb involve higher fracture energies, although other factors such as varied loading rates (see below) may also be involved.

Table 2. Fracture energies and numbers of IAF cases analyzed

Fracture location	Fracture Energy (J)		# of cases	
	Civilian°	Military°	Civilian	Military
Calcaneus	19.3±3.1 (14.1-26.2)	20.4±5.6 (3.6-29.6)	48	37
Tibial pilon	14.6±7.1 (0.9-37.9)	10.9±6.9 (1.3-28.7)	118	34
Tibial plateau	12.6±6.4 (0.6-33.2)	18.9±11.1 (4.3-39.6)	129	10
Acetabulum	16.9±8.9 (3.4-41.9)		79	1
Distal radius	4.9±1.8 (2.8-9.0)		20	

° Values are shown as mean±standard deviation (range)

The fracture energies for all civilian cases analyzed ranged from 0.6 to 41.9 Joules (J). The distribution of energies was highly dissimilar between different IAF locations, (Figure 6) with no overlap whatsoever between the calcaneal and distal radius fractures. For the military cases, fracture energies ranged from 1.3 to 39.6 J. In general, there were no differences between the fracture energies of military and civilian cases.

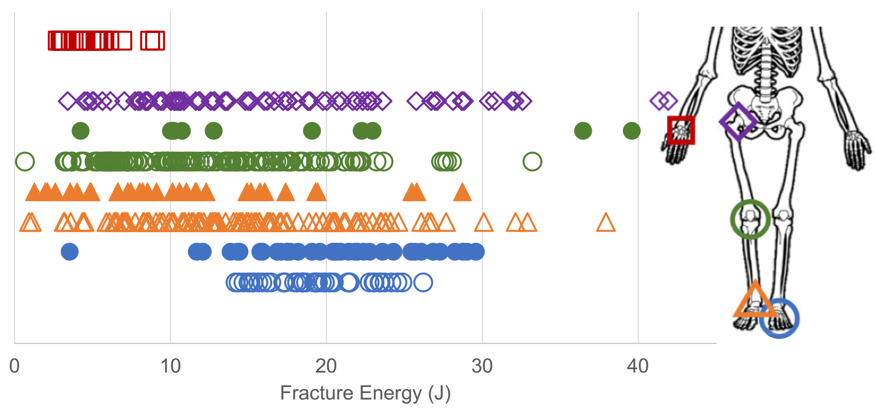

Figure 6. Graphical comparison of the fracture energies computed in civilian subjects with datapoints colored according to the joint (see skeleton to right for key). Open symbols are for civilian cases and closed symbols for military cases.

When axial fracturing impacts are delivered to a joint, energy transfer across the joint is distributed over the articular surface through the contact area, which can vary considerably from joint to joint. This means tissues of the different joints are subjected to different mechanical insults during the fracturing event due solely to their different contact areas. To enable comparisons of the fracture energies across different joints, we therefore normalized to characteristic joint-specific contact areas (Table 3). We queried the published literature for generally accepted averages of the

Table 3. Contact areas and PTOA rates of different joints.

Fracture location	Contact Area (cm^2)*	PTOA Rates*
Calcaneus	3.90 (3.10-5.36)	85.7 (60.4-95.4%)
Tibial pilon	6.28 (4.40-7.34)	48.1 (40.8-74.0%)
Tibial plateau	11.08 (10.65-11.50)	24.5 (11.0-36.5%)
Acetabulum	19.03 (14.70-26.77)	27.9 (12.0-39.5%)
Distal radius	1.87 (1.00-2.74)	43.4 (35.0-73.0%)

* Values are mean followed by range

relevant contact areas. We also queried the published literature for the different rates of PTOA in these different joints after an IAF.

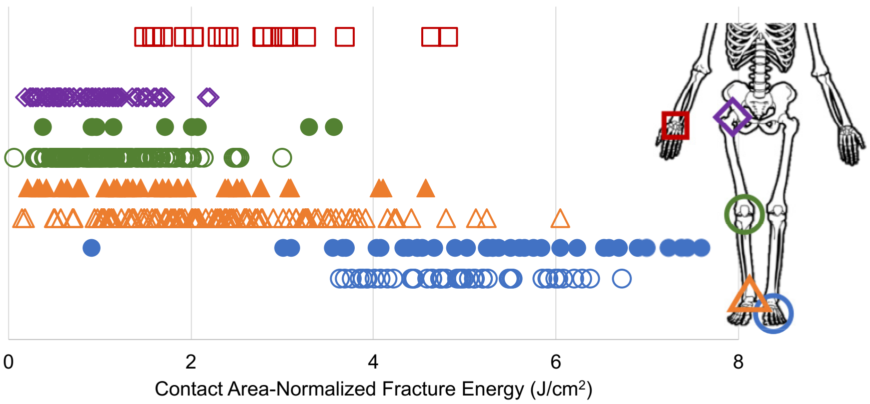

Figure 7. Graphical comparison of the fracture energies normalized to the characteristic contact area of the respective articular joint (see skeleton to right for key). Open symbols are for civilian cases and closed symbols for military cases.

The contact area-normalized fracture energies ranged from 0.06 to 6.73 J/cm^2 for all civilian cases (Figure 7). The contact area-normalized fracture energies ranged from 0.21 to 7.60 J/cm^2 for all military cases. There was a trend toward lower fracture energies in joints going from distal to proximal in the lower extremity with distal radial fractures having energies in the middle of the range

To study the influence of different loading rates, we turned to a different data source. Fortuitously, in May 2017, we were introduced to a group at the University of Virginia's Center for Applied Biomechanics (lead: Dr. Robert Salzar) that has been doing cadaveric lower extremity fracture studies for the past 15 years. They had recently turned their attention to scenarios akin to those experienced with blast injuries in the military. Data collected during their fracture experiments include accelerations, forces, displacements, bone strains, and video-radiography, with acoustic sensors used to precisely detect fracture initiation.

We recognized this as an opportunity to complement our CT-based post hoc fracture severity analysis work with their direct studies of the actual fracture event. Pre-op CT scans from 42 battlefield blast cases were analyzed for comparison with CT scans obtained from laboratory testing of 36 cadaveric lower extremity specimens. Three testing conditions designed to replicate battlefield blast fractures were used in the laboratory with low, intermediate, and high loading rates. Fracture energy measures were calculated from post-fracture CT scans using our validated methods. A new measure, the mean energy-release distance (MERD), was also calculated to characterize the location and distribution of fractures. The MERD was defined as the proximal distance from the distalmost aspect of the calcaneus at which 50% of the total fracture energy had been dissipated.

The battlefield blast cases had fracture energies of 15.2 ± 8.1J (mean ± SD) and MERDs of 63.4 ± 42.4mm (Figure 8). The laboratory low,

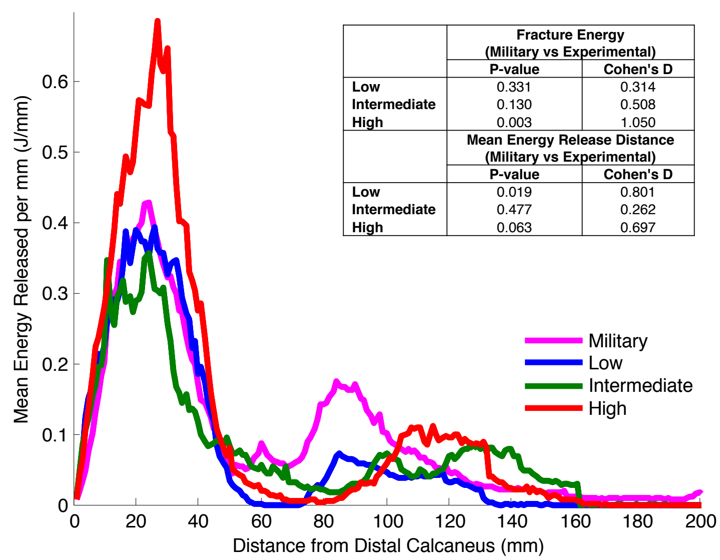

	Fracture Energy (Military vs Experimental)	
	P-value	Cohen's D
Low	0.331	0.314
Intermediate	0.130	0.508
High	0.003	1.050
	Mean Energy Release Distance (Military vs Experimental)	
	P-value	Cohen's D
Low	0.019	0.801
Intermediate	0.477	0.262
High	0.063	0.697

Figure 8. Plots of the mean fracture energy released for each group as it varies along the distance from the distalmost aspect of the calcaneus over the fractured lower extremity segment.

intermediate, and high impact conditions had fracture energies of 12.7 ± 7.8J, 19.5 ± 8.8J, and 23.5 ± 7.7J, along with MERDs of 33.6 ± 31.2mm, 53.6 ± 31.7mm, and 38.9 ± 25.9mm, respectively. There were no significant differences in the fracture energies between battlefield blast cases and the low ($p=0.33$) or intermediate ($p=0.13$) impact groups. The high impact group had significantly more energy released ($p=0.003$). Significant difference was seen between MERDs for the battlefield blast cases and the intermediate impact group ($p=0.019$), while no differences were seen with the intermediate ($p=0.48$) and high ($p=0.063$) impact groups.

These results indicate that the intermediate laboratory impact protocol produced fractures most closely representative of battlefield blast injuries in both overall fracture energy and in its distribution (MERD). This methodology can be used to inform and improve injury models by bridging the gap between experimental and clinical results, and we hope to continue working with the group in Virginia to develop these ideas.

Chronic elevated contact stress over-exposure

In the area of studying post-operative chronic contact stress elevation, we had to lean heavily on our complementary civilian data. Most recently, we specifically chose to focus on contact stress elevation in acetabular IAFs and have adapted prior methods for this purpose. We similarly extended our stress analysis methods to investigate IAFs of the calcaneus but have chosen to focus in this report instead on methods developed for the hip. For more details of all these methods, the reader is asked to read the dissertation of Dr. Kevin Dibbern, supported by this research funding (Dibbern KN. Utilizing objective measures of acute and chronic mechanical insult to determine their contributions to post-traumatic osteoarthritis risk. PhD thesis, University of Iowa, 2019. https://doi.org/10.17077/etd.92oy-stmy).

After obtaining Institutional Review Board (IRB) approval, a series of 75 patients at our institution who had undergone operative fixation of acetabular fractures between 2004 and 2016 were identified for having pre-operative and post-operative CT scans. Patients were excluded from study for having less than two-year radiographic follow-up, being under the age of 18 at the time of surgery, undergoing arthroplasty within the same hospital admission, or if they had associated femoral head fracture. Twenty-four patients declined to participate or were unreachable. Ten patients had undergone surgery within the past two years and thus did not have 2-year radiographic follow-up. One patient was 17 at the time of surgery. Of the remaining 40 patients, a total of 23 patients had adequate imaging and follow-up available for analysis.

Femoral and pelvic anatomy for each patient was segmented from post-operative CT scans to produce discrete element analysis (DEA) models using validated methods previously reported by our group (Townsend et. al. J Biomech. 2018 ;67:9-17). Bone geometries were extracted from CT using a semi-automated watershed-based algorithm. Errors in the automated surface detection and separation protocol were manually corrected, and triangulated surface models of the anatomy were generated and smoothed. Articular surfaces were approximated by projecting the acetabular and femoral subchondral surfaces a uniform distance of 1mm then subsequently smoothing the projected surfaces toward sphericity using a custom iterative smoothing algorithm. The resulting approximations of the chondral geometries have been shown to yield accurate contact stress computations from fractured surfaces.

Radiographs obtained at two years after surgery or later were evaluated for arthritic changes by two independent evaluators. Each evaluator assigned a Tönnis grade to each hip using the modified Tönnis grading description scale. When there was disagreement between observers, an arbitaror reviewed the studies and determined Tönnis grade. Patients having Tönnis grades 0 and

1 were included in a no PTOA group and Tönnis grades 2 and 3 were included in a PTOA group. Those patients who went on to total hip arthroplasty or femoral head resection prior to two year follow up were considered as Tönnis grade 3 equivalents for radiographic purposes.

DEA models were then aligned to a coordinate system defined by Bergmann et al. (J. Biomech. 2001;34:859-71) based on patient-specific anatomic landmarks on the bone surface models. The walking gait data obtained in that study of instrumented total hips was discretized into 13 evenly spaced time increments. DEA was then used to compute contact stress over an entire gait cycle for each case using boundary conditions for forces and rotations based on patient-specific body weights and defined by the Bergmann et. al. study. Forces were applied to the femur and directed toward the hip as dictated by the Bergmann data. Cartilage was assigned isotropic linear-elastic material properties (E=8MPa, ν= 0.42).

A total of 23 patients (15 developed OA and 8 did not) and 10 healthy volunteers (serving as normal controls) were included in the final analysis. The average age of the patients was 40±16.6 years at the time of surgery (42.5±16.6 years in the OA group and 34.6±15.1 years for the no OA group, p=0.32), and the average age of the controls was 34.6±8.7 years (p=0.34). The average BMI was 29.9±6.0 for the patients (29.5±6.7 in the OA group and 30.8±4.0 in the no OA group, p=0.66) and 35.0±7.2 for the controls (p=0.07). There were 19 males and 4 females in the patient group (2 males and 17 females in the OA group) and 6 males and 4 females in the control group.

Qualitatively, the contact stress distributions in the control hips gradually varied over the surface. For the fractured hips, particularly those in the PTOA group, there were much more focal contact stress elevations that varied in location over the gait cycle (Figure 9), attributable to residual local articular surface incongruities. Our findings relating these contact stress measures to PTOA outcomes are detailed in the latter portion of the next section (see below).

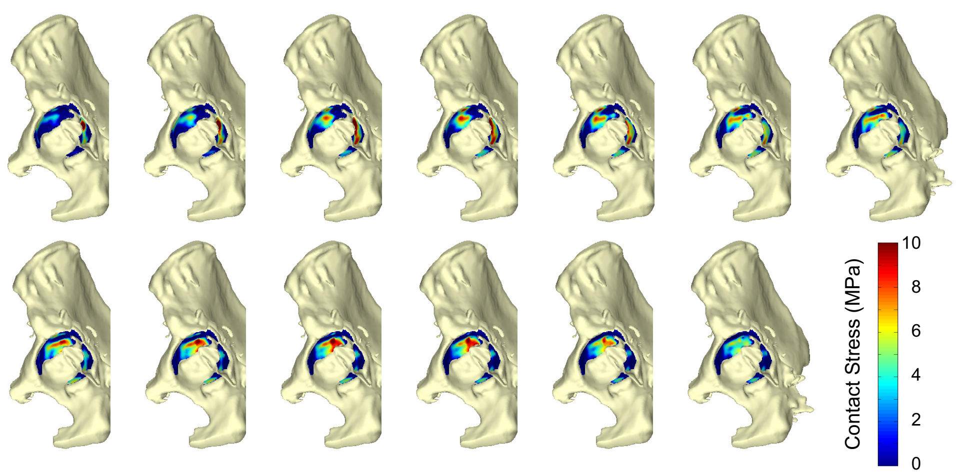

Figure 9. Contact stress distributions are computed at each of the 13 loaded poses for this fractured acetabulum to replicate the entire stance phase of gait.

Major Tasks 5 (PTOA radiographic frequency) and 6 (PTOA symptoms and quality of life) presented major challenges. Our partners at BAMC screened hundreds of patient medical records and encountered challenges that were all expected, but not to the degree experienced. For one, the initial DoD trauma registry search had limitations based on coding. The BAMC team cast a broad net so not to miss potential cases, but in the process got a large number of ankle fractures and non-articular cases from inaccurate coding. Additional screening methods and fastidious review of cases led to the successful accumulation of over 100 fractures. However, difficulties including 1) a lack of follow-up radiographs or other records to comment on OA status and 2) a lack of requisite CT imaging both hindered our collection of more outcome data. The follow up issue is a DoD medical system limitation that the team was unable to entirely overcome.

Detailed report of progress on Major Task 5

Clearly, the obtaining of reliable follow-up outcome data in the patients whose IAFs we analyzed proved our most difficult challenge. To address this shortcoming, we turned to the published literature to find average rates of PTOA development for each of the joints as a point of comparison (Table 3). For consistency across the studies, we defined PTOA as being present in joints when the Kellgren-Lawrence (KL) radiographic grade was greater than or equal to 2. To explore how acute fracture severity influences PTOA risk after IAF, we first examined correlations between the computed fracture energies and published PTOA rates. Then an additional data analysis step involved likewise examining correlations between contact area-normalized fracture energies and PTOA rates. Fracture energy alone did not correlate at all with the published rates of PTOA (Figure 10). However, when normalized to account for the fact that energy transfer across the joint is distributed over the contact area of the articular surface, fracture energy much more accurately explains differences in PTOA propensity (Figure 11).

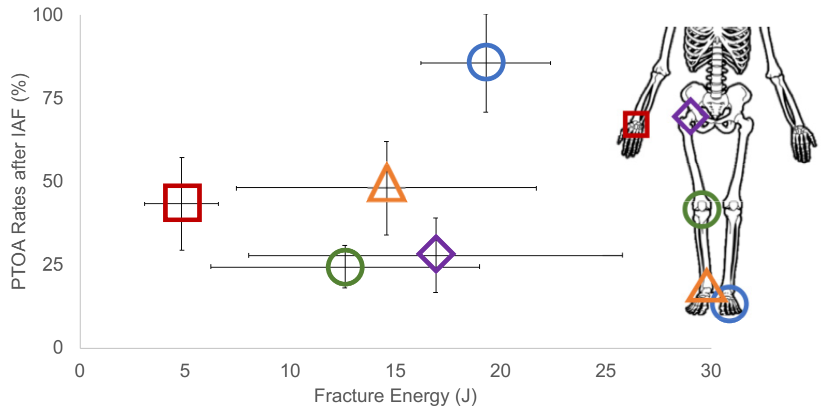

Figure 10. PTOA rates did not correlate with fracture energy for intra-articular fractures of articular joints involving the calcaneus (n=48), tibial pilon (118), tibial plateau (129), acetabulum (79), or distal radius (20).

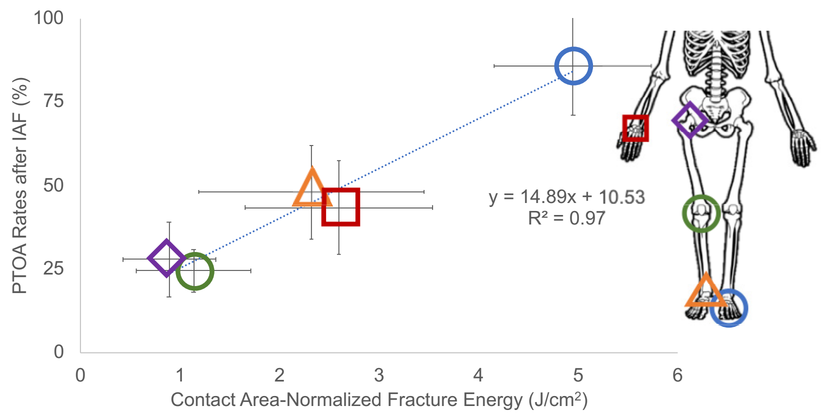

Figure 11. Correlation between the normalized fracture energies and the reported rates of PTOA for each of the joints of the body analyzed.

In addition to variations in contact area, there are also variations in the thickness of the cartilage and in the density of the subchondral bone, both of which may also partly explain differences in PTOA rates in different joints. Thicker cartilage might, for instance, provide more material to deform and thereby further distribute the impact. If there are larger areas of contacting cartilage over which to disperse the energy, then the damage in any given region might be lessened. The literature reports differences in cartilage thickness across joints to be smaller than the differences seen in contact area. As there are other, larger anatomical differences between these joints (e.g., presence/absence of a labrum, meniscus, etc.) it does pose a challenge for us to carefully consider other factors at play.

However, we would argue that variations in cartilage thickness are unlikely to be meaningful in this respect, because the fracturing impacts occur at such high rates of loading that there is very little opportunity for fluid flow in the cartilage, meaning that it is effectively much stiffer and therefore deforms little. For the ranges of cartilage thickness variation in these joints, it is hard to believe that the cartilage thickness appreciably influences the joint injury. As for variation in subchondral bone density across joints, it is implicitly captured by the fracture energy measurements, which incorporate bone density over inter-fragmentary surface areas involving subchondral bone.

Returning now to the PTOA risk attributable to IAF malreduction, we investigated the implications of chronic contact stress elevation following surgical repair of the acetabular IAF cases (see above for detail of methods). The hips from healthy volunteers were exposed to an average maximum contact stress of 7.4 ± 2.0 MPa (mean ± standard deviation). Hips from patients with acetabular fractures experienced an average maximum contact stress of 10.9 ± 3.4 MPa. Patients that developed PTOA had significantly higher maximum contact stresses in their hips than patients that did not (12.0 ± 3.8 MPa vs. 8.8 ± 0.7 MPa; p=0.008 – Figure 12). Patients that developed PTOA also had significantly higher maximum contact stresses than did subjects in the control group (p<0.001), while there was no significant difference in maximum contact stresses between the controls and the patients who did not develop PTOA (p=0.068). Over the course of the stance phase of gait, the PTOA group had higher maximum contact stress than the patients that didn't develop PTOA and the normal controls (Figure 13). The fracture patients that didn't develop PTOA also had consistently higher maximum contact stress than the normal control group.

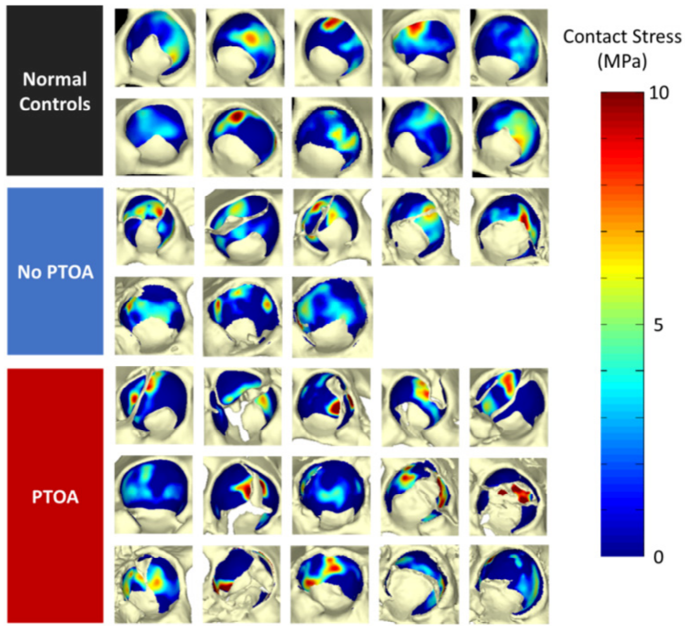

Figure 12. Contact stress distributions for the patients who had developed PTOA at two years after surgery were substantially more focal and had significantly higher peak values.

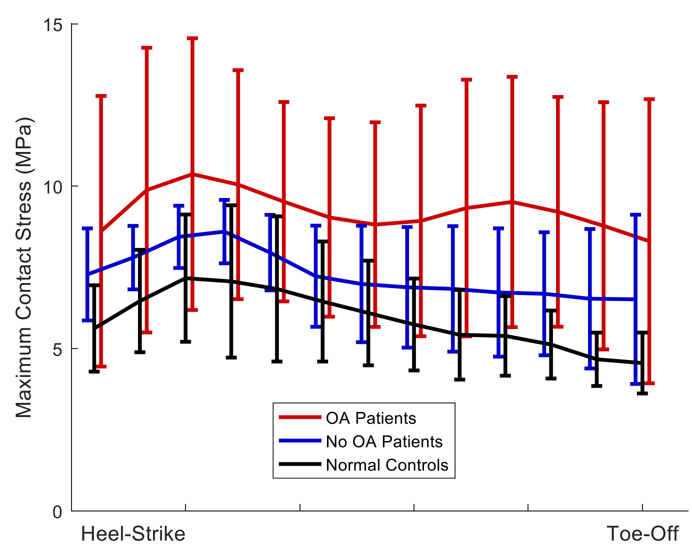

Figure 13. Over the entire stance phase of gait, the maximum contact stress in the OA group is higher than the no OA patients and normal hips.

If we consider the peak maximum contact stress across the entire gait cycle, differences in the groups become more apparent (Figure 14). There appears to be a threshold of maximum contact stress around 11 MPa, above which patients predictably progress to PTOA. Of note, this level barely exceeds the highest maximum contact stress seen in the normal control group, indicating that even slight perturbations in the joint surface from normal in some cases may portend degeneration. However, in our data nearly half of the patients that developed PTOA (7/15) would be missed by this threshold, demonstrating the multifaceted nature of PTOA. These patients may have incurred irreparable damage from the initial fracture, have diminished regenerative capacity, or be predisposed to its development by a number of other factors that led to degeneration of their articular cartilage, despite a comparatively normal mechanical environment.

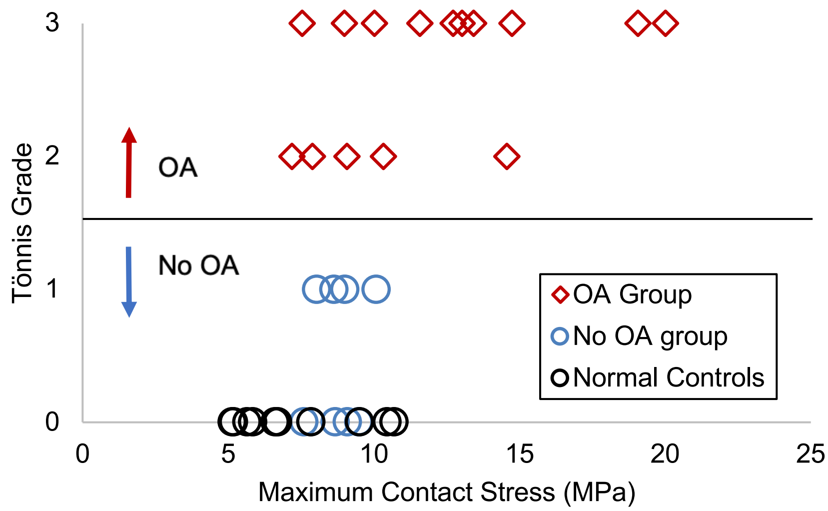

Figure 14. Elevated maximum contact stress is predictive of PTOA when contact stresses exceed those of normal.

In an effort to improve the model of PTOA risk arising from chronic contact stress elevation, DEA was used to compute deleterious contact stress exposure above a damage threshold at each step in the gait cycle. The basic premise of this approach is that contact stress itself is not dangerous, and it is in fact required for normal cartilage functioning. However, above a certain level it is known to be deleterious to cartilage health. Therefore, to assess the effects of chronic mechanical insult, previous work by our group established the concept of a damage threshold above which contact stresses become deleterious to cartilage health. By ignoring contact stresses below the damage threshold and combining the duration and magnitude of suprathreshold contact stresses, we derived a means to estimate the dose of chronic mechanical insult. We refer to this dose as the contact stress over-exposure.

In our study, we selected the damage threshold to be 5 MPa, based on our prior work. These deleterious contact stresses were then computed at each of the 13 steps of the gait cycle and multiplied by the time spent in each of the steps to obtain a stress-time over-exposure metric. Summed over the gait cycle, the cumulative contact stress over-exposure experienced by the articular surface was compared to Tönnis grades at 2 years post-operatively (Figure 15). For each patient, only the deleterious contact stress over-exposure was considered in our evaluation. We found a positive correlation (Pearson's correlation of 0.7) between the maximum contact stress over-exposure and the Tönnis grade. The maximum contact stress over-exposure seen in the no PTOA group was 0.98±0.45 MPa-s per gait cycle, while the PTOA group had maximum

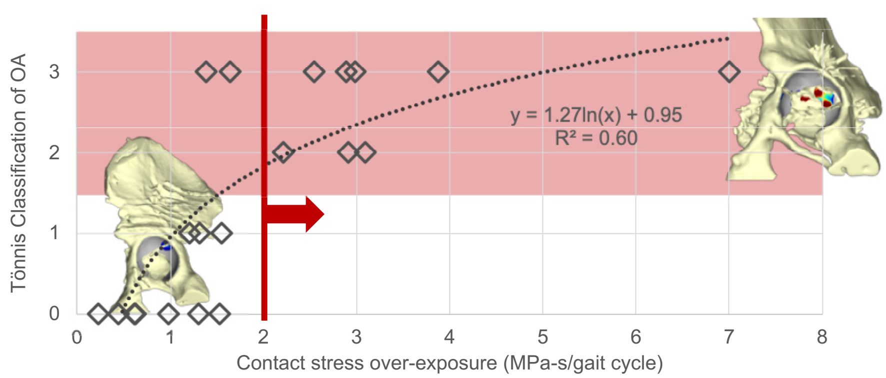

Figure 15. Maximum per gait cycle contact stress over-exposure vs. KL grade at minimum two-year clinical follow up.

contact stress over-exposures of 3.06±0.73 MPa-s per gait cycle, more than three times higher than in the no PTOA group. These differences were highly significant ($p<0.0001$). Perhaps more significant clinically, these data present a clear exposure threshold above which cases predictably progress to PTOA. Using a 2 MPa-s/gait cycle threshold to predict which cases progressed to OA yields a sensitivity of 100% and a specificity of 83.3%.

To get an overview of how the exposures differed for the no PTOA and PTOA groups, they are divided top and bottom in Figure 16. Comparing the two groups, it becomes clear that acetabular fractures in the group that degenerated to PTOA had larger regions of higher contact stress over-exposures. In contrast, cases with minimal or no radiographic evidence of PTOA had less severe incongruities that resulted in regions of over-exposure that were smaller in size and magnitude.

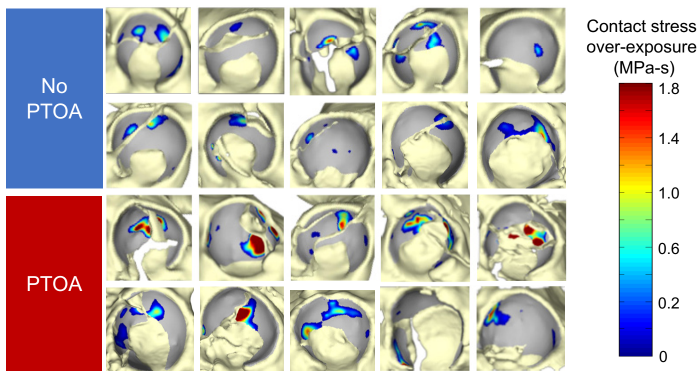

Figure 16. The distributions of contact stress over-exposure in the series of acetabular fractures studies are shown here, arranged according to their PTOA status.

CONCLUSION: PTOA Risk Prediction Models Utilizing Pathomechanical Factors

Limitations related to challenges in achieving adequate patient follow up notwithstanding, we were able to complete combined fracture severity and contact stress analyses on a series of civilian patients having sustained IAFs of either their distal tibial pilon, the acetabulum, or the calcaneus. These results are summarized below and presented in the context of defining PTOA risk prediction models based on the pathomechanical factors analyzed.

A receiver operating characteristic curve, or ROC curve, is a graphical plot showing the diagnostic ability of a binary classifier system as its discrimination threshold is varied. Consider a two-class prediction problem (binary classification), in which the outcomes are labeled either as positive (p) or negative (n). There are four possible outcomes from a binary classifier. If the outcome from a prediction is p and the actual value is also p, then it is called a true positive; however, if the actual value is n then it is said to be a false positive. Conversely, a true negative has occurred when both the prediction outcome and the actual value are n, and false negative is when the prediction outcome is n while the actual value is p. Plotted in tabular form, this is a contingency table.

Contingency Table		True Condition	
		Positive	Negative
Predicted condition	Positive	True positive (TP)	False positive (FP), Type I error
	Negative	False negative (FN), Type II error	True negative (TN)
		True positive rate (TPR) = TP/(TP+FN)	False positive rate (FPR) = FP/(FP+TN)

The ROC curve is created by plotting the true positive rate (TPR), also known as the sensitivity, against the false positive rate (FPR), or 1-specificity, at various threshold settings. The ROC curve graphically displays the trade-off between sensitivity and specificity and is useful in assigning the best cut-offs for clinical use. Overall accuracy is expressed as the area under the ROC curve (AUC) and provides a useful parameter for comparing test performance. The shape of a ROC curve and the AUC helps us estimate the discriminative power of a test. The closer the curve is located to the upper-left hand corner and the larger the area under the curve, the better the test is at discriminating between diseased and non-diseased. The area under the curve can have any value between 0 and 1 and it is a good indicator of the goodness of the test. A perfect diagnostic test has an AUC 1.0. whereas a nondiscriminating test has an area 0.5.

Sixteen patients with articular fractures of the tibial pilon were enrolled in an IRB-approved study. Patients were selected for having both pre- and post-op CT imaging with a minimum of 24 months of radiographic follow-up. Acute fracture severity metrics and maximum contact stress over-exposures were both significantly correlated with PTOA severity ($\rho=0.82$, $p<0.001$ and $\rho=0.65$, $p=0.007$, respectively). When thresholds were chosen to produce the optimal predictive performance, the injury severity measure had an AUC of 0.93, the contact stress over-exposure measure had an AUC of 0.98 and a combined measure of the two had an AUC of 1.00 indicating a perfect delineation of cases that did/did not develop PTOA (Figure 17).

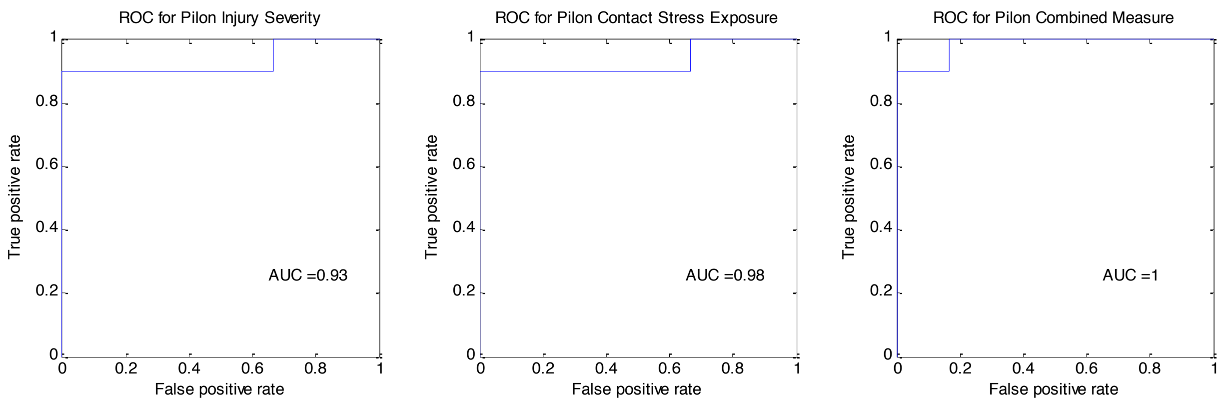

Figure 17. ROC curves for the tibial pilon of the combined injury severity measure, contact stress over-exposure, and the combined measure of injury severity and contact stress over-exposure. AUCs are displayed on each graph.

Nineteen patients with articular fractures of the acetabulum were enrolled in an IRB approved study. Patients were selected for having both pre- and post-op CT imaging with a minimum of 12 months of radiographic follow-up. Maximum contact stress over-exposures and the injury severity measures were both significantly correlated with PTOA severity ($\rho=0.67$, $p=0.002$ and $\rho=0.45$, $p=0.05$, respectively). The fracture severity measure had an AUC of 0.90, the contact stress over-exposure measure had an AUC of 0.87 and a combined measure of the two had an AUC of 0.91 (Figure 18).

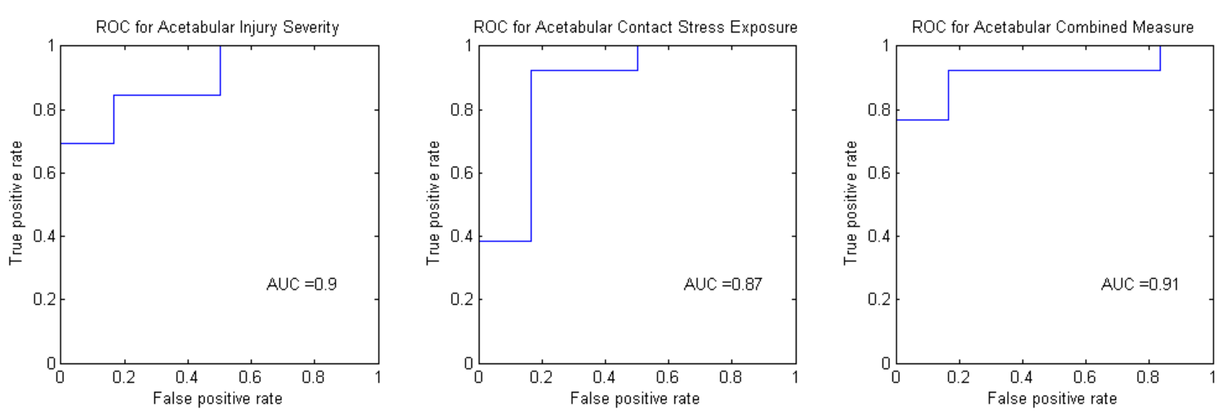

Figure 18. ROC curves for predictors of PTOA development in acetabular fractures. The combined measure of injury severity, the measure of contact stress over-exposure, and the combined measures of injury severity and contact stress over-exposure are plotted from left to right with AUCs displayed on each graph.

Thirty-three patients with articular fractures of the calcaneus were enrolled in an IRB-approved study. Patients were selected for having both pre- and post-op CT imaging with a minimum of 18 months of radiographic follow-up. Both the acute fracture severities and maximum contact stress over-exposures significantly correlated with PTOA severity (ρ=0.52, p=0.002 and ρ=0.48, p=0.004, respectively). The acute fracture severity metric had an AUC of 0.83, the contact stress over-exposure measure had an AUC of 0.82 and a combined measure of the two had an AUC of 0.88 (Figure 19).

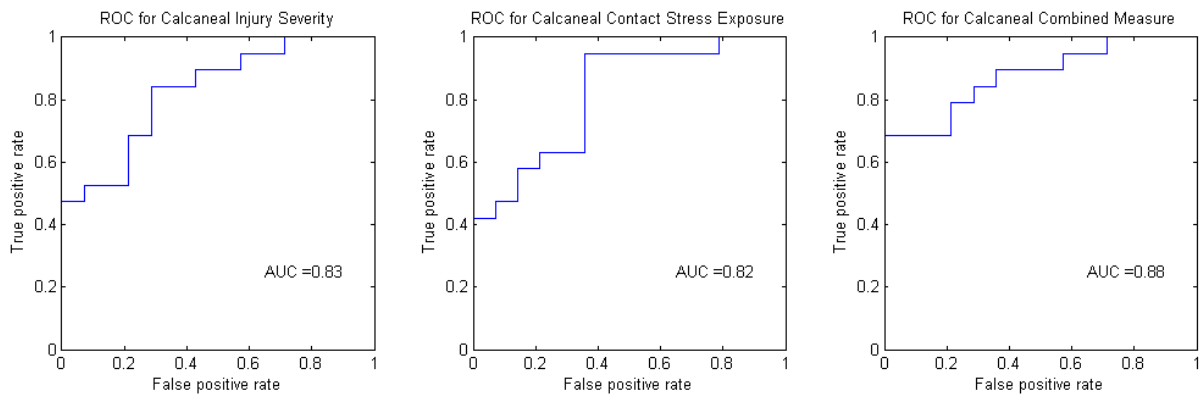

Figure 19. ROC curves for the calcaneus of the combined injury severity measure, contact stress over-exposure, and the combined measure of injury severity and contact stress over-exposure. AUCs are displayed on each graph.

The relative impact of the acute fracture severity and contact stress over-exposure related to malreduction (shown in Figure 20) has significant clinical implications for the treatment of IAFs. These were the first studies to objectively quantify both the severity of initial injury and the accuracy of surgical reduction in patients with IAFs of the pilon, acetabulum, or calcaneus. The results of this study confirm literature findings that surgical reduction quality, as measured by contact stress over-exposure, is predictive of PTOA risk. However, the results also indicate that, in addition to the surgical reduction, the severity of the initial injury plays a critical role in PTOA risk. This elucidates a potential reason for the disconnect between advances in surgical care and the lack of improvement observed in PTOA prevention after IAFs. Acute biological damage caused by fracture is not effectively treated but appears to be a significant contributor to PTOA

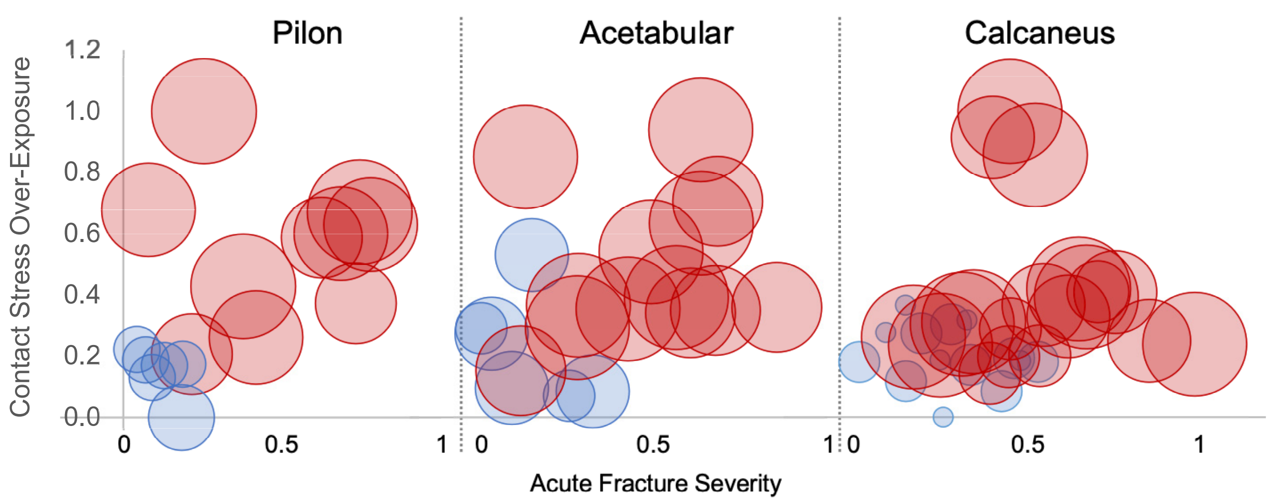

Figure 20. Fractures with lower acute fracture severity and contact stress over-exposure had lesser degrees of PTOA (KL grades 0&1 shown as smaller blue bubbles and KL grades ≥2 as larger red bubbles).

risk. Therefore, to improve management of these challenging injuries, novel biological interventions may be needed in addition to improvements in mechanical restoration of the articular surface to substantially reduce PTOA risk.

What opportunities for training and professional development has the project provided?

Mr. Kevin Dibbern, the graduate research assistant who worked on this project, completed his PhD in Biomedical Engineering in August 2019. Dr. Anderson served as his primary advisor, and in that capacity not only directed Mr. Dibbern's work, but also mentored him in related technical and professional development matters. This involved bi-weekly one-on-one meetings, having Mr. Dibbern give regular presentations in the laboratory related to this work, and having Mr. Dibbern attend national/international conferences at which the work was presented.

How were the results disseminated to communities of interest?

Over the entirety of the funding period, four articles have been published and seven additional manuscripts are written and in various stages of journal submission/review. We have presented our research findings at national and international conferences all over the world, in 37 presentations to date. The audiences have ranged from the military health community, to the orthopedic surgeon community, to orthopedic research scientists.

What do you plan to do during the next reporting period to accomplish the goals?

Nothing to Report

4. **Impact**

What was the impact on the development of the principal discipline(s) of the project?

To our knowledge, we continue to be the only group utilizing objective quantitative fracture severity metrics to stratify PTOA risk after IAF. Correspondingly, we are the first to document a clear relationship between the acute mechanical insult to the joint and later PTOA risk. Additionally, our patient-specific computational modeling results are the first to demonstrate the relationship between cumulative contact stress over-exposure and PTOA after IAFs. We are in the process of finalizing these analyses (and others) and have prepared manuscripts for submission (see Appendix).

What was the impact on other disciplines?

Nothing to Report

What was the impact on technology transfer?

Nothing to Report

What was the impact on society beyond science and technology?

Nothing to Report

5. **Changes/Problems**

Changes in approach and reasons for change

Nothing to Report

Actual or anticipated problems or delays and actions or plans to resolve them

Nothing to Report

Changes that had a significant impact on expenditures

Nothing to Report

Significant changes in use or care of human subjects, vertebrate animals, biohazards, and/or select agents

Nothing to Report

Significant changes in use or care of human subjects

Nothing to Report

Significant changes in use or care of vertebrate animals.

Not Applicable

Significant changes in use of biohazards and/or select agents

Not Applicable

6. **Products**

Publications, conference papers, and presentations

- Journal publications

1. Kempton LB, Dibbern KA, Anderson DD, Morshed S, Higgins TF, Marsh JL, McKinley TO. Objective metric of energy absorbed in tibial plateau fractures corresponds well to clinician assessment of fracture severity. J Orthop Trauma. 2016;30(10):551–556. PMC5035182. Federal support acknowledged.

2. Dibbern K, Kempton LB, Higgins TF, Morshed S, McKinley TO, Marsh JL, Anderson DD. Fractures of the tibial plateau involve similar energies as the tibial pilon but greater articular surface involvement. J Orthop Res. 2017;35(3):618–624. PMC5218984. Federal support acknowledged.

3. Townsend KC, Thomas-Aitken HD, Rudert MJ, Kern AM, Willey MC, Anderson DD, Goetz JE. Discrete element analysis is a valid method for computing joint contact stresses in the hip before and after acetabular fracture. J Biomech. 2018;67:9–17. PMC5767141. Federal support acknowledged.

4. Rao K, Dibbern K, Day M, Glass N, Marsh JL, Anderson DD. Correlation of fracture energy with Sanders Classification and post-traumatic osteoarthritis following displaced intra-articular calcaneus fractures. J Orthop Trauma. J Orthop Trauma. 2019;33(5):261–266. PMC6476631. Federal support acknowledged.

5. Dibbern K, Kern A, Anderson DD. A universally applicable, objective CT-based method for quantifying articular fracture severity (submitted). Federal support acknowledged.

6. Dibbern K, McKinley TO, Marsh JL, Anderson DD. Toward a unifying understanding of the influence of acute fracture severity on risk of post-traumatic osteoarthritis following intra-articular fractures (ready for submission). Federal support acknowledged.

7. Thomas-Aitken H, Dibbern K, CarlLee T, Marsh JL, Willey M, Goetz J, Anderson DD. Elevated joint contact stress is associated with radiographic measures of osteoarthritis in operatively treated acetabular fractures at two years (ready for submission). Federal support acknowledged.

- Books or other non-periodical, one-time publications.

1. Dibbern KN. Utilizing objective measures of acute and chronic mechanical insult to determine their contributions to post-traumatic osteoarthritis risk. PhD thesis, University of Iowa, 2019. https://doi.org/10.17077/etd.92oy-stmy.
2. Anderson DD, Wilken J, Brockett C, Redmond A. (2021) Predicting and Preventing Post-traumatic Osteoarthritis of the Ankle. In Ledoux W, Telfer S, Iaquinto J (Eds.) Foot and Ankle Biomechanics, (pp. TBD). Amsterdam, Netherlands: Science & Technology Books, Elsevier.

- Other publications, conference papers, and presentations. [* indicates produced a manuscript]

1. *Dibbern KN, Kempton LB, Higgins TF, McKinley TA, Marsh JL, Anderson DD. Comparison of objective fracture severity measures in tibial plateau and pilon fractures. <u>39th Annual Meeting of the American Society of Biomechanics</u>, August 5–8, 2015, Columbus, Ohio.
2. *Kempton LB, Dibbern K, Anderson DD, Morshed S, Higgins T, Marsh JL, McKinley T. Objective metric of energy absorbed in tibial plateau fractures corresponds well to clinician assessment of fracture severity. <u>31st Annual Meeting of the Orthopaedic Trauma Association</u>, October 7–10, 2015, San Diego, California.
3. *Dibbern KN, Kempton LB, Higgins TF, McKinley TA, Marsh JL, Anderson DD. Energy absorbed in fracturing is similar in tibial plateau and pilon fractures over a full spectrum of severity. <u>83rd Annual Meeting of the American Academy of Orthopaedic Surgeons</u>, March 1–5, 2016, Orlando, Florida.
4. *Kempton LB, Dibbern K, Anderson DD, Morshed S, Higgins T, Marsh JL, McKinley T. CT-based metric of tibial plateau fracture energy corresponds well to clinician assessment of fracture severity. <u>83rd Annual Meeting of the American Academy of Orthopaedic Surgeons</u>, March 1–5, 2016, Orlando, Florida.
5. *Dibbern KN, Kempton LB, McKinley TO, Higgins TF, Marsh JL, Anderson DD. Quantifying tibial plateau fracture severity: Fracture energy agrees with clinical rank ordering. <u>62nd Annual Meeting of the Orthopaedic Research Society</u>, March 5–8, 2016, Orlando, Florida.
6. *Townsend KC, Rudert MJ, Kern AM, Willey MC, Anderson DD, Goetz JE. Validation of hip joint contact stresses computed using discrete element analysis. <u>62nd Annual Meeting of the Orthopaedic Research Society</u>, March 5–8, 2016, Orlando, Florida.
7. *Dibbern KN, Higgins TF, Kempton LB, McKinley TO, Marsh JL, Anderson DD. Objective fracture energy assessment of tibial plateau fractures loosely corresponds to Schatzker classification. <u>62nd Annual Meeting of the Orthopaedic Research Society</u>, March 5–8, 2016, Orlando, Florida.

8. *Rao K, Dibbern KN, Phisitkul P, Marsh JL, Anderson DD. Relating fracture severity to post-traumatic osteoarthritis risk after intra-articular calcaneal fractures. 62nd Annual Meeting of the Orthopaedic Research Society, March 5–8, 2016, Orlando, Florida.

9. Mosqueda JM, Dibbern KN, Willey MC, Marsh JL, Anderson DD. Elevated contact stress after surgical reduction of acetabular fractures correlates with progression to post-traumatic osteoarthritis. 40th Annual Meeting of the American Society of Biomechanics, August 2–5, 2016, Raleigh, North Carolina.

10. *Dibbern KN, Kempton LB, Higgins TF, McKinley TO, Marsh JL, Anderson DD. Clinical fractures of the tibial plateau involve similar energies as the tibial pilon. 40th Annual Meeting of the American Society of Biomechanics, August 2–5, 2016, Raleigh, North Carolina.

11. *Rao K, Dibbern KN, Phisitkul P, Marsh JL, Anderson DD. Post-traumatic OA risk relative to intra-articular calcaneal fracture severity. 32nd Annual Meeting of the Orthopaedic Trauma Association, October 5–8, 2016, National Harbor, Maryland.

12. *Holland TC, Dibbern KN, Marsh JL, Anderson DD, Willey MC. Objective prediction of post-traumatic OA risk following acetabular fractures based on severity. 63rd Annual Meeting of the Orthopaedic Research Society, March 19–22, 2017, San Diego, California.

13. Dibbern KN, Caldwell L, Lawler E, Anderson DD. Less energy is absorbed in fracturing the distal radius than in lower extremity fractures. 63rd Annual Meeting of the Orthopaedic Research Society, March 19–22, 2017, San Diego, California.

14. Dibbern KN, Kern AM, Anderson DD. A universally applicable objective CT-based method for quantifying articular fracture severity. 63rd Annual Meeting of the Orthopaedic Research Society, March 19–22, 2017, San Diego, California.

15. Dibbern KN, Willey MC, Phisitkul P, Glass NA, Marsh JL, Anderson DD. Fracture severity predicts OA risk following intra-articular fractures. 2017 OARSI World Congress on Osteoarthritis, April 27–30, 2017, Las Vegas, Nevada.

16. Rivera JC, Dibbern KN, Marsh JL, Anderson DD. Objective CT-based assessment of severity in articular fractures of the tibial pilon. 26th Annual Scientific Meeting of the Limb Lengthening and Reconstruction Society, July 21– 22, 2017. Park City, Utah.

17. Dibbern KN, Rivera J, Marsh JL, Anderson DD. Objective CT-based assessment of severity in articular fractures of the tibial pilon. 2017 Military Health System Research Symposium, August 27–30, 2017, Kissimmee Florida.

18. Dibbern KN, Rivera JC, Marsh JL, Anderson DD. Objective metrics of tibial pilon fracture severity predict secondary amputation. 2018 AAOS/OTA/SOMOS/ORS Extremity War Injuries XIII Symposium (EWI XIII), January 21–23, 2018, Washington, DC.

19. Dibbern KN, Rivera JC, Marsh JL, Anderson DD. Objective assessment of tibial pilon articular fracture severity predictive of secondary amputation. 64th Annual Meeting of the Orthopaedic Research Society, March 10–13, 2018, New Orleans, Louisiana.

20. Thomas HD, Dibbern KN, Holland TC, CarlLee T, Rao K, Marsh JL, Willey MC, Goetz JE, Anderson DD. Joint contact stress correlates with clinical measures of osteoarthritis in

surgically reduced acetabular fractures. 64th Annual Meeting of the Orthopaedic Research Society, March 10–13, 2018, New Orleans, Louisiana.

21. Anderson DD. Alex Stacoff Lecture: Enabling Post-Traumatic OA Risk Prediction from Pathomechanics. 2018 International Foot and Ankle Biomechanics (i-FAB) Meeting, April 10, 2018, New York City, New York.

22. Thomas HD, Dibbern KN, Holland TC, Marsh JL, Willey MC, Goetz JE, Anderson DD. Elevated contact stress after acetabular fracture correlates with development of radiographic OA. 2018 OARSI World Congress on Osteoarthritis, April 26–29, 2018, Liverpool, United Kingdom.

23. Anderson DD. Enabling Post-Traumatic Osteoarthritis Risk Prediction from Pathomechanics. Engineering Solutions for Health: Biomedical Engineering Research Strategy, June 6, 2018, University of Calgary, Calgary, AB Canada.

24. Dibbern KN, Perry BJ, Spratley EM, Salzar RS, Rivera JC, Anderson DD. Novel severity measures link fractures from cadaveric experiments to those in battlefield blast cases. 8th World Congress of Biomechanics, July 8–12, 2018, Dublin, Ireland.

25. Thomas-Aitken HD, Dibbern KN, Holland TC, Marsh JL, Willey MC, Goetz JE, Anderson DD. Elevated contact stress after acetabular fracture correlates with the development of radiographic OA. 8th World Congress of Biomechanics, July 8–12, 2018, Dublin, Ireland.

26. Dibbern KN, Holland TC, Thomas-Aitken HD, CarlLee T, Willey MC, Goetz JE, Marsh JL, Anderson DD. Contact stress over-exposure correlates with OA development in acetabular fractures. 42nd Annual Meeting of the American Society of Biomechanics, August 8–11, 2018, Rochester, Minnesota. 2018. 2018 **[Received ASB Clinical Biomechanics Award.]**

27. Thomas HD, Dibbern KN, CarlLee TL, Marsh JL, Willey MC, Goetz JE, Anderson DD. Elevated joint contact stress is associated with radiographic measures of osteoarthritis in operatively treated acetabular fractures at two years. 34th Annual Meeting of the Orthopaedic Trauma Association, October 17–20, 2018, Orlando, Florida.

28. Dibbern KN, Thomas-Aitken H, CarlLee T, Willey M, Goetz J, Marsh JL, Anderson DD. Contact stress over- exposure correlates with PTOA risk in acetabular fractures. 65th Annual Meeting of the Orthopaedic Research Society, February 2–5, 2019, Austin, Texas.

29. Dibbern KN, McKinley T, Marsh JL, Anderson DD. Toward a unifying understanding of the influence of acute fracture severity on PTOA risk following intra-articular fractures. 65th Annual Meeting of the Orthopaedic Research Society, February 2–5, 2019, Austin, Texas.

30. Anderson DD. Enabling Post-Traumatic OA Risk Prediction from Pathomechanics. Biophysics of Bone and Cartilage Research Group Seminar, April 4, 2019, University of Eastern Finland, Kuopio, Finland.

31. Dibbern K, McKinley TO, Marsh J, Anderson DD. The influence of acute fracture severity on OA risk following intra-articular fractures. Osteoarthritis Research Society International 2019 World Congress, May 2–5, 2019, Toronto, Ontario, Canada.

32. Dibbern KN, McKinley TO, Marsh JL, Anderson DD. The relationship between acute intra-articular fracture severity and the risk of post-traumatic osteoarthritis. XXVII Congress of the International Society of Biomechanics (ISB 2019), held in conjunction with the 43rd Annual Meeting of the American Society of Biomechanics (ASB 2019), July 31–August 4, 2019, Calgary, Canada.

33. Anderson DD. Enabling Post-Traumatic Osteoarthritis Risk Prediction from Pathomechanics. Center for Applied Biomechanics Seminar, October 23, 2019, University of Virginia, Charlottesville, Virginia.

34. Dibbern KN, Engelken M, Thomas-Aitken Holly D, Holland T, Willey MC, Marsh JL, Anderson DD. Objective mechanical measures predict post-traumatic OA risk after intra-articular fracture of the acetabulum. 66th Annual Meeting of the Orthopaedic Research Society, February 8–11, 2020, Phoenix, Arizona.

35. Dibbern KN, Rao K, Day M, Marsh JL, Anderson DD. Objective mechanical measures predict post-traumatic OA risk after intra-articular fracture of the calcaneus. 66th Annual Meeting of the Orthopaedic Research Society, February 8–11, 2020, Phoenix, Arizona.

36. Dibbern KN, Willey MC, Marsh JL, Anderson DD. Objective mechanical measures predict post-traumatic OA risk after intra-articular fracture of the tibial plafond. 66th Annual Meeting of the Orthopaedic Research Society, February 8–11, 2020, Phoenix, Arizona. [**New Investigator Recognition Award (NIRA) Finalist**.]

37. Dibbern KN, Rao K, Day M, Willey MC, Marsh JL, Anderson DD. Objective mechanical measures predict post- traumatic OA risk after intra-articular fracture of the hindfoot and ankle. International Foot & Ankle Biomechanics Meeting 2020, April 5–8, 2020, Sao Paulo, Brazil.

Website(s) or other Internet site(s)

Nothing to Report

Technologies or techniques

Our prior objective, CT-based methods for determining the energy expended in a bone fracture were extended to enable their use in more fracture types. The new methodology requires only a pre-operative CT-scan of the fractured joint. The CT images are then segmented, identifying all bone fragments to generate 3D models of the fracture fragments. Surfaces are then smoothed to remove imaging artifacts and to prepare the data for use in a surface classification algorithm. An automated classifier then identifies fractured surfaces on the fragments, with a graph cut method used to create a clear boundary between the intact and fractured bone surfaces. Manual adjustment of this boundary is performed to finalize the fractured surface identification. The CT Hounsfield Unit intensities are then sampled along the fractured surface for use in obtaining a bone density distribution over the surface. The fractured areas are then scaled by these location specific densities and multiplied by a density dependent energy release rate to obtain the fracture energy. Articular comminution can be quantified by measuring the fracture edge length along the articular surface from the fractured surface boundaries. The new methodology was validated by comparing the fracture energies obtained for a series of 20 pilon fractures that had previously been assessed using the existing methods.

We recognize the need for broad dissemination of the research methods developed in the course of this work that allow study of the pathways responsible for PTOA. Perhaps the most effective means for sharing the techniques is through the presentation of our findings at scientific meetings and as peer-reviewed published manuscripts. In the latter case, we will submit or have submitted on our behalf to the National Library of Medicine's PubMed Central an electronic version of any final, peer-reviewed manuscripts upon acceptance for publication, to be made publicly available no later than 12 months after the official date of publication. We will strive to produce such scientific outputs in a timely manner and to report on all relevant data derived during the project in as broad a range of venues as possible.

Inventions, patent applications, and/or licenses

Nothing to Report

Other Products

- Follow-on additional funding

Currently Funded Grants

2017 – 2020 Orthopaedic Trauma Association
An Imaging Framework for Clinically Testing New Treatments to Prevent Post-Traumatic OA
$79,982 Total Costs (Co-Principal Investigator)

The main goal of this project is to test the value of a new low-cost, low-dose standing CT system for efficient early detection of both joint degeneration and elevated contact stress. This work would provide better early indicators of PTOA development that could complement the predictive methods developed in the current project.

2018 – 2022 US Department of Defense, CDMRP Peer Reviewed Medical Research Program Focused Program Award (W81XWH-18-1-0658)
Translating Metabolic Responses to Mechanical Insult into Early Interventions to Prevent PTOA
Project 1: Small-scale Early Phase Clinical Trial of Amobarbital to Reduce PTOA Risk in Tibial Pilon Fractures
$2,320,698 Subproject Total Costs (Co-Investigator, Project 1)
Project 2: Integrating Pathomechanical PTOA Risk into Clinical Decision-making Following IAF
$2,420,192 Subproject Total Costs (Project Lead, Project 2)
$9,999,762 Total Costs

The goal of this program is to translate approaches targeting harmful chondrocyte metabolic responses to mechanical insult that drive progressive joint destruction into multi-faceted therapies to prevent, delay, or mitigate PTOA after IAFs and other traumatic injuries. The methods developed and the PTOA prediction models tested in the current project provided critical groundwork for this program.

Pending Grants

2020 – 2022 Arthritis Foundation
3D Joint Space Width from Weight Bearing CT as an Imaging Biomarker of PTOA
$677,679 Total Costs (Principal Investigator)

The main goal of this project is to develop an early imaging biomarker of PTOA working from low-cost, low-dose standing CT for efficient early detection of both joint degeneration and elevated contact stress. This work would provide better early indicators of PTOA development that could complement the predictive methods developed in the current project.

7. **Participants & Other Collaborating Organizations**

What individuals have worked on the project?

Name: Donald D. Anderson, PhD
Project Role: PI
Researcher Identifier (e.g. ORCID ID): 0000-0002-1640-6107
Nearest person month worked: 2.4
Contribution to Project: Dr. Anderson leads the research team at the University of Iowa, guiding development and analysis related to the project.

Name: J. Lawrence Marsh, MD
Project Role: Investigator
Researcher Identifier (e.g. ORCID ID): 0000-0002-3494-6289
Nearest person month worked: 0.6
Contribution to Project: Dr. Marsh is the clinical lead at the University of Iowa, providing insight regarding the scope of the clinical problem and ensuring clinical applicability of decisions related to the project.

Name: M. James Rudert, PhD (30 Sep 2017 – 30 Mar 2018)
Project Role: Investigator
Nearest person month worked: 4
Contribution to Project: Dr. Rudert, an expert in mechanical measurement and fracture testing/simulation work, works closely with Mr. Dibbern to support measurements and computation. Dr. Rudert was taken off the team as of 30 Mar 2018 as he retired.

Name: Joshua E. Johnson, PhD (01 Jul 2018 – 29 Sep 2018)
Project Role: Investigator
Nearest person month worked: 4
Contribution to Project: Dr. Johnson was hired to replace Dr. Rudert on the team, and he began employment 01 Jul 2018.

Name: Kevin Dibbern, PhD
Project Role: Graduate Research Assistant
Researcher Identifier (e.g. ORCID ID): 0000-0002-8061-4453
Nearest person month worked: 6
Contribution to Project: Mr. Dibbern was actively involved in developing algorithms, writing analysis code, and performing analysis of the CT data.

Has there been a change in the active other support of the PD/PI(s) or senior/key personnel since the last reporting period?

Nothing to Report

What other organizations were involved as partners?

Nothing to Report

8. **Special Reporting Requirements**

COLLABORATIVE AWARDS: The Collaborating/Partnering PI at BAMC (Dr. Jessica Rivera) is submitting a separate progress report for that site.

9. **Appendices**

A collection of journal publications and abstracts (please see above *Products* for a complete listing) from the entirety of the funding period that supplements, clarifies and supports the text of this report are attached as appendices.

Objective Metric of Energy Absorbed in Tibial Plateau Fractures Corresponds Well to Clinician Assessment of Fracture Severity

Laurence B. Kempton, MD, Kevin Dibbern, BS,† Donald D. Anderson, PhD,† Saam Morshed, MD,‡ Thomas F. Higgins, MD,§ J. Lawrence Marsh, MD,† and Todd O. McKinley, MD**

Objectives: Determine the agreement between subjective assessments of fracture severity and an objective computed tomography (CT)-based metric of fracture energy in tibial plateau fractures.

Methods: Six fellowship-trained orthopaedic trauma surgeons independently rank-ordered 20 tibial plateau fractures in terms of severity based on anteroposterior and lateral knee radiographs. A CT-based image analysis methodology was used to quantify the fracture energy, and agreement between the surgeons' severity rankings and the fracture energy metric was tested by computing their concordance, a statistical measure that estimates the probability that any 2 cases would be ranked with the same ordering by 2 different raters or methods.

Results: Concordance between the 6 orthopaedic surgeons ranged from 82% to 93%, and concordance between surgeon severity rankings and the computed fracture energy ranged from 73% to 78%.

Conclusions: There is a high level of agreement between experienced surgeons in their assessments of tibial plateau fracture severity, and a slightly lower agreement between the surgeon assessments and an objective CT-based metric of fracture energy. Taken together, these results suggest that experienced surgeons share a similar understanding of what makes a tibial plateau fracture more or less severe, and an objective CT-based metric of fracture energy captures much but not all of that information. Further research is ongoing to characterize the relationship between surgeon assessments of severity, fracture energy, and the eventual clinical outcomes for patients with fractures of the tibial plateau.

Key Words: tibial plateau fracture, fracture energy, quantifying fracture severity

(*J Orthop Trauma* 2016;30:551–556)

INTRODUCTION

Fracture severity is commonly assessed by treating orthopaedic surgeons to determine prognosis and decide optimal treatment. Outcomes of intraarticular fractures are influenced by multiple patient, surgeon, and injury factors. The location of a fracture and its morphology, the quantity of articular surface involvement, and the extent of acute mechanical damage all play a role in defining the severity of a fracture. Fracture "severity" spans a spectrum from low to high. Low-severity fractures have characteristics such as minimal displacement or comminution and are thought to have an excellent prognosis with nonoperative treatment. High-severity fractures have characteristics like extensive displacement and comminution and are generally indicated for operative treatment with good to fair prognosis.

These indices, taken together, clearly indicate individual injury specificity. Orthopaedic surgeons formulate treatment strategies based largely on subjective criteria and clinical experience while accounting for patient-specific demographic and medical conditions. However, subjective methods of fracture assessment such as morphology and classification are often poorly reproducible among orthopaedic surgeons and are inherently unreliable.[1–3] There is a risk that relying on such methods may lead to poorly conceived treatment algorithms because they are not grounded in objective data.

The greater the amount of energy dissipated in the creation of a fracture (ie, the fracture energy), the greater the fracture severity. Accurate and reliable measures of the fracture energy can provide objective data for orthopaedic surgeons to use in making treatment decisions and predicting prognosis.

Accepted for publication May 18, 2016.
From the *Department of Orthopaedic Surgery, Indiana University School of Medicine, Indianapolis, IN; †Department of Orthopaedics and Rehabilitation, The University of Iowa, Iowa City, IA; ‡Department of Orthopaedic Surgery, Orthopaedic Trauma Institute, University of California, San Francisco, San Francisco, CA; and §Department of Orthopaedics, University of Utah School of Medicine, Salt Lake City, UT.
Supported by the National Institute of Arthritis and Musculoskeletal and Skin Diseases of the National Institutes of Health under award numbers P50AR055533 and R21AR061808. The content is solely the responsibility of the authors and does not necessarily represent the official views of the National Institutes of Health. This work was also supported by the Assistant Secretary of Defense for Health Affairs through the Peer Reviewed Medical Research Program under Award No. W81XWH-15-2-0087. Opinions, interpretations, conclusions and recommendations are those of the author and are not necessarily endorsed by the Department of Defense. The research was also aided by a grant from the Foundation for Orthopaedic Trauma (FOT).
Presented in part at the Annual Meeting of the Orthopaedic Trauma Association, October 9, 2015, San Diego, CA.
Thomas Higgins is a member of the Board of Directors of the OTA, has stock ownership in Orthogrid and Summit Med Ventures, and is a paid consultant for DePuy Synthes. Todd McKinley is a paid consultant for Bioventus. The remaining authors report no conflict of interest.
Supplemental digital content is available for this article. Direct URL citations appear in the printed text and are provided in the HTML and PDF versions of this article on the journal's Web site (www.jorthotrauma.com).
Reprints: Laurence Kempton, MD, Department of Orthopaedic Surgery, Indiana University School of Medicine, 1801 N. Senate Blvd. Ste 535, Indianapolis, IN 46240 (e-mail: Lkempton1@iuhealth.org).

DOI: 10.1097/BOT.0000000000000636

Previous investigations have demonstrated that objective computed tomography (CT)-based measures of fracture energy in tibial pilon fractures correlate with (1) surgeon assessment of injury severity and (2) 2-year radiographic and functional outcomes.[4,5] In this work, we explored whether this technique of objective fracture energy measurement could also be used to stratify the severity of tibial plateau fractures in a manner that would agree with expert opinions of fracture severity. Specifically, we hypothesized that an objective CT-based measure of fracture energy would correspond to subjective surgeon assessment of fracture severity.

MATERIALS AND METHODS

A fellowship-trained orthopaedic trauma surgeon (TOM) purposefully selected 20 cases from a series of 50 consecutive tibial plateau fractures to represent a full spectrum of fracture severity and to avoid having multiple fractures cluster around a common level of severity. Fracture classifications included orthopaedic trauma association (OTA) 41-B3 and 41-C3, reflecting the use of CT in assigning classifications and a heavy emphasis on articular surface involvement and depression.[6] Patients sustaining the fractures ranged in age from 18 to 70 years old. There were 12 males and 8 females. Our Institutional Review Board approved use of the patient data. See **Table**, **Supplemental Digital Content 1** (http://links.lww.com/BOT/A715) for a summary of demographic information.

Six fellowship-trained orthopaedic trauma surgeons from 4 separate institutions independently rank-ordered the fractures in order of severity based on the appearance of the fractures on AP and lateral knee radiographs. The only instructions given to the raters were to rank the cases in order of least to most severely injured. Subjectively, they used the number and size of fragments, the amount and direction of displacement, percentage of articular surface involved, and whatever other features they felt were important based on their clinical experience. Raters were blinded to independently obtain CT-derived data and patient information.

A previously validated CT-based image analysis approach was used to quantify the fracture energy based on measurement of the fracture-liberated surface area and accounting for bone density. This method has been shown to be accurate in calculating fracture energy (ie, the amount of energy dissipated in fracturing the bone),[7,8] but the extent of its clinical utility is still under investigation. Fracture energy is expressed in the units of Joules (J), which are equivalent to Newton-meters or kg-m^2/s^2. Software, custom-written in MATLAB, was used to identify all fracture fragments working from standard-of-care axial CT image data. The surfaces of the fragments were then classified as subchondral, cortical, or interfragmentary based on their associated CT intensities and their local geometric character (surface roughness, curvatures, etc). The surface classifications were subsequently manually confirmed to be accurate, or modified as needed, by an experienced analyst (Fig. 1). The interfragmentary surface areas of all the fracture fragments were summed to provide a single aggregate measure of the fracture-liberated surface area. Bone density values were obtained based on previously established relationships with Hounsfield intensity of CT pixels,[9] and the fracture-liberated surface areas were scaled accordingly to reflect the influence of bone density on the fracture properties. Fracture energy was calculated from a previously validated formula based on the fracture mechanics principle that energy is directly proportional to fracture-liberated surface area scaled by bone density in a brittle solid.[7,8]

We tested our hypothesis by comparing the surgeon rank orderings of fracture severity in this series of tibial plateau fractures with CT-based measurements of fracture energy. The agreement between fracture severity assessments among the surgeons, and between each of the surgeons and the fracture

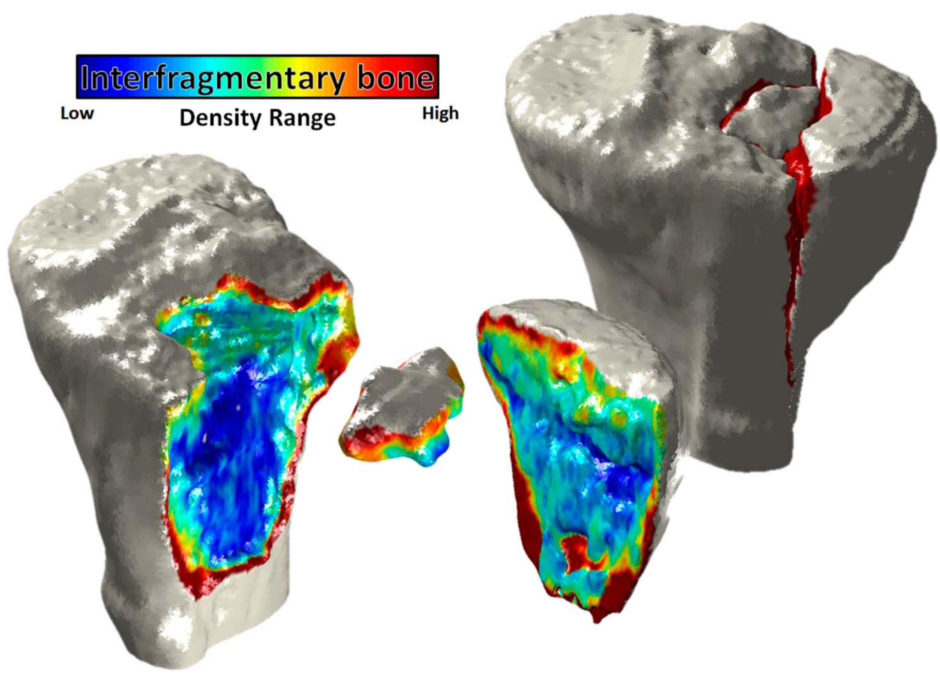

FIGURE 1. Custom-written software was used to measure the surface area of the fracture-liberated cancellous (interfragmentary) bone surfaces, colored according to their local density in the exploded view to the left. The fracture-liberated surface area and bone densities were both used to calculate fracture energy. **Editor's Note:** A color image accompanies the online version of this article.

energy metric, was tested by computing their concordance. The injury severity rankings of 2 cases were deemed concordant if the case with the higher ranking of injury severity by 1 rater/metric also had the higher ranking by a second. The concordance was calculated as the number of concordant pairs divided by the total number of possible pairings. This sample-based statistical measure was used to estimate the probability that 2 cases would be ranked with the same ordering. Random assignment of fracture severity by 2 reviewers would be expected to result in a concordance of 0.5 because any case pairing would have a 50% chance of being concordant.

RESULTS

Fracture energies ranged from 5.5 J to 36.7 J (see **Table**, **Supplemental Digital Content 1**, http://links.lww.com/BOT/A715). There was a high level of agreement between the 6 experienced surgeons in their assessments of tibial plateau fracture severity, with concordances ranging from 82% to 89%, with a mean of 85% (Fig. 2). The concordance between surgeon severity rankings and the fracture energy severity ranking were slightly less high, ranging from 73% to 78%, with a mean of 74%.

Case 19 (as ranked by rater 1) is an example of excellent agreement between orthopaedic surgeons and fracture energy. Severity rankings ranged from 17 to 20 with a fracture energy of 24.5 J (Fig. 3). Substantial articular surface comminution and normal bone density led to a high fracture energy calculation. This feature, as well as substantial fracture displacement, knee dislocation, and bicondylar fracture morphology all contributed to high ranking by the orthopaedic surgeons. Despite the good overall agreement observed between surgeon assessments of fracture severity and the fracture energy metric, there were some notable exceptions. Case 18 demonstrated substantial discrepancy between the objective fracture energy metric and all 6 subjective ratings (Fig. 4). The orthopaedic surgeons all rated this fracture as high in severity, whereas the fracture energy value was modest (11.9 J). The radiographs demonstrate significant fracture malalignment, which would not be reflected in the fracture energy. In contrast, case 7 was a clear outlier with a much higher fracture energy value (17.9 J) relative to the low severity rank assigned by all 6 raters (Fig. 5). The common "split-depression" (OTA 41-B3) was typically deemed lower severity by all surgeons, but closer inspection of the sagittal CT section demonstrates significant comminution leading to a higher fracture energy measurement.

DISCUSSION

The purpose of this study was to determine whether a CT-based fracture energy metric could provide an objective, quantifiable measure of tibial plateau fracture severity by comparing it to the current gold standard, subjective expert surgeon opinion. We found a high level of agreement (85%) regarding fracture severity among the 6 orthopaedic trauma subspecialists. The level of agreement between surgeon assessments of fracture severity and fracture energy was 74%, suggesting that fracture energy has clinical relevance. These results demonstrate that fracture energy reasonably mirrors expert opinion regarding the relative fracture severity over a full spectrum of tibial plateau fractures. This builds on the findings of previous investigations of tibial pilon fractures and shows that fracture energy may be used as a measure of injury severity in other intraarticular fractures as well.

The two major benefits of using fracture energy rather than clinician assessment are its ability to physically quantify severity and its objective nature. Quantifying fracture energy allows for distribution of fracture severity over continuous scales ranging from the entire spectrum of injury severity to subtle differences not appreciated by clinical assessment. In contrast, current classification schemes place fractures into one of several categories and often do not distinguish between substantially different injuries. Objectivity in calculating fracture energy is also valuable because it prevents clinician bias and disagreement resulting from subjective assessments and ensures reproducibility of calculations through rigorous algorithms.

The Schatzker classification and OTA classification are 2 common subjective methods that categorize tibial plateau fractures and convey information about fracture severity. The

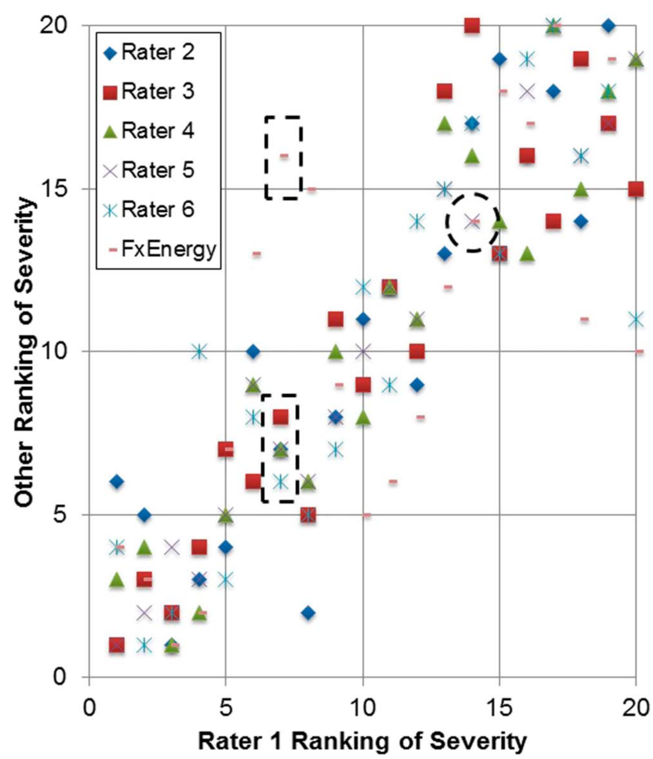

FIGURE 2. Representative rank ordering of fracture severity by 6 orthopaedic trauma surgeons and by fracture energy. The y-axis represents severity ranking as assigned by raters 2–6 and according to the calculated fracture energy. The x-axis represents the rank ordering of rater 1. As an example, there was high agreement between rater 1 and raters 2 through 6 at rater-1 injury number 7, but this fracture's rank according to fracture energy calculation was much higher (black dashed boxes). At rater-1 injury number 14, the rank according to fracture energy was the same as the rank assigned by raters 1 and 5 (dashed circle). **Editor's Note:** A color image accompanies the online version of this article.

FIGURE 3. Example of high level of agreement between orthopaedic surgeons and fracture energy calculation. These AP and lateral knee radiographs demonstrate a bicondylar tibial plateau fracture with substantial articular surface comminution and displacement and an associated knee dislocation.

interobserver reliability of assigning fractures within these 2 classifications based on radiographs ranges from 0.38 to 0.47 and from 0.36 to 0.43 (Kappa statistic), respectively.[1–3,10] When the classifications are based on CT, the reliabilities increase to 0.76 and 0.73, respectively.[10] Although concordance values cannot be directly compared with correlation, our concordance rates of 73%–78% fracture energy and surgeon ranking suggest a similar or better level of agreement relative to current classification strategies. Although this study does not necessarily support incorporating fracture energy calculations into clinical practice, it demonstrates clinical relevance of fracture energy. Therefore, fracture energy can be used to quantify injury severity as an objective, continuous variable in studies comparing 2 groups of fractures to determine extent of group similarity. This is superior to common methods of comparing severity between groups using fracture classification.

It may also be that fracture energy predicts outcomes as a function of treatment. Perhaps excellent outcomes can be expected after nonoperative treatment of a low-severity fracture (fracture energy of 6 J), whereas poor outcomes with nonoperative treatment (and good outcome with operative treatment) can be expected for a high-severity fracture (fracture energy of 30 J). If that were the case, then measurement of fracture energy would be helpful to determine operative indications, as well as predict future patient function.

There are several inherent inaccuracies and discrepancies in CT-based measurements and surgeon observations. First, the fracture energy calculation was based solely on fracture-liberated surface area and bone density. It does not

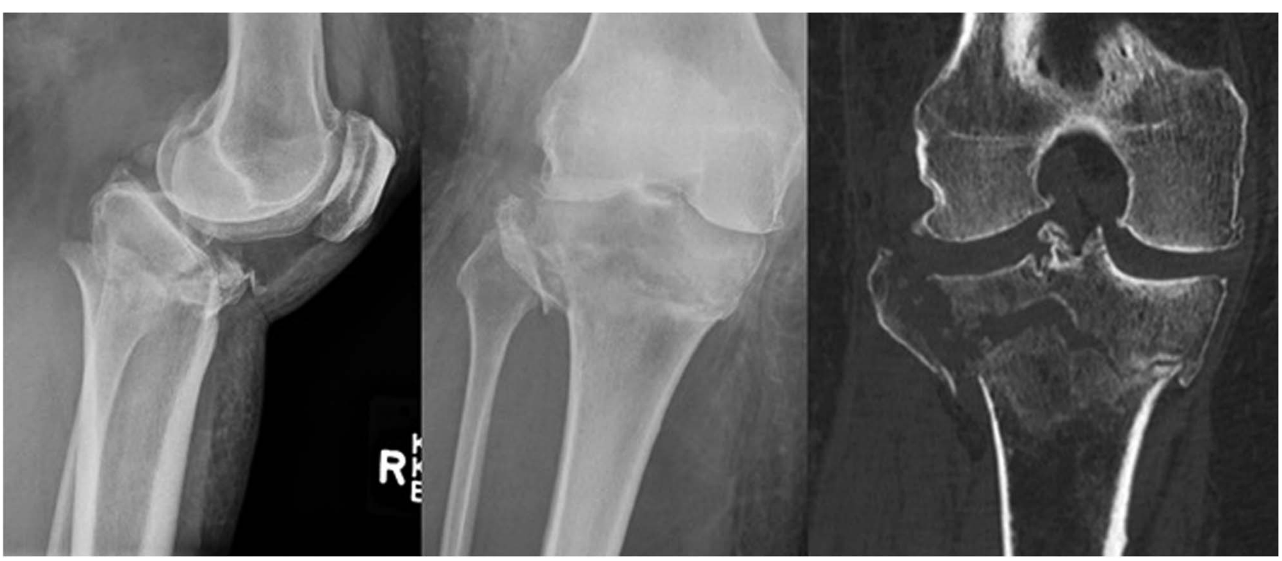

FIGURE 4. Example of high clinician ranking but modest fracture energy. These AP and lateral knee radiographs and a representative coronal CT cut demonstrate osteopenia and substantial metaphyseal impaction without many separate pieces of comminution. The ranking surgeons considered these factors in their assessment of severity, but the fracture energy calculation did not.

FIGURE 5. Example of high fracture energy but low surgeon ranking. These AP and lateral knee radiographs and representative sagittal CT cut demonstrate a fracture that surgeons ranked low in severity because of minimal comminution and depression at the weight-bearing portion of the articular surface and very little overall fracture displacement. However, comminution throughout the posterior central portion of the tibial plateau substantially contributed to an increased fracture energy calculation.

yet account for other fracture features observed by surgeons, such as fracture displacement, malalignment (Fig. 4), fracture morphology (eg, extent of articular surface comminution vs. metaphyseal comminution), or the ease of fixing the fracture, all of which may influence outcomes. Decreased bone density also directly reduces objective energy measurements. In contrast, it is possible that surgeons examining radiographs would ascribe a higher severity to an osteopenic fracture based on fracture fixation difficulties often encountered in such injuries. This would lead to higher severity ranking by surgeons compared with lower fracture energy calculations. Another factor leading to higher surgeon ranking of severity relative to fracture energy is that the surface area metric is based on brittle material assumptions[11] and does not account for plastic deformation. Therefore, impacted metaphyseal and articular surface fragments, which often have significant compaction of underlying trabecular bone, may have absorbed higher levels of energy than were measured. This could lead to an artificially lower fracture energy calculation, particularly in fractures with significant articular surface comminution. Finally, a limitation of the study unrelated to the technique for measuring fracture energy is that the orthopaedic surgeons judged fracture severity based solely on plain radiographs, but the fracture energy calculation was based on CT data. Therefore, there were likely instances in which certain fracture characteristics not appreciated on radiographs may have led to underestimation of fracture severity by surgeon assessment.

Fracture displacement, undeniably one of the most important clinical assessment criteria, was not included in the fracture energy metric. This was because regression analysis in our previous work[7] identified fracture energy and articular comminution as statistically significant post-traumatic osteoarthritis predictors ($P < 0.01$), but not fragment displacement ($P = 0.35$). Actually, fracture energy and fracture displacement were only loosely linked in that work. This may partly be because injury CT scans are often obtained after the application of a temporary external distractor.

This work is a preliminary interrogation of a novel method to yield objective evidence that may eventually prove useful to guide treatment decisions. However, there are no data yet from our study that correlate fracture energy and clinical outcomes. Surgeon rank-order assessment of fracture severity is a reasonable subjective index but has no objective jurisdiction in predicting outcomes. In this study, we chose to use this subjective measure as there is currently no other standard against which to compare fracture energy. Further investigation is ongoing to determine whether quantified relationships between objective fracture energy indices and objective measurements of clinical outcomes can be established.

In conclusion, an objective CT-based measurement of fracture energy demonstrated good concordance with fellowship-trained orthopaedic trauma surgeon subjective assessment of injury severity in tibial plateau fractures, adding to previous work reporting similar findings for tibial pilon fractures. Ongoing investigation will determine the clinical utility of these measurements.

REFERENCES

1. Walton NP, Harish S, Roberts C, et al. AO or Schatzker? How reliable is classification of tibial plateau fractures? *Arch Orthop Trauma Surg.* 2003;123:396–398.
2. Maripuri SN, Rao P, Manoj-Thomas A, et al. The classification systems for tibial plateau fractures: how reliable are they? *Injury*. 2008;39:1216–1221.
3. Charalambous CP, Tryfonidis M, Alvi F, et al. Inter- and intra-observer variation of the Schatzker and AO/OTA classifications of tibial plateau fractures and a proposal of a new classification system. *Ann R Coll Surg Engl.* 2007;89:400–404.
4. Anderson DD, Mosqueda T, Thomas T, et al. Quantifying tibial plafond fracture severity: absorbed energy and fragment displacement agree with clinical rank ordering. *J Orthop Res.* 2008;26:1046–1052.
5. Thomas TP, Anderson DD, Mosqueda TV, et al. Objective CT-based metrics of articular fracture severity to assess risk for posttraumatic osteoarthritis. *J Orthop Trauma.* 2010;24:764–769.

6. Marsh JL, Slongo TF, Agel J, et al. Fracture and dislocation classification compendium—2007: orthopaedic Trauma Association classification, database and outcomes committee. *J Orthop Trauma.* 2007;21(suppl 10):S1–S133.
7. Beardsley CL, Anderson DD, Marsh JL, et al. Interfragmentary surface area as an index of comminution severity in cortical bone impact. *J Orthop Res.* 2005;23:686–690.
8. Thomas TP, Anderson DD, Marsh JL, et al. A method for the estimation of normative bone surface area to aid in objective CT-based fracture severity assessment. *Iowa Orthop J.* 2008;28:9–13.
9. Ciarelli MJ, Goldstein SA, Kuhn JL, et al. Evaluation of orthogonal mechanical properties and density of human trabecular bone from the major metaphyseal regions with materials testing and computed tomography. *J Orthop Res.* 1991;9:674–682.
10. Brunner A, Horisberger M, Ulmar B, et al. Classification systems for tibial plateau fractures; does computed tomography scanning improve their reliability? *Injury*. 2010;41:173–178.
11. Von Rittinger P. *Lehrbruch der Aufbereitskunde*. Berlin: Ernst Kokn; 1867.

Fractures of the Tibial Plateau Involve Similar Energies as the Tibial Pilon but Greater Articular Surface Involvement

Kevin Dibbern,[1] Laurence B. Kempton,[2] Thomas F. Higgins,[3] Saam Morshed,[4] Todd O. McKinley,[2] J. Lawrence Marsh,[1] Donald D. Anderson[1]

[1]Department of Orthopaedics and Rehabilitation, the University of Iowa, Iowa City, Iowa, [2]Department of Orthopaedic Surgery, Indiana University School of Medicine, Indianapolis, Indiana, [3]Department of Orthopaedics, University of Utah School of Medicine, Salt Lake City, Utah, [4]Department of Orthopaedic Surgery, University of California, San Francisco, San Francisco, California

Received 1 March 2016; accepted 30 June 2016
Published online 18 July 2016 in Wiley Online Library (wileyonlinelibrary.com). DOI 10.1002/jor.23359

ABSTRACT: Patients with tibial pilon fractures have a higher incidence of post-traumatic osteoarthritis than those with fractures of the tibial plateau. This may indicate that pilon fractures present a greater mechanical insult to the joint than do plateau fractures. We tested the hypothesis that fracture energy and articular fracture edge length, two independent indicators of severity, are higher in pilon than plateau fractures. We also evaluated whether clinical fracture classification systems accurately reflect severity. Seventy-five tibial plateau fractures and 52 tibial pilon fractures from a multi-institutional study were selected to span the spectrum of severity. Fracture severity measures were calculated using objective CT-based image analysis methods. The ranges of fracture energies measured for tibial plateau and pilon fractures were 3.2–33.2 Joules (J) and 3.6–32.2 J, respectively, and articular fracture edge lengths were 68.0–493.0 mm and 56.1–288.6 mm, respectively. There were no differences in the fracture energies between the two fracture types, but plateau fractures had greater articular fracture edge lengths ($p < 0.001$). The clinical fracture classifications generally reflected severity, but there was substantial overlap of fracture severity measures between different classes. Similar fracture energies with different degrees of articular surface involvement suggest a possible explanation for dissimilar rates of post-traumatic osteoarthritis for fractures of the tibial plateau compared to the tibial pilon. The substantial overlap of severity measures between different fracture classes may well have confounded prior clinical studies relying on fracture classification as a surrogate for severity.
 J Orthop Res 35:618–624, 2017.

Keywords: tibial plateau; tibial pilon; fracture severity; post-traumatic OA

Post-traumatic osteoarthritis (PTOA) commonly occurs following a variety of joint injuries. Articular fractures of the lower extremity are particularly at risk of PTOA, and they often result from similar injury mechanisms. Despite similarities in the injuries, PTOA develops in 23–44% of tibial plateau fractures before 15 years[1,2] but in as many as 74% of tibial pilon fractures.[3] The reasons for this difference are not well understood. It is known that outcomes of articular fractures are influenced by the severity of the damage sustained at the time of injury and as a result of abnormal loading associated with changes to articular congruity, joint alignment, and joint stability after healing.[4–6]

The primary goals in treating articular fractures are to restore limb alignment and precisely reduce any articular displacement to decrease the likelihood of PTOA. The severity of the fracture correlates highly with the risk of PTOA, so treating surgeons have adopted fracture severity assessment methods to aid in their treatment decision-making. However, conventional systems for classifying fractures and their severity are highly subjective, have poor reliability, and cannot reliably predict risk of PTOA.[7–13]

The damage sustained at the time of injury can be objectively assessed though physical manifestations of the fracture severity: the amount of energy involved in fracturing a bone (i.e., the fracture energy) and the amount of articular surface involvement. It has been demonstrated in fractures of the tibial pilon that these fracture severity metrics significantly correlate with PTOA incidence.[14–16] This provides a possible explanation for differences found in the rates of PTOA development in tibial pilon and plateau fractures; that is, greater energy is absorbed or articular surface involved in creating tibial pilon fractures compared to plateau fractures.

In this study, an objective CT-based methodology for measuring fracture energy and articular surface involvement was used to explore the hypothesis that fracture severity metrics are higher in pilon fractures compared to plateau fractures. In addition, we assessed the relationship between the fracture severity measures and traditional categorical fracture classification systems to determine how well the classifications reflected severity.

METHODS

Fellowship-trained orthopedic trauma surgeons enrolled 75 patients with tibial plateau fractures spanning an entire spectrum of severity in this multi-institutional level III diagnostic study. These were compared with 52 patients having sustained tibial pilon fractures, enrolled in a similar manner. An Institutional Review Board approved use of the patient data, collected during standard-of-care clinical treatment.

Fracture severities were calculated using a previously validated, objective, CT-based image analysis methodology.[15,17]

Grant sponsor: National Institute of Arthritis and Musculoskeletal and Skin Diseases; Grant numbers: R21AR061808, P50AR055533; Grant sponsor: Peer Reviewed Medical Research Program; Grant number: W81XWH-15-2-0087; Grant sponsor: Foundation for Orthopaedic Trauma.
Correspondence to: Donald D. Anderson (T: +1-319-335-7528; F: +1-319-335-7530; E-mail: don-anderson@uiowa.edu)

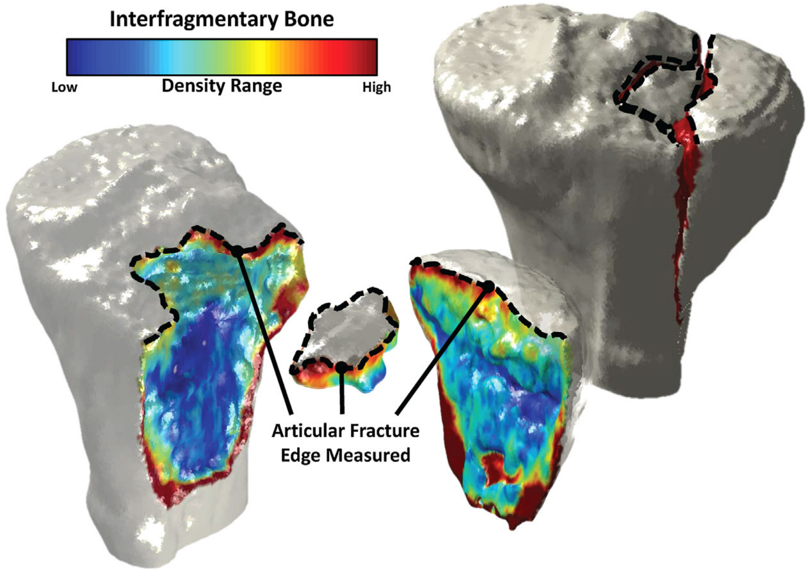

Figure 1. Custom-written software was used to measure surface area of pre-injury cortical and subchondral bone surfaces and post-injury-exposed interfragmentary bone surfaces. The fracture-liberated surface area and the bone densities across that surface were used to calculate fracture energy. The length of the edge between the subchondral and interfragmentary bone surfaces (the articular fracture edge length—highlighted with dashed black lines) was used to quantify articular surface involvement.

This technique quantifies fracture energy based upon measurement of the fracture-liberated surface area, accounting for variations in bone density over the interfragmentary surfaces (Fig. 1). Software, custom-written in MATLAB (MathWorks, Inc., Natick, MA), was used to identify all fracture fragments working from CT scan data. The surfaces of the fragments were then classified as intact cortical, subchondral, or de novo interfragmentary based upon their CT intensities and local geometric character (surface roughness, curvatures, etc.). The surface classifications were then manually evaluated and modified as needed by an expert analyst (Fig. 1). The interfragmentary surface areas of all of the fracture fragments were then summed to provide a measure of the fracture-liberated surface area. Bone densities were estimated from the CT Hounsfield intensities at each CT scan pixel using previously established relationships.[18,19] The location-specific bone density was then used to appropriately scale fracture-liberated surface areas by density-dependent energy release rates to obtain the fracture energy.[15–17] An additional measure reflecting the amount of articular surface involvement was derived by quantifying the articular fracture edge length, defined as the length of the edge at the intersection between interfragmentary and subchondral bone surfaces.

Fracture energies and articular fracture edge lengths were obtained for all pilon and plateau fractures enrolled in the study. A *t*-test statistic was used to test the hypothesis that the fracture severity characteristics differed between the two fracture locations. In order to gain further insight regarding any differences in the two fracture types, cases of similar fracture energies were qualitatively evaluated for energies at the low end, at an intermediate value, and at the high end of the fractures studied.

The fractures were also characterized using two different fracture classification systems, based upon consensus evaluation by three fellowship-trained orthopedic traumatologists (LBK, TOM, JLM). The Schatzker classification system was developed as a method for identifying groups of tibial plateau fractures with distinct pathomechanical and etiological factors.[20] This system has well-established clinical utility in guiding treatments and predicting outcomes.[21] The AO/OTA classification system, on the other hand, seeks to categorize fractures based upon their morphological characteristics in order of increasing complexity and severity, where severity "implies anticipated difficulties of treatment, the likely complications, and the prognosis."[22–24] Where the Schatzker classification seeks to categorize intra-articular fractures of the tibial plateau alone, the AO/OTA classification system is applicable to a broader set of fractures. The fracture energies computed for fractures in different Schatzker and AO/OTA classes were compared to test how well the classification systems reflected severity.

RESULTS

The range of fracture energies measured for tibial plateau fractures was 3.2–33.2 Joules (J). The range of fracture energies for pilon fractures was 3.6–32.2 J (Fig. 2a). The fracture energies (mean ± standard deviation) of the plateau fractures were 13.3 ± 6.8 J, and they were 14.9 ± 7.1 J for the pilon fractures. The distribution of energies for each fracture type was similar. Although these types of fractures are highly idiosyncratic, the smallest fragments in the plateau fractures tended to be smaller than those in the pilon fractures.

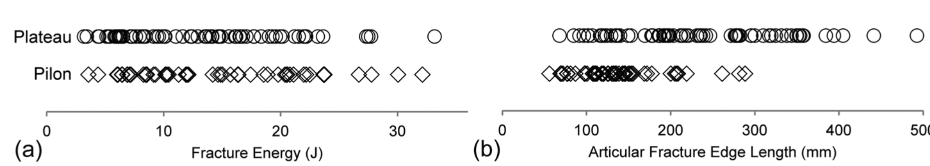

Figure 2. Tibial plateau and pilon (a) fracture energy and (b) articular fracture edge length values distributed over a full spectrum of injury severity.

The range of articular fracture edge lengths measured for tibial plateau fractures was 68.0–493.0 mm. The range of articular fracture edge lengths for pilon fractures was 56.1–288.6 mm (Fig. 2b). The articular fracture edge lengths (mean $\pm$ standard deviation) of the plateau fractures were 231.4 ± 94.7 mm, and they were 138.1 ± 54.9 mm for the pilon fractures. Fractures of the tibial plateau had greater articular fracture edge lengths than those of the pilon ($p < 0.001$).

Qualitative comparisons of tibial plateau and pilon fractures with low, intermediate, and high fracture energies showed similarities in the number and size of the fragments in each range and supported the observations regarding the amount of articular surface involvement (Fig. 3). The lower energy fractures were selected at 3.2 J and 3.6 J for the plateau and pilon, respectively. The lower energy pilon fracture had two fragments, while the lower energy plateau fracture had three. The largest two fragments on each were similar in size between the plateau and pilon, while the third fragment seen on the plateau was much smaller. The intermediate energy fractures were selected at 14.2 J and 14.9 J for the plateau and pilon, respectively. Again, similar quantities and sizes of fragments were found for the two different anatomical sites. Finally, the higher energy fractures were selected at 27.3 J and 24.6 J for the plateau and pilon, respectively. These higher energy fractures had numerous smaller fragments and involved substantial diaphyseal extension.

Fracture classifications for the plateau injuries ranged from Schatzker I to VI (Table 1). The plateau fractures ranged in AO/OTA class from 41-B1 to 41-C3 and the pilon fractures ranged from 43-B1 to 43-C3 (Table 2). The average fracture energies and articular fracture edge lengths for the most part increased with increasing Schatzker (Fig. 4) and AO/OTA classification (Fig. 5), indicating general agreement between the fracture classes and the severity metrics associated with such fractures. However, the severity metrics varied, in some instances considerably, within individual classes. In addition to the overall fracture

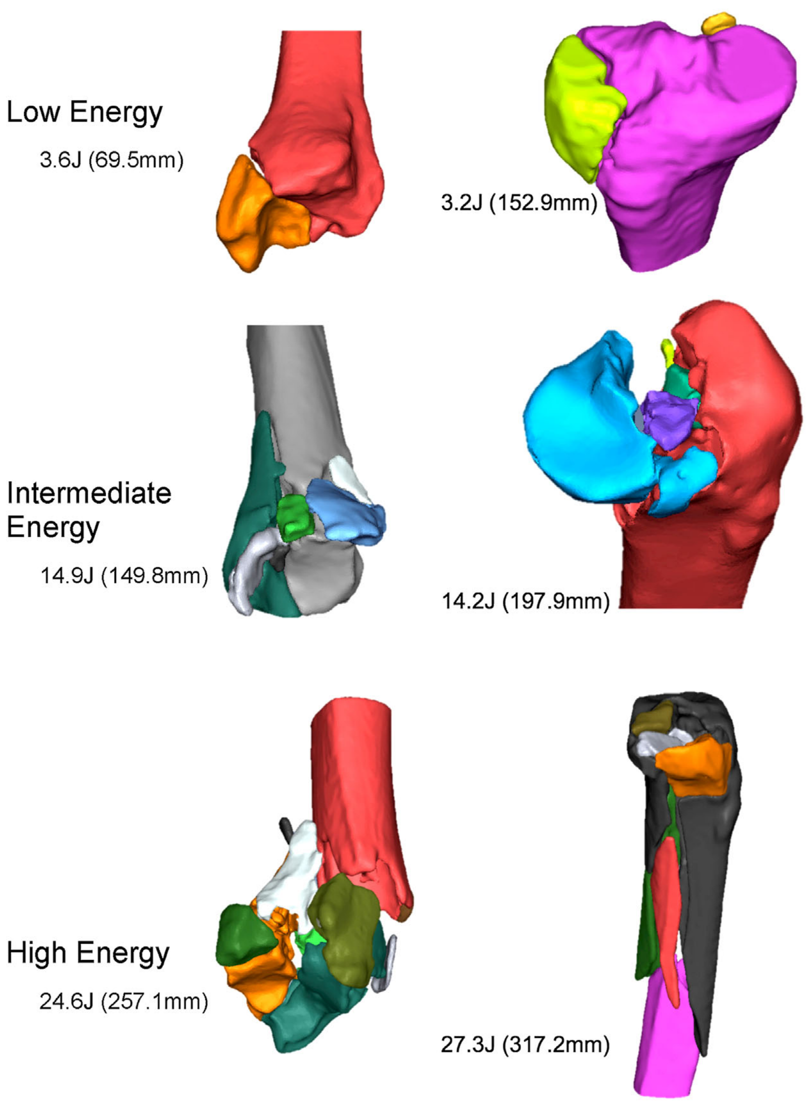

Figure 3. Fracture energy comparison between tibial pilon (left) and plateau (right) injuries. Different colors are assigned to individual fragments in these graphical representations. Articular fracture edge length values are shown for reference, in parentheses.

Table 1. Distribution of Tibial Plateau Fractures, Fracture Energies, and Articular Fracture Edge Lengths by Schatzker Fracture Classification

Schatzker Class	Number of Cases	% of Total	Fracture Energy (J)	Articular Fracture Edge Length (mm)
I	3	4	9.3 (6.9)	134.6 (40.7)
II	27	36	8.8 (4.2)	227.7 (83.0)
III	0	0	—	—
IV	16	21	11.9 (4.8)	225.3 (92.3)
V	5	7	13.7 (3.0)	247.8 (129.9)
VI	24	32	19.8 (6.1)	253.6 (110.8)

Values are mean (standard deviation).

energies of pilons and plateaus being similar, the ranges and medians of fracture energies for AO/OTA B3 and C3 fractures of pilons and plateaus were also quite similar. The same was not true of articular fracture edge lengths, with the ranges and medians of pilons being substantially smaller than those of plateaus. Finally, the higher fracture classes consistently demonstrated a wider range of fracture severity metric values than was observed for less complex fracture patterns, although there were relatively fewer fractures seen in the less complex categories.

DISCUSSION

There were no differences in the fracture energies between the pilon and plateau fracture types, but there were differences in the articular fracture edge lengths. Similar injury mechanisms typically lead to these two fractures, and previous studies show a substantially lower incidence of PTOA resulting from tibial plateau fractures compared to pilon fractures. PTOA represents an organ-level injury response that is complex and likely joint-specific. Impact tolerance of the proximal tibia may be explained by differences in joint morphology/anatomy, cartilage thickness, the subchondral bone, inflammatory response after injury, mechanics of joint load distribution, or a variety of other factors.

Differences in size and joint morphology between the tibial plateau and pilon provide possible explanations for differences in PTOA risk. This is consistent with the greater amount of articular surface involvement and comminution seen in the tibial plateau fractures, although greater surface involvement would generally be expected to increase PTOA risk. Another anatomical confounder could stem from the large difference in the size of the articular surfaces between the two joints. The tibial plateau has a significantly larger articulating surface ($\sim$1,200 mm^2) than the tibial pilon ($\sim$600 mm^2).[24,25] The tibio-talar joint could therefore experience a higher energy per unit area transmitted upon fracturing than the tibio-femoral joint. The higher energy per unit area could result in a larger degree of acute chondrocyte damage or death in the pilon when compared to the plateau. This presents an area for future development of the fracture severity measure to include bone or fracture-specific characteristics.

Substantial differences in soft tissue structures could also contribute in multiple ways. The tibial plateau has a dense, load-bearing, fibrocartilaginous meniscus and other substantial soft tissues. It is reasonable to assume that in contrast with the robust bony load bearing in the ankle, the soft tissue support in the knee may aid in preventing post-fracture deterioration, despite similar energies involved in the injuries. Further confounding this possibility is variable/occult comorbidity to these soft tissues associated with fractures of the tibial plateau. Previous studies have demonstrated approximately double the incidence of PTOA of the knee in plateau fractures with meniscectomies compared to those where the meniscus was reconstructed (74% vs. 37%).[26] In the context of surgical fracture reduction, the integrity of the soft tissues around the joint is seldom a focus of attention. Finally, the appeal of using fracture energy to assess severity in this context is that it is an indirect indicator of injury to the articular cartilage, as well as the bone. Ideally, a measure of fracture severity reflects the amount and the distribution of energy transmitted across the articular surface. The larger

Table 2. Distribution of Fracture Energies and Articular Fracture Edge Lengths for Tibial Plateau and Pilon Fractures by AO/OTA Fracture Classification

	Plateau				Pilon			
AO/OTA Class	Number of Cases	% of Total	Fracture Energy (J)	Articular Fracture Edge Length (mm)	Number of Cases	% of Total	Fracture Energy (J)	Articular Fracture Edge Length (mm)
B1	4	5	8.6 (5.8)	134.5 (33.2)	5	10	7.1 (2.2)	94.4 (26.8)
B2	2	3	16.9 (4.6)	299.8 (120.1)	1	2	6.1 (–)	120.6 (–)
B3	45	60	10.1 (4.4)	227.9 (88.3)	15	29	10.2 (5.0)	127.1 (38.5)
C1	2	3	21.4 (0.3)	140.8 (79.1)	2	4	17.5 (14.6)	99.6 (1.4)
C2	5	7	17.5 (7.6)	220.1 (100.5)	12	23	19.7 (6.3)	124.1 (61.0)
C3	17	23	20.3 (6.0)	276.7 (110.6)	17	33	18.1 (5.1)	169.1 (52.8)

Values are mean (standard deviation).

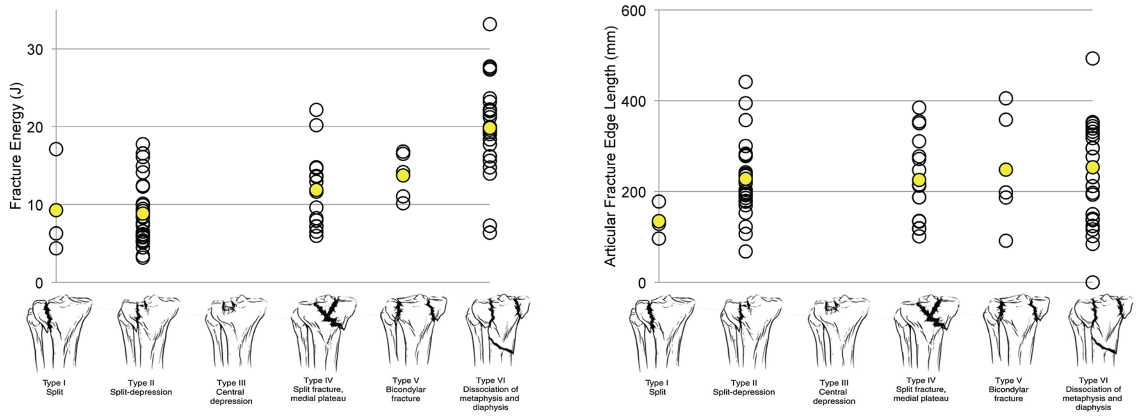

Figure 4. Range of fracture energies and articular fracture edge lengths as they vary over the Schatzker classes of tibial plateau fractures.

the quantity of energy, the more initial cartilage damage and subsequent degeneration would be predicted. Other joint-specific factors influential in this respect include the cartilage thickness and the rigidity of the subchondral and underlying metaphyseal bone. The cartilage of the tibial plateau is significantly thicker ($\sim$3 mm) than for the tibial pilon ($\sim$1.5 mm). The intra-tissue strains at the time of injury would therefore be expected to be more severe in the thinner cartilage of the pilon compared to the plateau.

The larger range of fracture energies seen in higher classes of the fracture classifications (C3, Schatzker V and VI) may reflect the fact that more complex and variable injuries make up these classes. However, the higher class fracture patterns were not necessarily more severe (i.e., did not always have higher fracture energies). This suggests that fracture classifications are less reflective of severity for the more complex fracture patterns. A surprisingly wide range of fracture energy was seen for the fracture classifications that we assessed, suggesting that these classifications are not a reliable surrogate for fracture severity. Combining fracture classification, which categorizes the morphologic characteristics of the fracture, with objecive measurement of fracture energy would provide a more complete assessment of articular fractures.

Historically, studies comparing different groups of fractures have used AO/OTA fracture classification to show that the groups had similar fracture characteristics and severity. Perhaps the most useful conclusion from these data is that prior studies failing to demonstrate group equivalence simply by showing no statistical difference in fracture classification type are missing critical information about underlying differences in fracture severity. Assigning "high energy" and "low energy" based on injury mechanism and fracture pattern is largely subjective and fails to sufficiently stratify severity. The data presented in this study provide strong evidence of the utility that fracture energy has in the context of clinical research.

This study is not without limitations. The accuracy of the fracture energy calculations may suffer either

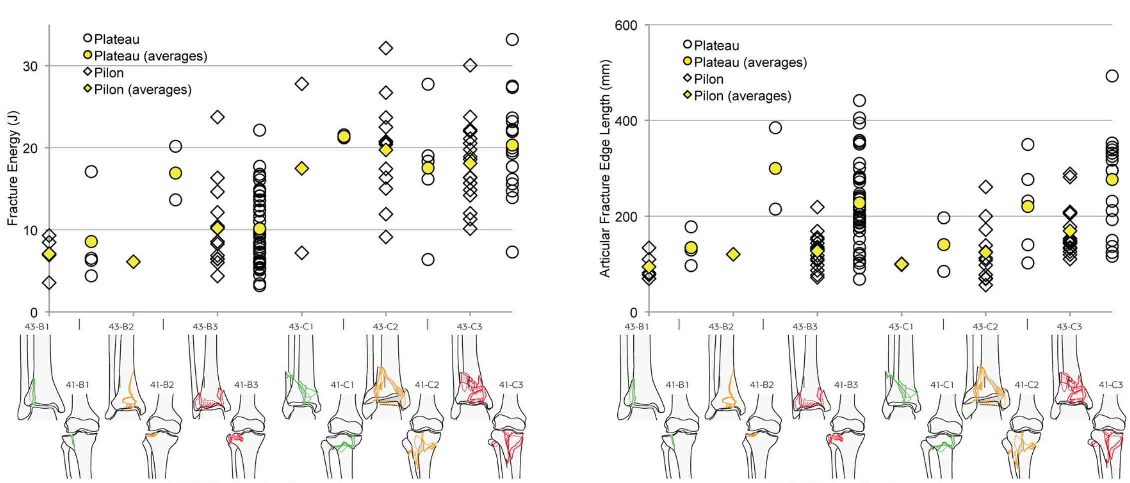

Figure 5. Range of fracture energies and articular fracture edge lengths as they vary over the different AO/OTA classes for the tibial plateau and pilon fractures.

when small bone fragments are missed in segmentation from CT or when there is substantial compaction of bone. The volumes of the smallest fragments segmented were on the order of 10–20 mm^3. We cannot rule out inaccuracies associated with missing smaller fragments but would not expect for those to contribute appreciably to fracture energy absorption. Bone compaction was not assessed in our measurements but again, given the relatively low density of cancellous bone subject to compaction, it is unlikely that this would introduce substantial inaccuracy. Another limitation is that soft tissue status was not available for inclusion in the assessments of fracture severity. Ultimately, a more robust predictive algorithm may involve not only calculation of fracture energy but also some measure of soft tissue status. A present lack of follow-up data prevented the evaluation of the relationships between fracture severity and outcomes in the plateau and pilon fractures. Establishing these relationships is the objective of ongoing study in these patients, who are all being followed prospectively.

PTOA is a complex disease with many contributing factors. The findings in this study disprove our hypothesis that tibial pilon fractures have a higher energy absorbed than plateau fractures across the spectrum of injury, but they raise new questions about differences in the amount of articular surface involvement. Our results show similar energy absorption profiles with greater articular involvement in the tibial plateau, suggesting that it may be more tolerant of impact injury compared to the distal tibia. This possibility will need to be tested further as longer term outcome data become available for the specific patients analyzed in this study.

ACKNOWLEDGMENTS

The content is solely the responsibility of the authors and does not necessarily represent the official views of the National Institutes of Health. Opinions, interpretations, conclusions, and recommendations are those of the author and are not necessarily endorsed by the Department of Defense. The research was also aided by a grant from the Foundation for Orthopaedic Trauma. The authors gratefully acknowledge the dedicated image segmentation efforts of Ms. Janelle Lala.

AUTHORS' CONTRIBUTIONS

All authors made substantial contributions to the research design, data acquisition, and analysis/interpretation of data. K.D., L.K., T.M., J.L.M., and D.D.A. were involved in the drafting of the paper, and all authors provided subsequent critical review. All authors have read and approved the final submitted manuscript.

REFERENCES

1. Honkonen SE. 1995. Degenerative arthritis after tibial plateau fractures. J Orthop Trauma 9:273–277.
2. Volpin G, Dowd GS, Stein H, et al. 1990. Degenerative arthritis after intra-articular fractures of the knee. Long-term results. J Bone Joint Surg Br 72:634–638.
3. Marsh JL, Weigel DP, Dirschl DR. 2003. Tibial plafond fractures. How do these ankles function over time? J Bone Joint Surg Am 85:287–295.
4. Anderson DD, Chubinskaya S, Guilak F, et al. 2011. Post-traumatic osteoarthritis: improved understanding and opportunities for early intervention. J Orthop Res 29:802–809.
5. Anderson DD, Marsh JL, Brown TD. 2011. The pathomechanical etiology of post-traumatic osteoarthritis following intraarticular fractures. Iowa Orthop J 31:1–20.
6. McKinley TO, Rudert MJ, Koos DC, et al. 2004. Pathomechanic determinants of posttraumatic arthritis. Clin Orthop Relat Res 427:S78–S88.
7. Brunner A, Horisberger M, Ulmar B, et al. 2010. Classification systems for tibial plateau fractures; does computed tomography scanning improve their reliability? Injury 41:173–178.
8. Charalambous CP, Tryfonidis M, Alvi F, et al. 2007. Inter- and intra-observer variation of the Schatzker and AO/OTA classifications of tibial plateau fractures and a proposal of a new classification system. Ann R Coll Surg Engl 89:400–404.
9. Dirschl DR, Adams GL. 1997. A critical assessment of factors influencing reliability in the classification of fractures, using fractures of the tibial plafond as a model. J Orthop Trauma 11:471–476.
10. Dirschl DR, Ferry ST. 2006. Reliability of classification of fractures of the tibial plafond according to a rank- order method. J Trauma 61:1463–1466.
11. Maripuri SN, Rao P, Manoj-Thomas A, et al. 2008. The classification systems for tibial plateau fractures: how reliable are they? Injury 39:1216–1221.
12. Swiontkowski MF, Sands AK, Agel J, et al. 1997. Interobserver variation in the AO/OTA fracture classification system for pilon fractures: is there a problem? J Orthop Trauma 11:467–470.
13. Walton NP, Harish S, Roberts C, et al. 2003. AO or Schatzker? How reliable is classification of tibial plateau fractures? Arch Orthop Trauma Surg 123:396–398.
14. Thomas TP, Anderson DD, Mosqueda TV, et al. 2010. Objective CT-based metrics of articular fracture severity to assess risk for posttraumatic osteoarthritis. J Orthop Trauma 24:764–769.
15. Thomas TP, Anderson DD, Marsh JL, et al. 2008. A method for the estimation of normative bone surface area to aid in objective CT-based fracture severity assessment. Iowa Orthop J 28:9–13.
16. Anderson DD, Mosqueda T, Thomas T, et al. 2008. Quantifying tibial plafond fracture severity: absorbed energy and fragment displacement agree with clinical rank ordering. J Orthop Res 26:1046–1052.
17. Beardsley CL, Anderson DD, Marsh JL, et al. 2005. Interfragmentary surface area as an index of comminution severity in cortical bone impact. J Orthop Res 23:686–690.
18. Ciarelli MJ, Goldstein SA, Kuhn JL, et al. 1991. Evaluation of orthogonal mechanical properties and density of human trabecular bone from the major metaphyseal regions with materials testing and computed tomography. J Orthop Res 9:674–682.
19. Snyder SM, Schneider E. 1991. Estimation of mechanical properties of cortical bone by computed tomography. J Orthop Res 9:422–431.
20. Schatzker J, McBroom R, Bruce D. 1979. The tibial plateau fracture. The Toronto experience 1968–1975. Clin Orthop Relat Res 138:94–104.
21. Rademakers MV, Kerkhoffs GM, Sierevelt IN, et al. 2007. Operative treatment of 109 tibial plateau fractures: five- to 27-year follow-up results. J Orthop Trauma 21:5–10.

22. Müller M. 1990. The comprehensive classification of fractures of long bones. Berlin: Springer-Verlag. p 176–179.
23. Marsh JL, Slongo TF, Agel J, et al. 2007. Fracture and dislocation classification compendium—2007: Orthopaedic Trauma Association classification, database and outcomes committee. J Orthop Trauma 21:S1–S133.
24. Fukubayashi T, Kurosawa H. 1980. The contact area and pressure distribution pattern of the knee. A study of normal and osteoarthrotic knee joints. Acta Orthop Scand 51:871–879.
25. Li W, Anderson DD, Goldsworthy JK, et al. 2008. Patient-specific finite element analysis of chronic contact stress exposure after intraarticular fracture of the tibial plafond. J Orthop Res 26:1039–1045.
26. Papagelopoulos PJ, Partsinevelos AA, Themistocleous GS, et al. 2006. Complications after tibia plateau fracture surgery. Injury 37:475–484.

Journal of Biomechanics 67 (2018) 9–17

Contents lists available at ScienceDirect

Journal of Biomechanics

journal homepage: www.elsevier.com/locate/jbiomech
www.JBiomech.com

Discrete element analysis is a valid method for computing joint contact stress in the hip before and after acetabular fracture

Kevin C. Townsend [a,b], Holly D. Thomas-Aitken [a,b], M. James Rudert [a], Andrew M. Kern [a,b], Michael C. Willey [a], Donald D. Anderson [a,b], Jessica E. Goetz [a,b,*]

[a] Department of Orthopaedics, Rehabilitation, University of Iowa, Iowa City, IA, USA
[b] Department of Biomedical Engineering, University of Iowa, Iowa City, IA, USA

A R T I C L E I N F O

Article history:
Accepted 13 November 2017

Keywords:
Discrete element analysis
Acetabular fracture
Hip
Contact stress
Tekscan

A B S T R A C T

Evaluation of abnormalities in joint contact stress that develop after inaccurate reduction of an acetabular fracture may provide a potential means for predicting the risk of developing post-traumatic osteoarthritis. Discrete element analysis (DEA) is a computational technique for calculating intra-articular contact stress distributions in a fraction of the time required to obtain the same information using the more commonly employed finite element analysis technique. The goal of this work was to validate the accuracy of DEA-computed contact stress against physical measurements of contact stress made in cadaveric hips using Tekscan sensors. Four static loading tests in a variety of poses from heel-strike to toe-off were performed in two different cadaveric hip specimens with the acetabulum intact and again with an intentionally malreduced posterior wall acetabular fracture. DEA-computed contact stress was compared on a point-by-point basis to stress measured from the physical experiments. There was good agreement between computed and measured contact stress over the entire contact area (correlation coefficients ranged from 0.88 to 0.99). DEA-computed peak contact stress was within an average of 0.5 MPa (range 0.2–0.8 MPa) of the Tekscan peak stress for intact hips, and within an average of 0.6 MPa (range 0–1.6 MPa) for fractured cases. DEA-computed contact areas were within an average of 33% of the Tekscan-measured areas (range: 1.4–60%). These results indicate that the DEA methodology is a valid method for accurately estimating contact stress in both intact and fractured hips.

1. Introduction

It has been reported that as many as one in four acetabular fracture patients will rapidly progress to develop post-traumatic osteoarthritis (PTOA) of the hip (Bhandari et al., 2006; Dirschl et al., 2004; Matta, 1996; Saterbak et al., 2000). The likelihood of developing PTOA after an intra-articular fracture has been associated with quality of articular reduction and increases in joint contact stress (Anderson et al., 2011; Kern and Anderson, 2015). Residual incongruity is common in surgically reconstructed acetabular fractures, where incongruities of 1–3 mm are often considered satisfactory reductions (Borrelli et al., 2002; Moed et al., 2003) despite biomechanical studies demonstrating that 1 mm and 2 mm articular step-offs increase joint contact stress by 23% and 48%, respectively (Malkani et al., 2001).

The primary goal of surgical reduction is restoration of an anatomic joint surface, the necessity of which has been illustrated by numerous mechanical studies across both fractured and intact joints showing a direct correlation between elevated joint contact stress and development of osteoarthritis (Anderson et al., 2011; Hadley et al., 1990; Kern and Anderson, 2015; Maxian et al., 1995; Segal et al., 2009, 2012). This association indicates that joint contact stress may be useful as a predictor of a patient's risk for developing PTOA. Though joint contact stress can be obtained *in vivo* (Anderson et al., 2003; Bergmann et al., 2001, 1999; Hodge et al., 1989, 1986), such measurements are highly invasive and are only realistic in small patient cohorts and under extremely controlled conditions.

Joint contact stress is most commonly assessed in living patients using non-invasive computational modeling techniques such as finite element analysis (FEA) (Harris et al., 2012; Henak et al., 2014a; Rhyu et al., 2011). Unfortunately, the technical burden required to develop and run patient-specific FE models is substantial, with mesh generation and establishment of numerically

* Corresponding author at: Orthopaedic Biomechanics Lab, 2181 Westlawn Building, Iowa City, IA 52242-1100, USA.

E-mail address: jessica-goetz@uiowa.edu (J.E. Goetz).

https://doi.org/10.1016/j.jbiomech.2017.11.014
0021-9290/

stable contact conditions requiring many days or weeks of effort, and model run-times that range from hours to days depending on model complexity. Consequently, even purportedly large-scale patient-specific FEA investigations have been limited to less than 15–20 patients (Harris et al., 2012; Henak et al., 2014a; Li et al., 2008).

Discrete element analysis (DEA) is another computational method that has been utilized for determining intra-articular contact stress in many different joints (Anderson et al., 2010b; Chao et al., 2010; Volokh et al., 2007). In DEA, cartilage is modeled as an array of compressive springs between rigid bony surfaces, eliminating the need for development of a continuum mesh and greatly simplifying model generation relative to FEA. Contact stress is computed by balancing applied loads with cartilage spring forces using numerically stable and rapidly executing methods that provide solutions within seconds. While DEA methodology sacrifices continuum mechanics information and the use of advanced material property definitions, it can provide joint contact stress estimations in a fraction of the time required to obtain similar information using FEA, making it an appealing technique for application to larger patient cohorts (Anderson et al., 2010b; Segal et al., 2009, 2012).

DEA models of articular joints can be developed using specimen-specific cartilage surfaces (Abraham et al., 2013; Segal et al., 2009, 2012) or approximated cartilage surfaces – most often generated by prescribing a uniform projection from subchondral bone (Anderson et al., 2007; Kern and Anderson, 2015). In some DEA models of the hip, cartilage surfaces have been defined as spherically congruent projections from the subchondral bone (Genda et al., 2001; Yoshida et al., 2006), which results in calculation of contact stress values lower than those measured in physical experiments (Hodge et al., 1989, 1986). In contrast, systematic exploration of many of the assumptions of the DEA methodology has shown that projected cartilage surfaces and rigid underlying bone result in calculation of contact stress values higher than those measured physically (Anderson et al., 2010a), and even DEA performed using specimen-specific cartilage data results in contact stress at least 15% higher than that obtained using FEA (Abraham et al., 2013). Given that specimen-specific DEA models tend to over-predict, and spherically approximated DEA models tend to under-predict hip contact stress, there would seem to be some level of model approximation that could yield accurate calculations of contact stress using the DEA methodology.

To obtain hip contact stresses in acetabular fracture patients using DEA, model generation must be from a CT scan, which (without the use of a contrast agent) does not show cartilage. As metal artifact from fracture fixation hardware precludes use of MRI scans, and contrast from a CT arthrogram would leak through fractured surfaces, it is presently not possible to obtain cartilage geometry directly from clinical imaging in acetabular fracture patients. Therefore, cartilage information must be approximated from bony geometry for these patients, an approximation that it is important validate to determine the accuracy of resulting contact stress calculations. The objective of this work was to determine if DEA estimates of contact stress in both intact and imperfectly reduced fractured hips are valid by comparing DEA-computed contact stress to those physically measured from cadaveric preparations.

2. Methods

2.1. Specimen preparation

Two fresh-frozen cadaveric hemipelves were used for physical loading experiments. Specimen 1 was from a 170 cm, 63.5 kg, 71 year old male, and Specimen 2 was from a 183 cm, 79.4 kg, 37 year old male. Each was carefully dissected free of soft tissues down to the joint capsule and the acetabular labrum. The ilium was cut in an approximately transverse plane 10 cm superior to the acetabulum to fit in a pre-existing potting device. Using previously described instrumentation (Martin et al., 2015), the cut pelvis was oriented so that a vertically directed load along the axis of the femur corresponded with the hip loading vector during maximum load during walking (15 degrees abduction and 25 degrees flexion) (Bergmann et al., 2001). The ilium was embedded in a polymethylmethacrylate (PMMA) block in this position. The specimen was then inverted and the femur was transected mid-shaft and embedded vertically in a 5-cm diameter PMMA cylinder.

2.2. Loading apparatus

The experimental loading apparatus (Fig. 1) was mounted in an MTS Bionix 858 test machine (MTS Inc., Minneapolis, MN). The lower assembly consisted of a compound sine plate and a set of dual orthogonal linear bearings (an XY-stage) attached to the load cell. The upper assembly was a short metal tube attached to the MTS linear/rotary actuator. For testing, each specimen was inverted and the pelvic PMMA block was bolted to the sine plate, which controlled hip flexion/extension and abduction/adduction. The femoral PMMA cylinder was locked into the upper tube so that the MTS could simultaneously apply axial load and femoral rotation. Once oriented in the testing fixture, the entire joint capsule was excised and the acetabular labrum was partially removed to permit insertion of the Tekscan sensor. Upon opening the joint, we visually confirmed macroscopically normal cartilage in Specimen 1 and noted the focal defect in Specimen 2 was sufficiently medial within the acetabulum so as to not be loaded in any testing poses. Specimens were sprayed copiously with saline throughout the potting process and each loading test to prevent cartilage dehydration/degeneration.

2.3. Testing: intact specimens

Specimen 1 was tested in a heel-strike pose (16.3° flexion; −5.5° abduction; 5.4° external rotation), and Specimen 2 was positioned to simulate heel-strike, mid-stance (0° flexion; −8.3° abduction; 6.7° external rotation), and toe-off (−6.9° flexion; −4° abduction; 8.7° external rotation) of normal walking gait (Bergmann et al., 2001). At the beginning of each test, the MTS was used to distract the femur from the acetabulum for insertion of a calibrated hip-specific pressure sensor (Model 4402, Tekscan, Inc. Boston, MA) (Rudert et al., 2014). The sensor was lubricated with petroleum jelly to minimize shear damage. Two investigators held the sensor with the outermost ring of the sensor even with the lateral rim of the acetabulum while the MTS actuator pushed the femoral head into contact with the acetabulum with 50 N of force. This compressive force then held the sensor in place for testing. For each test, the actuator applied a ramp load to 1000 N, and joint contact pressure data were then recorded by the Tekscan sensor.

With the load still applied, a threaded rod was installed to lock the relative positions of the sine plate and femur tube (Fig. 1, right) so that the specimen and sensor could be removed from the MTS as a rigid construct and transported for CT scanning (0.39 mm × 0.39 mm × 0.5 mm voxels). The sensing elements of the Tekscan sensor were visible in the CT scans (Fig. 2), allowing for the Tekscan sensor location to be spatially registered to the adjacent bony anatomy. After CT scanning, the locking rod was removed, the femur and the Tekscan sensor were removed from the acetabulum, and the specimen was remounted in the MTS for the next gait pose. A newly calibrated Tekscan sensor was inserted and the pressure recording/CT-scan sequence was repeated.

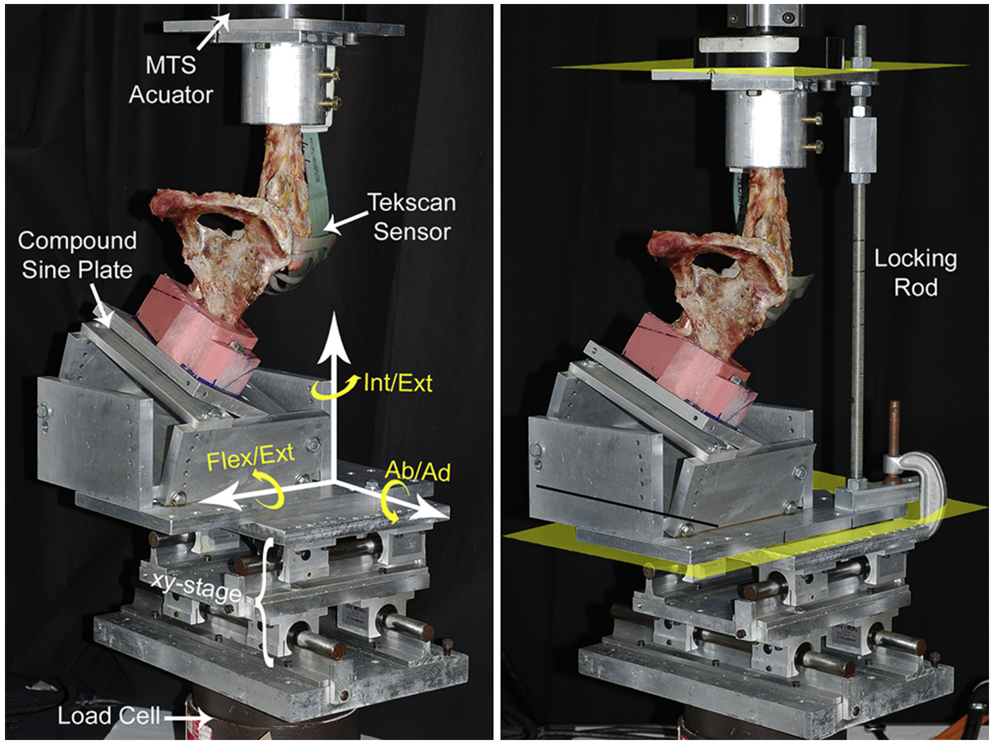

Fig. 1. Photographs of the experimental loading fixture mounted in the MTS. The hip is inverted relative to its physiologic orientation. The individual fixturing components are indicated, and the axes about which anatomic rotations occur are shown (left). Upon completion of loading, a locking rod was added to the fixture (right) to maintain the relative positions of the femoral pot and the compound sine plate, and the portion of the device between the two yellow planes was transferred to the CT scanner for imaging. (For interpretation of the references to color in this figure legend, the reader is referred to the web version of this article.)

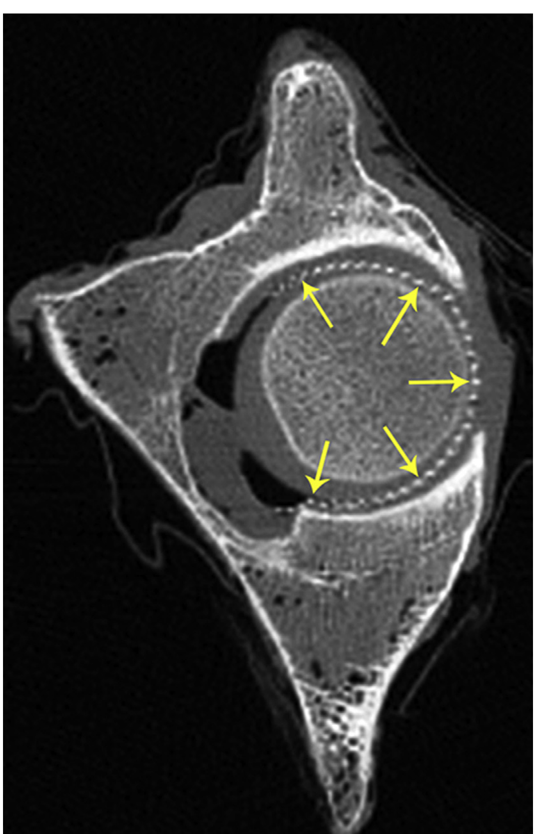

Fig. 2. CT scan slice with the conductive wires of the Tekscan sensor visible (arrows).

2.4. Testing: mal-reduced fracture specimens

After completion of the experiments in the various gait poses, an acetabular fracture was created in each specimen using a combination of saw and osteotome cuts. Fractures were fixed by an orthopaedic trauma surgeon using two interfragmentary screws and a buttress plate supported by two distal and two proximal screws (Fig. 3). In Specimen 1, the fracture was intentionally reduced with a uniform 2-mm recessed step-off, and in Specimen 2 the fracture was reduced with an intentional inter-fragmentary gap plus a 1–2 mm recessed step-off. These malreductions are surgically realistic and would likely be considered acceptable reductions in a clinical setting (Ebraheim et al., 2007; Matta et al., 1986). The loading/pressure recording/CT-scan sequence was repeated at each gait pose in the fractured specimens.

2.5. DEA model generation

Two sets of DEA models were generated for comparison to the physical loading experiments. The first set incorporated specimen-specific cartilage thickness information obtained from an MRI scan (dual echo steady-state; 0.5 mm isotropic voxels) (Abraham et al., 2015) acquired prior to testing while the specimen was intact and unloaded. Femoral head and acetabular articular cartilage surfaces and underlying bony anatomy were manually segmented from the MRI scans using OsiriX software (Pixmeo, Geneva, Switzerland) and converted into triangulated surfaces using Geomagic Studio (Geomagic Inc., Research Triangle Park, NC). Cartilage thickness was defined as the perpendicular distance from each triangular facet on the articular surface to the subchondral bone. An iterative closest point algorithm was used to align the MRI-derived bone surfaces with CT-derived bone surfaces obtained with the bones locked in each testing position. Those

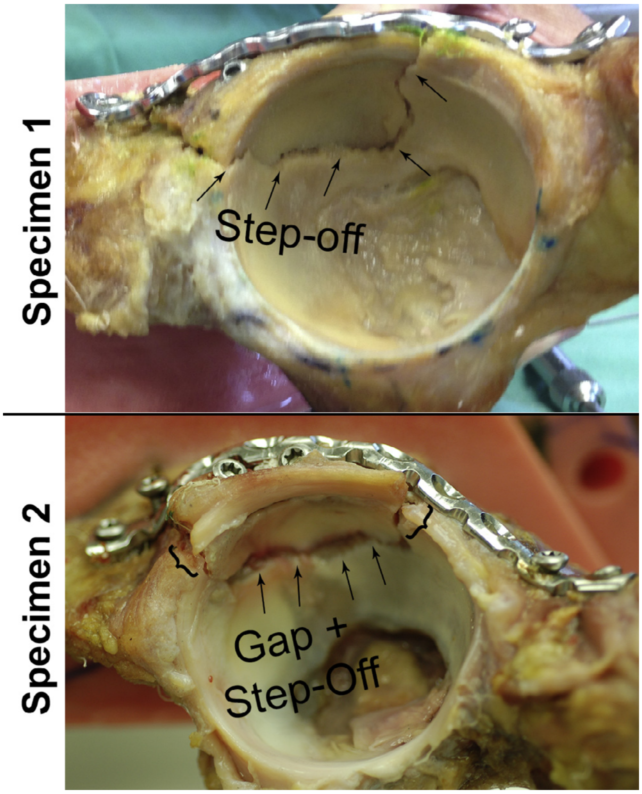

Fig. 3. Photographs of the two different posterior wall fracture malreductions used for validating DEA-computed contact stress. Specimen 1 had a fairly uniform 2 mm step-off around the entirety of the fragment (arrows), while the majority of the malreduction in Specimen 2 was deeper in the acetabulum (arrows). Along the acetabular rim, the fracture fragment was relatively well aligned (brackets), making this a very clinically realistic pattern of malalignment. The blue lines on the labrum in Specimen 1 were intended to assist returning the specimen to the MTS in the same femoral rotation after fracture. These lines are absent in Specimen 2 because instead of the tissue, the PMMA blocks were marked during testing for this purpose. (For interpretation of the references to color in this figure legend, the reader is referred to the web version of this article.)

transformations were then applied to the MRI-derived specimen-specific cartilage surfaces in order to bring them into the orientations used during physical loading experiments.

The second set of DEA models was generated entirely from the CT scans obtained after each physical loading experiment, simulating the most realistic option for DEA model generation in acetabular fracture patients. For these models, the cartilage surface was generated from each post-testing CT scan by isolating femoral head and acetabular subchondral bone from the full bone surfaces, and projecting that subchondral bone geometry 1 mm into the joint space along local surface normals. These projected articular surfaces were then iteratively smoothed towards sphericity using a custom algorithm (Shivanna, 2006). The Euclidean distance of each cartilage surface vertex from the center of a sphere fit to the entire projected surface was calculated. The location of each cartilage surface vertex was adjusted along a ray connecting that vertex to the sphere center by a distance equal to the difference between the vertex's radius and the average radius of the neighboring vertices within a 2 mm neighbor threshold. A 0.05 mm maximum radial change for each of smoothing 5 iterations was allowed, permitting a total maximum radial change of 0.25 mm, approximately half the distance of a CT voxel. The number of smoothing iterations was determined empirically from the intact heel strike model of Specimen 1 by choosing the number of iterations after which the DEA-computed contact stresses were closest to the physically measured contact stress data. As the goal of this work was to validate the results of a standardized modeling approach, these parameters were applied uniformly to generate the other seven projected-cartilage DEA models.

2.6. Contact stress calculations

The Tekscan sensor was calibrated (Rudert et al., 2014) before and upon completion of testing, and equal weighting was applied to the pre-test and post-test calibration curves when converting Tekscan raw pressure values (0–255) into contact stress values (MPa). A sensor was used for a maximum of two tests to limit the effects of sensor degradation.

For all DEA models, cartilage was assigned isotropic linear-elastic material properties ($E = 8$ MPa, $\nu = 0.42$). Boundary and loading conditions applied to the models were identical to the physical loading experiments. DEA contact stress solutions were computed using a Newton's method solver implemented in MATLAB (Mathworks, Natick, MA) to match DEA spring forces with applied boundary conditions (Kern and Anderson, 2015). Run time for each DEA model was approximately 10 s in Matlab 2013b running on a desktop computer (IntelCore i7-6700 3.4 Gz; 16384 MB RAM; 64-bit operating system).

2.7. Contact stress comparisons

The piezoresistive wires of the Tekscan sensor were visible in each CT scan (Fig. 2), permitting direct segmentation and 3D surfacing of the Tekscan sensor as it was positioned in the joint during testing. Tekscan pressure data were mapped onto the 3D sensor

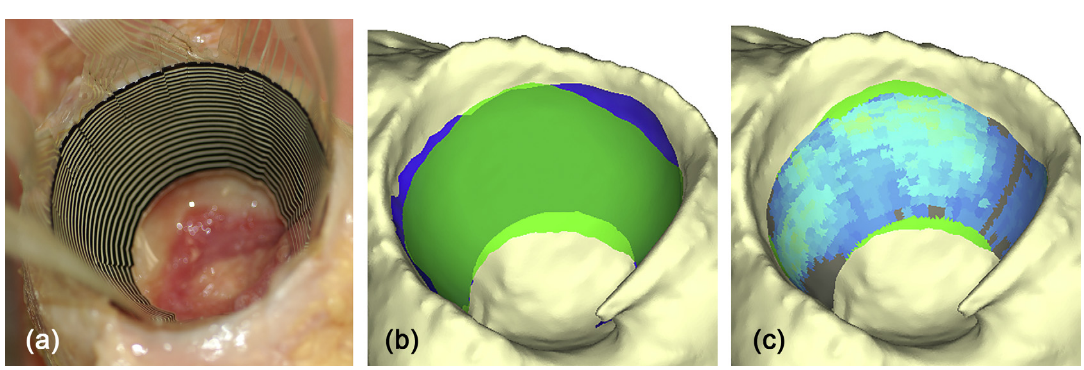

Fig. 4. (a) Photograph of the Tekscan sensor positioned inside the acetabulum of Specimen 1 for experimental testing. The circumferential rings of the sensor (black) are visible. (b) Surface model corresponding to Specimen 1 illustrating the segmented acetabular cartilage surface (blue) and the segmented Tekscan sensor (green). (c) Tekscan data were project to the cartilage surface to spatially register the Tekscan pressure data for direct comparison with DEA-generated contact stress distributions. (For interpretation of the references to color in this figure legend, the reader is referred to the web version of this article.)

geometry by subdividing the triangulated 3D sensor surface (mesh size ~ 0.0295 mm^2) into the 21 circumferential rings and 52 radial spokes of the physical sensor (sensel size 1.923 mm^2), which resulted in approximately 65 surface triangles per Tekscan sensel. Every triangular facet within a sensel was assigned the measured value of that sensel. A ray casting technique was then used to identify the surface vertex on the acetabular cartilage surface closest location of each Tekscan sensor vertex (Fig. 4). Spatial agreement between Tekscan and DEA data sets was then assessed using point-to-point correlation, omitting locations where both DEA and Tekscan were reporting zero stress. Peak contact stress and contact area were also compared between DEA models and physical loading experiments.

3. Results

3.1. Specimen-specific cartilage models

Average cartilage thickness for Specimen 1 was 0.96 mm on the femoral head and 1.34 mm on the acetabulum. The average cartilage thickness for Specimen 2 was 1.33 mm on the femoral head and 1.67 mm on the acetabulum. Contact stress values computed using specimen-specific cartilage DEA models were highly correlated with Tekscan-measured values for intact hips (correlations greater than 0.94 in all phases of the gait cycle – Table 1). Specimen-specific cartilage DEA models also accurately approximated Tekscan-measured peak contact stress (average difference of 11%; range: 4–25%) for the intact state. Contact areas from DEA were within an average of 33% (range: 18–48%) of the physical measurements for intact hips.

Contact stress values computed using specimen-specific cartilage DEA models of a malreduced posterior wall acetabular fracture were also highly correlated with Tekscan-measured values (correlations greater than 0.91 – Table 1). Peak contact stress values computed were also within an average of 11% (range: 9–15%) of the Tekscan-measured values. DEA-computed contact areas were within 30% (range: 16–36%) of physical measurements for the malreduced fractures.

Point-by-point absolute difference maps show visually that cartilage-specific DEA predictions had similar contact stress distributions as the Tekscan measurements (Fig. 5). Areas of high contact stress in the DEA models appeared to be in similar locations as high contract stresses measured during physical testing. In the malreduced fracture state, both specimens exhibited bimodal contact anterior and posterior to the fragment. The fracture fragment in Specimen #1 was uniformly recessed 2 mm and did not contact the femoral head at heel strike. The fracture fragment for Specimen #2 had a better reduction near the acetabular rim, and thus the fragment did experience load at all instances of gait investigated in this work.

3.2. CT-projected cartilage models

DEA models of intact hips with cartilage surfaces that were projected from CT scans and smoothed using our algorithm were also able to accurately approximate physical measurements of contact stress and area. DEA-computed contact stress values were highly correlated with Tekscan-measured values for intact hips (correlations greater than 0.93 in all phases of the gait cycle – Table 1). Peak contact stress in the projected cartilage models was within an average of 12% (range: 4–29%) of the Tekscan measurements for the intact hips, and contact areas were within an average of 12% (range: 4–29%).

DEA-computed contact stress values for the malreduced posterior wall acetabular fractures also highly correlated with Tekscan-measured values (correlations greater than 0.88 in all phases of the gait cycle – Table 1). As for the specimen-specific cartilage models, peak contact stress computed with projected cartilage DEA models of malreduced posterior wall acetabular fractures had excellent agreement (average within 6%; range: 0–12%) with the Tekscan-measured contact forces. Contact areas were within 48% (range: 29–60%) for the malreduced fractures.

Point-by-point absolute difference maps of the projected cartilage DEA contact stress maps (Fig. 6) show agreement between DEA-generated and Tekscan measured contact stress that is very similar (though not identical) to the good agreement found using specimen-specific cartilage models. Areas of high contact stress on the acetabular cartilage appeared in similar locations on the projected-cartilage DEA models and the Tekscan sensor. Models of both malreduced fracture specimens exhibited similar contact stress and loading patterns as those seen with the cartilage-specific models and the Tekscan measurements.

4. Discussion

The goal of this work was to validate the use of a DEA methodology for estimating contact stress in the context of acetabular fractures. We demonstrated that with the use of specimen-specific cartilage thickness information, there was excellent agreement in terms of peak contact stress, contact area, and spatial correlation between DEA-computed and Tekscan-measured contact stress. Unfortunately, specimen-specific cartilage data is likely to remain unavailable when dealing with acetabular fractures patients, and implementation of DEA for obtaining contact stress in fractured joints will continue to rely on cartilage surface models extrapolated from clinical CT data. This work demonstrated that with an appropriate smoothing algorithm applied to a cartilage surface extrapolated from bony geometry, the resulting DEA contact stress estimations had excellent agreement with physically measured intra-articular contact stress values ($R^2 \geq 0.93$ for intact state, $R^2 \geq 0.88$ for fractured state).

Table 1
Comparative contact area, peak contact stress, and stress correlation data for the intact and malreduced posterior wall fracture experiments. HS – heel strike; MS – mid stance; TO – toe off.

Specimen	State	Position	Contact area (mm^2)			Peak contact stress (MPa)			Stress correlation	
			Tekscan	Specimen-specific cartilage DEA	Projected cartilage DEA	Tekscan	Specimen-specific cartilage DEA	Projected cartilage DEA	Specimen-specific cartilage DEA	Projected cartilage DEA
1	Intact	HS	1562	808	1174	2.8	3.5	2.0	0.95	0.97
2	Intact	HS	928	651	616	5.7	5.9	6.1	0.95	0.93
2	Intact	MS	667	419	455	6.8	6.4	6.5	0.94	0.93
2	Intact	TO	515	421	522	5.1	5.5	5.5	0.99	0.94
1	Fractured	HS	821	528	580	4.7	5.1	4.4	0.94	0.97
2	Fractured	HS	627	426	250	11.3	9.7	11.3	0.96	0.88
2	Fractured	MS	652	421	274	7.1	6.0	6.7	0.91	0.90
2	Fractured	TO	587	496	330	6.9	6.4	7.7	0.95	0.88

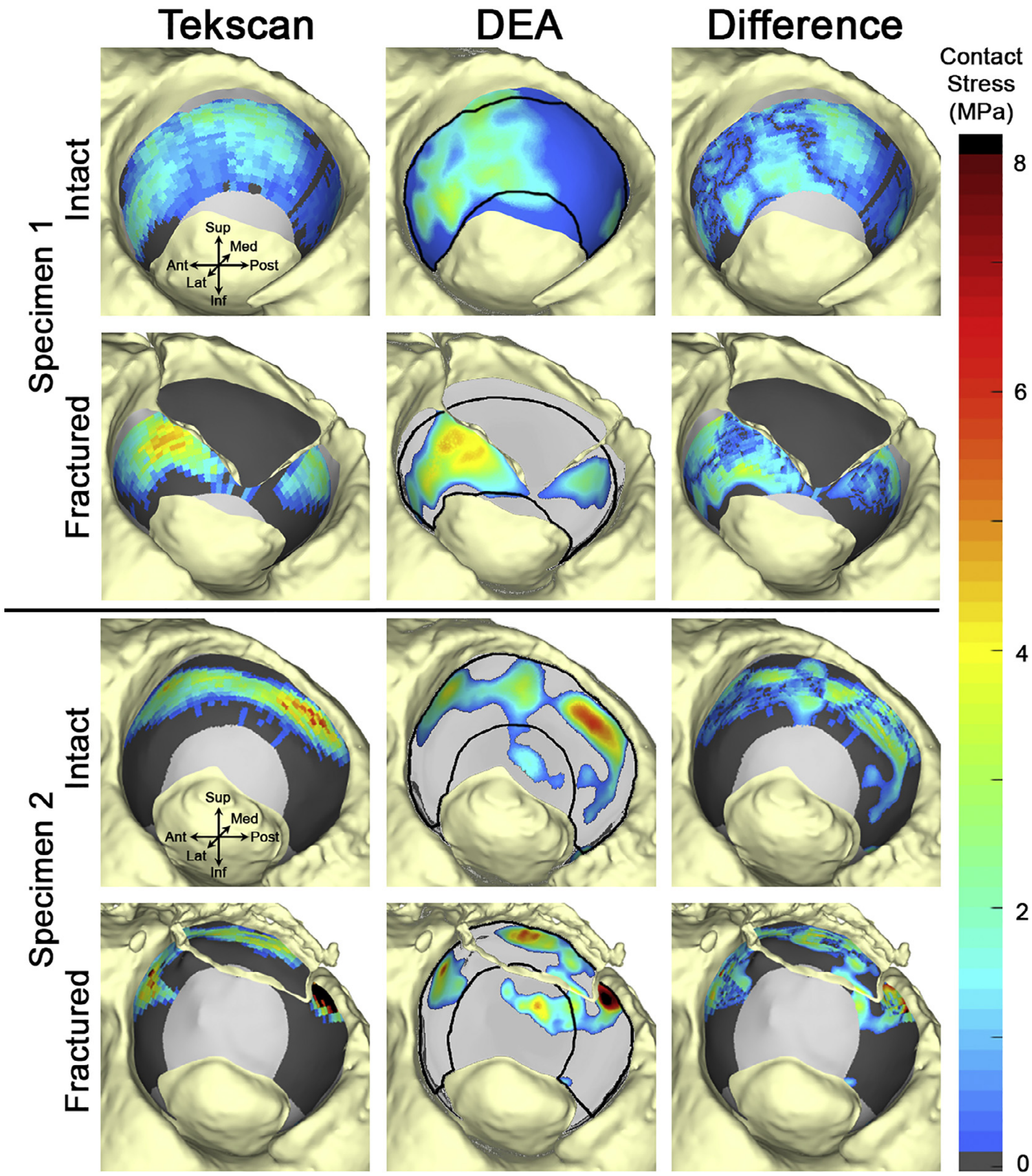

Fig. 5. Contact stress distributions at heel strike for the intact and fractured states of both specimens obtained from DEA models generated with specimen-specific cartilage thickness. The leftmost column shows the acetabular cartilage in light gray and the Tekscan sensor surface in dark gray with the mapped contact stresses shown as indicated on the colorbar. Dark gray indicates that the Tekscan sensor registered no contact at that location under load. In the center column, the light gray shows all acetabular cartilage in the DEA models with a black line denoting the edge of the Tekscan sensor which is not shown. The rightmost column shows difference maps which are the absolute value of the Tekscan maps minus the DEA maps. Contact stress values above 8 MPa are represented in black, with a maximum contact stress value of 11.3 MPa. The presence of a fracture disrupts the peripheral contact distribution of the intact joints and appears to shift stresses anterosuperiorly and medially within the acetabulum.

While this work was to the best of our knowledge the first to use a Tekscan sensor to explore contact stress in the hip after an acetabular fracture, a variety of comparative information about joint contact stress in intact hips and in hips with acetabular fractures is available from studies using pressure-sensitive film. The average contact area across all DEA models in our work was 6.3 cm^2 in intact hips and 4.1 cm^2 in fractured hips, values similar to the range of contact areas that have been measured for intact hips (range: 4.3–6.8 cm^2) and fractured hips (range: 2.9–5.3 cm^2) using pressure-sensitive film (Hak et al., 1998; Konrath et al., 1998b; Olson et al., 1995; Olson et al., 1996). Peak contact stress values measured in this work ranged from 2.0–6.5 MPa for intact hips and 4.4–11.3 MPa for fractured hips. These peak stress values were on the lower end of the range reported for experiments using pressure-sensitive film (5.6–10.5 MPa for intact; 6.3–20.5 MPa for fractured) (Hak et al., 1998; Konrath et al., 1998b; Olson et al., 1995). This is likely in part due to the higher spatial resolution of pressure-sensitive film compared to the Tekscan sensor permitting measurement of highly localized higher peak pressures and the fact that our loading experiments used approximately half of the applied load of those previous studies.

Despite the excellent agreement between the DEA-computed and the experimentally measured contact stresses in a variety of hip positions, this work has several limitations. Neither the DEA model nor the cadaveric testing included an acetabular labrum. Omitting a labrum was determined acceptable for this work because while the labrum affects intra-articular fluid pressure and joint lubrication (Ferguson et al., 2003; Song et al., 2012), cadaveric and computational studies have indicated that absence of an intact acetabular labrum minimally affect hip stability or

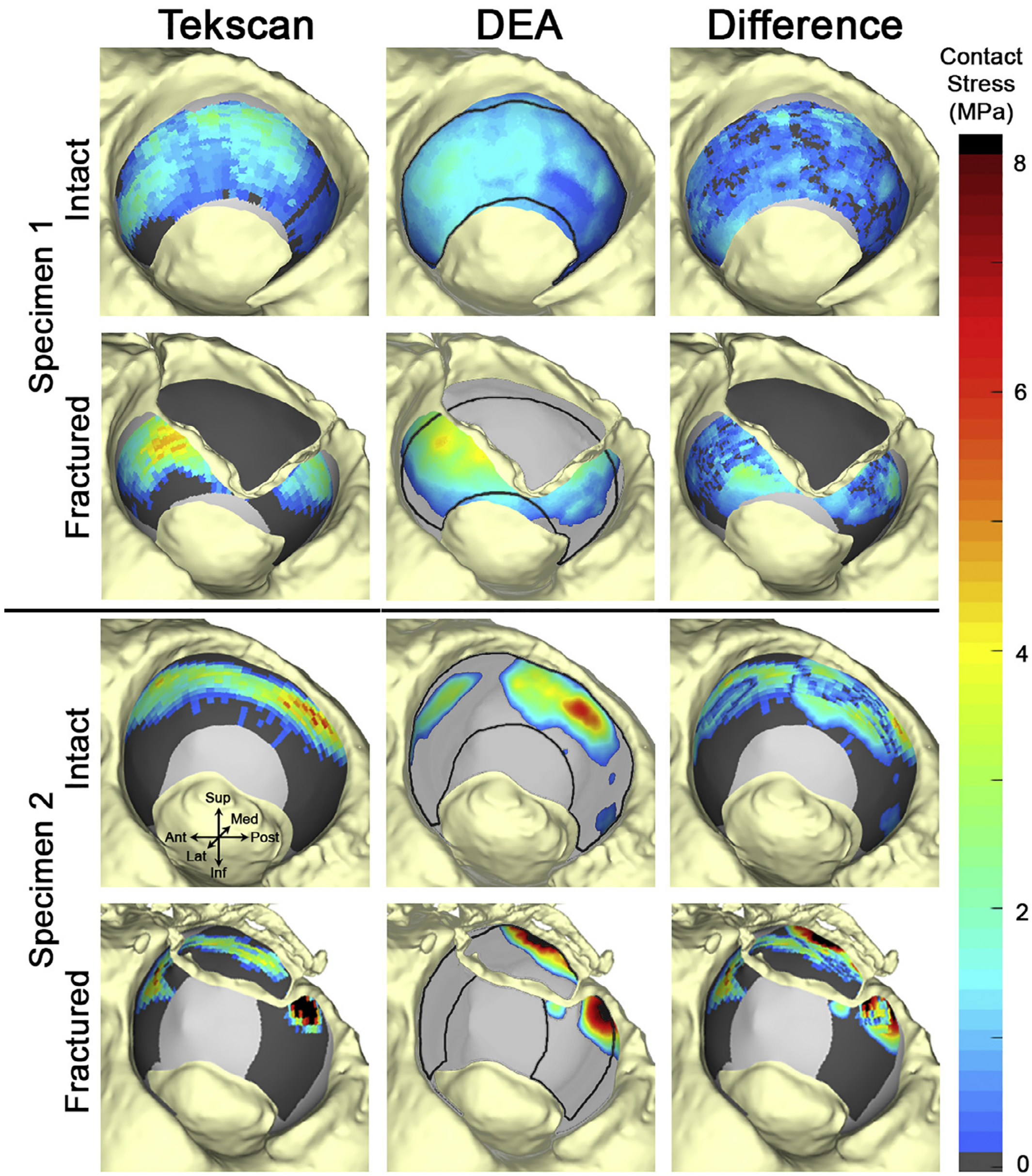

Fig. 6. Contact stress distributions at heel strike for the intact and fractured states of both specimens obtained using DEA models generated by projecting cartilage from CT scans. The leftmost column shows the acetabular cartilage in light gray and the Tekscan sensor surface in dark gray with the mapped contact stresses shown as indicated on the colorbar. Dark gray indicates that the Tekscan sensor registered no contact at that location under load. In the center column, the light gray shows all acetabular cartilage in the DEA models with a black line denoting the edge of the Tekscan sensor which is not shown. The rightmost column shows difference maps which are the absolute value of the Tekscan maps minus the DEA maps. Contact stress values above 8 MPa are represented in black, with a maximum contact stress value of 11.3 MPa. The presence of a fracture disrupts the peripheral contact distribution of the intact joints and appeared to shift stresses posteromedially within the acetabulum.

intra-articular contact stress in normal hips (Crawford et al., 2007; Henak et al., 2011; Konrath et al., 1998a; Myers et al., 2011). Furthermore, the labrum is likely to be disrupted in a fractured hip.

The 1 mm projected cartilage thickness was thinner than the MRI-measured cartilage thickness in our specimens, and on the very low end of literature values reported for acetabular or femoral head cartilage thickness (Adam et al., 1998; Athanasiou et al., 1994; Shepherd and Seedhom, 1999). This thickness was selected because it resulted in DEA contact patch locations being most consistent with the physically measured contact. Thicker cartilage projections seemed to prevent the femoral head from seating in the acetabulum, and the DEA computed contact stress pattern appeared as rim loading (Fig. 7) that did not correspond to the measured spatial pattern of contact stress (Fig. 6). Peak contact stress and contact area were most sensitive to changes in cartilage modulus with a 1 mm cartilage projection, yet even then, key measures of contact stress were minimally affected by variation in cartilage Young's modulus (Fig. 7). This greater effect of geometry than material properties on stress is similar to findings in other orthopaedic soft tissues (Hansen et al., 2017).

While the loading conditions used in this work were similar to loads seen *in vivo*, some of the loading characteristics and model assumptions limit generalization to a wider clinical population. While we did vary the position of the hip to simulate multiple instances of the stance phase of gait, we did not vary the applied load (1000 N). Furthermore, hip positions used in this work were based upon the average of the instrumented hip data acquired by Bergmann, et al. (Bergmann et al., 2001, 1999), and thus were representative of hip orientation in elderly individuals rather than those typically suffering acetabular fractures. Thus, joint contact

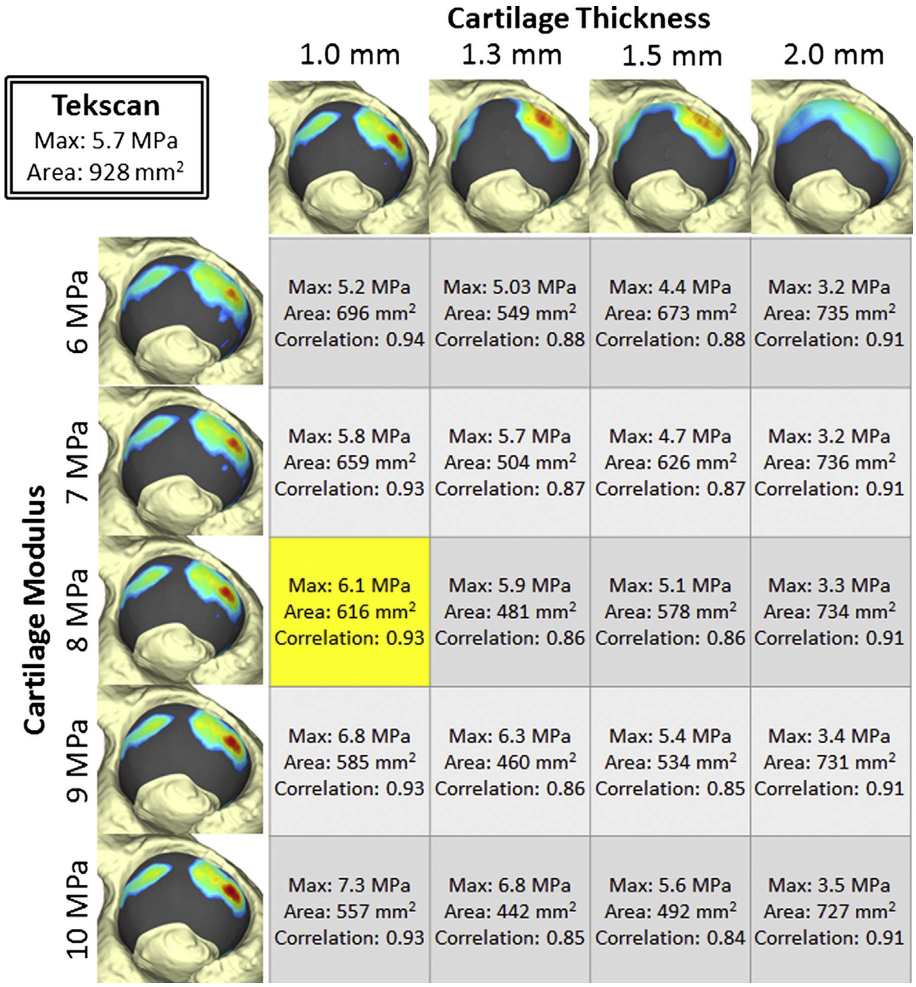

Fig. 7. Sensitivity of computed contact stresses on projected cartilage thickness and cartilage modulus values. All models are of Specimen 2 at heel strike, with the Tekscan measured data shown in the box on the upper left. Contact stress maps on the left are from models with 1 mm cartilage projections and variable Young's Modulus for cartilage. Contact stress maps along the top are for variable thickness cartilage projections and a constant 8 MPa Young's modulus. The data shown in yellow result from the modeling parameters that were validated. (For interpretation of the references to color in this figure legend, the reader is referred to the web version of this article.)

data determined in this work should be considered representative examples of contact patterns that may develop in a fractured acetabulum rather than a complete description of contact stress occurring in the acetabulum after a posterior wall fracture.

We elected to report the agreement between DEA and contact stress measurements in positions simulating gait, however we also tested Specimen 1 in several arbitrary abduction poses not representative of gait and found similar agreement between DEA and physically measured contact stresses. Peak contact stress at 11° of abduction was 6.84 MPa and 6.80 MPa for the DEA and Tekscan, respectively. At 5° abduction, DEA predicted a maximum contact stress of 4.88 MPa compared to Tekscan measurement of 4.66 MPa. At 4° adduction, DEA predicted a maximum contact stress of 5.53 MPa and Tekscan measured 5.27 MPa. Testing was performed in the ab/adducted poses only with an intact acetabulum due to concerns about stability of the experimental setup with the fracture fragment location relative to the acetabular loading pattern in these poses.

The use of DEA to assess contact stress in the hip has previously been validated (Abraham et al., 2013) using comparisons to FE models and to pressure-sensitive film measurements of contact stress in cadavers (Anderson et al., 2007; Henak et al., 2014b). That work emphasized the non-spherical nature of the femoral head and encouraged the use of specimen-specific cartilage thickness to obtain realistic results (Abraham et al., 2013). However, in cases of intra-articular fractures, specimen-specific cartilage thickness is unavailable. In this work, we have shown that our DEA methodology is valid for cases of an incongruent fractured acetabulum, and further, if a suitable smoothing algorithm is applied, a cartilage surface projected from underlying subchondral bone will yield valid contact stress information. This allows for implementation of DEA in cases of intra-articular hip fractures in which standard clinical CT imaging is the standard of care, thereby facilitating large, patient-specific population studies of contact stress in studies of acetabular fractures.

Conflict of interest

No author has a conflict of interest with this work resulting from commercial relationships.

Acknowledgements

This work was funded by NIH grant AR055533. The NIH had no role in study design or in the collection, analysis, interpretation, or presentation of the data. The authors would like to thank Mr. Thomas Baer for his assistance with photography and Mr. Kevin Dibbern for his assistance with data visualization.

References

Abraham, C.L., Bangerter, N.K., McGavin, L.S., Peters, C.L., Drew, A.J., Hanrahan, C.J., Anderson, A.E., 2015. Accuracy of 3D dual echo steady state (DESS) MR arthrography to quantify acetabular cartilage thickness. J. Magn. Reson. Imaging 42, 1329–1338.

Abraham, C.L., Maas, S.A., Weiss, J.A., Ellis, B.J., Peters, C.L., Anderson, A.E., 2013. A new discrete element analysis method for predicting hip joint contact stresses. J. Biomech. 46, 1121–1127.

Adam, C., Eckstein, F., Milz, S., Putz, R., 1998. The distribution of cartilage thickness within the joints of the lower limb of elderly individuals. J. Anat. 193 (Pt 2), 203–214.

Anderson, A.E., Ellis, B.J., Maas, S.A., Weiss, J.A., 2010a. Effects of idealized joint geometry on finite element predictions of cartilage contact stresses in the hip. J. Biomech. 43, 1351–1357.

Anderson, D.D., Goldsworthy, J.K., Li, W., Rudert, M. James, Tochigi, Y., Brown, T.D., 2007. Physical validation of a patient-specific contact finite element model of the ankle. J. Biomech. 40, 1662–1669.

Anderson, D.D., Iyer, K.S., Segal, N.A., Lynch, J.A., Brown, T.D., 2010b. Implementation of discrete element analysis for subject-specific, population-wide investigations of habitual contact stress exposure. J. Appl. Biomech. 26, 215–223.

Anderson, D.D., Van Hofwegen, C., Marsh, J.L., Brown, T.D., 2011. Is elevated contact stress predictive of post-traumatic osteoarthritis for imprecisely reduced tibial plafond fractures? J. Orthopaedic Res.: Off. Publ. Orthopaedic Res. Soc. 29, 33–39.

Anderson, I.A., MacDiarmid, A.A., Lance Harris, M., Mark Gillies, R., Phelps, R., Walsh, W.R., 2003. A novel method for measuring medial compartment pressures within the knee joint in-vivo. J. Biomech. 36, 1391–1395.

Athanasiou, K.A., Agarwal, A., Dzida, F.J., 1994. Comparative study of the intrinsic mechanical properties of the human acetabular and femoral head cartilage. J. Orthopaedic Res.: Off. Publ. Orthopaedic Res. Soc. 12, 340–349.

Bergmann, G., Deuretzbacher, G., Heller, M., Graichen, F., Rohlmann, A., Strauss, J., Duda, G.N., 2001. Hip contact forces and gait patterns from routine activities. J. Biomech. 34, 859–871.

Bergmann, G., Graichen, F., Rohlmann, A., Deuretzbacher, G., Morlock, M., Heller, M., Duda, G.N., 1999. GAIT98 version June99 The hip joint: Contact forces, gait data and load cycles. Feie Universitat, Berlin, Germany, CD-ROM.

Bhandari, M., Matta, J., Ferguson, T., Matthys, G., 2006. Predictors of clinical and radiological outcome in patients with fractures of the acetabulum and concomitant posterior dislocation of the hip. J. Bone Joint Surg. Br. 88, 1618–1624.

Borrelli Jr., J., Goldfarb, C., Ricci, W., Wagner, J.M., Engsberg, J.R., 2002. Functional outcome after isolated acetabular fractures. J. Orthopaedic Trauma 16, 73–81.

Chao, E.Y., Volokh, K.Y., Yoshida, H., Shiba, N., Ide, T., 2010. Discrete element analysis in musculoskeletal biomechanics. Mol. Cell Biomech. 7, 175–192.

Crawford, M.J., Dy, C.J., Alexander, J.W., Thompson, M., Schroder, S.J., Vega, C.E., Patel, R.V., Miller, A.R., McCarthy, J.C., Lowe, W.R., Noble, P.C., 2007. The 2007 Frank Stinchfield Award. The biomechanics of the hip labrum and the stability of the hip. Clin. Orthop. Relat. Res. 465, 16–22.

Dirschl, D.R., Marsh, J.L., Buckwalter, J.A., Gelberman, R., Olson, S.A., Brown, T.D., Llinias, A., 2004. Articular fractures. J. Am. Acad. Orthopaedic Surg. 12, 416–423.

Ebraheim, N.A., Patil, V., Liu, J., Sanford Jr., C.G., Haman, S.P., 2007. Reconstruction of comminuted posterior wall fractures using the buttress technique: a review of 32 fractures. Int. Orthop. 31, 671–675.

Ferguson, S.J., Bryant, J.T., Ganz, R., Ito, K., 2003. An in vitro investigation of the acetabular labral seal in hip joint mechanics. J. Biomech. 36, 171–178.

Genda, E., Iwasaki, N., Li, G., MacWilliams, B.A., Barrance, P.J., Chao, E.Y., 2001. Normal hip joint contact pressure distribution in single-leg standing–effect of gender and anatomic parameters. J. Biomech. 34, 895–905.

Hadley, N.A., Brown, T.D., Weinstein, S.L., 1990. The effects of contact pressure elevations and aseptic necrosis on the long-term outcome of congenital hip dislocation. J. Orthopaedic Res.: Off. Publ. Orthopaedic Res. Soc. 8, 504–513.

Hak, D.J., Hamel, A.J., Bay, B.K., Sharkey, N.A., Olson, S.A., 1998. Consequences of transverse acetabular fracture malreduction on load transmission across the hip joint. J. Orthopaedic Trauma 12, 90–100.

Hansen, W., Shim, V.B., Obst, S., Lloyd, D.G., Newsham-West, R., Barrett, R.S., 2017. Achilles tendon stress is more sensitive to subject-specific geometry than subject-specific material properties: a finite element analysis. J. Biomech. 56, 26–31.

Harris, M.D., Anderson, A.E., Henak, C.R., Ellis, B.J., Peters, C.L., Weiss, J.A., 2012. Finite element prediction of cartilage contact stresses in normal human hips. J. Orthopaedic Res.: Off. Publ. Orthopaedic Res. Soc. 30, 1133–1139.

Henak, C.R., Abraham, C.L., Anderson, A.E., Maas, S.A., Ellis, B.J., Peters, C.L., Weiss, J.A., 2014a. Patient-specific analysis of cartilage and labrum mechanics in human hips with acetabular dysplasia. Osteoarthritis Cartilage 22, 210–217.

Henak, C.R., Ellis, B.J., Harris, M.D., Anderson, A.E., Peters, C.L., Weiss, J.A., 2011. Role of the acetabular labrum in load support across the hip joint. J. Biomech. 44, 2201–2206.

Henak, C.R., Kapron, A.L., Anderson, A.E., Ellis, B.J., Maas, S.A., Weiss, J.A., 2014b. Specimen-specific predictions of contact stress under physiological loading in the human hip: validation and sensitivity studies. Biomech. Model. Mechanobiol. 13, 387–400.

Hodge, W.A., Carlson, K.L., Fijan, R.S., Burgess, R.G., Riley, P.O., Harris, W.H., Mann, R.W., 1989. Contact pressures from an instrumented hip endoprosthesis. J. Bone Joint Surg. Am. 71, 1378–1386.

Hodge, W.A., Fijan, R.S., Carlson, K.L., Burgess, R.G., Harris, W.H., Mann, R.W., 1986. Contact pressures in the human hip joint measured in vivo. Proc. Natl. Acad. Sci. USA 83, 2879–2883.

Kern, A.M., Anderson, D.D., 2015. Expedited patient-specific assessment of contact stress exposure in the ankle joint following definitive articular fracture reduction. J. Biomech. 48, 3427–3432.

Konrath, G.A., Hamel, A.J., Olson, S.A., Bay, B., Sharkey, N.A., 1998a. The role of the acetabular labrum and the transverse acetabular ligament in load transmission in the hip. J. Bone Joint Surg. Am. 80, 1781–1788.

Konrath, G.A., Hamel, A.J., Sharkey, N.A., Bay, B.K., Olson, S.A., 1998b. Biomechanical consequences of anterior column fracture of the acetabulum. J. Orthopaedic Trauma 12, 547–552.

Li, W., Anderson, D.D., Goldsworthy, J.K., Marsh, J.L., Brown, T.D., 2008. Patient-specific finite element analysis of chronic contact stress exposure after intraarticular fracture of the tibial plafond. J. Orthopaedic Res.: Off. Publ. Orthopaedic Res. Soc. 26, 1039–1045.

Malkani, A.L., Voor, M.J., Rennirt, G., Helfet, D., Pedersen, D., Brown, T., 2001. Increased peak contact stress after incongruent reduction of transverse acetabular fractures: a cadaveric model. J. Trauma 51, 704–709.

Martin, C.T., Heiner, A.D., Baer, T.E., Pugely, A.J., Noiseux, N.O., 2015. Protrusio after medial acetabular wall breach in total hip arthroplasty. Iowa Orthopaedic J. 35, 99–107.

Matta, J.M., 1996. Fractures of the acetabulum: accuracy of reduction and clinical results in patients managed operatively within three weeks after the injury. J. Bone Joint Surg. Am. 78, 1632–1645.

Matta, J.M., Mehne, D.K., Roffi, R., 1986. Fractures of the acetabulum. Early results of a prospective study. Clin. Orthop. Relat. Res., 241–250

Maxian, T.A., Brown, T.D., Weinstein, S.L., 1995. Chronic stress tolerance levels for human articular cartilage: two nonuniform contact models applied to long-term follow-up of CDH. J. Biomech. 28, 159–166.

Moed, B.R., Carr, S.E., Gruson, K.I., Watson, J.T., Craig, J.G., 2003. Computed tomographic assessment of fractures of the posterior wall of the acetabulum after operative treatment. J. Bone Joint Surg. Am. 85-a, 512–522.

Myers, C.A., Register, B.C., Lertwanich, P., Ejnisman, L., Pennington, W.W., Giphart, J. E., LaPrade, R.F., Philippon, M.J., 2011. Role of the acetabular labrum and the iliofemoral ligament in hip stability: an in vitro biplane fluoroscopy study. Am. J. Sports Med. 39 (Suppl.), 85S–91S.

Olson, S.A., Bay, B.K., Chapman, M.W., Sharkey, N.A., 1995. Biomechanical consequences of fracture and repair of the posterior wall of the acetabulum. J. Bone Joint Surg. Am. 77, 1184–1192.

Olson, S.A., Bay, B.K., Pollak, A.N., Sharkey, N.A., Lee, T., 1996. The effect of variable size posterior wall acetabular fractures on contact characteristics of the hip joint. J. Orthopaedic Trauma 10, 395–402.

Rhyu, K.H., Kim, Y.H., Park, W.M., Kim, K., Cho, T.J., Choi, I.H., 2011. Application of finite element analysis in pre-operative planning for deformity correction of abnormal hip joints–a case series. Proc. Inst. Mech. Eng. H 225, 929–936.

Rudert, M.J., Ellis, B.J., Henak, C.R., Stroud, N.J., Pederson, D.R., Weiss, J.A., Brown, T. D., 2014. A new sensor for measurement of dynamic contact stress in the hip. J. Biomech. Eng. 136, 035001.

Saterbak, A.M., Marsh, J.L., Nepola, J.V., Brandser, E.A., Turbett, T., 2000. Clinical failure after posterior wall acetabular fractures: the influence of initial fracture patterns. J. Orthopaedic Trauma 14, 230–237.

Segal, N.A., Anderson, D.D., Iyer, K.S., Baker, J., Torner, J.C., Lynch, J.A., Felson, D.T., Lewis, C.E., Brown, T.D., 2009. Baseline articular contact stress levels predict incident symptomatic knee osteoarthritis development in the MOST cohort. J. Orthopaedic Res.: Off. Publ. Orthopaedic Res. Soc. 27, 1562–1568.

Segal, N.A., Kern, A.M., Anderson, D.D., Niu, J., Lynch, J., Guermazi, A., Torner, J.C., Brown, T.D., Nevitt, M., 2012. Elevated tibiofemoral articular contact stress predicts risk for bone marrow lesions and cartilage damage at 30 months. Osteoarthritis Cartilage 20, 1120–1126.

Shepherd, D.E., Seedhom, B.B., 1999. Thickness of human articular cartilage in joints of the lower limb. Ann. rheumatic Dis. 58, 27–34.

Shivanna, K., 2006. Automating Patient-Specific Diarthrodial Joint Contact Model Development. University of Iowa.

Song, Y., Ito, H., Kourtis, L., Safran, M.R., Carter, D.R., Giori, N.J., 2012. Articular cartilage friction increases in hip joints after the removal of acetabular labrum. J. Biomech. 45, 524–530.

Volokh, K.Y., Chao, E.Y., Armand, M., 2007. On foundations of discrete element analysis of contact in diarthrodial joints. Mol. Cell Biomech. 4, 67–73.

Yoshida, H., Faust, A., Wilckens, J., Kitagawa, M., Fetto, J., Chao, E.Y., 2006. Three-dimensional dynamic hip contact area and pressure distribution during activities of daily living. J. Biomech. 39, 1996–2004.

Correlation of Fracture Energy With Sanders Classification and Post-traumatic Osteoarthritis After Displaced Intra-articular Calcaneus Fractures

Karan Rao, BSE, Kevin Dibbern, MS,*† Molly Day, MD,* Natalie Glass, PhD,* J. Lawrence Marsh, MD,* and Donald D. Anderson, PhD*†*

Objectives: To quantify fracture severity for a series of displaced intra-articular calcaneal fractures (DIACFs) and to correlate it with Sanders classification, post-traumatic osteoarthritis (PTOA), and patient outcomes.

Design: Retrospective review and fracture severity analysis.

Setting: Level 1 trauma center affiliated with the University of Iowa in Iowa City, IA.

Patients/Participants: Thirty-six patients with 48 DIACFs were selected from 153 patients previously treated. All patients 18 years of age and older who had available electronic preop and postop computed tomography (CT) scans, good-quality postop and follow-up radiographs, and a follow-up ≥18 months were selected for study.

Intervention: Fractures were treated with percutaneous reduction, using multiple small stab incisions and fluoroscopy to guide manipulation of articular fragments using cork screws or Steinmann pins, with subsequent fixation using 3.5- and 4.0-mm screws.

Main Outcome Measurements: Preop CT scans were used to grade fractures according to the Sanders classification and to quantify fracture severity. Fracture severity was objectively quantified using a CT-based measure of fracture energy. PTOA was assessed on follow-up radiographs using the Kellgren–Lawrence scale. Patient outcomes were assessed using the Short Form 36 (SF-36) questionnaire and a visual analog scale pain score.

Results: Fracture energies for the 48 DIACFs ranged from 14.1 to 26.2 J (19.3 ± 3.1 J) and correlated with Sanders classification (rho = 0.53, P = 0.0001); type I (16.3 ± 0.9 J); type II (18.0 ± 2.7 J); type III (20.8 ± 2.8 J); and type IV (22.0 ± 0.7 J). Fracture energy was higher for fractures in which the subtalar joint developed PTOA (19.5 ± 2.7 J) than for those that did not (18.9 ± 3.3 J), but the difference did not reach statistical significance. The Sanders classification predicted PTOA risk [odds ratio (OR) = 4.04, 95% confidence interval = 1.43–11.39, P = 0.0084]. No relationship was observed between fracture energy and visual analog scale pain scores. Higher fracture energy correlated with lower SF-36 scores.

Conclusions: Fracture energy positively correlates with Sanders classification for DIACFs, which can be used to identify more severe fractures at greater risk of progressing to PTOA.

Key Words: fracture energy, calcaneus fractures, intra-articular fractures, fracture severity, post-traumatic osteoarthritis

Level of Evidence: Prognostic Level III. See Instructions for Authors for a complete description of levels of evidence.

(*J Orthop Trauma* 2019;33:261–266)

INTRODUCTION

The energy involved in fracturing a bone, by definition the fracture energy, can be measured from clinical computed tomography (CT) scan data and used to objectively quantify fracture severity. CT-based methods for quantifying fracture energy have previously been described for tibial plateau and pilon fractures.[1–3] Fracture energy as a measure of severity may improve on current fracture classification systems, which are categorical and prone to poor interobserver reliability.[4]

Displaced intra-articular calcaneal fractures (DIACFs) frequently result in post-traumatic osteoarthritis (PTOA). Previous studies have shown that fracture energy correlates with PTOA risk in tibial pilon fractures.[1,2,5] However, the prognostic value of fracture energy in predicting PTOA risk and clinical outcomes has not been evaluated in DICAFs. Our CT-based measurement technique has the potential to impact clinical research, treatment decisions, and counseling of patients with DIACFs regarding progression of osteoarthritis.

The primary purpose of this study was to quantify fracture severity by calculating fracture energy for a series of

Accepted for publication December 21, 2018.

From the Departments of *Orthopaedics and Rehabilitation, and †Biomedical Engineering, The University of Iowa, Iowa City, IA.

Research reported in this publication was supported by the National Institute of Arthritis and Musculoskeletal and Skin Diseases of the National Institutes of Health under Award Number P50 AR055533. The content is solely the responsibility of the authors and does not necessarily represent the official views of the National Institutes of Health. This work was also supported by the Assistant Secretary of Defense for Health Affairs through the Peer Reviewed Medical Research Program under Award No. W81XWH-15-2-0087. Opinions, interpretations, conclusions, and recommendations are those of the author and are not necessarily endorsed by the Department of Defense.

The authors report no conflict of interest.

Supplemental digital content is available for this article. Direct URL citations appear in the printed text and are provided in the HTML and PDF versions of this article on the journal's Web site (www.jorthotrauma.com).

Reprints: Donald D. Anderson, PhD, University of Iowa, Orthopaedic Biomechanics Laboratory, 2181 Westlawn Building South, Iowa City, IA 52242 (e-mail: don-anderson@uiowa.edu).

DOI: 10.1097/BOT.0000000000001432

DIACFs and to correlate these values with fracture classification and PTOA risk. A secondary purpose was to correlate fracture severity with patient-reported clinical outcomes. We hypothesized that fracture severity would correlate with Sanders classification and be a significant predictor of PTOA after DIACFs. We also hypothesized that patients sustaining fractures with greater fracture energy would have poorer clinical outcomes.

METHODS

To assess fracture energy and correlate it with key dependent variables, a convenience sample of patients with DIACF was chosen from a larger series of patients who were identified. Thirty-six patients with 48 DIACFs were selected for study from among 153 patients who had been treated (see **Figure**, **Supplemental Digital Content 1**, http://links.lww.com/JOT/A649, which shows sample selection for the study). The patients selected were 18 years of age and older, had available electronic preop and postop CT scans, and good-quality postop and follow-up radiographs. Patients younger than 18 years of age, with extra-articular fractures, without preop CT scans, and having follow-up <18 months were excluded. The patients' charts and radiographs were accessed retrospectively after Institutional Review Board approval. Demographic data and patient characteristics are shown in Table 1.

Preop Fracture Classification

Preop CT scans were used to determine the Sanders classification.[6] A fellowship-trained orthopaedic trauma surgeon, a fellowship-trained orthopaedic foot and ankle surgeon, and a PGY-3 orthopaedic resident independently classified each fracture using the Sanders classification. Discrepancies were adjudicated by majority vote of 3 members, where each member had 1 vote. Approximately 11/48 fractures had a 1-grade discrepancy in independent evaluation of the Sanders classification, and an additional 2/48 had a separation of 2 grades, before subsequent consensus.

TABLE 1. Patient Characteristics

Total patients/calcanei	36/48
Sex (patients/calcanei):	
Male	33 (91.7%)/44 (91.7%)
Female	3 (8.3%)/4 (8.3%)
Age (n = 36)	18–70 y (43.1 ± 11.8)
BMI (n = 35)	26.9 ± 4.0 kg/m^2 (19.5–36.8)
Mechanism of injury:	
Fall	34 (94%)
Car accident	2 (6%)
Unilateral fracture	24 (67%)
Bilateral fractures	12 (33%)
Follow-up time (mo)	19.4–84 (43.6 ± 18.4)
Sanders classification:	
I	2 (4%)
II	24 (50%)
III	19 (40%)
IV	3 (6%)
Open injury	3/36 (8%)
Polytrauma	12/36 (33%)
Tobacco users	15/36 (42%)
Workers compensation	15/36 (42%)
Underlying disease	13/36 (36%)

BMI, body mass index.

Operative Protocol and Articular Step-off

Fractures were treated with percutaneous reduction, using multiple small stab incisions and fluoroscopy to guide manipulation of articular fragments using cork screws or Steinmann pins, with subsequent fixation using 3.5- and 4.0-mm screws.[7,8] No mini open incisions or plates were used. All procedures were performed by either a fellowship-trained orthopaedic trauma surgeon or a fellowship-trained orthopaedic foot and ankle surgeon. Surgical reduction was assessed by measuring the posterior articular surface residual step-off using a semiautomated 3D step-off measurement tool coded in MATLAB (MathWorks, Inc, Natick, MA) software. Three patients with 4 fractures did not have postop CT scans available to assess articular step-off but were still included in the study.

Assessment of Fracture Severity

The CT-based approach for assessing fracture severity relies on computing fracture energy, which is quantified by measuring the fracture-liberated surface area and accounting for bone density.[1,5] Mechanical energy involved in a fracture liberates new surface area in a brittle solid (bone), and that energy is proportional to the interfragmentary surface area.[1,2,5,9] Previous studies have shown this method to accurately calculate fracture energy.[2] To determine fracture-liberated surface area, custom-written MATLAB software was used to identify fracture fragments from CT images. CT intensities and local fracture lines were used to further classify surfaces of bone fragments as cortical, subchondral, or interfragmentary. An image segmentation expert manually confirmed the accuracy of the surface classifications and made modifications as needed. The interfragmentary surface area was computed for each fractured face identified on the model. The Hounsfield Unit intensities from the CT scan were sampled at each vertex of these fractured faces, averaged, and scaled by a conversion factor to obtain the location-specific bone density for each face. This location-specific bone density was then used to appropriately scale the fracture-liberated surface area by density-dependent energy release rates to obtain the fracture energy for each fractured area (Fig. 1). This entire process takes on the order of 4 hours from the time the CT study is received until the fracture energy is obtained.

Assessment of Post-traumatic Osteoarthritis and Clinical Outcomes

PTOA was assessed on follow-up radiographs using the Kellgren–Lawrence (KL)[10] scale. The same 3 clinicians independently assigned a KL grade to the subtalar joint using available postop anteroposterior, lateral, and Broden radiographs

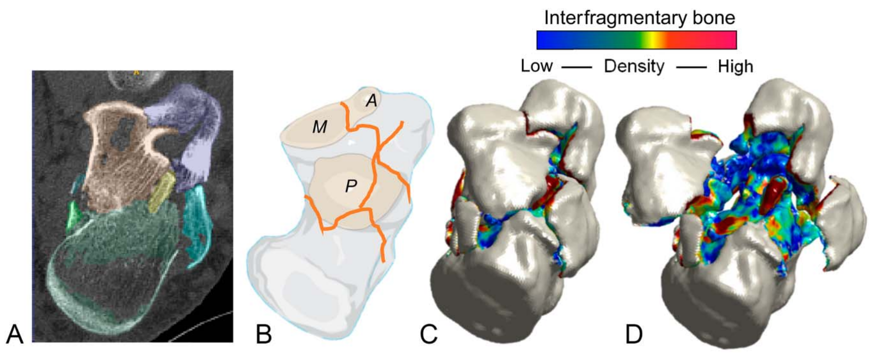

FIGURE 1. Superior views of a Sanders type III intra-articular fracture of the calcaneus. From left to right: (A) patient-specific CT slice with overlay of image segmentation of fracture fragments; (B) 2 fracture lines coursing through the posterior talar articular surface demonstrating a Sanders type III fracture pattern; (C) 3D model of the fracture generated by custom-written MATLAB software; and (D) exploded view showing interfragmentary bone surfaces and CT-derived densities used to calculate the fracture energy. A, anterior talar articular facet; M, middle talar articular facet; P, posterior talar articular facet. **Editor's Note:** A color image accompanies the online version of this article.

of the calcaneus. The radiographs were assessed at follow-up times ranging from 19 to 84 months, with a median follow-up time of 43 months. Disagreement in evaluation of KL grades was adjudicated by majority vote of all 3 evaluators. A KL grade ≥2 met criteria for PTOA.

Patients were clinically evaluated using functional outcome questionnaires scored from chart review. To evaluate clinical health score trends, fracture energy was arbitrarily divided into 3 categorical energy ranges ("low," "medium," and "high") with the goal of having an approximately equal number of fractures in each category. Two clinical health outcome scores were obtained: the visual analog scale (VAS) for pain, and the Short Form 36 (SF-36) quality of life survey. The SF-36 is a widely used quality of life survey composed of a physical component summary (PCS) and a mental component summary (MCS), with each category scoring from 0 to 100, and higher scores representing better outcomes.[11]

Statistical Methods

Statistical analyses were completed using SAS software version 9.4 (SAS Institute, Inc, Cary, NC). A P value <0.05 was considered statistically significant. For continuous outcomes between 2 groups, the t test was applied for variables that were normally distributed, and the Wilcoxon Rank-Sum test was used for variables without normal distributions. Adjustments for multiple comparisons were completed. Spearman correlation coefficients were used to describe relationships between fracture energy, Sanders classification, VAS pain scores, SF-36 scored, and step-off. Logistic regression was used to model the association between fracture energy, Sanders classification, and PTOA risk. Interobserver reliability was assessed using Kendall's τ coefficient of concordance.

RESULTS

Fracture Energy and Sanders Classification as Predictors of Post-traumatic Osteoarthritis

Of the 48 calcaneus fractures, 2 (4%) were classified as Sanders type I, 24 (50%) as type II, 19 (40%) as type III, and 3 (6%) as type IV (inter-rater reliability coefficient of concordance τ = 0.3). The fracture energies for the 48 DIACFs ranged from 14.1 to 26.2 J, with a mean ± SD of 19.3 ± 3.1 J. There was a statistically significant positive linear correlation between Sanders classification and mean fracture energy (rho = 0.53, P = 0.0001). The mean ± SD fracture energy for each Sander's class are as follows: type I [16.31 ± 0.98 J] (n = 2), type II [18.03 ± 2.73 J] (n = 24), type III [20.79 ± 2.80 J] (n = 19), and type IV [21.98 ± 0.73 J] (n = 3) (Fig. 2).

Fracture energies showed overlap across different grades of PTOA (see **Table**, **Supplemental Digital Content 2**, http://links.lww.com/JOT/A650, which shows mean fracture energy and follow-up time, along with the number of fractures for each radiographic grade of PTOA). Approximately 14/48 fractures had a 1-grade discrepancy in independent evaluation of KL grades, and an additional 4/48 fractures had a 2-grade discrepancy, before subsequent consensus; 1/48 fractures had a 3-grade discrepancy, as assessed by a PGY-3 resident and an orthopaedic trauma surgeon (inter-rater reliability coefficient of concordance τ = 0.6, P = 0.0074). Stratifying these data by the presence of radiographic PTOA (KL ≥ 2), the fracture energy was higher for fractures in which the subtalar joint developed PTOA (19.5 ± 2.7 J) than for those fractures in which the subtalar joint did not (18.9 ± 3.3 J), but the difference did not reach statistical significance [OR = 1.37, 95% confidence interval (CI) = 0.53–3.51, P = 0.52] (Fig. 3).

Twenty-nine of 48 subtalar joints (60%) showed radiographic evidence of PTOA. The median follow-up time for joints that developed PTOA was 49.0 (20.9–84.0) months.

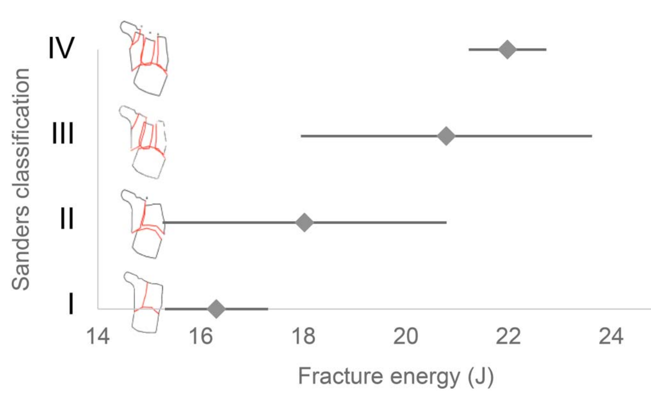

FIGURE 2. Relationship between Sanders classification and fracture energy. Diamond markers represent the mean, and the horizontal bars represent the SD. (rho = 0.53, P = 0.0001). **Editor's Note:** A color image accompanies the online version of this article.

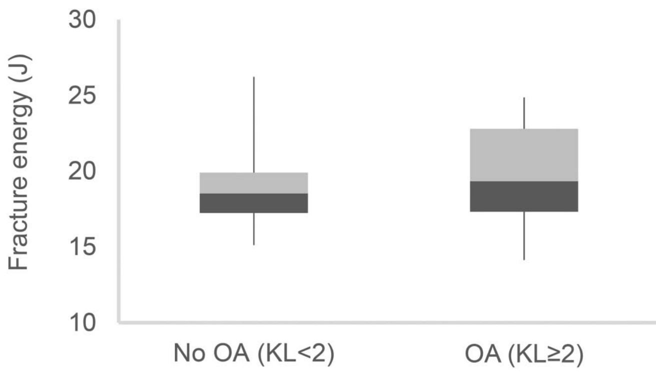

FIGURE 3. Fracture energy (J) versus PTOA development in the subtalar joint for calcaneus fractures. Twenty-nine subtalar joints developed radiographic PTOA with an energy of 19.5 ± 3.3 J. Nineteen subtalar joints did not show radiographic evidence of PTOA, with a mean energy of 18.9 ± 2.8 J (P = 0.5314).

The average follow-up time for joints that did not develop PTOA was 28.0 (19.4–58.0) months. Follow-up time was associated with PTOA (OR = 3.208, 95% CI = 1.389–7.405, P = 0.0063).

Eight patients (22%) with 10 affected subtalar joints were treated with subtalar arthrodesis (KL = 4). The median time to subtalar fusion, from the time of injury, was 34.6 (15.0–78.0) months. The fracture energies observed for these fractures (19.4 ± 3.5 J) were not significantly different from those that did not result in fusion (19.3 ± 3.0 J, OR = 1.05, 95% CI = 0.34–3.24, P = 0.9343).

The Sanders classification positively correlated with the risk of developing PTOA (OR = 4.04, 95% CI = 1.43–11.39, P = 0.0084), and the results were significant even when adjusted for follow-up time between the PTOA and non-PTOA groups (OR = 4.60, 95% CI = 1.30–16.28, P = 0.0179). For Sanders type I fractures, no evidence of PTOA was observed. For type II fractures, an equal number of subtalar joints developed PTOA as did not. A greater percentage (72%) of subtalar joints developed PTOA in Sanders type III and IV fractures (Table 2). The Sanders classification did not correlate with the likelihood of subtalar arthrodesis (OR = 1.39, 95% CI = 0.48–4.00, P = 0.5399).

Clinical Outcomes and Functional Scores

VAS pain scores were available for all 36 patients, and SF-36 scores were available for 28 of 36 patients (see **Table, Supplemental Digital Content 3**, http://links.lww.com/JOT/A651, which shows VAS and SF36 scores across fracture energy). Taken across the aggregate fracture energy range, there was a weak negative correlation between fracture energy and VAS pain scores (rho = −0.13, P = 0.3764). Patient-reported SF-36 PCS were lower for high-energy fractures. This result was more pronounced in patients with bilateral fractures (rho = −0.76, P = 0.0018, n = 14). There were no significant associations observed between fracture energy and SF-36 MCS, although there was a trend for lower scores with higher energy fractures.

Somewhat unexpectedly, patients who developed PTOA did not report significantly higher VAS pain scores than patients who did not (see **Table, Supplemental Digital Content 4**, http://links.lww.com/JOT/A652, which shows VAS and SF-36 scores with respect to PTOA). However, both SF-36 PCS and MCS were lower among patients who developed PTOA than in those who did not [PCS (PTOA: 34.7, no PTOA: 45.0; P = 0.013), MCS (PTOA: 47.9, no PTOA: 55.8; P = 0.045)]. An inverse relationship was observed between Sanders classification and VAS pain scores. Although generally decreasing with higher Sanders classification, SF-36 MCS scores did not differ significantly across Sanders fracture types, while SF-36 PCS scores significantly decreased.

Outcomes by Surgical Reduction

With respect to the quality of surgical reduction, 25 of 44 fractures (56.8%) measured a step-off <2 mm, and 19 of 44 fractures (43.2%) measured a step-off >2 mm. No correlation was observed between fracture energy and articular step-off. A nonsignificant positive association was observed between articular step-off and KL grades (see **Table, Supplemental Digital Content 5**, http://links.lww.com/JOT/A653, which shows articular step-off for fractures by a KL grade). Similarly, a positive correlation was observed between Sanders classification and articular step-off, but the finding was also not statistically significant.

DISCUSSION

Correlation of Fracture Energy with Sanders Classification

The energy range for DIACFs was found to be 14.14–26.87 J. Dibbern et al[3] used a similar methodology and reported fracture energies for tibial plateau fractures (3.2–33.2 J) and for pilon fractures (3.6–32.2 J). Thomas et al[1] reported pilon fracture energy range from 5.2 to 27.2 J. Compared with plateau and pilon fractures, the energy range for calcaneus fractures seems to be narrower and focused on the upper end of the spectrum, suggesting it may take consistently more

TABLE 2. Number and Percent of Fractures in Which the Subtalar Joint Progressed to PTOA and Joint Fusion, Across the Sanders Classification

Sanders Type	PTOA Absent (KL < 2)	PTOA Present (KL ≥ 2)	% OA	Joint Fusion	% Joint Fusion
I	2	0	0	0	0
II	12	12	50	5	21
III	5	14	74	4	21
IV	0	3	100	1	33

energy to break the calcaneus. Although the shape and density of the calcaneus cancellous bone are different than the plateau and pilon, MATLAB software accounts for differences in Hounsfield CT density values, which reflect the differences in density of the cancellous bone. Fracture morphology and the size of the articular contact area for a given joint both influence the energy absorption.[12,13] The shorter length of the calcaneus and the smaller contact area may limit the amount of energy absorbed, suggesting the calcaneus shatters in response to a higher, more concentrated distribution of energy compared with long bones such as the tibia.

Fracture classification systems are often used to provide a clinician-assessed indicator of fracture severity but suffer from poor interobserver reliability when clinicians' place fracture patterns into categorical classification schemes.[3,4] This study demonstrated poor interobserver reliability in classifying DICAFs by the Sanders classification (concordance $\tau = 0.6$, $P = 0.0074$). The Sanders classification is commonly used to assess DIACFs and has been previously found to be prognostic of long-term patient outcomes.[14–17] We found that fracture energy generally increased with Sanders classification. This is an expected result; the Sanders classification is based on the number of fracture lines through the posterior facet. More fracture lines through the posterior facet generally correlate with greater interfragmentary surface area, translating into higher energy. There was, however, considerable overlap among classification of fracture types and fracture energy, which may in part be explained by the fact the Sanders classification assesses only the number of intra-articular fracture lines, whereas the fracture energy calculation accounts for extra-articular extension of the fracture, which may vary across otherwise similar Sanders grades.

Fracture Energy as a Predictor of Post-traumatic Osteoarthritis

In this study, 61% of patients developed radiographic evidence of PTOA, and 22% of patients progressed to subtalar joint fusion, at a median of 36 months after injury. Previous studies have demonstrated that fracture severity metrics applied to tibial pilon fractures strongly correlate with subsequent PTOA.[1,2,4] In this study, this relationship was less evident for DIACFs. Although mean energy was higher for fractures in which the subtalar joint progressed to PTOA, there was significant energy overlap with those that did not. The pathogenesis of PTOA is heterogeneous and may result from persistence of a pathologic process initiated at the time of initial joint trauma or a combination of pathological and inflammatory processes that take place in damaged tissue.[18] In addition, independent risk factors such as obesity, smoking, age, sex, and activity levels are likely to confound the relationship between fracture energy and PTOA.

The clinical significance of fracture energy is that it (1) provides a truly objective assessment of fracture severity, (2) provides a means to test how well-subjective classification schemes reflect fracture severity, (3) can guide surgeon decision-making for minimally invasive versus open intervention techniques, and (4) may predict and inform patients of their PTOA risk. Of course, these clinical benefits can only be fully realized once fracture energy can be routinely quantified in practice.

This study also assessed the effect of another important variable, the residual mechanical environment caused by persistent articular step-offs. Multiple studies have suggested that fractures with an incongruous reduction (ie, step-off >2 mm) are associated with early PTOA; however, evidence is less clear on the relationship between poor reduction and worse long-term clinical outcomes.[9,18–21] In this study, fracture energy did not correlate with articular step-off, but there was a positive association between KL grade and articular step-off, as well as between Sanders classification and articular step-off; however, these differences were not significant. Articular step-off is an important source of expected PTOA, but other factors including cartilage loss at time of surgery and abnormal alignment of the body leading to uneven wear also influence PTOA risk from the time of surgical intervention to arthritis development.

Correlation to Clinical Outcomes

The clinical outcome assessed by SF-36 scores significantly correlated with PTOA. Fracture energy showed a weak negative correlation to SF-36 PCS scores, and scores were significantly different between PTOA and non-PTOA groups after an energy cutoff of 20 J ($P = 0.049$). SF-36 scores also decreased with increasing levels of the Sanders classification. These findings are consistent with previous literature reporting SF-36 outcome scores after DIACFs.

Trends with the VAS pain scores were less definitive. VAS pain scores did not correlate with either fracture energy or Sanders classification in any predictable or expected way. In addition, they did not correlate with PTOA at follow-up. Interestingly, VAS pain scores were highest for "low" energy fractures and lowest for "intermediate" energy fractures. VAS scores were higher for patients who showed radiographic evidence of PTOA. VAS pain scores did not relate to the Sanders classification. The Sanders classification has been shown to be prognostic with SF-36 and VAS pain scores, but sample size was a limitation in observing similar statistically significant trends.

Limitations

KL grading has previously been demonstrated in the literature to be subjective with moderate interobserver reliability in the subtalar joint.[22–25] In this study, interobserver reliability in assessing PTOA on plain radiographs was in the moderate range ($\tau = 0.6$). The lack of CT imaging to assess PTOA was a limitation, and further research assessing PTOA with weight-bearing CT scans may more accurately characterize subtalar PTOA. Another limitation was the form in which the VAS pain scores were charted on a 3-point range in patient records (eg, "moderate pain, VAS 4–6"), instead of a true 10-point scale. This may explain the significant overlap in pain scores and limited statistical significance observed with fracture energy.

Sample size was also a limitation. Ideally, a higher fracture energy suggests a more severe fracture pattern (which we observed with Sanders classification), which in turn should reflect a higher PTOA risk. Possible confounding factors between fracture energy and PTOA risk include anatomical reduction (<2 mm), sex, age, body mass index, comorbidities, and a shorter follow-up time in the non-PTOA group. Radiographic PTOA was assessed in this study. Defining PTOA from a biological and pain perspective creates additional complexities as the pathogenesis of PTOA is in itself complex, as is how patients interpret and report pain. The Sanders classification positively correlated with the risk of developing PTOA, consistent with literature,[17] but did not correlate with risk of subtalar fusion. Weak positive correlations between KL grades and articular step-off, as well as between Sanders classification and articular step-off were observed, which may have reached statistical significance with a larger sample size.

CONCLUSIONS

CT-based measurement of fracture energy in DIACFs showed a narrower range compared with tibial pilon and plateau fractures and is at the upper end of energy, suggesting that it takes consistently more energy to break the calcaneus. Fracture energy correlated with Sanders classification, but several factors contribute to significant energy overlaps between Sanders categories. Fracture energy, Sanders classification, and articular step-off all correlate with subsequent PTOA, but the association of fracture energy with PTOA is not as strong as it was in the tibial pilon.

ACKNOWLEDGMENTS

The authors acknowledge Dr Phinit Phisitkul for his expert assessment of Kellgren–Lawrence grades and Sanders classification. The authors also acknowledge the dedicated segmentation efforts of Mr. Denis Cuvalo.

REFERENCES

1. Thomas TP, Anderson DD, Mosqueda TV, et al. Objective CT-based metrics of articular fracture severity to assess risk for posttraumatic osteoarthritis. *J Orthop Trauma.* 2010;24:764–769.
2. Anderson DD, Mosqueda T, Thomas TP, et al. Quantifying tibial plafond fracture severity: absorbed energy and fragment displacement agree with clinical rank ordering. *J Orthop Res.* 2008;26:1046–1052.
3. Dibbern K, Kempton LB, Higgins TF, et al. Fractures of the tibial plateau involve similar energies as the tibial pilon but greater articular surface involvement. *J Orthop Res.* 2017;35:618–624.
4. Lauder AJ, Inda DJ, Bott AM, et al. Interobserver and intraobserver reliability of two classification systems for intra-articular calcaneal fractures. *Foot Ankle Int.* 2006;27:251–255.
5. Thomas TP, Anderson DD, Marsh JL, et al. A method for the estimation of normative bone surface area to aid in objective CT-based fracture severity assessment. *Iowa Orthop J.* 2008;28:9–13.
6. Sanders R, Fortin P, Dipasuale T, et al. Operative treatment in 120 displaced intra-articular calcaneal fractures: results using a prognostic computed tomography scan classification. *Clin Orthop.* 1993;290:87–95.
7. Marsh JL, Boyer JS, Sullivan J, et al. A percutaneous technique for reduction and internal fixation of displaced intra-articular calcaneal fractures. *JBJS Essent Sug Tech.* 2011;1:e9.
8. Tantavisut S, Phisitkul P, Westerlind BO, et al. Percutaneous reduction and screw fixation of displaced intra-articular fractures of the calcaneus. *Foot Ankle Int.* 2017;38:367–374.
9. Beardsley CL, Anderson DD, Marsh JL, et al. Interfragmentary surface area as an index of comminution severity in cortical bone impact. *J Orthop Res.* 2005;23:686–690.
10. Kellgren JH, Lawrence JS. Radiological assessment of osteo-arthrosis. *Ann Rheum Dis.* 1957;16:494–502.
11. Laucis NC, Hays RD, Bhattacharyya T. Scoring the SF-36 in orthopedics: a brief guide. *J Bone Jt Surg Am.* 2015;97:1628–1634.
12. Sohn HS, Yoon YC, Cho JW, et al. Incidence and fracture morphology of posterolateral fragments in lateral and bicondylar tibial plateau fractures. *J Orthop Trauma.* 2015;29:91–97.
13. Zhai Q, Hu C, Xu Y, et al. Study of posterior articular depression in Schatzker IV fractures. *Orthopedics.* 2015;38:e124–e128.
14. Rammelt S, Zwipp H, Schneiders W, et al. Severity of injury predicts subsequent function in surgically treated displaced intraarticular calcaneal fractures. *Clin Orthop Relat Res.* 2013;471:2885–2898.
15. Tennent TD, Calder PR, Salisbury RD, et al. The operative management of displaced intra-articular fractures of the calcaneum: a two-centre study using a defined protocol. *Injury.* 2001;32:491–496.
16. Zhang T, Su Y, Chen W, et al. Displaced intra-articular calcaneal fractures treated in a minimally invasive fashion: longitudinal approach versus sinus tarsi approach. *J Bone Jt Surg Am.* 2014;96:302–309.
17. Sanders R, Vaupel ZM, Erdogan M, et al. Operative treatment of displaced intraarticular calcaneal fractures: long-term (10-20 years) results in 108 fractures using a prognostic CT classification. *J Orthop Trauma.* 2014;28:551–563.
18. Riordan EA, Little C, Hunter D. Pathogenesis of post-traumatic OA with a view to intervention. *Best Pract Res Clin Rheumatol.* 2014;28:17–30.
19. Buckley R1, Tough S, McCormack R, et al. Operative compared with nonoperative treatment of displaced intra-articular calcaneal fractures. *J Bone Jt Surg Am.* 2002;84-A:1733–1744.
20. Goldfarb CA, Rudzki JR, Catalano LW, et al. Fifteen-year outcome of displaced intra-articular fractures of the distal radius. *J Hand Surg Am.* 2006;31:633–639.
21. Lutz M, Arora R, Krappinger D, et al. Arthritis predicting factors in distal intraarticular radius fractures. *Arch Orthop Trauma Surg.* 2011;131:1121–1126.
22. Mayich DJ, Pinsker E, Mayich MS, et al. An analysis of the use of the Kellgren and Lawrence grading system to evaluate peritalar arthritis following total ankle arthroplasty. *Foot Ankle Int.* 2013;34:1508–1515.
23. Menz HB, Munteanu SE, Landorf KB, et al. Radiographic classification of osteoarthritis in commonly affected joints of the foot. *Osteoarthr Cartil.* 2007;15:1333–1338.
24. Kraus VB, Kilfoil TM, Hash TW II, et al. Atlas of radiographic features of osteoarthritis of the ankle and hindfoot. *Osteoarthr Cartil.* 2015;23:2059–2085.
25. Dekker TJ, Walton D, Vinson EN et al. Hindfoot arthritis progression and arthrodesis risk after total ankle replacement. *Foot Ankle Int.* 2017;38:1183–1187.

Summer 2019

Utilizing objective measures of acute and chronic mechanical insult to determine their contributions to post-traumatic osteoarthritis risk

Kevin Nathaniel Dibbern
University of Iowa

Follow this and additional works at: https://ir.uiowa.edu/etd
Part of the Biomedical Engineering and Bioengineering Commons

UTILIZING OBJECTIVE MEASURES OF ACUTE AND CHRONIC MECHANICAL

INSULT TO DETERMINE THEIR CONTRIBUTIONS TO POST-TRAUMATIC

OSTEOARTHRITIS RISK

by

Kevin Nathaniel Dibbern

A thesis submitted in partial fulfillment
of the requirements for the Doctor of Philosophy
degree in Biomedical Engineering in the
Graduate College of
The University of Iowa

August 2019

Thesis Supervisor: Professor Donald D. Anderson

ACKNOWLEDGEMENTS

This work would not have been possible without the support from many individuals in the Department of Orthopedics and Rehabilitation and the Orthopedic Biomechanics Laboratory, as well as from our collaborators at the University of Indiana. I would like to thank Drs. J. Lawrence Marsh, Michael Willey, Lawrence Kempton, and Todd McKinley for their support and invaluable clinical expertise, Dr. Andrew Kern for his teaching and mentoring, and Holly Thomas-Aitken, as well as Drs. Karan Rao, and Tai Holland for their aid in the many hours of analysis required to complete these studies. Also, I acknowledge and would like to thank the many students who have helped in the support of this work, in particular, Megan Andrew, Dennis Cuvalo, Matt Engelken, James Hiller, Mike Ho, Erin McFadden, Jessica Mosqueda, Kara Schneider, and Janelle Lala. Finally, I would like to sincerely thank my advisor, Dr. Donald D. Anderson, for the outstanding mentoring and guidance he has provided.

ABSTRACT

Intra-articular fractures (IAFs) are challenging injuries to study and treat clinically. Following IAF, different joints and even different regions within joints have been shown to have varying degrees of tolerance to injury severity and surgical reduction accuracy. Therefore, to determine the true effects of surgical reduction accuracy on post-traumatic osteoarthritis (PTOA) development, more sensitive and objective measures of articular injury and restoration are needed. To that end, this work details the development of objective measures of injury severity and models of restoration. Two hypotheses were posed: that surgical reduction accuracy is correlated with injury severity, and that injury severity more greatly influences outcomes than the surgical reduction.

To quantify the effects of acute injury severity on PTOA development, objective measures of the energy involved in fracturing as well as the degree of damage to the articular surface were created. Differences in the area over which the damage was delivered were also accounted for as a normalization of the fracture energy to a given joint. Inclusion of this latter factor enabled more accurate study of damage to the important areas of the bone. From these measures, a combined severity score was created that could be applied to any IAF. It was demonstrated to be predictive of the degree of PTOA development in the hip, hindfoot, and ankle.

The effects of surgical reduction accuracy were measured through contact stress, a measure that detects when forces are concentrated over small areas. When these stresses are too high and persist over time, they are associated with chronic joint degeneration. Therefore, the exposure to the contact stresses during a simulated walking gait after fracture reconstruction was

computed for each patient. The over-exposures computed over this gait cycle were strongly associated with PTOA development in all 3 joints studied.

By measuring injury severity and reduction accuracy on the same patients with IAFs of the hip, hindfoot, or ankle, relative contributions to PTOA risk were determined for each joint. Significant correlations between injury severity and reduction accuracy were found supporting our first hypothesis. The second hypothesis was refuted, as reduction accuracy was also significantly associated with PTOA development in all 3 joints. An overall model combining the injury severity and reduction accuracy measure for each case was created to assess the total mechanical contributions to PTOA. This model achieved 100% accuracy in the ankle, 88% in the calcaneus, and 91% in the acetabulum.

PUBLIC ABSTRACT

Intra-articular bone fractures are challenging injuries from both the perspective of scientific study and that of clinical treatment. Following such injuries, different joints have been found to have different apparent tolerances to the severity of the initial injury and the accuracy of their restoration after surgical treatment. Therefore, to determine the true effects of this surgical accuracy on patient outcomes, more sensitive and objective measures of the severity of injury and accuracy of restoration are needed. To that end, this work details the development of objective measures of injury severity and models of restoration accuracy. Two hypotheses were posed: that the surgical restoration accuracy is correlated with the injury severity, and that the injury severity more greatly influences outcomes than the restoration accuracy.

The injury severity was objectively quantified using measures of the energy involved in creating the fracture. The differences in area over which damage was delivered and amount of energy in important regions of bone were also accounted for to better assess damage across highly varied joint anatomies. These measures were demonstrated to be predictive of patient outcomes in the hip, hindfoot, and ankle.

The effects of surgical restoration accuracy were measured through contact stress, a measure that detects when forces are concentrated over small areas. When these stresses are too high and persist over time, they are associated with chronic joint degeneration. Therefore, the exposure to the contact stresses during a simulated walking gait after fracture reconstruction was computed for each patient. The stress over-exposures computed over this gait cycle were also strongly associated with patient outcomes in all three joints studied.

By measuring injury severity and restoration accuracy on the same patients with IAFs of the hip, hindfoot or ankle, the relative contributions of each factor to patient outcomes were

determined for each joint. Significant correlations between injury severity and restoration accuracy were found, a result that supports our first hypothesis. The second hypothesis was refuted, as reduction accuracy was also significantly associated with patient outcomes. An overall model combining the injury severity and restoration accuracy measures for each case was created to best assess and predict patient outcomes. This model achieved 100% accuracy in the ankle, 88% in the calcaneus, and 91% in the acetabulum.

TABLE OF CONTENTS

LIST OF TABLES

LIST OF FIGURES

TABLE OF NOMENCLATURE

	Unit of measure	**Description**
Fracture energy	Joules	The energy involved in liberating surface area during a fracture based upon the strain energy release rate and Hounsfield Unit intensity. Used to objectively assess the severity of injury.
Contact area-normalized fracture energy	Joules/cm^2	Averaged fracture energy as scaled to literature values of contact area. Used to control for differences in the area over which energy is transmitted across the joint. Estimates damage on a per unit area basis to help control for highly varied anatomy.
Normalized fracture energy	Joules/cm^2	Articular surface area normalized fracture energy. Scaled to articular surface areas that receive primary loading from impacts as classified on segmentations from CT scans. Differentiated from the contact area-normalized fracture energy by enabling use on a patient-specific basis. Also estimates damage on a per unit area basis.
Articular comminution energy	Joules	Fracture energy dispersed within 1 cm of the joint surface. Measured by projecting a plane 1 cm from the average normal direction of the articular surface in each fragment. Used to estimate the energy dissipated across the articular surface.
Contact stress	MPa	The forces between two mated articular surfaces distributed over discrete areas.
Contact stress over-exposure	MPa*s	The magnitude of contact stress over a given damage threshold scaled by the amount of time per gait cycle that it is exposed to those stresses. Used to assess residual incongruity and predict cartilage degeneration.

PREFACE

The purpose of this work was ultimately to determine the effects of injury severity and surgical reduction accuracy on patient outcomes after intra-articular fracture. This first necessitated creating improved measures of injury severity that could be utilized across joints. Therefore, the substantial development burden described within details the progression from fracture energy providing inadequate correlations with post-traumatic osteoarthritis (PTOA) across joints, to improving predictions by controlling for damage per unit area, and, ultimately, to including a measure of articular comminution in order to create a more comprehensive combined measure of injury severity that best describes PTOA risk for comparing against measures of surgical reduction accuracy. The surgical reduction accuracy was quantified by a more proven measure, the contact stress over-exposure. Development of this measure described in this document built upon an established model in the ankle, validated preliminary work in the hip, and new model in the calcaneus. The results and discussion sections explore the data first from a context of establishing the new measures of injury severity then move toward determining the relative contributions of injury severity and reduction accuracy to patient outcomes.

CHAPTER 1 - INTRODUCTION

The management of intra-articular fractures (IAFs) represents a common but challenging task for orthopedic traumatologists, especially when bone fragments are substantially displaced from their native anatomical position. IAFs are characterized by extension into the joint that causes disruption of the smooth articular surface. Surgical management aims to provide stable fixation of fragments in an anatomically reduced position to ensure osseous union and restore the native mechanical environment of the joint. One of the basic tenets of fracture care is that the smooth articular surface must be precisely restored, although the literature suggests that the requisite degree of precision varies by joint. The task of achieving this precise restoration of anatomy is made more challenging by a number of frequently concurrent complexities of IAFs like higher energy mechanisms that create more fragments, comminution, and displacement[1, 3-5].

IAFs are associated with rates of arthritic development up to 20 times higher than extra-articular fractures as damage to the joint is followed by rapid degeneration to post-traumatic osteoarthritis (PTOA)[6]. PTOA represents the end stage organ-level failure of an injured joint [7]. It creates a tremendous burden for the patients and the economy, with disability comparable to end stage heart failure and annual healthcare costs in the U.S. estimated to exceed $12 billion[8]. Despite the prevalence, cost, and investment in new techniques and medicine over the past 50 years, the rates of PTOA following IAF have not substantially declined[7]. The reasons are multifactorial but most probably involve under-appreciated factors in PTOA pathogenesis.

Our best understanding of PTOA pathogenesis after IAFs can be described by the three primary components of its onset and progression: the acute articular injury, the surgical reduction accuracy, and the resulting pathobiological responses to the first two factors. The acute articular injury results directly from the injurious event and is described as the degree of damage to the joint brought about by the initial impact. The surgical reduction accuracy can be thought of as ameliorating the chronic components of IAF damage. Poor reductions can adversely impact the mechanical environment of the joint after the fracture with mal-reduced fragments after fixation altering the location, magnitude, and duration of stresses from those of a normal joint [3]. These changes frequently result in the progressive degeneration of articular joints. Pathobiological contributions to PTOA development result from the inability of the joint as an organ to restore homeostasis and can lead to failure of the joint[9]. Restoration of homeostasis is impeded by things like the residual incongruity and harmful biological responses to severe acute injuries [10, 11]. Though these three constitutive components of PTOA pathogenesis are known, and the pathomechanical components are the focus of treatment, their relative contributions to PTOA risk remain largely unknown.

Acute injury severity is widely known to influence PTOA risk after IAF but is not always considered as an independent explanation of poor patient outcomes. As more severe fractures require more challenging surgical restorations, it has been proposed that PTOA may result primarily from surgical mal-reduction. Unfortunately, there are no clinically available methods to objectively assess this important factor in a way that would enable determination of its relative contribution to patient outcomes. Instead, fracture severity assessment has relied upon joint-specific categorical fracture classification systems that suffer from poor inter-observer reliability [12, 13]. The most useful clinical classification systems focus on categorizing fractures according to various features of articular fractures that can be readily identified from radiographs or CT scans. Typically, these features include: the number of fractures, their relative locations in the bone—especially the proximity and interaction with the articular surface, and the amount of fragment displacement. Such features, however, are not amenable to reliable and objective assessment and have failed to provide contextual information on PTOA risk.

To remedy these shortcomings, novel CT-based analysis methods have been developed to aid in the objective quantification of IAF severity[1, 14-20]. The origin of these methods was the clinical axiom that “the extent of bone, cartilage, and soft tissue damage is directly related to the energy imparted to these structures”[21]. In the case of a brittle solid, this energy can be directly related to the amount of fracture-liberated surface area and the density of the material fractured. At the high rates of loading seen in fracturing events, bone behaves as a brittle solid, and the fracture-liberated surface area and bone density can both be determined from CT scans [16, 20]. Therefore, the amount of energy in a fracture can be determined from clinically available data. This approach was originally developed using laboratory models (first, a dense polyether-urethane foam surrogate material, then in bovine bone segments) and subsequently extended for use in human clinical series[15-18]. Over the past decade, these techniques were further developed to enable large scale study of fracture severity in the clinical research setting[19, 22]. This presents an opportunity to objectively study the influence of acute fracture severity on PTOA.

Chronic pathomechanical factors, often resulting from surgical mal-reduction, are the most thoroughly studied and treated causes of PTOA progression[3, 23-27]. Mechanical factors under surgical control involve everything from ligament reconstruction to joint alignment and restoration of surface congruency. For this reason, it has been thought that cases progressing to PTOA do so primarily from a failure to adequately restore normal joint mechanics. Literature has even suggested that precise fracture reductions with step-offs less than 2mm are necessary to achieve optimal restoration and forestall PTOA[28-30]. However, it is known that different joints—and even different regions within the same joint—can respond differently to IAFs. For example, there is clinical evidence that the accuracy of reduction as measured by step-off after an acetabular or tibial plafond fracture is highly correlated with outcomes while, by comparison, incongruities of the tibial plateau are well-tolerated[3, 28, 29, 31, 32]. Because of these inconsistencies, what constitutes optimal management of IAFs is frequently debated with arguments based more on anecdotal observation and intuition rather than on rigorous scientific evidence[7].

Recently, patient-specific computational modeling methods to estimate joint contact stresses have been developed to provide objective evidence through which the chronic mechanical environment of the joint can be evaluated[25, 33, 34]. Such models can help address the questions outlined above and definitively answer what constitutes adequate or even optimal surgical management. Preliminary studies have demonstrated significant correlations between quality of surgical reduction, as measured by contact stress, and PTOA development. However, there are cases with well-reduced fractures that still develop OA. This brings us back to the central question: if surgical methods are improving, why aren't PTOA rates decreasing? The most logical conclusion is that the acute severity of injury plays a larger role in PTOA risk than has been previously appreciated.

Despite a high likelihood of interplay between the three factors, there is a paucity of published evidence examining their relative contributions in any objective manner.Pathomechanical factors, for example, cannot be considered without accounting for the acute severity and pathobiological responses. If a joint has a high amount of damage from acute fracture severity, the surgery is more challenging and thereby less likely to restore surface congruity, leading to chronic joint pathomechanics. Conversely, poor surgical restorations also contribute to the PTOA rates seen when studying a spectrum of acute fracture severities as the more severe fractures are more likely to have poor restorations. Tying these factors together are the pathobiological responses that serve to potentiate PTOA as a disease as a direct result of these acute and chronic factors. For acute severity, in 2011, Tochigi et al. found that chondrocyte death propagates from the fracture edges[9]. Coleman followed this up with studies that outlined potential mechanisms of action for both acute and chronic factors related to chondrocyte respiratory function that cause cartilage degeneration toward PTOA[10, 11, 35]. These works have demonstrated an opportunity for intervention as we begin to understand potential methods to treat not only the chronic factors surgically, but the acute factors biologically[35].

It is in this context that the present work was performed to develop methods that enable injury severity and reduction accuracy to be well characterized in individual patients in order to study their relative contributions to PTOA risk. Method development was driven by two hypotheses. The first hypothesis is that the severity of articular injury correlates with reduction accuracy. It was posed to determine if this long held notion has an objective mechanical basis. The second hypothesis is that the injury severity more greatly influences PTOA risk than the reduction accuracy. This hypothesis is founded in the context of stagnant PTOA rates after injury despite ostensibly improved surgical care. These questions are central to the future of IAF treatment and could potentially have different answers in the context of different joints.

CHAPTER 2 – LITERATURE REVIEW

PTOA after intra-articular fractures

The clinical management of displaced IAFs focuses primarily on the surgical reduction and stabilization of articular fragments. However, even in the best of hands, an IAF still frequently leads to disabling PTOA. IAF commonly occurs in the hindfoot, ankle, knee, hip, and wrist; after IAF, PTOA occurs in 25-85% of these joints (Table 1). Across joints of the upper and lower extremities, the incidence of PTOA has remained stubbornly unchanged despite decades of improvements in technology and surgical management[7]. Marsh et al. 2002 first questioned the assumption that excellent surgical restoration will prevent PTOA, asking whether anatomic reduction improves outcomes. If it does not, then the acute severity of fracture may explain why PTOA rates have not changed.

Table 1. PTOA rates in joints of the upper and lower extremity after IAF

Site of IAF	PTOA Rate
Calcaneus[36-38]	85.7 (60.4-95.4%)
Distal Tibia[39-41]	48.1 (40.8-74.0%)
Proximal Tibia[42-45]	24.5 (11.0-36.5%)
Acetabulum[3, 29, 46]	27.9 (12.0-39.5%)
Distal radius[47-49]	43.4 (35.0-73.0%)

The idea that PTOA risk after IAF is related to the fracture type and its severity is widely held, even across different surgical treatment approaches[3, 50, 51]. Clinical assessment of IAF severity is most often completed using categorical classification systems or rank ordering for study of severity within a series. Using these techniques, some have even found that initial severity may be the primary determinant of PTOA development[51-55]. Conversely, it has also been found that different joints and even different areas within joints have different tolerances for articular reduction, most often quantified through step-off and gap measurements that are, unfortunately, insensitive and unreliable. Despite this limitation in measurement capability, articular reduction has been demonstrated to be an important factor in PTOA outcomes of acetabular fractures, with step-offs greater than 1 mm having fewer good clinical results[29]. By comparison, tibial plateau fractures are very tolerant of reduction inaccuracy with step-offs greater than 10mm showing acceptable functional results[3]. In other IAFs, like those of the tibial plafond, the impact of reduction is less clear with reduction being closely associated with injury severity. The fractures subjectively judged as most severe were considered to have the worst reductions while the cases that were least severe had the best reductions[55, 56]. This makes the impact of reduction challenging to disentangle from the injury severity. Therefore, in order to understand the development of PTOA and identify optimal strategies to treat it in each joint, careful, objective measurements are required along with knowledge of the general idiosyncrasies of each joint's characteristic tolerance to injury and reduction.

Radiographic grading of PTOA

Radiographic grading of osteoarthritis is also necessary in the study of PTOA development. The Kellgren-Lawrence (KL) classification system is a common scale used for grading osteoarthritis in articular joints. It is a widely accepted measure of arthrosis and has been shown to have good inter-observer reliability[57]. The KL classification is graded from 0 to 4 with grade 0 showing no signs of osteoarthritis, grade 1 having doubtful presence of joint space narrowing and osteophytes, grade 2 with definite narrowing and osteophytes, grade 3 with multiple osteophytes, definite narrowing, some sclerosis and possible deformity, and grade 4 presenting as large osteophytes, marked narrowing of the joint space, and severe sclerosis with definite deformity of the bone (Figure 1). Grades 2 and above are typically considered to mark the presence of PTOA development after injury.

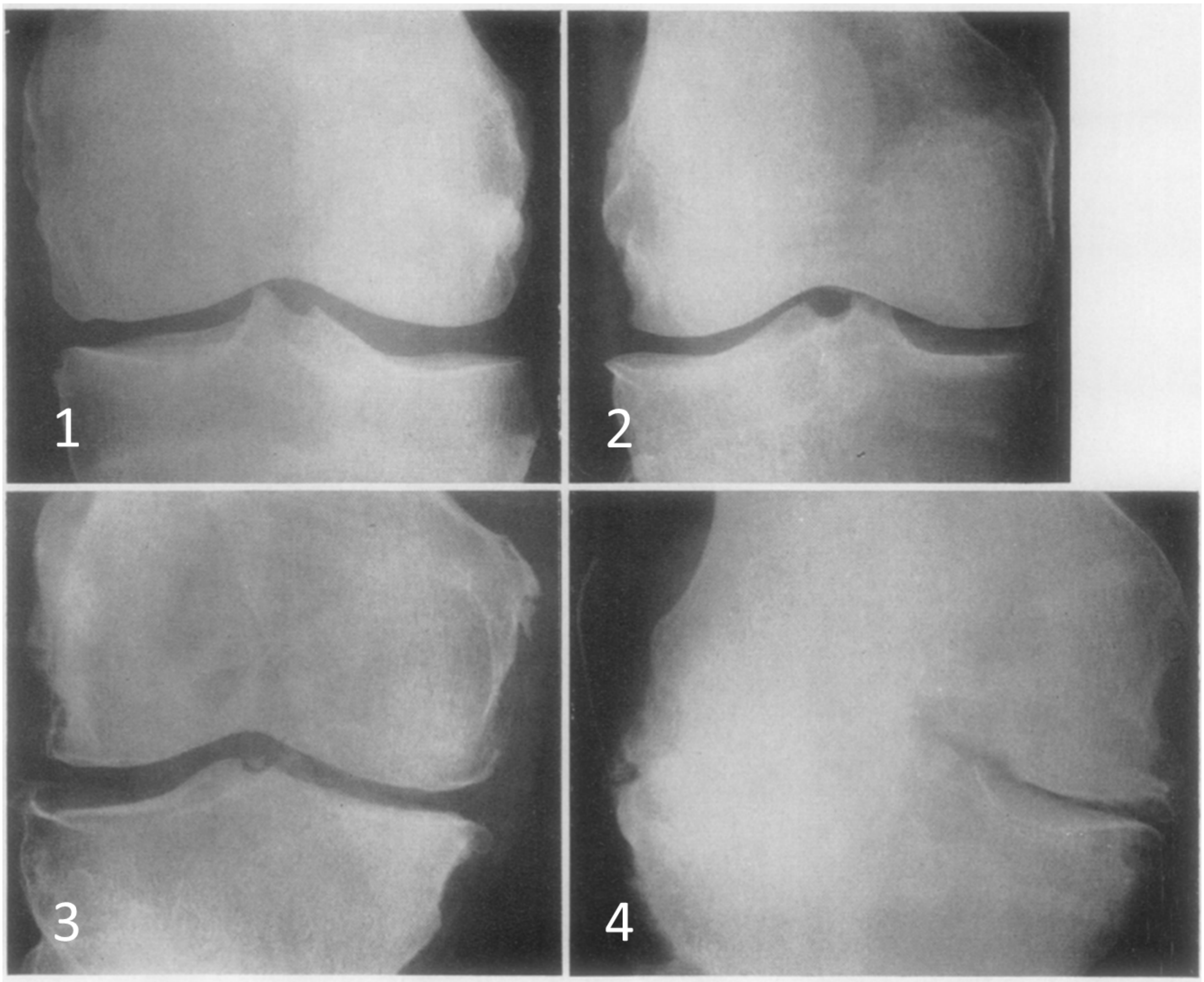

Figure 1. Kellgren-Lawrence classification grades 1-4 demonstrated in the tibial plateau (modified from original to label different grades)[57].

The Tönnis classification is another commonly used measure of radiographic arthritis that was specifically created for the hip. It is graded from 0 to 3 with grade 0 having no arthritis, grade 1 having increased sclerosis, minor joint space narrowing and no or minor loss of head sphericity, grade 2 having small bone cysts, moderate joint space narrowing and moderate loss of head sphericity, and grade 3 representing severe arthritis with large bone cysts, severe joint space narrowing/obliteration and severe deformity of the femoral head[58, 59] (Figure 2). Grades 2 and above are considered to indicate the presence of PTOA development but, occasionally, grade 1 has also been used.

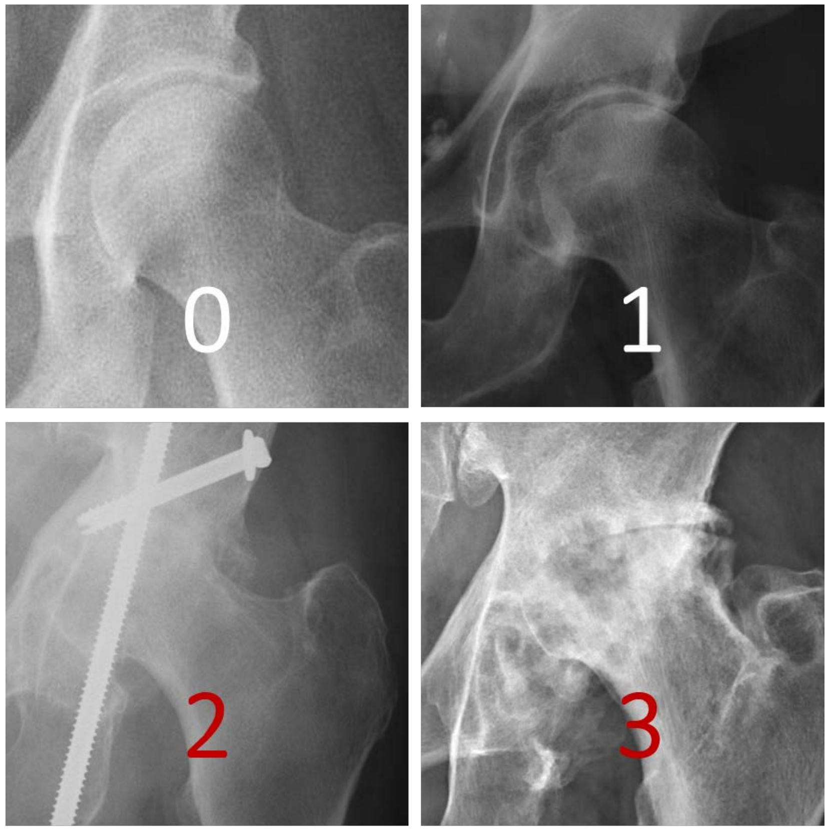

Figure 2. Tönnis grades 1-3 from the upper right to the lower right with grade 0, a normal hip, shown in the upper left.

<u>PTOA in calcaneal fractures</u>

Perhaps in no other joint is injury severity considered as central to PTOA outcomes as in the hindfoot after displaced intra-articular calcaneal fractures (DIACFs). Sanders et al. developed a classification for DIACFs based on evaluation of the number of fracture lines traversing the posterior facet[60]. In the original study, this Sanders classification was demonstrated to have a strong correlation with outcomes, with 73% of type II fractures repaired by open reduction and internal fixation having good clinical results compared to only 9% of type IV fractures that were similarly treated. A subsequent study of long-term follow-up found significant differences in rates of subtalar fusion between type II and III fractures with 47% of type III fractures requiring fusion compared to only 19% of type II fractures[38]. Comparing radiographic grading of arthritis, 70% of type II fractures and 90% of type III fractures had the highest two grades of arthritis. These findings are of particular interest as 95% of fractures were reported as having anatomic reduction postoperatively, defined as a step-off between 0 and 1 mm, indicating that differences in long term outcomes were due to differences in the initial injury. A study by Rao et al. found similar correlations in percutaneously reduced fractures with 46% of patients having Sanders type I or II fractures and 77% of those having type III and IV fractures developing PTOA. In this study, however, positive correlations that trended toward significance were observed between post-reduction step-off and both KL grade and Sanders classification. This could implicate surgical reduction as contributing to at least a small component of PTOA risk in DIACFs.

PTOA in tibial plafond fractures

Contributors to the development of PTOA after IAF in the tibial plafond are more complicated. Some clinical evidence has found reduction accuracy to be strongly correlated with PTOA development[61]. Mechanical studies have also found elevated contact stresses from mal-reduced fractures to be predictive of PTOA development[25]. Other clinical studies by DeCoster et al. found no difference in outcomes of patients with good and poor reductions[55]. A study by Etter and Ganz suggests that there are other factors at play as perfect reductions did not guarantee good outcomes[52]. But, as Marsh et al. noted, “one of the biggest challenges for research on the effect of articular reduction is to disentangle the effect of injury to the articular surface from … the reduction."[62] This is particularly true in the tibial plafond where there also exists a significant correlation between initial injury and outcomes. Studies of rank ordering of reduction quality and initial severity, and PTOA grade found significant correlations with both [55, 56]. Therefore, without the ability to accurately assess the degree of initial injury or the degree to which loading characteristics have been altered, it will not be possible to determine the influence of reduction quality on PTOA risk in fractures of the tibial plafond.

PTOA in acetabular fractures

Acetabular fractures, like calcaneal fractures, have a much clearer association between outcomes and predictors. In acetabular fractures, the literature provides a significant amount of evidence that accurate reduction is paramount in forestalling PTOA development[29, 63-66]. Matta was the first to classify acetabular reduction by measuring the residual incongruity between fragments as a step-off. His work established anatomic reduction as ≤1 mm of maximal articular displacement on any plain radiograph[65]. Reduction between 1 and 3 mm was considered satisfactory while reduction >3mm was unsatisfactory. For these three grades, he observed that anatomic reduction had 83% good clinical results while satisfactory had 68%; unsatisfactory reduction achieved good clinical results only 50% of the time. Subsequent studies found similar results with poor reductions strongly correlating to poor outcomes[27, 29, 66-68].

Despite significant study of reduction and outcomes in acetabular fractures, the effect of injury severity on acetabular fracture outcomes independent of reduction is unclear. Tannast, Najibi, and Matta studied the survivorship of 810 patients with operatively treated acetabular fractures but did not find significant differences in the survivorship by fracture type[27]. They did, however, find lower survivorship for cases having greater than 20 mm of initial displacement but did not report a correlation between reduction and displacement that may confound these results. Briffa, Pearce, Hill, and Bircher reported certain fracture types, specifically posterior column and T-shaped fractures, to have a statistically significant negative impact on outcomes[68]. Combined posterior wall and T-shaped fractures fared the worst. They claimed "[W]e may be reaching the limit of our operative capabilities, suggesting that the biology of the fracture (primary articular cartilage damage) has now become the limiting factor." However, they again did not report correlations between injury type and reduction in their series highlighting the need for objective measurement of both injury and reduction in clinical series to definitively determine their relative contributions.

Objective measures of acute severity

As detailed in the previous sections, PTOA risk is widely held to relate to fracture type and its severity, even across joints and different surgical approaches. However, none of the clinically available methods for assessing IAF injury objectively assess the severity of fracture. Instead, clinical fracture severity assessment has relied upon joint-specific categorical classification systems that have poor inter-observer reliability. As such, they fail to provide a consistent and continuous contextual indication of fracture severity as it relates to PTOA risk. To remedy these shortcomings, previous work was undertaken to objectively quantify IAF severity in a continuous manner. The methods were based upon the principle that mechanical energy is required to create new free surface area when fracturing a brittle solid and that the amount of energy required is directly related to the amount of de novo surface area. This approach was originally developed using laboratory models (first, a dense polyether-urethane foam bone surrogate material[17, 18] and then bovine bone segments[16]) and subsequently extended it to use in human clinical cases[15]. Over the past decade, these techniques have been further developed to enable larger-scale study of fracture severity in the clinical setting[1, 19, 20, 37].

Methods for computing fracture energy were originally developed using pre-operative CT scans of articular fractures along with their intact contralateral bones[1, 14, 20]. Idiopathic OA is rare in the ankle whereas PTOA commonly presents within a few years of tibial plafond fracture. This high propensity for PTOA makes study of these plafond fractures ideal for identifying factors that predispose joints to degeneration while avoiding potential confounding variables. These methods, therefore, segmented the boundary of all tibial fragments and on the intact contralateral to compute the surface area difference between them (Figure 3). The fracture energy was quantified by relating the energy absorbed to this computed fracture-liberated surface area and scaling it to account for variation in bone density. Articular comminution was quantified by determining the amount of inter-fragmentary surface area present within 1.5mm of the articular surface expressed as a percentage of the intact area on the same region of the contralateral distal tibia.

In these original studies, Thomas et al. found that fracture energies ranged from 5.2 to 27.2 Joules, and the articular comminution from 51 to 156%[1]. There were significant differences in fracture energy and articular comminution between the 11 patients that developed moderate to severe OA (KL≥2) and the 9 who did not (KL≤1). A combined injury severity score of both fracture energy and articular comminution was found to be highly correlated with PTOA development (R^2=0.70, Figure 4).

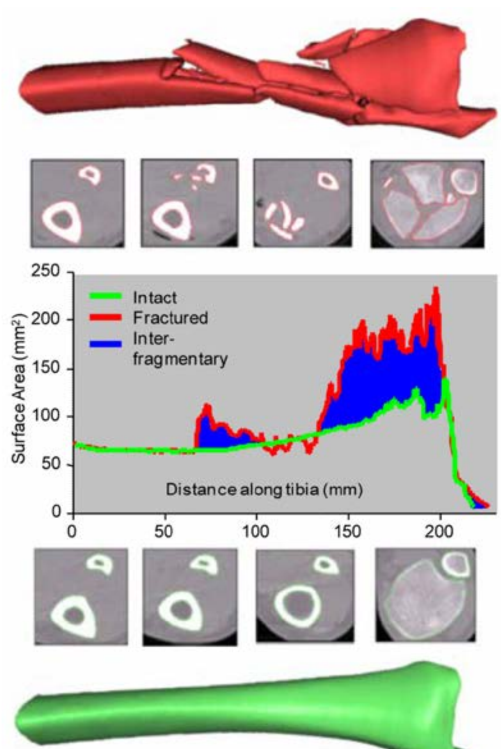

Figure 3. The surface area for the fractured (red) and intact contralateral (green) are plotted along the length of the tibia. The total inter-fragmentary surface area is graphically represented by the blue area between the intact and fractured curves. The severe disruption and fragmentation visible in the fractured metaphysis illustrate comminution[1].

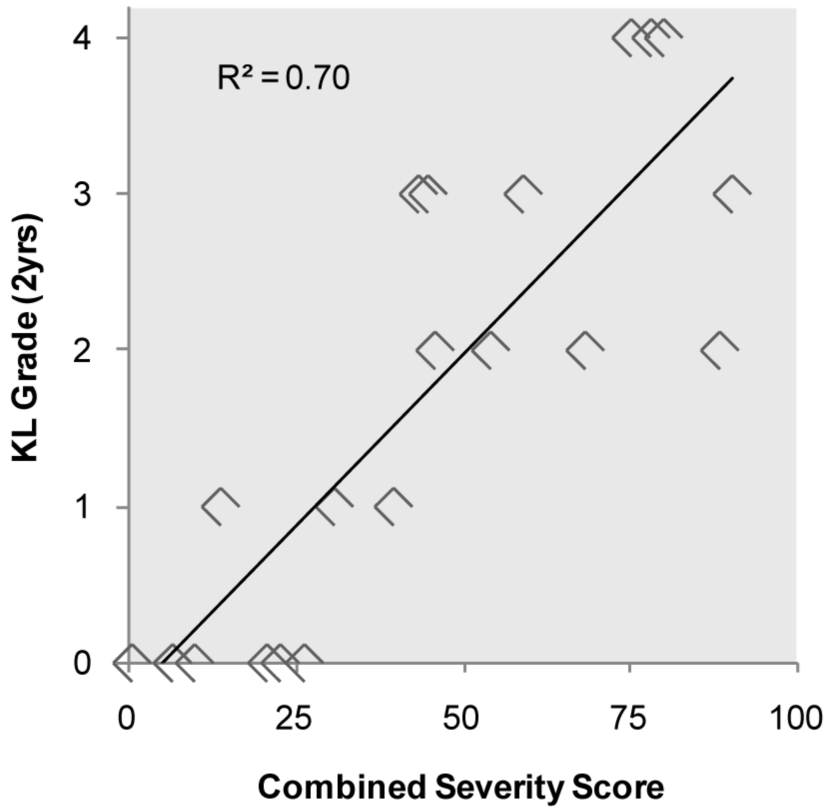

Figure 4. Linear regression modeled Kellgren-Lawrence (KL) arthrosis scores as a function of a combined severity score[1].

These results established fracture energy as an objective tool through which injury severity can be assessed. However, though their general concepts are translatable, the methods employed for measuring fracture energy and articular comminution were joint specific. They required an intact contralateral datum with which to compare liberated surface areas. Therefore, additional development was required to enable objective assessment of severity through fracture energy and articular comminution in joints outside of the tibial plafond.

Objective measures of surgical reduction

Though the pathogenesis and etiology of PTOA is not well understood, chronic exposure to elevated contact stresses resulting from residual articular surface incongruity have been implicated as an important mechanical factor. Surgical reduction is frequently assessed in literature by measuring the step-off or gapping left after fixation. These measures are understood to merely be surrogates for assessing the altered mechanical environment of the joint. Hadley, Brown, and Weinstein were among the first to report the adverse effects of elevated contact pressure on long term outcomes of hips[69]. Maxian, Brown, and Weinstein followed these results and were the first to establish preliminary thresholds for contact stress tolerance in cartilage of the human hip[70].

Anderson et al.'s work was the first to attempt quantification of these deleterious contact stress over-exposures using patient-specific finite element analysis (FEA)[71, 72]. Again, this work used IAFs of the ankle as a useful model due to the joint's low incidence of idiopathic PTOA and high incidence of PTOA within a few years of injury. This work quantified differences in contact stress exposures for fractured and intact contralateral ankles, identifying a strong correlation between the development of radiographic PTOA, as measured by KL grading two years postoperatively, and contact stress exposure.

Contact stress exposure was calculated across the tibial articulating surface using the following equation:

$$\hat{P}_{cumulative} = \sum_{i=1}^{13}((\hat{P}_i - P_d)\Delta t_i)$$

where $\hat{P}_{cumulative}$ was the spatial distribution of per-gait cycle cumulative contact stress over-exposure, expressed in MPa-seconds; $\hat{P}_i$ were the computed contact stress magnitudes at each node, with i varying across 13 loading increments over the stance phase of gait; $P_d$represented the scalar contact stress damage threshold taken only from those nodes where $\hat{P}_i$ was greater than

P_d, nodes where $\hat{P}_i$ was less than P_d where excluded from analysis; and Δt_i was the time, in seconds, associated with a given increment in the gait cycle.

In these studies, however, it has remained unclear whether injury severity remains linked to poor reductions or whether accurate reduction of the articular surface can improve patient outcomes. Larger cohorts of subjects are required to sufficiently answer these questions but model building in FEA is cumbersome and articular contact remains a challenge. This is especially true in cases where residual incongruities of the articular surface require substantial effort to be expended in mesh generation. To resolve these problems, Kern and Anderson developed a discrete element analysis (DEA) contact model of articular fractures[33].

DEA models contact between cartilage surfaces as a bed of compressive-only springs distributed over an implicit (not explicitly included in computation) rigid bony surface. While FEA runs take on the order of hours, run time for DEA models take on the order of minutes, facilitating patient-specific modeling. Kern and Anderson expanded its use to report contact in both intact and fractured human ankles. In this DEA formulation, surfaces were triangulated and springs along the contact surface were oriented along each triangular face's surface normal, with an un-deformed length equal to its associated cartilage thickness. The cartilage surface was modeled as a bed of compressive springs spanning from the articular surface to a rigid attachment at the implicit underlying subchondral bone surface. Contact was defined between intersections of apposed surfaces. Within intersecting regions, compound springs were created across the total cartilage thickness of the joint. Each spring responds according to Hooke's law:

$$f = kd$$

where f is the force exerted by the spring along its normal direction, d is the spring deformation, and k is the spring constant as a function of the cartilage Young's Modulus, E, Poisson's ratio, v, the length of the spring created from combined articular cartilage thicknesses, l, and the area of the spring's associated triangular surface, a, where

$$k = \frac{(1-v)E}{(1+v)(1-2v)}\frac{a}{l}$$

They validated DEA-computed contact stress using previously reported human cadaveric data[73]. Finally, they confirmed the utility of DEA contact stress computation in place of FEA for determining PTOA risk from contact stress over-exposures. A subsequent validation study was also performed for a model of contact stress in acetabular fractures by Townsend et al.[74].

Summary

Up to now, study of the interplay between acute and chronic mechanical factors has been limited due to the lack of ability to rapidly and objectively assess the pre-operative severity of the fracture and the postoperative mechanical environment of the joint. Fractures of the tibial plafond have proven useful in establishing objective methods that can achieve this goal by analyzing both acute and chronic mechanical contributors to PTOA development on a patient-specific basis. With the advent of fracture energy analysis and patient-specific discrete element analysis, we are now able to more comprehensively evaluate the interplay of these factors and to determine their relative contributions to patient outcomes across joints. This offers the unique opportunity to answer lingering questions posed in each joint as to the relative role that initial injury severity vs. surgical reduction quality play in PTOA risk. Specifically, we will seek to address two hypotheses: that severity of IAF fracture correlates with reduction quality and, subsequently, that the acute mechanical damage more greatly influences PTOA. To test these hypotheses, we will expand upon previous methods to create DEA models with relevant boundary conditions in the hip, ankle, and hindfoot as well as to develop and implement measures of fracture severity that can be utilized in all these joints. In conjunction with the recent investigations elucidating the pathobiological changes and mechanisms of PTOA development, this work aims to leverage patient-specific assessment capabilities toward a unifying understanding of all mechanical aspects of PTOA development.

CHAPTER 3 - METHODS

Improving measures of intraarticular injury severity

Fracture energy and articular comminution were previously established as objective measures of injury severity in the tibial plafond that are predictive of PTOA risk. It remained to be determined, however, whether these injury severity measures are likewise predictive of PTOA risk in other joints. To answer this question, major limitations of the previous analysis methods had to be addressed. Specifically, this involved eliminating the need for an intact contralateral datum and expediting the analysis time. Methods from work detailed below formed the foundation for establishing a fracture energy measure that could be extended to any joint. The following section will detail these methods and how they were expanded upon.

Fracture energy computation

The fracture energy computation requires 3d surface models of fractured bone. This involves segmenting CT scans of the fractured limbs to identify and separate bone fragments. Individual bone fragment volumes were identified using a semi-automated watershed transform-based algorithm implemented in MATLAB (The Mathworks, Natick, MA, USA) from purpose written code originally developed by Thomas, Kern, and Anderson [75]. Errors in separation of fragments were corrected using a custom graphical user interface written in MATLAB. From these segmentations, 3d models were produced and analyzed to identify new surfaces of bone liberated by the fracturing process. The procedure for identifying these surfaces relied heavily upon a surface classification algorithm trained to recognize fracture liberated surfaces based upon geometric and image intensity features (detailed below).

After segmenting bone fragments from CT scans, the resulting segmentations, stored as NIFTI files, were loaded into ITK-SNAP to correct errors and inconsistencies in the segmentation. After corrections were completed, ITK-SNAP was utilized to export all fragments as individual binary STL models, the 3d model format later used in delineating intact and fractured surfaces so that the interfragmentary fracture-liberated area could be quantified (Figure 5).

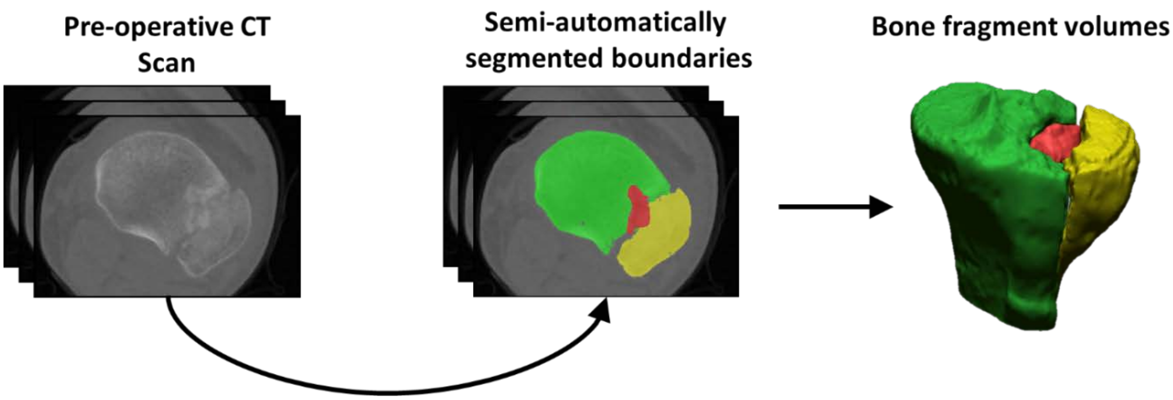

Figure 5. Semi-automated identification of bone fragments from preoperative CT imaging (colors represent each individually identified fracture fragment).

STL models were then imported into Geomagic Design X (3DS Systems, Rock Hill, SC), where a smoothing process was used to remove stair-step artifacts from the voxellated segmentations and a decimation routine was used to attain a more accurate representation of the bony surface in preparation for subsequent fracture severity computation. Each properly prepared STL surface file of a fracture fragment was then saved to be imported into the MATLAB bone surface classification algorithm (Figure 6 and Figure 7).

The classification of separate bone surfaces was performed to distinguish inter-fragmentary bone from intact bone to use in the subsequent computation of severity. Several optimally segmented and prepared sets of intact and fractured bone were painstakingly manually identified to be used in training a classifier implemented through the MATLAB function ‘predict’. This function implements the results of several machine learning classification strategies and options after training. Specifically, an ensemble of bagged decision trees was eventually used based on the promise it exhibited in preliminary studies. Bootstrap aggregation (bagging for short) is a powerful ensemble method that combines predictions from different machine learning models together to make a more accurate prediction than the constituent individual models. Bootstrap aggregation is generally applied to reduce the variance for algorithms that have high variance like the decision trees implemented herein. Initial training of the models was also performed in MATLAB using the ‘fitensemble’ function with the ‘bag’ option for classification using more than three predictors.

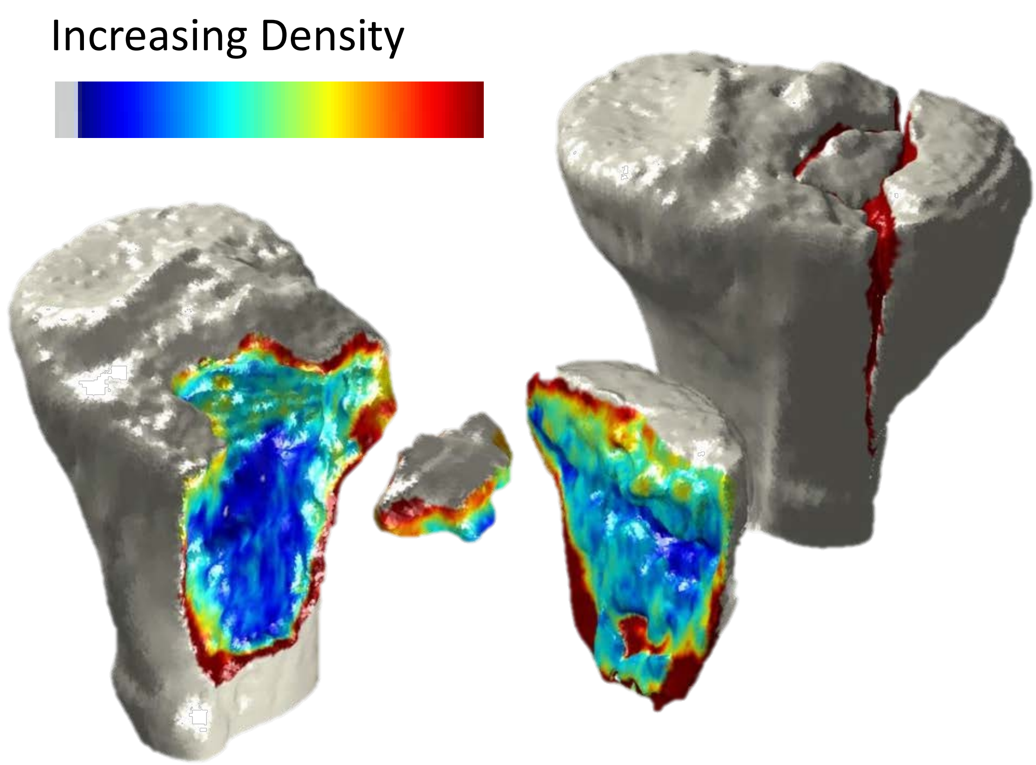

Figure 6. 3D surface models of the fractured bone for use in delineating intact and fractured surfaces so the interfragmentary fracture-liberated area could be quantified.

There were eight features selected for the classifier training task to aid in the optimal separation of intact and fractured bone surfaces. There were six image intensity-based features and two geometry-based features. The image intensity-based features were CT Hounsfield units, the image sheetness (second derivative of image intensity), and variations of the two at different depths from the normal direction of the bone model surface. The image sheetness is capable of detecting both direction and magnitude of edges, contrasted against original CT data. Obtaining the CT Hounsfield units was accomplished by sampling into the CT image at five depths along the normal direction of the surface of the STL model from 0mm to 2mm at 0.5mm intervals at each vertex. The mean, standard deviation, and difference in HU between the 0mm and 2mm depths were computed on the normal image and sheetness image and constituted the six image intensity-based features used in classification.

The geometry-based features were obtained purely from the STL model vertices without relation to the image intensity data. Minimum, maximum, and Gaussian curvatures were computed for each vertex. The Gaussian curvature is computed from a multiplication of the minimum and maximum curvatures, and only the maximum and Gaussian curvatures were used for classification purposes. They were selected to help the classifier better detect regions as intact bone when they have lower curvatures, because fractured bone surfaces tend to have much higher curvatures.

These features were then passed to the classifier which, based on the training data cases, computed the probability of a surface element as being from a fractured surface. The classifier was retrained for each different joint as needed to provide optimal identification of differences in intensities of fracture-liberated surfaces across highly varied bones like the dense, highly curved acetabulum from the flatter, less dense subchondral bone of the tibial plateau.

After classification of each vertex is computed, the identification of fracture-liberated surfaces was completed by a minimum-cut/maximum-flow graph cut algorithm. If this step was not included, the surface would be divided into heterogeneous regions of improperly classified vertices scattered throughout. Therefore, to achieve homogenous intact and fracture-liberated regions, the graph cut was performed. For the edge costs of the graph to decide where the cut should be made, predicted classification probabilities and surface curvatures were used (normalized between 0 and 1).

After the graph cut was performed to obtain a preliminary separation of the fracture-liberated surface regions, any spurious region classifications were manually corrected through a 3d user interface programmed in MATLAB. The interface consisted of a window displaying all fragments in their classified forms with the ability to select misclassified fragments. Selected fragments could then be independently opened to correct errors in classification. Errors in classification frequently occurred in cortical regions of high curvature.

Severity computation

Once fracture-liberated surfaces were identified, they could then be utilized to create an estimate of the energy involved in creating the fracture. The faces of each bone fragment that contained two or more vertices classified as fractured (after the graph cut) were included in the fractured area computation. The CT Hounsfield Unit (HU) intensity previously sampled at each of the three vertices in each face classified as fractured were averaged to obtain an approximation of bone density at the area of that face. Fracture energy was determined from these data using the following equation:

$$Energy(J) = \frac{1}{2} * [SA_{liberated}(m^2)] * \left[\left(\frac{HU}{10^{2.87}}\right)^{\left(\frac{1}{1.45}\right)}\left(\frac{g}{m^3}\right)\right] * \left[\frac{12000}{1.98}\left(\frac{J * m}{g}\right)\right]$$

where the first term, SA, is the liberated surface area, here scaled by $\frac{1}{2}$ to account for only the new surface area generated along the plane of fracture and not counting both sides of the fracture plane as it is segmented; the second term in brackets represents the density derived from the CT Hounsfield Unit intensity, HU in the equation, as empirically derived by Snyder et al. in 1991; the third bracketed term is the strain energy release rate, or the density-dependent energy scaling factor, empirically determined by Beardsley and first implemented by Thomas[1, 15, 17, 76]. The interfragmentary bone demonstrated in Figure 8 is shown with the densities mapped in color. The density, calculated in the second portion of the equation, is reported in grams/meter^3. The energy release rate is the same across all cases and the density does not account for patient factors such as age or gender. While this is a limitation, it has been established in prior work that such differences were relatively minor in the context of the articular fractures studied.

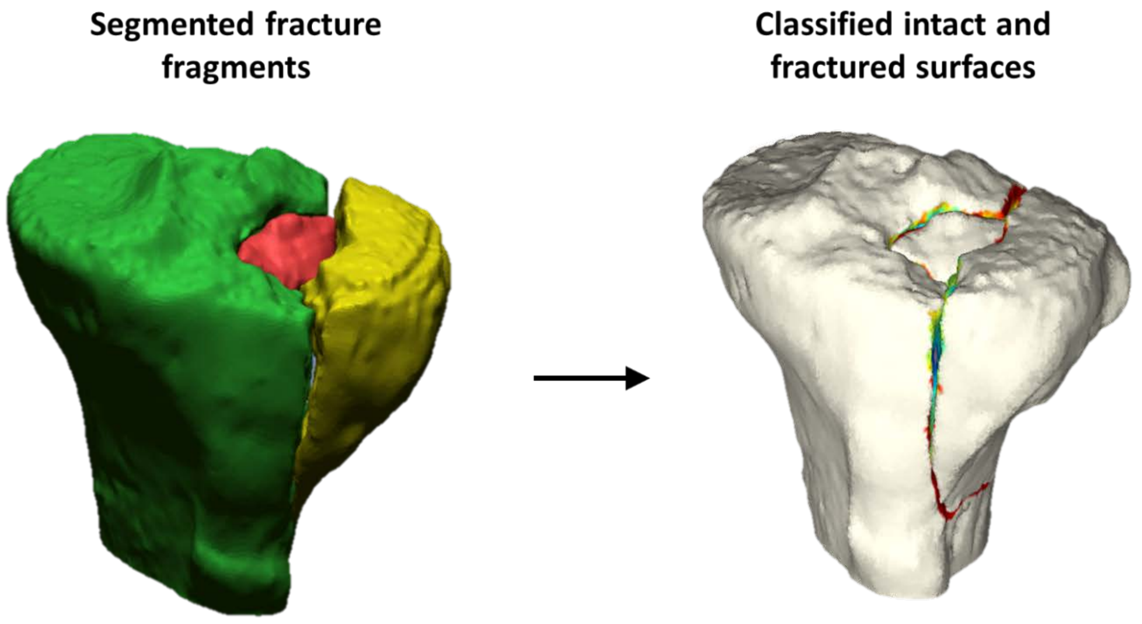

Figure 7. 3D models of the bone fragments are classified into intact and fracture liberated surfaces.

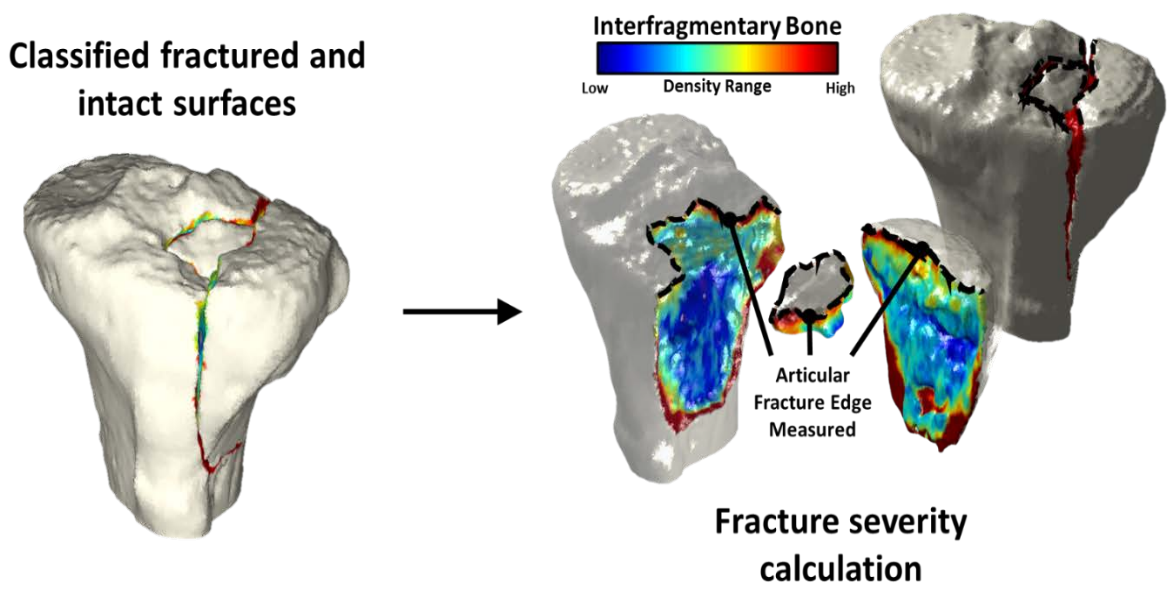

Figure 8. A graph cut was implemented to define the boundary between intact and fractured bone on each fragment so the fracture energy and articular fracture edge length could be computed.

Articular comminution and area measurement

Developing a new metric for computing articular comminution that can be applied in different joints was a priority of this work. Previously, the articular comminution measure had been computed as the interfragmentary surface area present within 1.5mm of the articular surface, expressed as a percentage of the surface area over the same portion of the intact datum tibia. It was only slightly correlated with the fracture energy measure (R^2=0.20) but when combined with it, yielded a significant correlation with outcomes. Therefore, keeping with these principles, but removing the requirement for the intact datum, a technique to examine the fracture energy within 1cm of the articular surface was developed. This necessitated the identification of the subchondral bone surface from the rest of the interfragmentary and intact bone. To accomplish this, a classifier was trained on subchondral bone surface geometries.

The classifier for identifying the subchondral bone surface regions utilized the same image intensity- and geometry-based features that had been previously used to aid in the identification of fracture-liberated bone area. The image-based features were the mean, standard deviation, and difference in intensities sampled at 0 mm and 2 mm into the bone surface from the STL models of the fragments for both the standard HU values and the sheetness image intensity values. The geometry-based features were the maximum and Gaussian curvatures. More so than for the interfragmentary bone surface classifier, the subchondral bone surface classifier required training for each individual joint to account for large differences in articular features across joints (Figure 9).

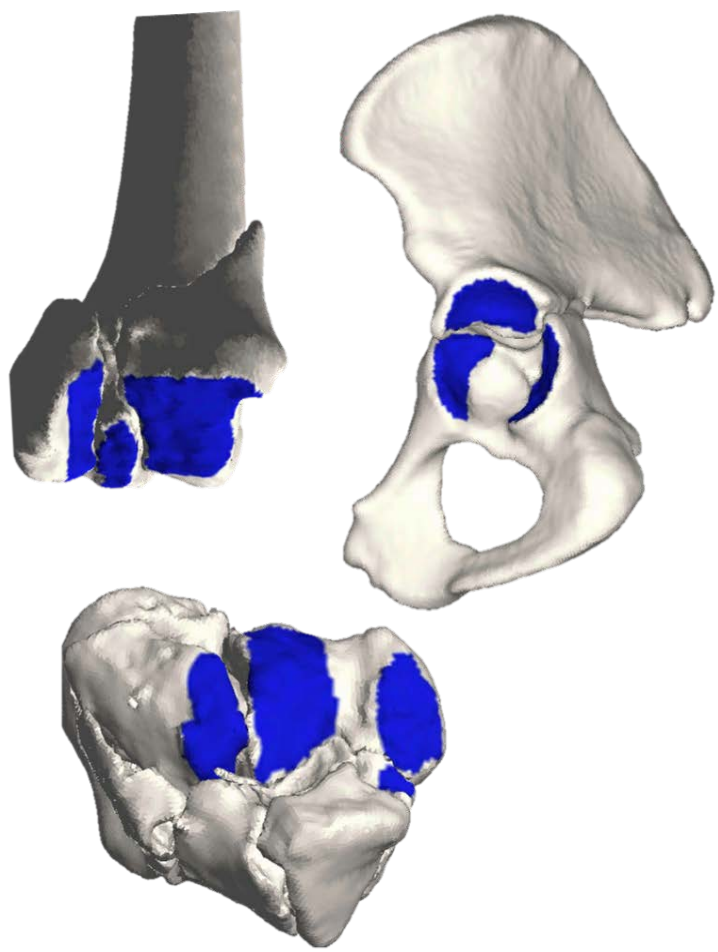

Figure 9. Vastly different articular geometries of articular surface that required classifier re-training.

A manual editing process of the subchondral bone surface classification was implemented in a similar manner to what was done for the interfragmentary bone surface classification. A key difference was that computation of the subchondral bone surface classification was limited to only fragments that were identified as containing components of the articular surface. This expedited computational efficiency and enabled for more rapid computation of the fracture energy within 1 cm of the subchondral bone surface.

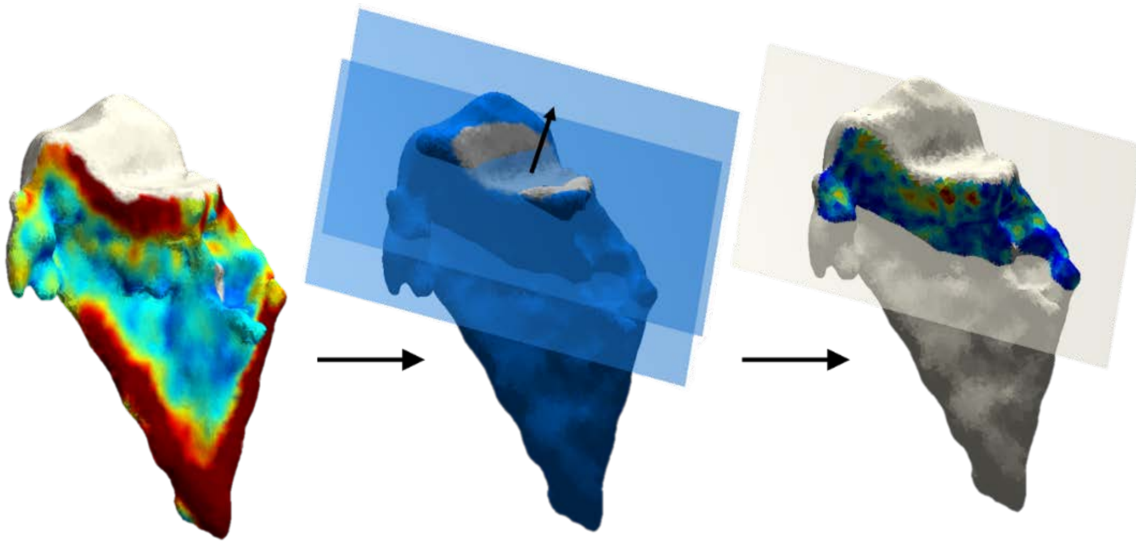

Figure 10. Subchondral energy measurement process. Previously classified (as intact or fracture liberated surface) articular fragments (left) have their subchondral surfaces identified through classification (middle), and subchondral energy is measured 10mm into the surface (shown in color on the right down to a plane marking 10mm into the bone) from the inverse of the average normal plane direction (shown with the arrow and two planes in the middle) of the articulation.

This articular comminution energy, or the subchondral energy, was computed after the finalized classification of both interfragmentary bone and subchondral bone surfaces. The subchondral energy was computed along the average normal of the subchondral bone surface pointing away from the articular surface as demonstrated in Figure 10. Liberated areas above the plane were also included in the computation to ensure that all energy was captured. This would be expected to lead to a slight overestimation of the subchondral energy but ensures that all energy is captured along curved surfaces.

A secondary benefit to the computation of subchondral bone surface energy is the implicit task of identifying the articular surface. This enables a trivial computation of the articular surface area to provide an area-normalized comminution metric. When axial fracturing impacts are delivered to a joint, energy transfer is distributed over the articular surface through the contact area. A metric of fracture energy scaled by area, therefore, is appealing in the context of assessing likely cartilage insult at the tissue level. As contact areas are more challenging to obtain but are related to joint size and surface area, this articular area measure could provide a reasonable estimate to control for differences in damage caused by differences in energy distribution (i.e. energy per unit area). The correlation between contact area and surface area for each joint studied is explored in the following sections. Fracture energy itself is a representation of how badly the bone in its entirety was disrupted, i.e. the damage at the bone level. As the energy of articular fractures necessarily must involve the articular surface, it is likely also distributed over that articular surface area. Therefore, to control for variable joint sizes both within and between bones and to provide an estimate of the damage done to the cartilage tissue by the energy passing through it, the area over which that energy passes can be used to normalize energy and potentially provide an improved estimate of IAF damage.

Normalized fracture severity study

The ability of the new fracture energy measure to explain differences in PTOA rates across fractures of five different joints (subtalar, ankle, knee, hip, and wrist) was studied. To enable comparisons of the fracture energies across different joints, we normalized by characteristic joint-specific contact areas. For this study a database of 319 patients having sustained IAFs that had been originally enrolled for fracture energy study without normalization were examined. Patients were selected for having pre-operative CT scans available for IAFs of the distal radius (n=22), acetabulum (n=79), proximal tibia (n=88), distal tibia (n=82), and calcaneus (n=48). An Institutional Review Board approved use of the imaging and patient data collected in the course of their standard-of-care clinical treatment.

Fracture energy was obtained for all fractures included in the study using previously validated, objective analysis methods working from preoperative CT scans [1, 14, 19]. In lieu of patient-specific contact areas that were not estimated, peer-reviewed literature was queried for generally accepted averages of the relevant contact areas (Table 2). Similarly, in lieu of appropriate duration longer-term clinical follow-up data for each individual patient, we again turned to the published literature to find average rates of PTOA development for each of the joints as a point of comparison. For consistency across the studies, we defined PTOA as being present in joints when the Kellgren-Lawrence radiographic grade was greater than or equal to two[3]. A summary of the PTOA rates for each joint and the source papers can be found in Table 2.

Table 2. PTOA rates and contact areas in the upper and lower extremity

	PTOA Rates	Contact Area (cm^2)
Calcaneus[36-38, 77-79]	85.7 (60.4-95.4%)	3.90 (3.10-5.36)
Distal Tibia[39-41, 80-82]	48.1 (40.8-74.0%)	6.28 (4.40-7.34)
Proximal Tibia[42-45, 83, 84]	24.5 (11.0-36.5%)	11.08 (10.65-11.50)
Acetabulum[29, 46, 74, 85-87]	27.9 (12.0-39.5%)	19.03 (14.70-26.77)
Distal radius[47-49, 88, 89]	43.4 (35.0-73.0%)	1.87 (1.00-2.74)

Finally, to explore how acute fracture severity influences PTOA risk after IAF, we first examined correlations between the computed fracture energies and published PTOA rates. Then an additional data analysis step involved likewise examining correlations between contact area-normalized fracture energies and PTOA rates. Pearson's correlations were computed to determine the significance of the relationships between joints.

<u>Surface area-normalized fracture energy as a patient-specific predictor of PTOA risk in individual joints</u>

After completing the previous study, the next logical step was to test patient-specific correlations between surface area-normalized fracture energy and actual (rather than prior published group average norms for) PTOA outcomes. This involved the analysis of 190 patients having sustained IAFs in a multi-institutional study. Patients were selected for having pre-operative CT scans and a minimum of 12-month radiographic follow-up available for IAFs of the calcaneus (n=48), distal tibia (n=71), and acetabulum (n=71). An Institutional Review Board approved the use of the imaging and patient data collected during the course of their standard-of care clinical treatment.

Fracture severity was analyzed for all fractures included in the study using previously validated, objective analysis methods on pre-operative CT scans. During axial fracturing impacts, energy transfer is distributed over the articular surface through the contact area. In lieu of computing patient-specific contact areas for such circumstances and to enable comparisons across joints, we normalized to patient-specific joint surface areas. Therefore, the first step in this study was to determine how well correlated average contact areas were with joint surface areas. This was completed by comparing the results of the literature review for contact area (as reported in the previous study above) with the average surface areas for these calcaneal, distal tibial, and acetabular fracture cases. Table 3 shows a comparison of these averages. As might be anticipated due to highly varied loading and geometric characteristics across joints, joint classified surface areas did not directly correspond to the literature reported values of contact area. The acetabulum and plafond showed surface areas were around 125-135% of the literature reported contact areas while the calcaneus was over 200% the size. The larger difference in the calcaneus is partially attributable to how it was measured. Literature only reported contact areas of the posterior facet of the calcaneus while the classifier described herein was also trained to identify the middle facet. The surfaces included for each joint are shown classified in blue in Figure 9. Of note is the inclusion of the entire sourcil in the acetabulum, the exclusion of the medial malleolus in the distal tibia, and the inclusion of the middle facet in the calcaneus. The criteria for inclusion was straightforward: all potential axial load bearing regions that frequently contained primary fracture lines were included in the surface area computation as these were the regions most likely to have the energy of impact transferred through them and damage is assumed to result from this energy transfer.

Table 3. Comparison of surface areas and average contact areas in the lower extremity.

	Surface Area(cm^2)	Contact Area (cm^2)
Calcaneus[36-38, 77-79]	8.11±1.24	3.90 (3.10-5.36)
Distal Tibia[39-41, 80-82]	8.06±1.94	6.28 (4.40-7.34)
Acetabulum[29, 46, 74, 85-87]	25.09±4.44	19.03 (14.70-26.77)

Follow-up was defined by radiographic measures of PTOA. In the calcaneus and distal tibia, the Kellgren-Lawrence (KL) radiographic grade was used, while in the acetabulum, the Tönnis grade was used. This was done because the joint-specific Tönnis grade has been shown to better reflect OA status in the hip than does the KL grade. The KL scale is graded from 0 to 4, where grades 2 and above are generally considered to represent the presence of arthritis. The Tönnis scale is graded from 0 to 3 where grades 2 and 3 are generally considered to represent arthritis. For consistency, analyses across joints were completed using only the binary PTOA status (i.e. presence or absence as defined radiographically above).

To explore how acute severity influences PTOA risk after IAF, Spearman correlations between fracture energy and the radiographic measures of PTOA for each joint. Finally, to determine if there exists a unified threshold above which joints progress to PTOA, logistic regressions were performed for each joint.

Discrete element analysis

Discrete element analysis (DEA) modeling, as described in the literature review, is a technique that models cartilage as a deformable bed of springs over an implicit rigid bone surface. The specifics of the computational implementation are described in the literature review and are performed in Matlab on the order of seconds rather than the hours required for finite element analysis (FEA)[33]. DEA was first implemented to study a limited series of fractures in the tibial plafond as a proof-of-concept and to get a general idea of the stresses seen in articular cartilage after fracture reconstruction. Building from these studies, several important considerations also hold true for DEA modeling in reconstructed IAFs across different joints. Due to the large amount of metal near the articular surfaces of reconstructed IAFs, MRI is precluded from providing measurements of local cartilage thickness. In the ankle, a uniform cartilage thickness assumption proved adequate for generating DEA models of contact stress that were similar to a physical validation model. This assumption is carried forward to models of the subtalar joint, where accurate identification of the articular cartilage thickness is not possible from post-operative CT scans but prior studies have established normative values of the cartilage thickness. Additionally, DEA contact patches are very similar in size and shape to those produced via FEA but they tend to produce consistently higher contact stress values. Therefore, the magnitudes of contact stress results should be interpreted with caution in a relative fashion, with DEA models being compared only with DEA models in the same joint or potentially by scaling them to comparable FEA models.

Analysis of results and PTOA development

Contact stress over-exposure

DEA-computed contact stress distributions are obtained throughout the stance phase of gait as implemented. In an effort to link contact stress to PTOA risk after IAF, a previously developed paradigm for evaluating the contact stress over-exposure was used. As contact stresses are not all deleterious in nature, this paradigm implements a threshold to exclude healthy stresses so that a potentially harmful per gait cycle over-exposure can be computed. The threshold was selected by performing a parameter sweep of all reasonable cutoffs for over-exposure, from 0 to 15 MPa. The optimal cutoff was selected by determining the highest number of correct selections for cases that developed PTOA. The results were then reported as MPa*s exposures, deriving from the equation described in the literature review on pages 15 and 16 where the amount of time (in seconds) joints were exposed to suprathreshold stresses was multiplied by magnitude of the stresses (MPa) to obtain the exposure (MPa*s). The P_d cutoff described in this equation as the damage threshold was then used for later statistics and comparisons.

Injury severity comparison

To better understand potential connections between injury severity and reduction accuracy, injury severity assessments were performed on all cases from pre-operative CT scans. The fracture energy, articular comminution energy, and joint area were analyzed. The fracture energy was normalized to joint area as an estimate of energy per unit area dissipated over the articular surface. The articular comminution energy, as described above was then combined with the normalized fracture energy to test if a composite score was more predictive of PTOA development. A final composite measure was created by combining the injury severity and reduction accuracy components of composite severity and contact stress over-exposure, respectively. The composite scores were then analyzed using receiver operating characteristic (ROC) curves to assess sensitivity and specificity and the area under the curve (AUC) was measured to provide metric of performance.

Contact stress over-exposure in the tibial plafond after IAF

Prior studies have examined the contact stresses as a measure of both the surgical reduction's ability to restore the mechanics of the joint after IAFs of the tibial plafond and how they relate to PTOA development. Those studies examined a series of 11 cases where 10 had sufficient follow-up and DEA results while nine had adequate pre-operative CT for fracture severity to be measured. This study expanded to 16 cases with pre- and post-operative CT scans to enable objective measurement of both IAF injury and reduction for comparison to PTOA.

Patient Selection and outcomes data

After obtaining IRB approval, cases selected for analysis were drawn from a clinical series of 36 patients sustaining unilateral tibial plafond fractures. Patients were chosen to represent the spectrum of severity from partial articular fractures to highly comminuted fractures involving the entire joint surface. Fractures were initially treated using a spanning external fixator and subsequent screw fixation of the articular surface. They were assessed as having varying degrees of residual incongruity.

Model generation

The cartilage geometries from the first nine cases with adequate imaging and follow-up reported from previous studies were utilized in this study[33, 90]. These cases were previously segmented from post-operative CT using iso-surfacing in OsiriX (Osirix software, www.osirixviewer.com) and repaired and smoothed using Geomagic Studio (Geomagic Studio; Geomagic, Research Triangle Park, NC)[90]. For the other seven cases, bony geometries of the tibia and talus were segmented from the post-operative CT scans using a semi-automated watershed transform-based algorithm implemented in MATLAB (The Mathworks, Natick, MA, USA) from purpose written code originally developed by Thomas, Kern, and Anderson.[87] Errors in separation of the bones were corrected using a custom graphical user interface written in MATLAB. The resulting NIFTI files were then loaded into ITK-SNAP to correct minor errors in the subchondral regions of the tibia and talus. Geomagic Design X (3D Systems Inc., Rock Hill SC) was used to repair and smooth the final bone models. As contrast-enhanced post-operative CT arthrographic imaging failed to reliably provide adequate cartilage imaging, a uniform 1.7mm cartilage projection was made by extrusion from the subchondral bone along the normal direction of the smoothed surfaces.

Anatomical alignment

CT data were acquired with patients supine and their ankle joints planar-flexed and externally rotated. Therefore, their posture was not a functionally neutral pose for the stance phase of walking and required alignment. The first nine cases were previously aligned by an experienced ankle surgeon to a neutral weight-bearing apposition using a procedure that involved working from weight bearing radiographs when available. A local coordinate reference frame was defined based on anatomical landmarks and centered in the talus. The flexion/extension axis of the ankle was defined along a line connecting the centers of the circles fitted to the condylar arcs of the talar dome. The origin was along this line splitting the distance between the two arcs of the talus. A projection of the primary axis onto a plane normal to the flexion/extension axis was used to define a second axis. Tibial and talar surfaces were translated together to ensure the talus' anatomic coordinate system was appropriately aligned to the global reference frame. The flexion/extension axis was defined as the global x direction and was sued to align the talus with the first metatarsal at 15° below horizontal. The tibia was then aligned so the angle between the shaft and the floor was 85°. The second 9 cases were aligned to the results of this robust initial alignment in Geomagic Design X. The medial-lateral x-axis was defined via the central axis of a fitted cylinder and the origin and second axis were defined as previously described. The final orientations of the bones were obtained by aligning them to one of the first 9 cases that they best matched anatomically.

Boundary conditions

Boundary conditions for the models were chosen to replicate the original DEA and FEA studies[33, 90]. The simulations were performed over the stance phase of gait using 13 quasi-static loading steps in which the ankle undergoes a flexion/extension arc ranging from 5° of plantar-flexion to 9° of dorsiflexion (Figure 11). During each quasi-static step in the flexion/extension arc, the tibia is axially loaded according to the forces reported for post-operative patients and proportional to the subject body weight and constrained in all directions except superior and inferior translation along its long axis. The talar rotations were free except flexion-extension, which was constrained to maintain the appropriate position for that stage of gait. Talar translations were free in all directions except for superior and inferior movement to resist the forces applied by the tibia. In every stage of the stance phase of gait the simulation prescribed the flexion-extension of the talus beneath the tibia as dictated by its position within gait. A fibular restraint was added to emulate the ankle mortise, modeled as a linear spring acting laterally on the talus, resisting medial-lateral translation from the initial position of the talus (spring constant = 100N/mm)[33, 90].

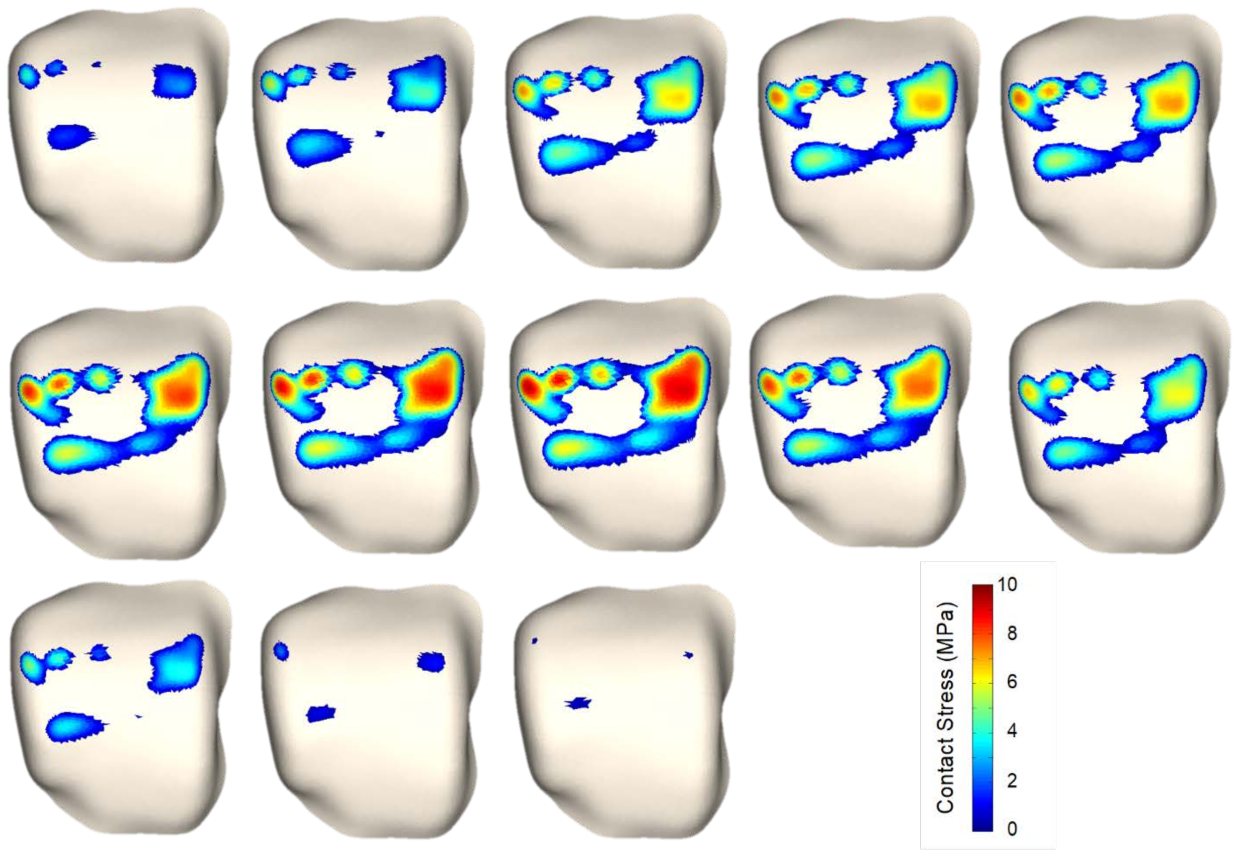

Figure 11. Contact stress (pressure) distributions on the superior dome of the talus after IAF of the tibial plafond. From the top left to the bottom right is heel-strike through toe-off of the 13 steps the stance phase of gait was discretized into. Top is anterior and left is lateral.

<u>Contact stress over-exposure in the calcaneus after IAF</u>

Patient Selection and outcomes data

To investigate the mechanical factors at play in the development of PTOA, contact stress was computed on patients with reconstructed intra-articular calcaneal fractures. Patients were chosen as a sample of convenience from a larger series of patients previously analyzed for fracture energy. Pre-operative scans were analyzed for fracture energy to determine the severity of the initial injury and post-operative CT scans were analyzed for contact stress to evaluate the joint mechanics after surgery. After obtaining Institutional Review Board (IRB) approval, thirty-six patients with 48 DIACFs were selected for study from among 153 patients that had been treated. The patients selected were age ≥ 18 years, had available electronic pre-operative and post-operative CT scans, and good quality post-op and follow up radiographs. Patients age < 18, extra-articular fractures, patients without pre-op CT scans, patients without post-op CT scans, and follow up < 18 months were excluded. Final selection for inclusion in this study was determined by convergence criteria in the contact stress modeling. Failed models were excluded.

Model Generation

Calcaneal and talar geometries for each patient were extracted from post-operative CT scans using the same semi-automated watershed-based algorithm from the plafond study (Figure 5). Errors in the automated surface detection and separation protocol were manually corrected using ITK-SNAP and STL models were exported. The triangulated surface models produced had residual artifact from voxelization of the anatomy, so they were subsequently smoothed and resampled to remove any errors and irregularities in the mesh (Geomagic Design X software, 3D Systems Inc., Rock Hill SC). Articular cartilage surfaces were approximated by projecting the calcaneal and talar subchondral surfaces of the posterior and middle facets a uniform distance of 1 mm. This projection was taken from literature values sampling from a healthy joint[91].

Therefore, cartilage in the fractured joints was assumed to be healthy at the time of injury with thicknesses maintained after surgical reduction. Additional considerations from these normative data are that the edges of the articular surfaces be tapered. Therefore, the cartilage surfaces were subsequently projected back toward the subchondral bone by 1 mm to simulate the natural tapering of cartilage thickness toward its outmost edges.

Anatomical alignment

The models were aligned to neutrally opposed bones in a weight bearing CT-scan of a well reduced calcaneal fracture not contained within the examined dataset. This case was selected to be representative of an average post-operative reconstruction from a series of 10 candidate cases. The alignment procedure was completed in Geomagic Design X by first aligning the talus of the representative bone to a global coordinate system centered at the subtalar joint [92]. The footpad of the WBCT was segmented and used to define the z-axis as orthogonal to it. The x and y planes were taken to be at the slot center of the subtalar joint. The y-axis was defined from the intersection of the plane defined by approximating the long axis of the third metatarsal (obtained with a cylinder fit) and a point passing through the center of the heel (taken from the mean of the heelpad segmentation) and orthogonal to the plane defined by the origin and orthogonal z-axis. The x-axis was orthogonal to this line and the z-axis defining and just

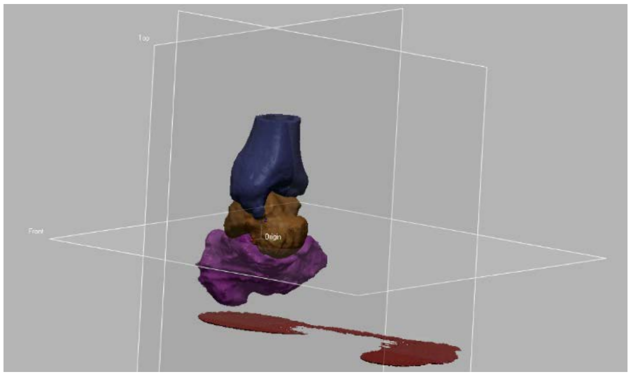

Figure 12. Alignment models segmented from weight-bearing CT with planes defining the appropriate alignment positions.

below the axis about which planar and dorsiflexion occur. The alignment models are shown in Figure 12.

Boundary conditions

Similar to the tibial plafond model, the boundary conditions were chosen to simulate the stance phase of gait in 13 quasi-static loading steps. Kinematics of the joint motion were defined by Arndt et. al.'s study using intracortical pins to assess relative talocalcaneal motion[92]. Talocalcaneal forces were defined from heel strike to toe-off from Giddings 2000 study of forces during walking[93]. As the Giddings study simulated healthy gait, a correction of the maximum forces was applied to reduce peak forces to 68% of their peak to match the post-operative forces observed in gait in the Stauffer et. al study(reported as over 500% of body-weight in the

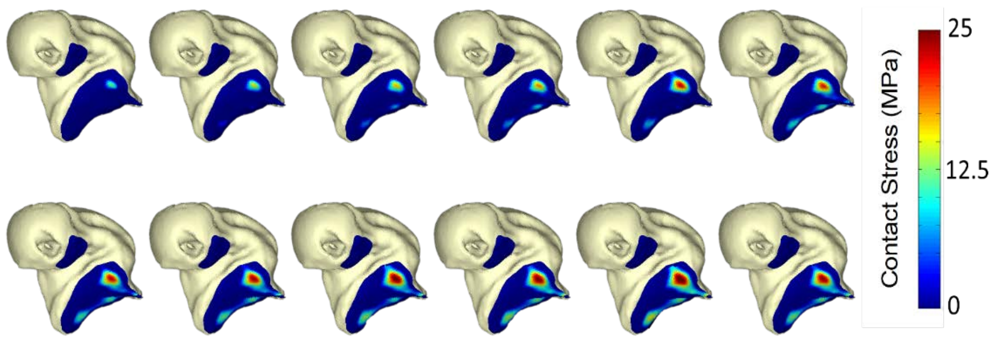

Figure 13. Inferior view of contact stresses on the talus after IAF of the calcaneus. From the top left to the bottom right are the 12 discretized steps of the gait cycle analyzed. The top is anterior and left is medial.

Giddings study)[94]. Patient-specific weights were utilized to be scaled by the percent of body-weight forces reported across the prescribed gait cycle. The talus was allowed to freely translate over the calcaneus with rotations rigidly prescribed in accordance with each quasi-static loading step. Anterior-posterior motion and medial-lateral motion were restricted with 350 N/mm springs to simulate the boney constraints of the navicular and forefoot as well as the strong ligamentous attachments. With these parameters the models were then analyzed using DEA to evaluate contact stress.

Contact stress over-exposure in the acetabulum after IAF

Patient Selection and outcomes data

After obtaining Institutional Review Board (IRB) approval, a series of 75 patients at a single institution who had undergone operative fixation of acetabular fractures between 2004 and 2016 were identified for having pre-operative and post-operative CT scans. Patients were excluded from study for having less than two-year radiographic follow-up, being under the age of 18 at the time of surgery, undergoing arthroplasty within the same hospital admission, or if they had associated femoral head fracture. Twenty-four patients declined to participate or were unreachable. Ten patients had undergone surgery within the past two years and thus did not have 2-year radiographic follow-up. One patient was 17 at the time of surgery. Of the remaining 40 patients, 22 patients had adequate imaging and follow-up available for contact stress analysis. A total of 19 had adequate imaging and follow-up for both fracture energy and contact stress analysis.

Radiographs obtained at a minimum of 12 months were evaluated for arthritic changes by two independent evaluators. Each evaluator assigned a Tönnis grade to each hip using the modified Tönnis grading description scale [95]. When there was disagreement between observers, an arbitrator (MW) reviewed the studies and determined Tönnis grade. Patients having Tönnis grades 0 and 1 were included in the no PTOA group and Tönnis grades 2 and 3 were included in the PTOA group. Those patients who went on to total hip arthroplasty were considered as Tönnis grade 3 equivalents for radiographic purposes.

Contact Stress Analysis

Femoral and pelvic geometries for each patient were extracted from post-operative CT scans using a semi-automated watershed-based algorithm (Figure 14). Errors in the automated surface detection and separation protocol were manually corrected, and triangulated surface models of the anatomy were generated and smoothed (Geomagic Design X software, 3D Systems Inc., Rock Hill SC). Articular surfaces were approximated by projecting the acetabular and femoral subchondral surfaces a uniform distance of 1 mm then subsequently smoothing the projected surfaces toward sphericity using a custom iterative smoothing algorithm[74]. The resulting approximations of the chondral geometries have been previously shown to yield accurate contact stress computations, even from fractured surfaces.

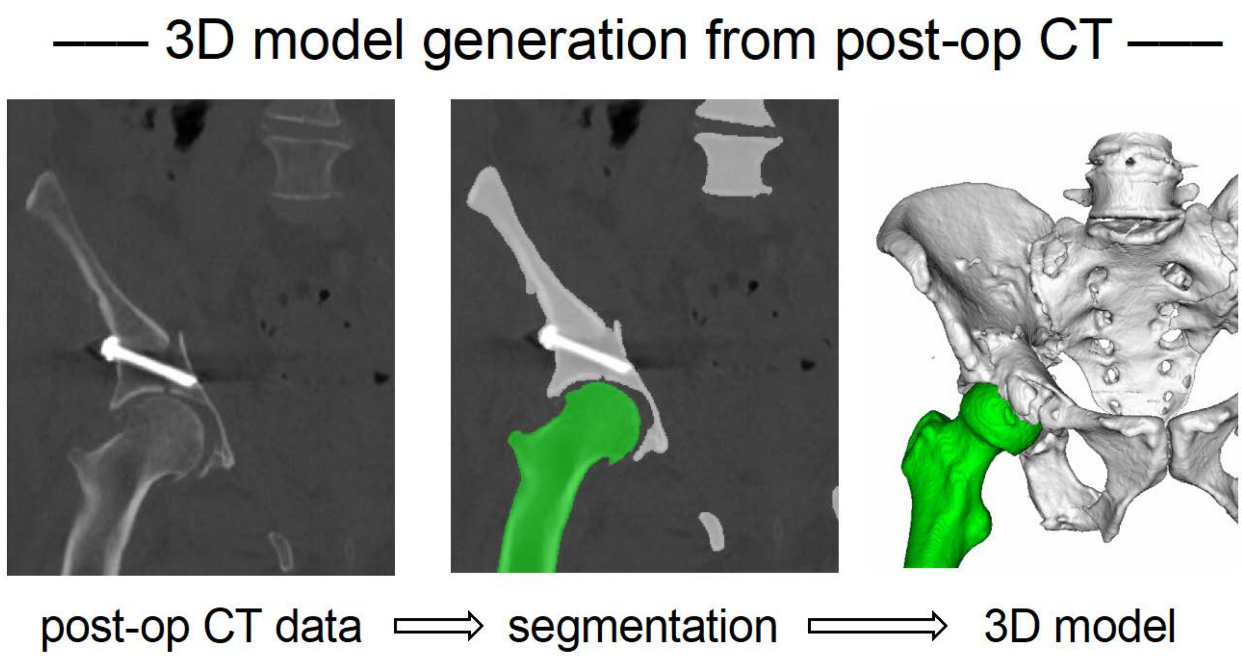

Figure 14. Patient-specific 3D models of the hip were generated from post-operative CT scans of the surgically reduced acetabular fractures.

The models were aligned to the hip joint coordinate system defined by Bergmann et. al. (2001) based on patient-specific anatomic landmarks on the bone surface models[2]. DEA was used to compute contact stress over an entire gait cycle for each case. Boundary conditions for forces and rotations were based on patient-specific body weights and were defined by the Bergmann et. al. study (2001) from instrumented total-hips[2]. The stance phase of gait was discretized into 13 quasi-static time steps to facilitate direct comparison of the resulting contact

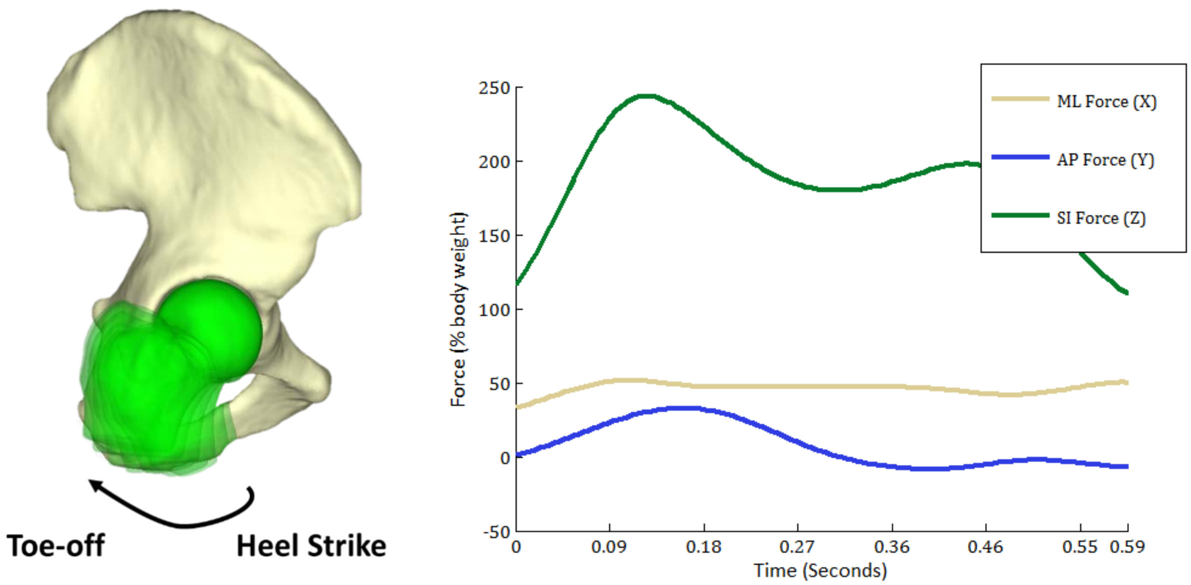

Figure 15. The gait cycle was discretized into 13 quasi-static time steps (shown overlaid on one another to the left) with forces and rotations obtained form the Bergman gait data (right) [2].

stress distributions (Figure 15 and Figure 16). Forces were applied to the femur and directed toward the hip as dictated by the Bergmann data. Cartilage was assigned isotropic linear-elastic material properties (E=8MPa, v= 0.42).

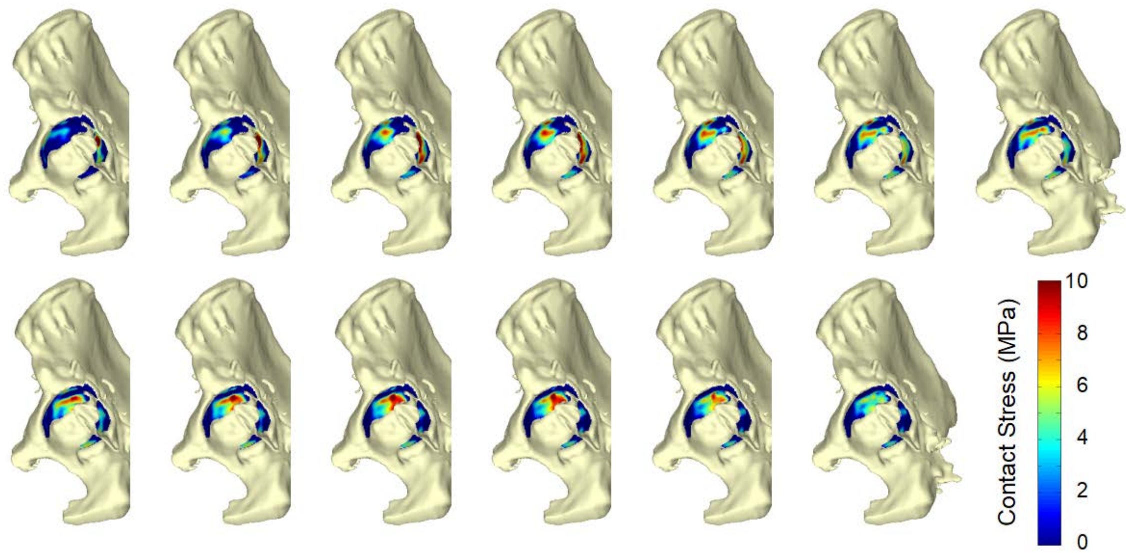

Figure 16. Contact stress distributions are computed at each of the 13 loaded poses to replicate the entire stance phase of gait.

Statistical Models of injury severity and reduction

The purpose of these studies was ultimately to determine the effect of articular reduction and injury severity on patient outcomes in various joints. Unpaired t-tests were used to compare results between the no PTOA and PTOA groups (defined as KL and Tönnis Grades ≥2). Spearman's rank-order correlations were computed to evaluate correlations between patient factors, predictors, and the ordinal radiographic outcomes. Spearman's correlations were used as the outcome variable was categorical in nature and therefore, not as amenable to study by Pearson's correlations which can consider continuous predictor and outcome variables.

CHAPTER 4 - RESULTS

Contact area-normalized fracture energy as a predictor of PTOA risk:

Initial data on contact area-normalized fracture severity was obtained from the literature normative reported values for contact area and PTOA rates across different joints. The fracture energies for all cases analyzed, measured as delineated in the methods above, ranged from 0.9 to 41.9 (J). The range of fracture energies for calcaneal fractures was 14.2 to 26.2J, for distal tibial fractures it was 0.9 to 38J, for proximal tibial fractures it was 3.2 to 33.2J, for acetabular fractures it was 4.5 to 41.9J, and for distal radial fractures it was 2.8 to 9.0J. The fracture energies (mean ± standard deviation) were 19.3±3.1J for calcaneal fractures, 15.3±7.3J for distal tibia fractures, 13.1±6.5J for proximal tibia fractures, 16.9±8.9J for acetabular fractures, and 4.9±1.8J for distal radius fractures. The distribution of energies was highly dissimilar between a number of these groups with no overlap whatsoever between the calcaneal and distal radius fractures (Figure 17).

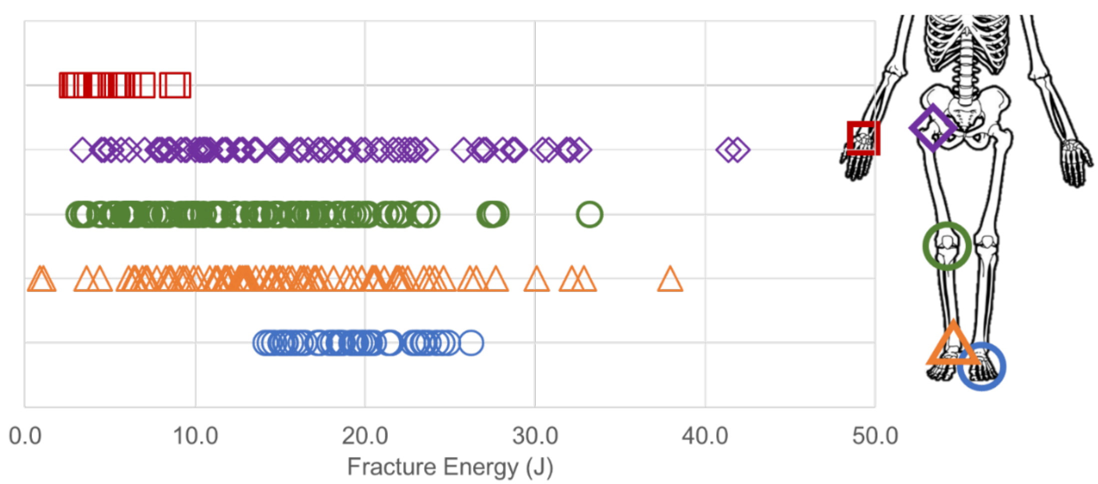

Figure 17. The distribution of fracture energies for calcaneal, distal tibial, proximal tibial, acetabular, and distal radial fractures.

The contact area-normalized fracture energies ranged from 0.14 to 6.73 J/cm^2 for all cases. The range of contact area-normalized fracture energies for calcaneal fractures was 3.63 to 6.73 J/cm^2, for distal tibial fractures it was 0.14 to 6.04 J/cm^2, for proximal tibial fractures it was 0.28 to 2.92 J/cm^2, for acetabular fractures it was 0.18 to 2.20J/cm^2, and for distal radial fractures it was 1.49 to 4.81 J/cm^2. The contact area-normalized fracture energies (mean ± standard deviation) were 4.94±0.79 J/cm^2 for calcaneal fractures, 2.44±1.17 J/cm^2 for distal tibia fractures, 1.16±0.57J/cm^2 for proximal tibial fractures, 0.89±0.47 J/cm^2 for acetabular fractures, and 2.59±0.94 J/cm^2 for distal radius fractures. There was a trend toward decreasing energy in joints going from distal to proximal in the lower extremity with distal radial fractures having energies in the middle of the range (Figure 18).

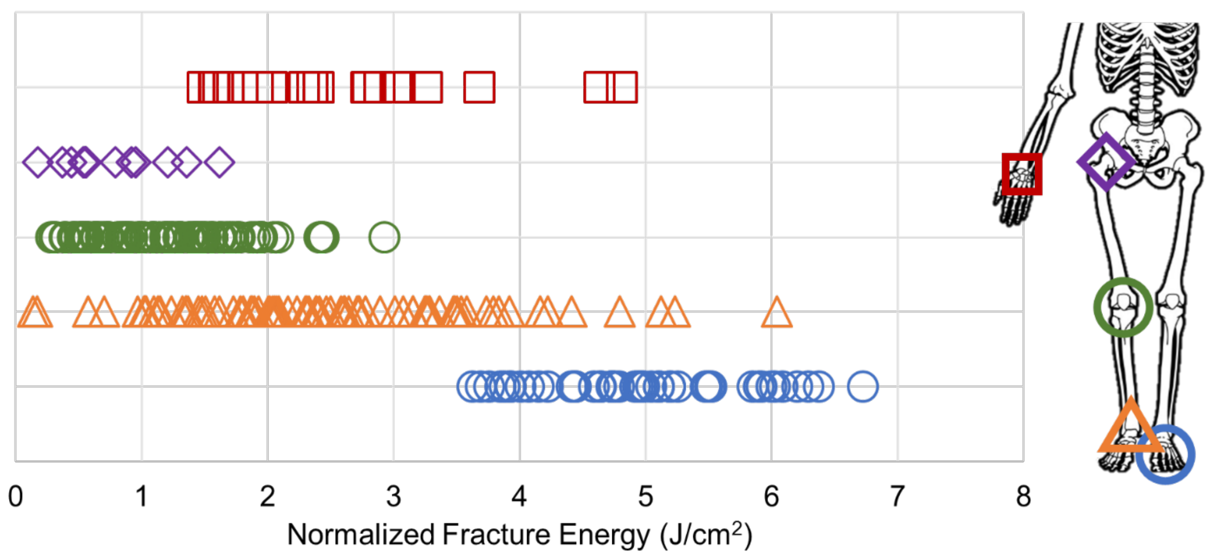

Figure 18. The distribution of fracture energies for calcaneal, distal tibial, proximal tibial, acetabular, and distal radial fractures scaled by the average contact area for each joint.

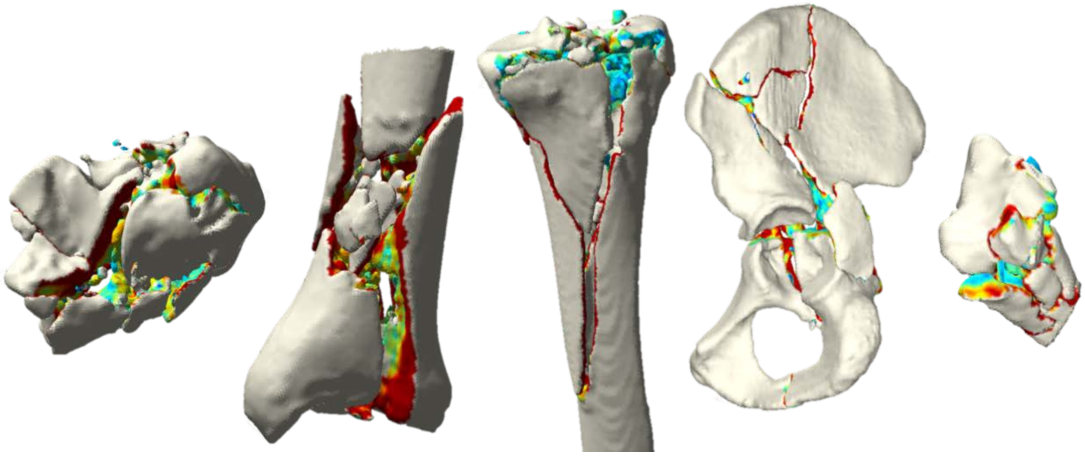

Figure 19. High energy fractures have similar characteristics across joints with many fragments, significant comminution, and disruption of the articular surface.

Qualitatively, high energy fractures in all five joints shared similar characteristics having similar size, number, and dispersion of fragments (Figure 19). Fractures at the lower energy end of the spectrum, however, did not demonstrate such similarities. When comparing fractures of similar energy across joints, there were perceptible differences in their appearance. An 8J fracture in the ankle can appear relatively minor while an 8J fracture of the distal radius can have a highly comminuted joint space with large diaphyseal extensions. Comparing joints with similar contact area-normalized fracture energies showed more consistent appearance across joints. A 4.29 J/cm^2 fracture of the distal radius is similarly comminuted with diaphyseal extension as is a 4.19 J/cm^2 fractures of the distal tibia (Figure 20).

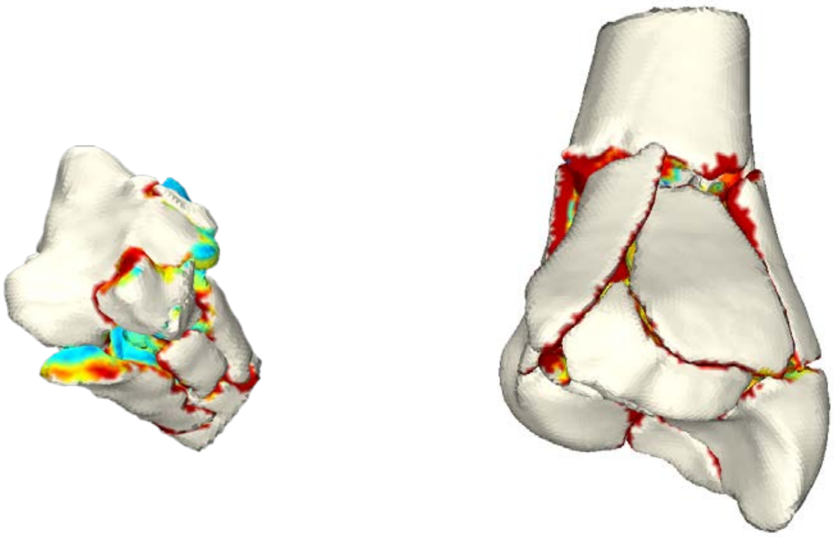

Figure 20. A 4.29 J/cm^2 fracture of the distal radius and a 4.19 J/cm^2 fracture of the distal tibia. Similar scaled fracture energy values tend to have visually similar degrees of damage.

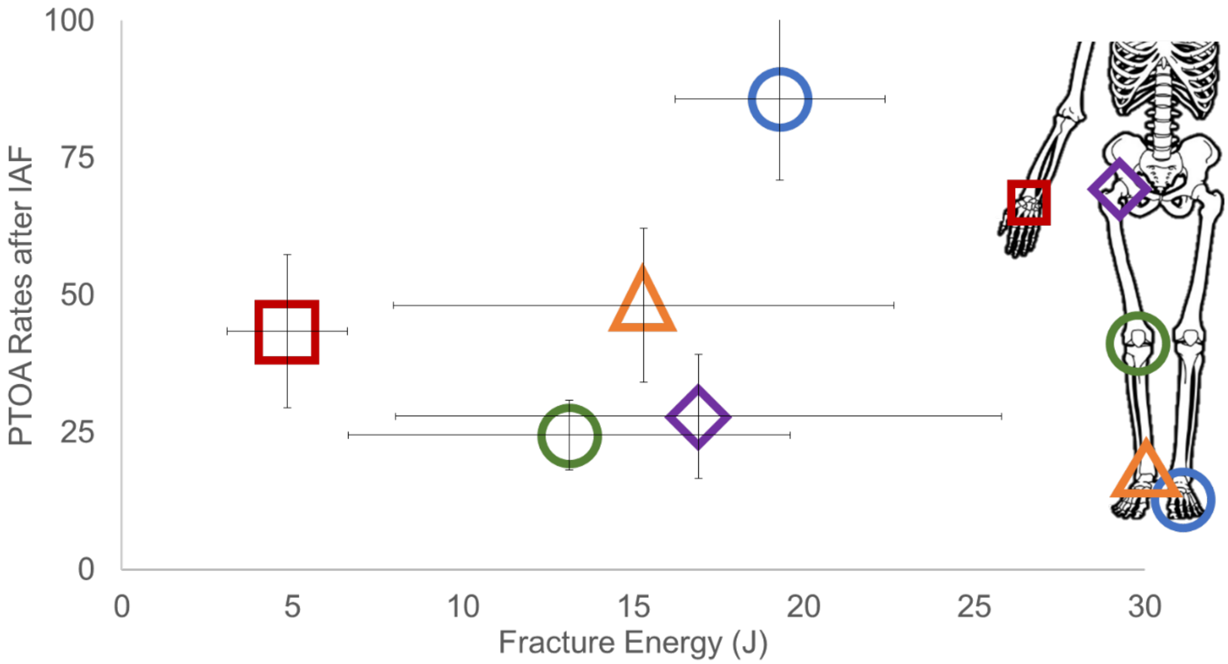

Figure 21. Fracture energies do not correlate with published rates of PTOA across the joints studied.

The computed fracture energies showed no correlation whatsoever with the published rates of PTOA across the joints studied (Figure 21). However, there was a highly significant correlation between contact area-normalized fracture energies and the rates of PTOA (Figure 22). The primary limitation to this study's results is that it is based on normative values of contact area and therefore cannot be interpreted on a patient-specific basis. Interpretation of these results is also limited by fact that it did not differentiate between groups for age, size, and gender differences.

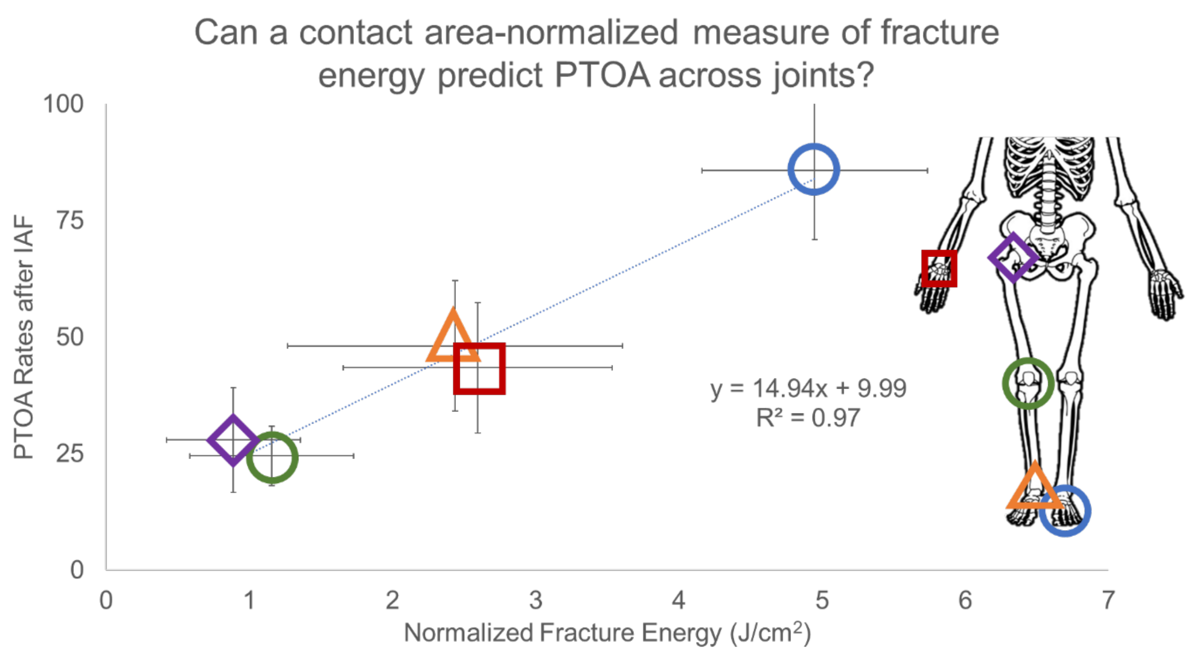

Figure 22. Area-normalized fracture energies have a highly significant correlation with rates of PTOA.

Articular surface area-normalized fracture energy as a predictor of patient-specific PTOA development in individual joints

Overall, 56.8% (108/190) of the patients studied developed PTOA by the time of their last radiographic follow-up. The PTOA rate in the plafonds studied was 52.1% (37/71), in the calcaneus it was 60.4% (29/48), and in the acetabulum it was 59.1% (42/71); PTOA rate was determined by a KL grade and Tönnis grade cutoff of ≥2 indicating the development of radiographic arthritis. The cases reported were not consecutive series and may have some selection bias, as the PTOA rates observed for them are not consistent with those previously reported in literature: 70-75% in the plafond[39], 83-92% in the calcaneus[38, 60], and 11-38% in the acetabulum[85].

As noted above, fracture energy ranged from 0.9 to 41.9J (17.7±7.5 J) for all cases. Fracture energies in patients who developed PTOA were significantly higher than those in the patients who did not (19.3±7.3 vs 15.5±7.1, $p<0.001$). Fracture energy in the tibial plafond ranged from 0.9 to 30.1J (14.6±6.5 J), in the calcaneus it ranged from 14.1J to 26.2J, and in the acetabulum it ranged from 4.5 to 41.9J (19.7±9.3J). Fracture energy was significantly higher in patients that developed PTOA in the plafond ($p=0.011$) and acetabulum ($p=0.021$), but not in the calcaneus ($p=0.51$).

Patient-specific contact area-normalized fracture energy ranged from 0.09 to 3.57 J/cm^2. The normalized fracture energies in patients who developed PTOA were significantly higher than in those who did not (17.5±8.8 vs 13.9±8.1, $p=0.004$). Normalized fracture energies ranged from 0.09 to 3.42 J/cm^2 (1.84±0.76 J/cm^2) in the tibial plafond, 1.24 to 3.56 J/cm^2 (2.42±0.47 J/cm^2) in the calcaneus, and 0.14 to 1.95 J/cm^2 (0.79±0.36 J/cm^2) in the acetabulum. The normalized fracture energy was significantly higher in patients that developed PTOA in the

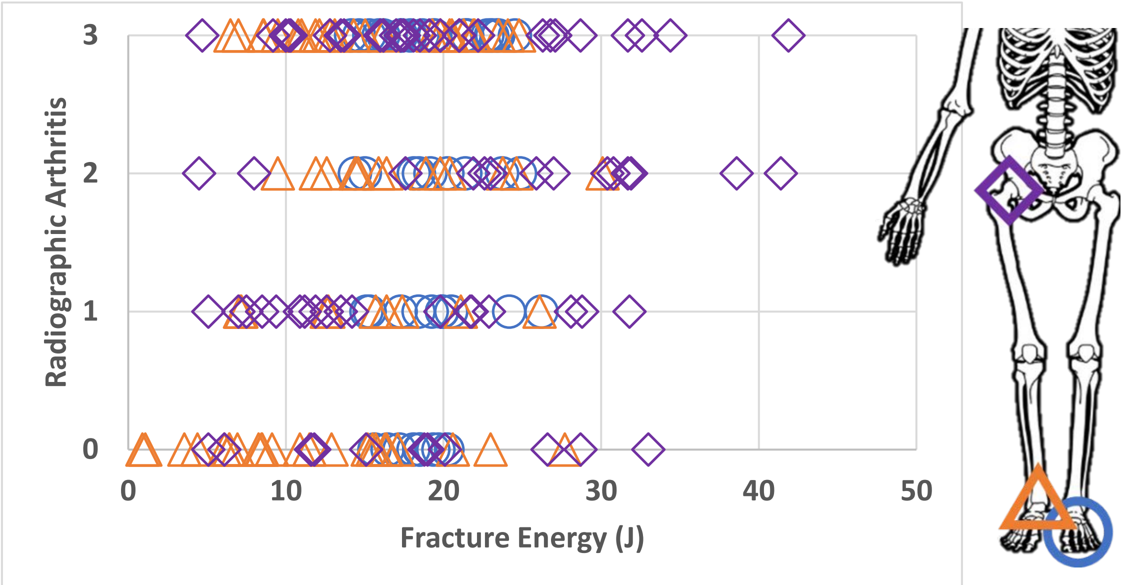

Figure 233. Fracture energy and grade of radiographic arthritis. The Tönnis grade was used for the acetabulum and a truncated Kellgren-Lawrence grade (where grades 3 and 4 were combined) was used for the calcaneus and tibial plafond.

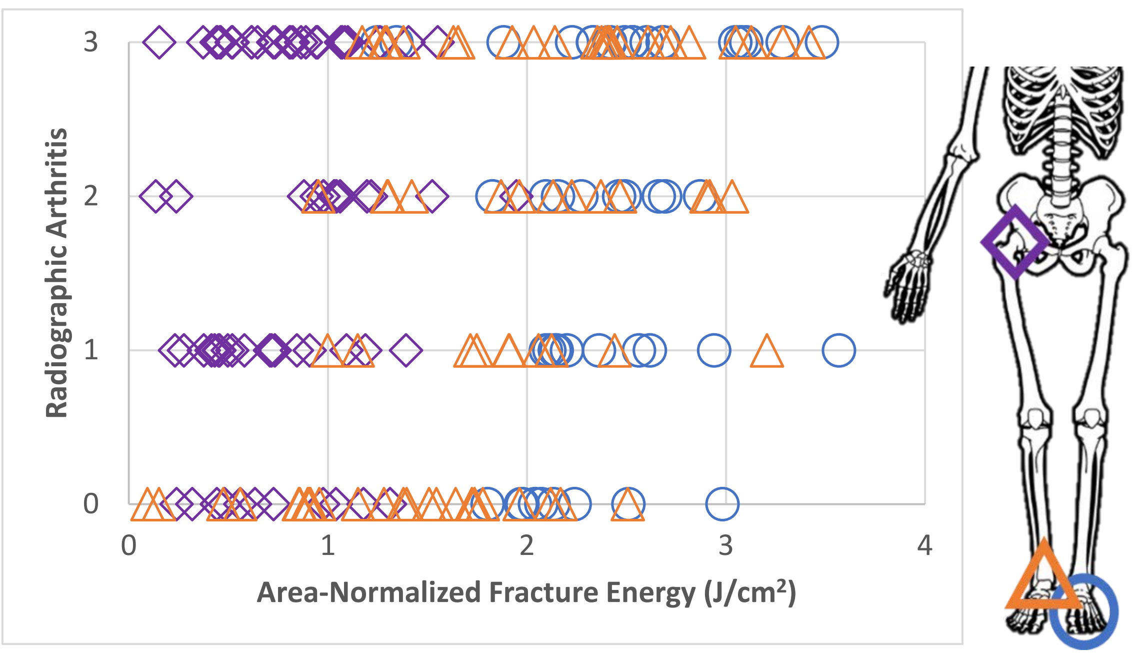

Figure 244. Area-normalized fracture energy and grade of radiographic arthritis. The Tönnis grade was used for the acetabulum and a truncated Kellgren-Lawrence grade (where grades 3 and 4) were combined was used for the calcaneus and tibial plafond.

plafond (2.18 vs 1.47 J/cm^2, p<0.001) and acetabulum (0.87 vs 0.68 J/cm^2, p=0.031), but not in the calcaneus (2.48 vs 2.12 J/cm^2, p=0.33). Figure 23 and Figure 24 show the distributions of fracture energy and normalized fracture energy, respectively versus radiographic grade for each joint.

Spearman's correlations between fracture energy, area, normalized fracture energy, radiographic OA grade, and OA status across all joints are shown in Table 4. Table 5, Table **6**Table 7 show Spearman's correlations between fracture energy, area, normalized fracture energy, radiographic OA grade, and OA status for the calcaneus, tibial plafond, and acetabulum, respectively. Across all cases, fracture energy had a small, but significant correlation with degree of OA development as well as OA status. Comparatively, normalized fracture energy had a slightly stronger correlation with degree of OA development that was highly significant. Broken down by joint, the fracture energy was significantly correlated with OA status in the plafond and acetabulum, but not the calcaneus. The degree of OA present was only significantly correlated with fracture energy and normalized fracture energy in the plafond. Normalized fracture energy was also significantly correlated with OA status in the plafond and acetabulum, but, once again, not in the calcaneus. In the calcaneus, the correlation appeared stronger but was not significant (p=0.062).

Logistic regressions of fracture energy, normalized fracture energy, and OA status across joints are shown in Table 8. Table 9, Table 10, and Table 11 show the results of these regressions for the calcaneus, tibial plafond, and acetabulum respectively. The confidence interval for the odds ratio across joints did not contain one, indicating that the results are significant for both the fracture energy and normalized fracture energy. They further revealed that for every Joule of increase in the fracture energy, there is an associated 3.2 to 12.6%

increased risk of PTOA development. Similarly, for each 0.1 J/cm^2 increase in area-normalized fracture energy, there was a corresponding 1.5 to 8.7% increase in PTOA risk. For individual joints, the odds ratios were also significant in the plafond and acetabulum, but not in the calcaneus. Additionally, the confidence intervals for the odds ratios were very large, indicating that more data is needed to reliably predict increased risk.

Table 4. Spearman correlations between objective measures of acute mechanical damage and PTOA status across fractures of the calcaneus, tibial plafond, and acetabulum. Significant correlations in bold. Coefficients are listed first followed by their p-value of significance.

All Cases Spearman Correlation Coefficients, N = 190 Prob > |r| under H0: Rho=0		
	Radiographic OA Grade	**OA**
Fracture energy	**0.189** **0.009**	**0.248** **<0.001**
Normalized Fracture Energy	**0.267** **<0.001**	**0.215** **0.003**

Table 5. Spearman correlations between objective measures of acute mechanical damage and PTOA status across fractures of the calcaneus. Significant correlations in bold. Coefficients are listed first followed by their p-value of significance.

Calcaneus Spearman Correlation Coefficients, N = 48 Prob > |r| under H0: Rho=0		
	KL Grade	**OA**
Fracture energy	0.102 0.491	0.090 0.547
Normalized Fracture Energy	0.271 0.062	0.248 0.090

Table 6. Spearman correlations between objective measures of acute mechanical damage and PTOA status across fractures of the tibial plafond. Significant correlations in bold. Coefficients are listed first followed by their p-value of significance.

Tibial Plafond Spearman Correlation Coefficients, N = 71 Prob > |r| under H0: Rho=0		
	KL Grade	**OA**
Fracture energy	**0.264** **0.026**	**0.286** **0.016**
Normalized Fracture Energy	**0.51749** **<.0001**	**0.466** **<.0001**

Table 7. Spearman correlations between objective measures of acute mechanical damage and PTOA status across fractures of the acetabulum. Significant correlations in bold. Coefficients are listed first followed by their p-value of significance.

Acetabular Spearman Correlation Coefficients, N = 71 Prob > |r| under H0: Rho=0		
	Tönnis Grade	**OA**
Fracture energy	0.129 0.282	**0.252** **0.033**
Normalized Fracture Energy	0.136 0.256	**0.257** **0.030**

Table 8. Results of logistic regressions of PTOA risk as predicted by the fracture energy in the top division in each table and by surface area-normalized fracture energy in the bottom division for all cases. For each regression, their respective parameter and odds ratio (OR) estimates are reported as well as a confidence interval of the OR.

Parameter	Estimate	Standard Error	Wald Chi-Square	Prob > ChiSq	OR Point Estimate	95% Wald Confidence Limits	
Constant	-1.025	0.405	6.409	0.0114			
Fracture energy	0.075	0.0221	11.5589	<0.001	1.078	1.032	1.126
Parameter	**Estimate**	**Standard Error**	**Wald Chi-Square**	**Prob > ChiSq**	**OR Point Estimate**	**95% Wald Confidence Limits**	
Constant	-0.493	0.310	2.529	0.1118			
Normalized Fracture Energy	0.049	0.018	7.704	0.006	1.050	1.015	1.087

Table 9. Results of logistic regressions of PTOA risk as predicted by the fracture energy in the top division in each table and by surface area-normalized fracture energy in the bottom division for the calcaneus. For each regression, their respective parameter and odds ratio (OR) estimates are reported as well as a confidence interval of the OR.

Calcaneal							
Parameter	**Estimate**	**Standard Error**	**Wald Chi-Square**	**Prob > ChiSq**	**OR Point Estimate**	**95% Wald Confidence Limits**	
Constant	-0.789	1.892	0.174	0.677			
Fracture energy	0.063	0.098	0.418	0.518	1.065	0.880	1.289
Parameter	**Estimate**	**Standard Error**	**Wald Chi-Square**	**Prob > ChiSq**	**OR Point Estimate**	**95% Wald Confidence Limits**	
Constant	-1.071	1.584	0.457	0.499			
Normalized Fracture Energy	0.062	0.065	0.911	0.340	1.064	0.937	1.209

Table 10. Results of logistic regressions of PTOA risk as predicted by the fracture energy in the top division in each table and by surface area-normalized fracture energy in the bottom division for the tibial plafond. For each regression, their respective parameter and odds ratio (OR) estimates are reported as well as a confidence interval of the OR.

Tibial Plafond							
Parameter	**Estimate**	**Standard Error**	**Wald Chi-Square**	**Prob > ChiSq**	**OR Point Estimate**	**95% Wald Confidence Limits**	
Constant	-1.366	0.640	4.556	0.033			
Fracture energy	0.100	0.0411	5.957	0.015	1.106	1.020	1.198
Parameter	**Estimate**	**Standard Error**	**Wald Chi-Square**	**Prob > ChiSq**	**OR Point Estimate**	**95% Wald Confidence Limits**	
Constant	-2.721	0.823	10.943	<0.001			
Normalized Fracture Energy	0.154	0.042	12.845	<0.001	1.166	1.072	1.269

Table 11. Results of logistic regressions of PTOA risk as predicted by the fracture energy in the top division in each table and by surface area-normalized fracture energy in the bottom division for the acetabulum. For each regression, their respective parameter and odds ratio (OR) estimates are reported as well as a confidence interval of the OR.

Acetabular							
Parameter	**Estimate**	**Standard Error**	**Wald Chi-Square**	**Prob > ChiSq**	**OR Point Estimate**	**95% Wald Confidence Limits**	
Constant	-0.847	0.5916	2.0474	0.1525			
Fracture energy	0.064	0.0289	4.8539	0.028	1.066	1.007	1.128
Parameter	**Estimate**	**Standard Error**	**Wald Chi-Square**	**Prob > ChiSq**	**OR Point Estimate**	**95% Wald Confidence Limits**	
Constant	-0.792	0.605	1.716	0.190			
Normalized Fracture Energy	0.151	0.073	4.217	0.040	1.162	1.007	1.342

Contact stress over-exposure in the tibial plafond after IAF

A total of 17 unilateral fractures of the tibial plafond were studied. For those included in the final analyses, the average age of the patients was 37.9±10.4 at the time of surgery (40.2±12.3 years in the OA group and 36.7±9.0 years for the no OA group, $p=0.59$). The average weight was 101.8±27.9 kg for the OA group and 85.0±8.6 kg in the normal controls. There were 10 males and 7 females in the patient group (7 males and 4 females in the OA group).

Fractured tibiotalar joints experienced an average maximum contact stress over-exposure of 0.69±0.17 MPa*s. Patients that developed PTOA had significantly higher maximum contact stress over-exposures in the tibiotalar joints than patients that did not (0.77±0.16 MPa*s in the OA group and 0.55±0.03 MPa*s in the No OA group, $p < 0.001$). Examining plots of the contact stresses, contact patches appeared more focal with higher peak contact stresses in cases that developed PTOA compared to more diffuse regions of lower contact stresses in the no PTOA groups (Figure 25).

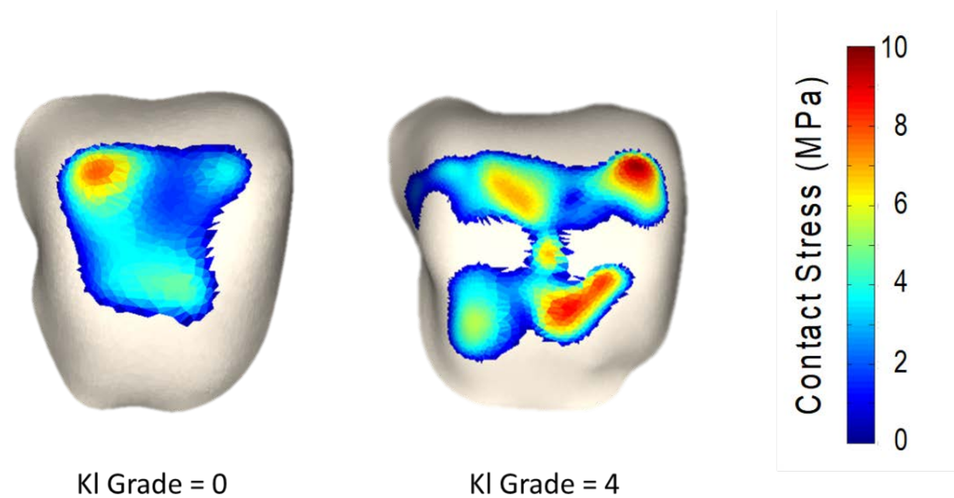

Figure 25. Contact stress distributions on the talar dome after tibial plafond IAF reconstruction. Cases that developed PTOA tended to have more focal and higher peak contact stresses than cases that did not.

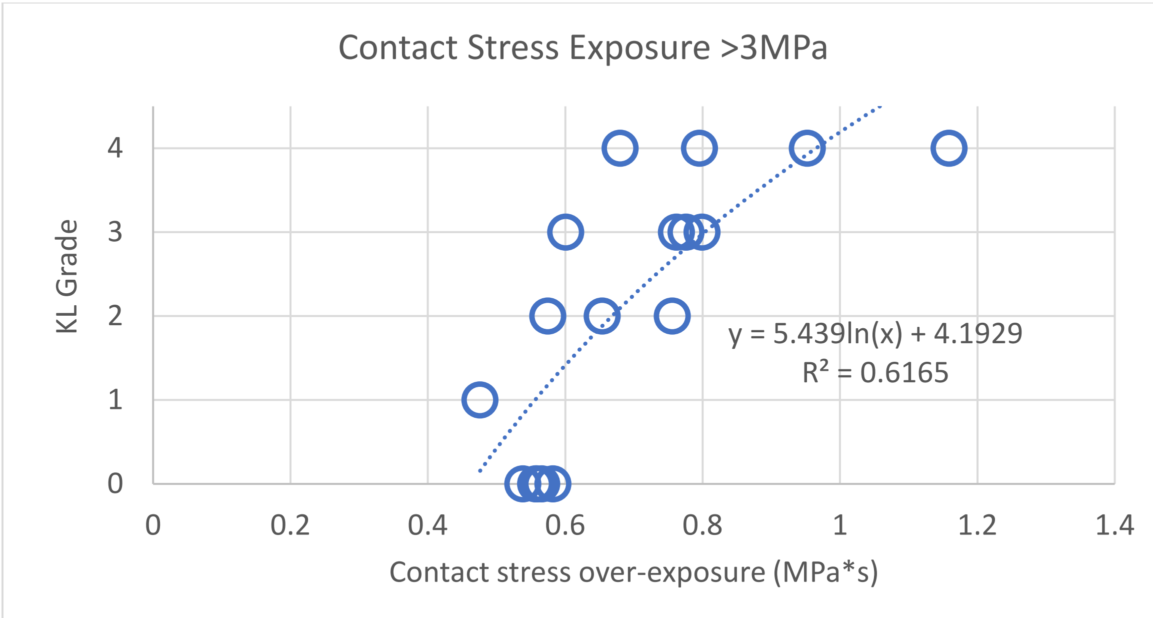

Figure 26. Contact stress over-exposure is highly correlated with PTOA outcomes in the tibial plafond after IAF reconstruction.

Contact stress over-exposure was found to be best correlated with patient outcomes when using a damage threshold of 3 MPa. The resulting exposures for each case are plotted above in Figure 26. There appears to be a clear delineation between exposures that develop PTOA and those that do not. Exposures above 0.6 MPa*s appear to predictably progress to PTOA development. There is also a strong correlation between the degree of radiographic arthritis and the quantity of over-exposure. It is important to note here that, as might be expected, the correlations reported do not directly explain the amount of variance in arthritis development as might be expected. This is because the KL grade is a categorical variable such that each grade will contain a range of continuous predictor values. The effect of this is that it will skew the assessment of variance toward a lower range and prevent it from having a directly interpretable meaning. Therefore, the R^2 values are merely included and discussed to generally assess each predictor against one another. Statistical evaluations of these correlations are performed with the Spearman's correlations as reported below in Table 12.

The measures of injury severity, as seen in the previous section, are also correlated with PTOA outcomes in this series of patients. The fracture energy and articular comminution energy are both moderately correlated with patient outcomes. The area-normalized fracture energy demonstrated a slightly stronger correlation with outcomes. It also demonstrated a potential cutoff above 1.5J/cm^2 that clearly demarcates the boundary between cases that did and did not develop radiographic PTOA above KL grade 2. The articular comminution energy, the energy absorbed within 10mm of the joint space, was the most highly correlated predictor. When combined with the normalized fracture energy, the results improved even further where a potential threshold at 0.2 would only misclassify one case.

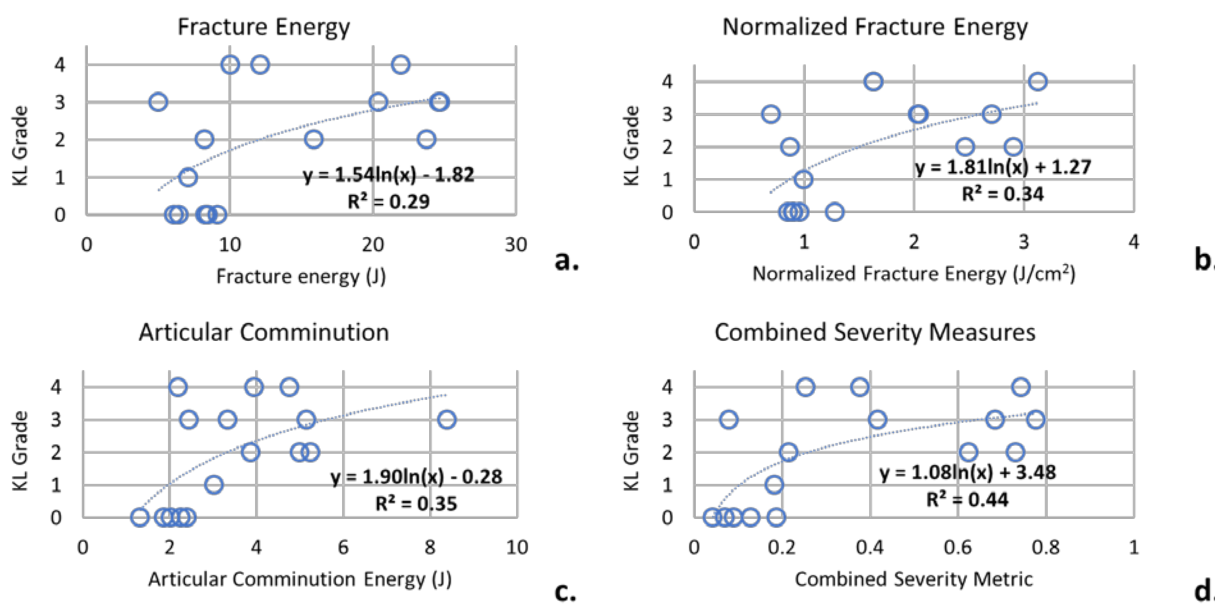

Figure 27. Correlations between measures of injury severity and radiographic outcomes in the tibial plafond. The area-normalized fracture energy, c, and the articular comminution, b, were normalized and combined equally to create the combined measure shown in d.

A further equally combined model of the composite injury severity measures shown in Figure 27d and the reduction accuracy (as quantified by the contact stress over-exposure in Figure 26) was created and is shown in Figure 29. This combined model explains over 70% of the variance in the degree of radiographically measured arthritic degeneration, further improving

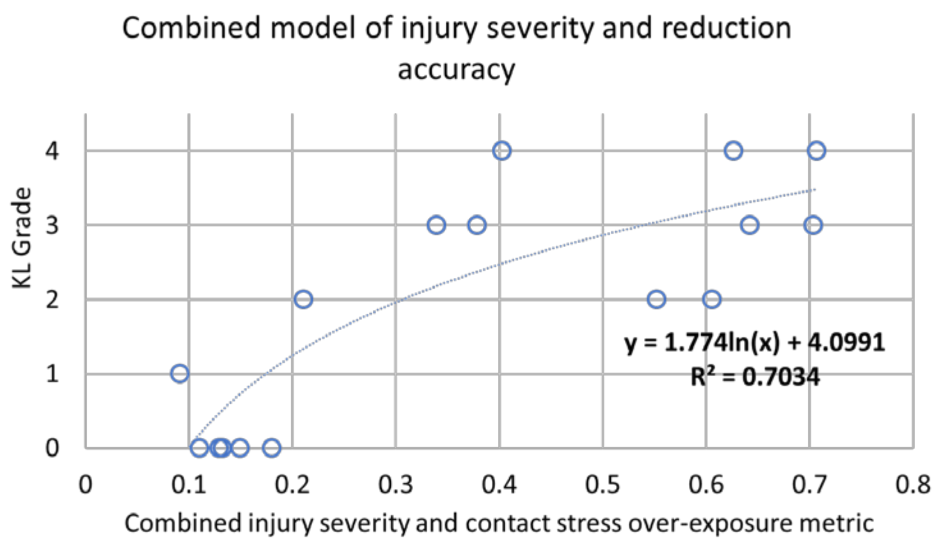

Figure 29. Combined model of the best objective measures of injury severity and reduction accuracy in the tibial plafond.

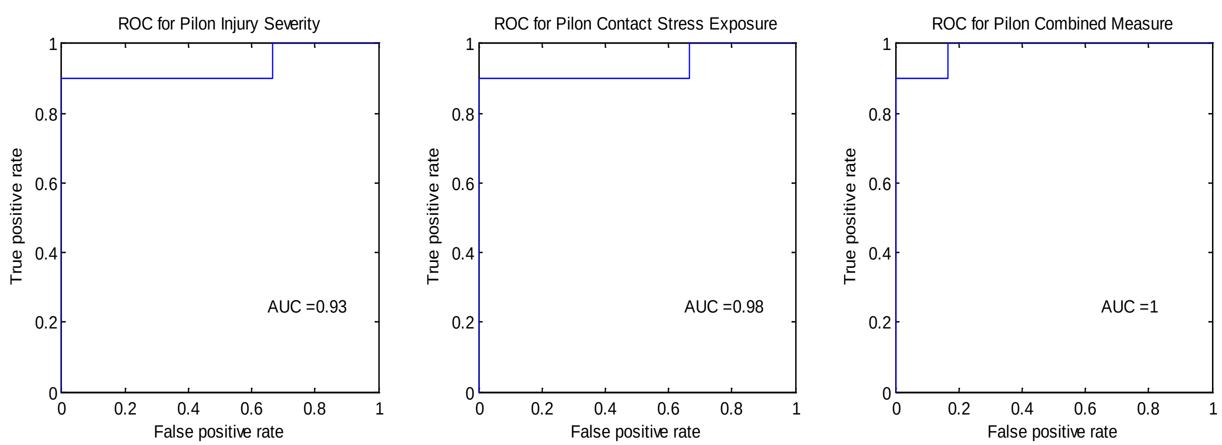

Figure 28. ROC curves for the tibial plafond of the combined injury severity measure, contact stress over-exposure, and the combined measure of injury severity and contact stress over-exposure. The AUC for each case is displayed on each graph.

upon its constitutive components. If a threshold were applied around 0.2, it would also achieve perfect delineation between cases that did and did not develop arthritis.

The accuracy of the model was demonstrated by the receiver operating characteristic (ROC) curves shown in Figure 28. The injury severity had excellent accuracy with an area under the curve (AUC) of 0.93 while the contact stress exposure measure had even higher accuracy with an AUC of 0.98. The combined measure of injury severity and contact stress over-exposure provided the best results with a perfect accuracy demonstrated by its AUC of 1.00.

To examine the relationships between the objective measures of injury severity and reduction accuracy, area-normalized fracture energy was plotted against contact stress over-exposure in Figure 26 and the combined severity metric from Figure 27d was plotted against the contact stress over-exposure above 3 MPa in Figure 31. Neither figure evinces a strong correlation between the injury severity and the reduction accuracy in these cases. Comparing the small blue bubbles that indicate KL grades of 0 and 1 to the large red bubbles indicating PTOA development of grades 2 through 4, we note that the former are clustered in the lower left-hand corner, indicating that cases that did not develop PTOA tended to have lower objective measures of injury severity and better reduction accuracy. Conversely, cases that had poor reductions and high injury severity predictably (found in the upper right corner) progressed to PTOA.

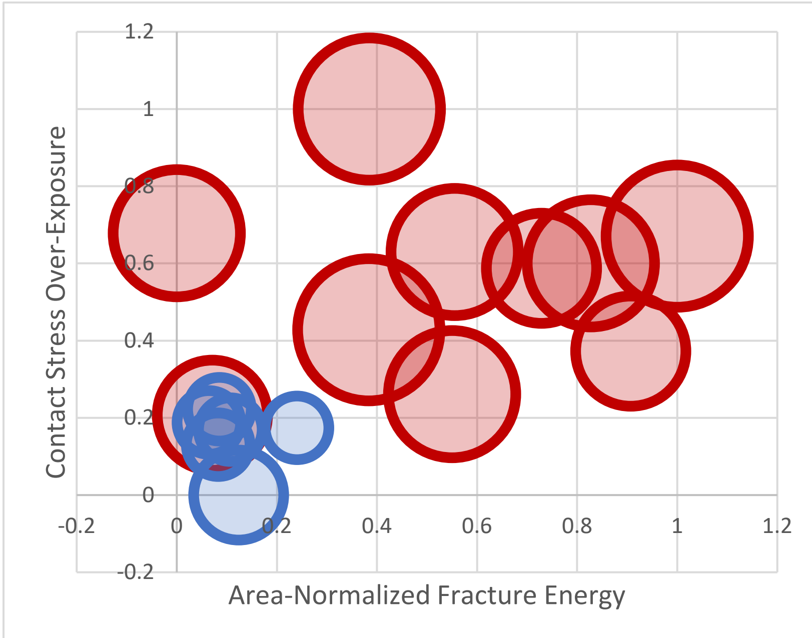

Figure 30. Normalized fracture energy is not correlated with contact stress over-exposure in fractures of the tibial plafond. High levels of contact stress over-exposure and area-normalized fracture energy are associated with higher grades of radiographic arthritis (KL 0-1 are shown as small blue bubbles and KL 2-4 are shown as larger red bubbles).

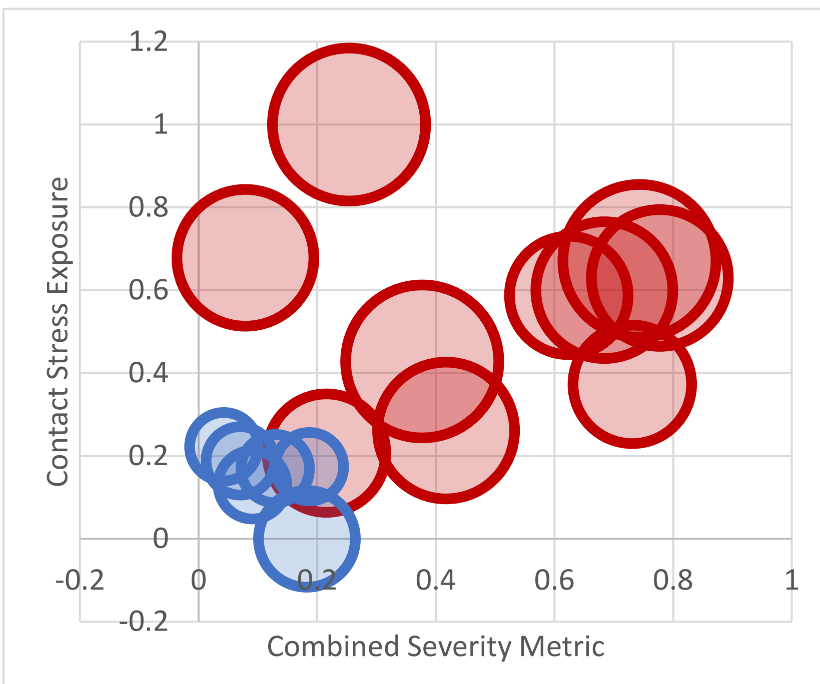

Figure 31. A combined metric to estimate the severity of articular injury is not correlated with contact stress over-exposure in the tibial plafond. Low levels of contact stress over-exposure and injury severity are associated with forestallment of PTOA (small blue bubbles) while high levels of both either or both were associated with PTOA development (large red bubbles).

The results of the Spearman's rank order correlations also demonstrated significant correlations between predictors and outcomes (Table 12). The two potential confounders, age and sex, were not significantly correlated to any of the predictors or outcomes. Fracture energy, articular comminution, area-normalized fracture energy, the injury severity composite, and stress and severity combined measures were all significantly correlated with radiographic outcomes of arthritis.

Table 12. Spearman's correlations of all predictors and radiographic outcomes in the tibial plafond. Significant correlations in bold.

Spearman Correlation Coefficients, N = 16									
	Fracture energy	**Articular comm**	**Area norm energy**	**Contact Stress Exposure**	**Injury Severity Composite**	**Stress & Severity**	**Age**	**Sex**	**KL**
Fracture energy	1.00000	**0.78824** **0.0003**	**0.91471** **<.0001**	0.42059 0.1048	**0.93529** **<.0001**	**0.76471** **0.0006**	-0.26510 0.3211	-0.44809 0.0817	**0.52064** **0.0387**
Articular comm	**0.78824** **0.0003**	1.00000	**0.72353** **0.0015**	0.42941 0.0969	**0.89412** **<.0001**	0.71765 0.0017	-0.16200 0.5489	-0.36407 0.1657	**0.54788** **0.0280**
Area norm energy	**0.91471** **<.0001**	**0.72353** **0.0015**	1.00000	0.44412 0.0848	**0.89706** **<.0001**	**0.74706** **0.0009**	-0.15758 0.5600	-0.19604 0.4668	**0.51761** **0.0400**
Contact Stress Exposure	0.42059 0.1048	0.42941 0.0969	0.44412 0.0848	1.00000	**0.51471** **0.0413**	**0.87647** **<.0001**	-0.02946 0.9138	0.08402 0.7571	**0.82636** **<.0001**
Injury Severity Composite	**0.93529** **<.0001**	**0.89412** **<.0001**	**0.89706** **<.0001**	**0.51471** **0.0413**	1.00000	**0.83235** **<.0001**	-0.18704 0.4879	-0.36407 0.1657	**0.64626** **0.0068**
Stress & Severity	**0.76471** **0.0006**	**0.71765** **0.0017**	**0.74706** **0.0009**	**0.87647** **<.0001**	**0.83235** **<.0001**	1.00000	-0.12960 0.6324	-0.16803 0.5339	**0.79912** **0.0002**
Age	-0.26510 0.3211	-0.16200 0.5489	-0.15758 0.5600	-0.02946 0.9138	-0.18704 0.4879	-0.12960 0.6324	1.00000	**0.67313** **0.0043**	-0.20993 0.4352
Sex	-0.44809 0.0817	-0.36407 0.1657	-0.19604 0.4668	0.08402 0.7571	-0.36407 0.1657	-0.16803 0.5339	**0.67313** **0.0043**	1.00000	-0.12970 0.6321
KL	**0.52064** **0.0387**	**0.54788** **0.0280**	**0.51761** **0.0400**	**0.82636** **<.0001**	**0.64626** **0.0068**	**0.79912** **0.0002**	-0.20993 0.4352	-0.12970 0.6321	1.00000

Contact stress over-exposure in the calcaneus after IAF

A total of 41 fractures from 32 patients were studied. Of the 41 patient-specific fracture models created, 33 reached convergence and were included in final analyses. There was no significant difference in KL graded outcomes between the patients whose models converged and those that did not. Both normal controls also reached convergence. For those included in the final analyses, the average age of the patients was 43.3 at the time of surgery (42.2±7.7 years in the OA group and 44.5±13.4 years for the no OA group, $p=0.56$). The average BMI was 26.7±4.0. There were 30 males and 3 females in the patient group (16 males and 1 female in the OA group).

The subtalar joints in the PTOA group were exposed to an average maximum contact stress over-exposure of 1.22±0.45 MPa*s (mean ± standard deviation). Fractured subtalar joints experienced an average maximum contact stress over-exposure of 0.99±0.19 MPa*s. This difference was highly significant ($p=0.005$). Examining plots of the contact stresses, contact patches appeared more focal with higher peak contact stresses in cases that developed PTOA compared to more diffuse regions of lower contact stresses in the no PTOA groups (Figure 32).

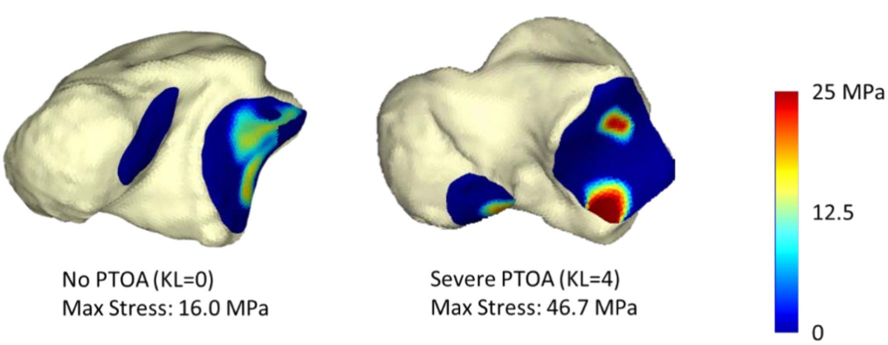

Figure 32. Differences in the maximum contact stress patches shown between a case that did not develop PTOA and a case that developed severe PTOA.

The results of the fracture energy analysis were similar to what was previously reported on the entire series of 48 fractures, fracture energy in the subgroup of 33 that reached convergence was not significantly correlated with PTOA outcomes (p=0.08). When considering the area-normalized fracture energy, differences were significant (2.54±0.40 MPa*s in the OA group versus 2.24±0.38 MPa*s in the no OA group, p=0.04).

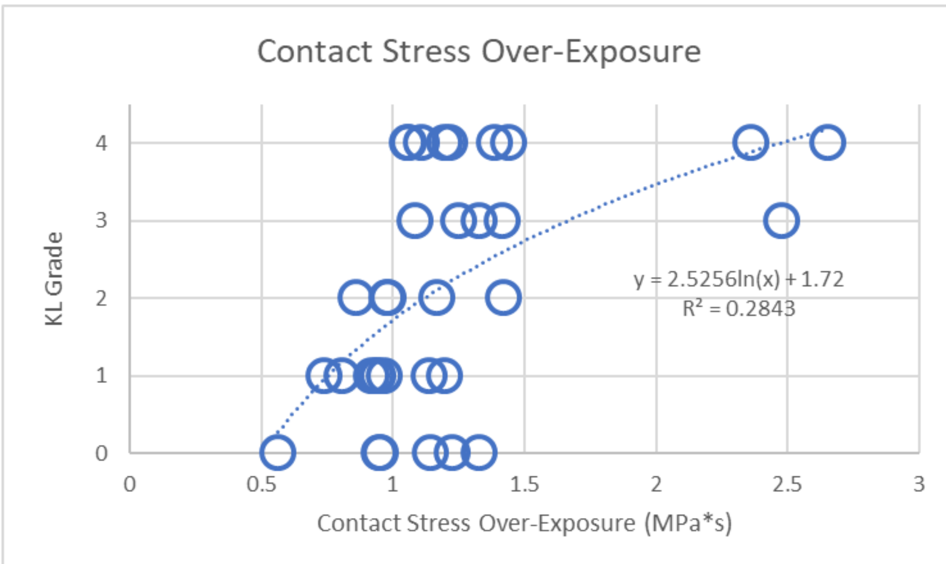

Figure 33. Contact stress over-exposure is correlated with PTOA outcomes after IAF in the calcaneus.

Contact stress over-exposure was found to be best correlated with patient outcomes when using a damage threshold of 10MPa. This is significantly higher than the 3MPa found in the tibiotalar joint in the previous section. The resulting exposures for each case are plotted above in Figure 33. There is not a clear delineation between exposures that develop PTOA and those that do not in the subtalar joint. Exposures above 1.25 MPa*s appear to be more likely to progress to PTOA development. There is also a small to moderate correlation between the degree of radiographic arthritis and the quantity of over-exposure with the over-exposure potentially explaining 28.4% of the variance in arthritis development. As noted in the discussion of the plafond results, it is important to note that these variances are skewed low by the comparison of a categorical and continuous variables and have no directly interpretable meaning. Therefore, they are merely reported as a reference for comparison across predictors. Statistical analysis of correlations was performed using Spearman's correlations in Table 13.

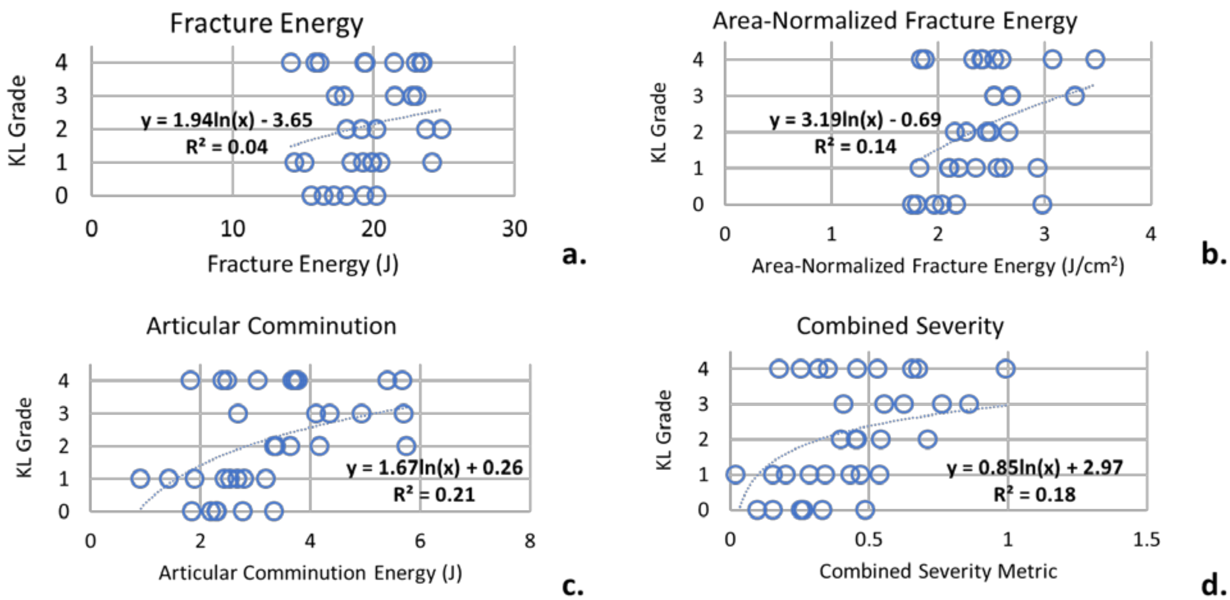

Figure 34. Correlations between measures of injury severity and radiographic outcomes in the calcaneus after IAF. The area-normalized fracture energy, c, and the articular comminution, b, were normalized and combined equally to create the combined measure shown in d.

Some measures of injury severity, as seen earlier in this document, are also correlated with PTOA outcomes in this subset of that prior series of 48 patients. The fracture energy was not correlated with outcomes ($R^2 = 0.04$, Figure 34a). The area-normalized fracture energy demonstrated a slightly stronger correlation with outcomes (R^2=0.14, Figure 34c), but was still not significant. The articular comminution as a measure of injury severity was the most correlated with patient radiographic outcomes, but its association was still rather modest. The articular comminution energy also appeared to demonstrate a potential cutoff around 3.5J, above which cases were likely to degenerate to PTOA. Correspondingly, the average differences in articular comminution energy were also highly significant (3.90±1.15J in the OA group vs 2.33±0.64J in the no OA group, $p<0.001$). When combined with the normalized fracture energy, the correlation with degree of arthritic outcomes improved slightly, but did not demonstrate as clear of a threshold above which cases predictably progressed to PTOA as was seen previously in the plafond.

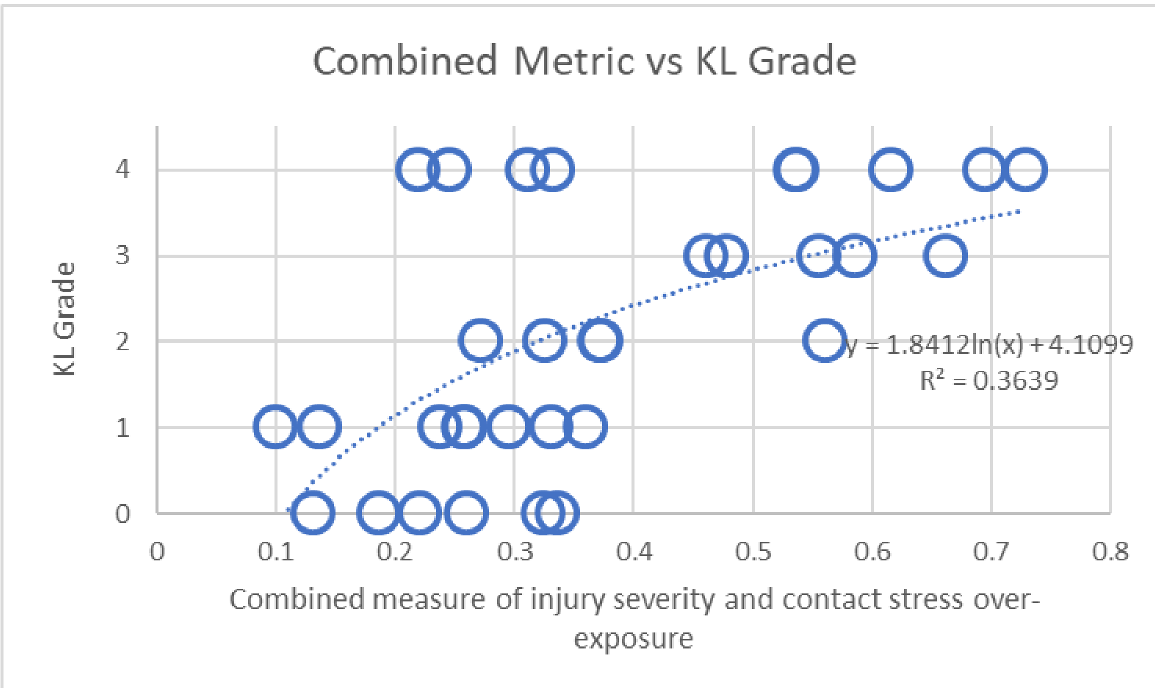

Figure 35. Combined model of the best objective measures of injury severity and reduction accuracy in reconstructed IAFs of the calcaneus.

A second combined model, this time of equal parts composite injury severity score (figure 34d) and contact stress over-exposure (Figure 33), was created (Figure 35). It demonstrated improved correlation with KL graded degree of radiographic arthritis over both of its constitutive components explaining over 36% of the variance in PTOA development. The metric also had a clear threshold around 0.4 above which cases predictably progressed to PTOA development.

The ROC curves, as shown in Figure 36, demonstrate the relative predictive accuracy of each measure. The combined injury severity measure provided equivalent predictive accuracy to that of the contact stress over-exposure measure, though both were slightly less predictive in this joint than in the plafond. Again, the combined measure of injury severity and contact stress over-exposure provided the best predictive accuracy of any model.

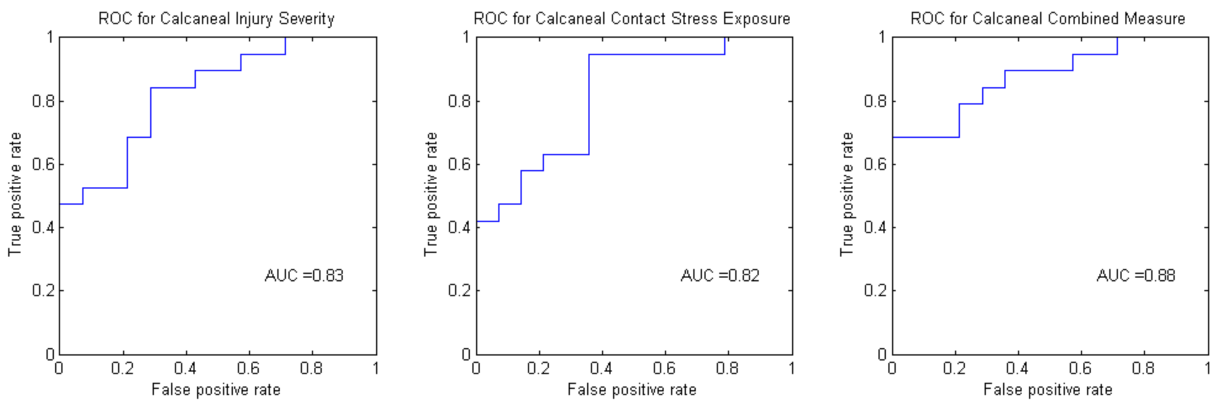

Figure 36. ROC curves for the calcaneus of the combined injury severity measure, contact stress over-exposure, and the combined measure of injury severity and contact stress over-exposure. The AUC for each case is displayed on each graph.

Examining the relationships between the objective measures of injury severity and reduction accuracy, area-normalized fracture energy was plotted against contact stress over-exposure in Figure 37 and the combined severity metric from Figure 34d was plotted against the contact stress over-exposure above 10 MPa in Figure 37. Neither finds a correlation between the injury severity and the reduction accuracy in these cases. Looking at the small blue bubbles that indicate KL grades of 0 and 1 in relation to the large red bubbles indicating PTOA development of grades 2-4, cases that did not develop PTOA tended to have lower objective measures of injury severity and better reduction accuracy, showing them clustered in the lower left-hand corner. This is more apparent in the combined measure of severity in Figure 38. Conversely, cases that had poor reductions and high injury severity predictably progressed to PTOA in the upper right.

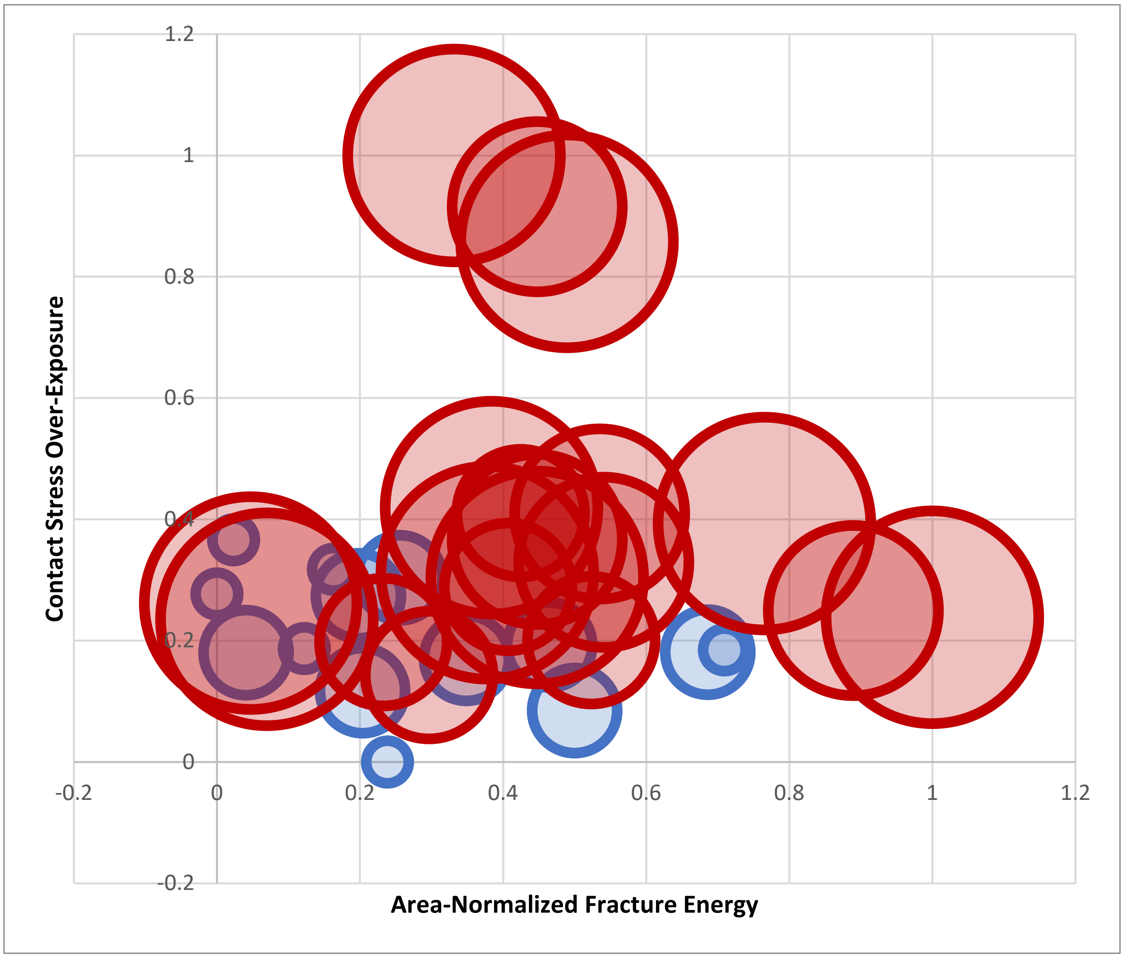

Figure 37. Normalized fracture energy is not correlated with contact stress over-exposure in the calcaneus. Cases that have low contact stress over-exposures demonstrate a lesser degree of radiographic arthritis (demonstrated by the larger red bubbles).

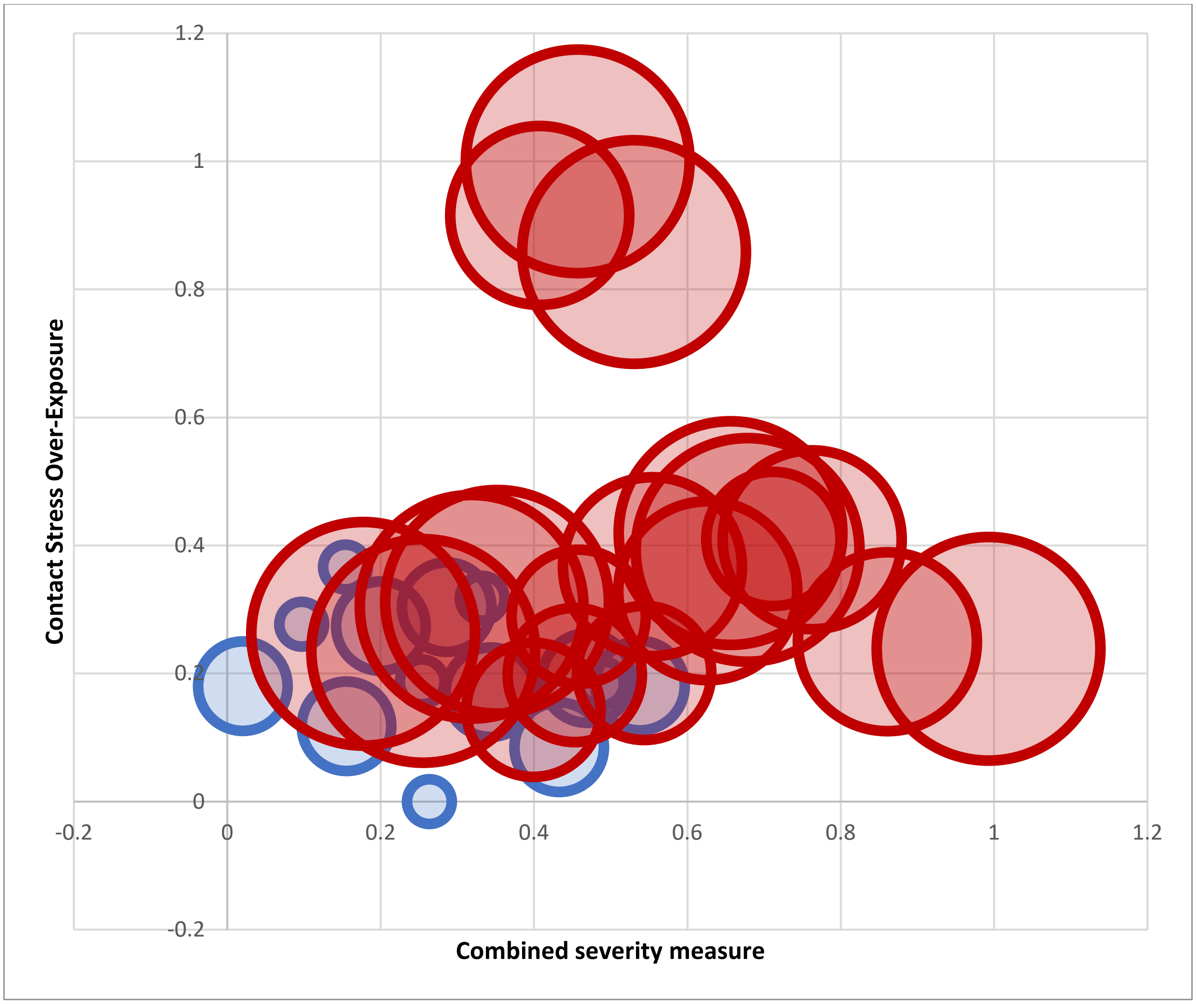

Figure 38. Combined severity measure is not correlated with contact stress over-exposure in the calcaneus. Cases that have low severity and contact stress over-exposures demonstrate lesser degrees of radiographic arthritis (demonstrated by larger red bubbles).

The results of the Spearman's rank order correlations found significant correlations between some of the predictors and outcomes (Table 13). The two potential confounders, age and sex, were not significantly correlated to any of the predictors or outcomes. Fracture energy by itself was not a significant predictor of outcomes but was significantly associated with Sanders classification, the gold standard clinical assessment of injury severity in the subtalar joint. Measures of contact stress exposure, articular comminution, the injury severity composite score, and stress and severity combined measures were all significantly correlated with radiographic outcomes of arthritis. The articular comminution energy and injury severity composite were even more strongly predictive of the degree of arthritic development than the Sanders classification.

Table 13. Spearman correlation coefficients for predictors of PTOA in the subtalar joint after IAF of the calcaneus.

Spearman Correlation Coefficients										
	Contact Stress Exposure	**Fracture Energy**	**Articular Comm**	**Area norm energy**	**Injury Severity Composite**	**Stress& Severity**	**Sanders**	**Age**	**Sex**	**KL**
Contact Stress Exposure	1.00000	-0.04546 0.8017	**0.44472 0.0095**	0.13574 0.4513	**0.34592 0.0486**	**0.68549 <.0001**	0.05781 0.7493	-0.112 0.4636	0.06642 0.7134	**0.52030 0.0019**
Fracture Energy	-0.04546 0.8017	1.00000	0.520 0.0565	**0.68361 <.0001**	**0.56973 0.0005**	**0.45107 0.0084**	**0.44250 0.0099**	-0.09051 0.6164	0.09410 0.6024	0.20942 0.2421
Articular Comm	**0.44472 0.0095**	0.520 0.0565	1.00000	**0.53900 0.0012**	**0.85853 <.0001**	**0.77463 <.0001**	0.20482 0.2529	-0.26601 0.1346	0.22142 0.2156	**0.48516 0.0042**
Area norm energy	0.13574 0.4513	**0.68361 <.0001**	**0.53900 0.0012**	1.00000	**0.87362 <.0001**	**0.71615 <.0001**	0.26449 0.1369	-0.285 0.1102	0.02215 0.9026	**0.35936 0.0400**
Injury Severity Composite	**0.34592 0.0486**	**0.56973 0.0005**	**0.85853 <.0001**	**0.87362 <.0001**	1.00000	**0.85227 <.0001**	0.22580 0.2064	-0.31095 0.0782	0.07749 0.6682	**0.45646 0.0076**
Stress& Severity	**0.68549 <.0001**	**0.45107 0.0084**	**0.77463 <.0001**	**0.71615 <.0001**	**0.85227 <.0001**	1.00000	0.21224 0.2357	-0.26206 0.1407	0.06642 0.7134	**0.57250 0.0005**
Sanders	0.05781 0.7493	**0.44250 0.0099**	0.20482 0.2529	0.26449 0.1369	0.22580 0.2064	0.21224 0.2357	1.00000	-0.13558 0.4519	0.10604 0.5570	**0.41419 0.0166**
Age	-0.112 0.4636	-0.09051 0.6164	-0.26601 0.1346	-0.285 0.1102	-0.31095 0.0782	-0.26206 0.1407	-0.13558 0.4519	1.00000	-0.028 0.8541	-0.16129 0.3699
Sex	0.06642 0.7134	0.09410 0.6024	0.22142 0.2156	0.02215 0.9026	0.07749 0.6682	0.06642 0.7134	0.10604 0.5570	-0.028 0.8541	1.00000	0.30612 0.08
KL	**0.52030 0.0019**	0.20942 0.2421	**0.48516 0.0042**	**0.35936 0.0400**	**0.45646 0.0076**	**0.57250 0.0005**	**0.41419 0.0166**	-0.16129 0.3699	0.30612 0.08	1.00000

Contact stress over-exposure in the acetabulum after IAF

A total of 22 patients were included in the final analysis. Fifteen out of 22 patients developed OA. The mean follow-up time for joints that developed PTOA was 33.1 (12.8-69) months. The mean follow-up time for joints that did not develop OA was 31.6 (12.2-76) months. Follow-up time was not significantly associated with PTOA ($p=0.82$). The average age of the patients was 39.7 ± 16.2 years at the time of surgery (42.7 ± 16.6 years in the OA group and 33.3 ± 13.1 years for the no OA group, $p=0.19$). The average BMI was 30.4 ± 6.4 for the patients (29.7 ± 7.0 in the OA group and 32.7 ± 3.1 in the no OA group, $p=0.24$). There were 18 males and 4 females in the patients studied (2 females in the OA group).

Qualitatively, the contact stress over-exposure distributions in the cases that did not develop OA were smaller and varied more gradually over the surface than those in the OA group (Figure 16). For those in the PTOA group, there were much more focal contact stress elevations that led to higher regions of over-exposure and varied in location over the gait cycle, attributable to larger local articular surface incongruities. All hips from patients with acetabular fractures experienced an average maximum contact stress exposure of 4.41 ± 1.53 MPa*s. Patients that developed PTOA had significantly higher maximum contact stress exposures in their hips than patients that did not (5.00 ± 1.38 MPa*s vs. 3.15 ± 0.96 MPa*s; $p=0.003$).

The range of fracture energies for the 19 cases on which it was computed was 7.0-41.4 J (18.3 ± 9.6 J). As was found in the larger study of injury severity reported earlier in this document, for the cases that developed PTOA, fracture energy was significantly higher than for those that did not (22.2 ± 9.2 J in the OA group and 10.0 ± 3.1 in the group that did not develop OA, $p<0.001$).

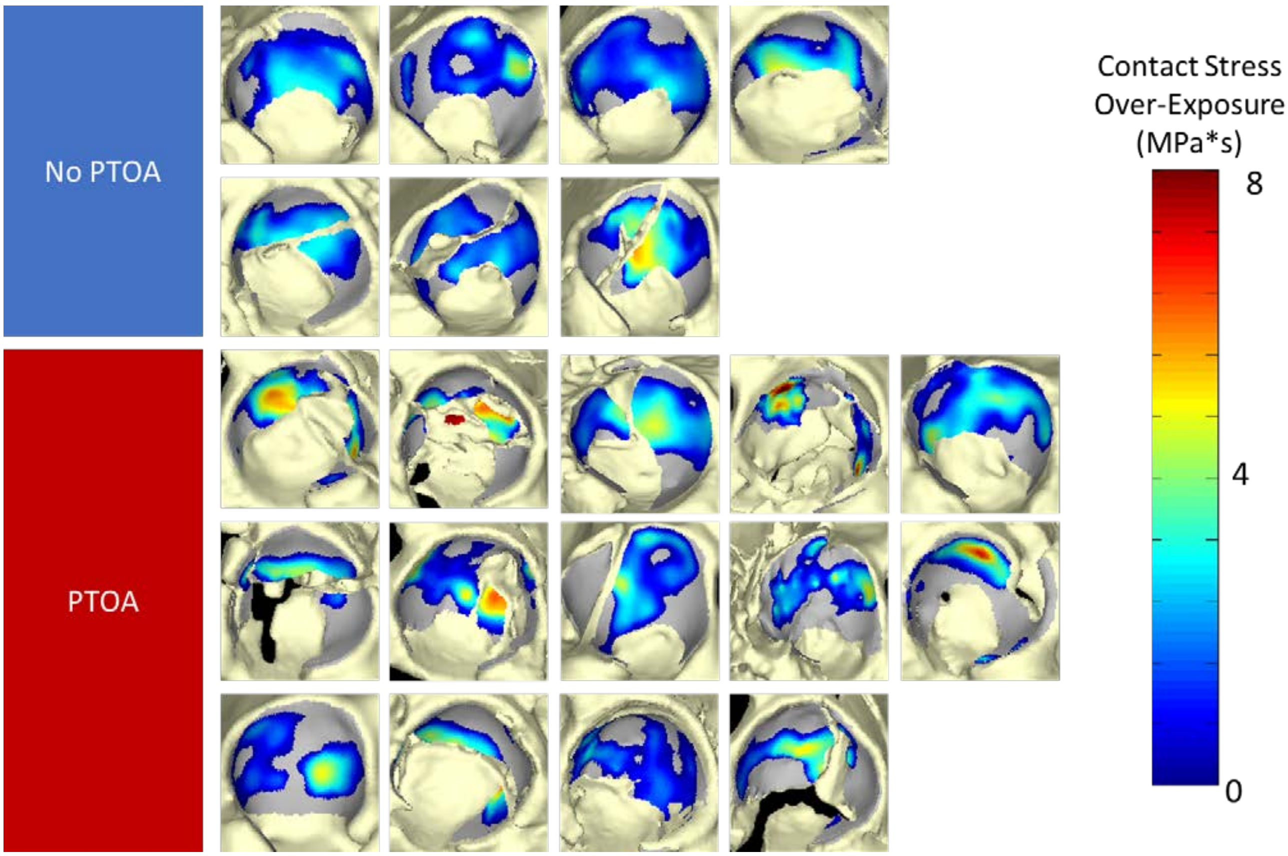

Figure 39. The contact stress over-exposure distributions for the patients who had developed PTOA at two years after surgery were substantially more focal and had significantly higher peak values.

Contact stress over-exposure was found to be best correlated with patient outcomes when using a damage threshold of 1 MPa. This is lower than the 3MPa found in the tibiotalar joint and substantially lower than the 10MPa found for the calcaneal fractures in the previous section. The resulting exposures for each case are plotted above in Figure 399. There is delineation between exposures that develop PTOA in the acetabulum around 4 MPa*s. There is also a moderate correlation between the degree of radiographic arthritis and the quantity of over-exposure with the over-exposure potentially explaining 41% of the variance in arthritis development (Figure 4040). As noted in the discussion of the plafond and calcaneal results, it is important to be aware that these variances are skewed low by the comparison of categorical and continuous variables and have no directly interpretable meaning. Therefore, they are merely reported as a reference for comparison across predictors. Statistical analysis of correlations was performed using Spearman's correlations in Table 14.

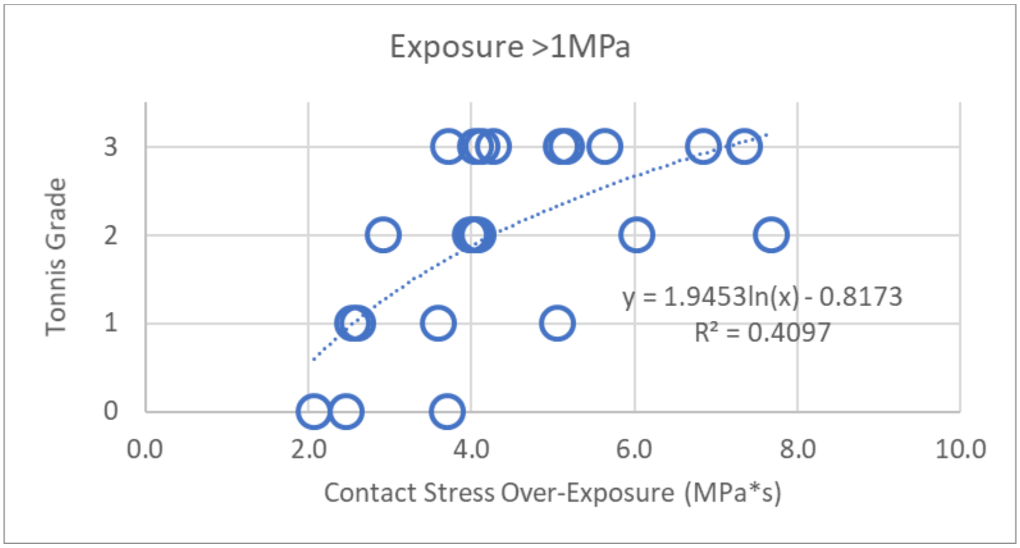

Figure 40. Contact stress over-exposure is correlated with PTOA outcomes after IAF of the acetabulum.

Measures of injury severity, as seen earlier in this document, are also correlated with PTOA outcomes in this subset of that prior series of 71 acetabular fracture patients. The fracture energy had a small correlation with outcomes ($R^2 = 0.23$, Figure 41a). The articular comminution and area-normalized fracture energy measures demonstrated similar small correlations with outcomes (R^2=0.20 and $R^2 = 0.22$, Figure 41b and 41c, respectively). The fracture energy appeared to demonstrate a potential cutoff around 15J; above this value, cases were likely to degenerate to PTOA. When the normalized fracture energy and articular comminution were taken in equal parts to form a combined model, the correlation with degree of arthritic outcomes improved substantially (R^2=0.36) and a clear threshold above which cases predictably progressed to PTOA emerged around 0.4.

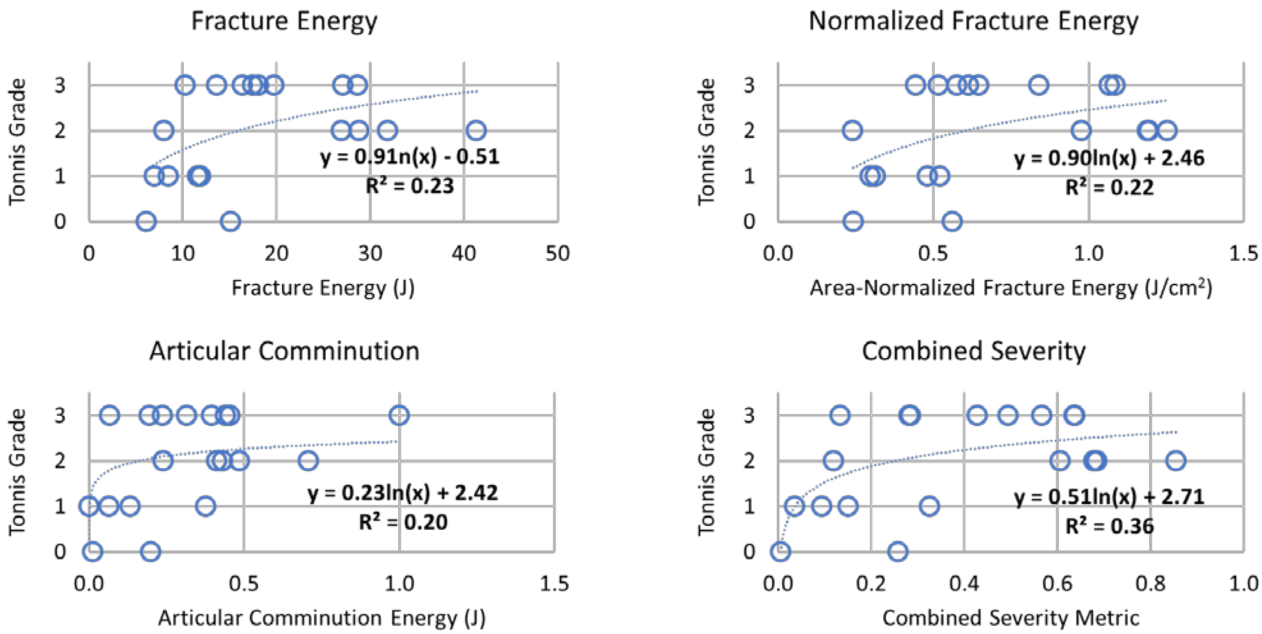

Figure 41. Correlations between measures of injury severity and radiographic outcomes in the acetabulum after IAF. The area-normalized fracture energy, c, and the articular comminution, b, were normalized and combined equally to create the combined measure shown in d.

Another combined model of equal parts composite injury severity score (Figure 41d) and contact stress over-exposure (Figure 40), was created (Figure 42). It demonstrated improved correlation with KL graded degree of radiographic arthritis over both of its constitutive components, explaining over 46% of the variance in PTOA development. The metric also had a clear threshold around 0.4 above which cases predictably progressed to PTOA development.

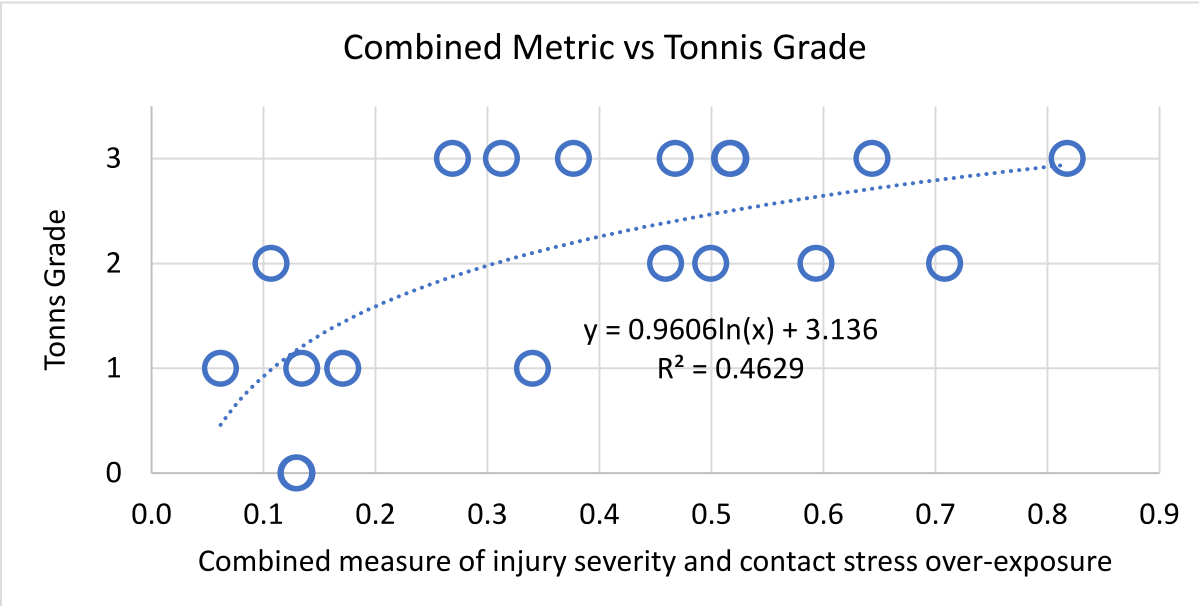

Figure 43. Combined model of injury severity and reduction accuracy predicts PTOA development in the acetabulum.

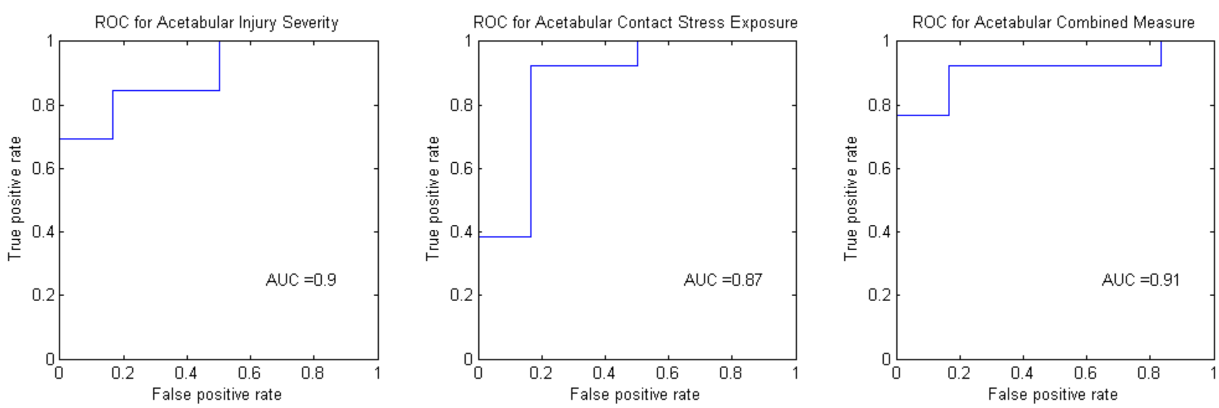

Figure 42. ROC curves for predictors of PTOA development in acetabular fractures. The combined measure of injury severity, the measure of contact stress over-exposure, and the combined measures of injury severity and contact stress over-exposure were plotted from left to right.

The ROC curves again demonstrated the predictive accuracy of each model for acetabular fractures in Figure 43. The combined measure of injury severity was slightly more predictive than the contact stress over-exposure measure while both had good to excellent accuracy. As with the plafond and calcaneus, the combined measure provided the highest overall accuracy with an AUC of 0.91.

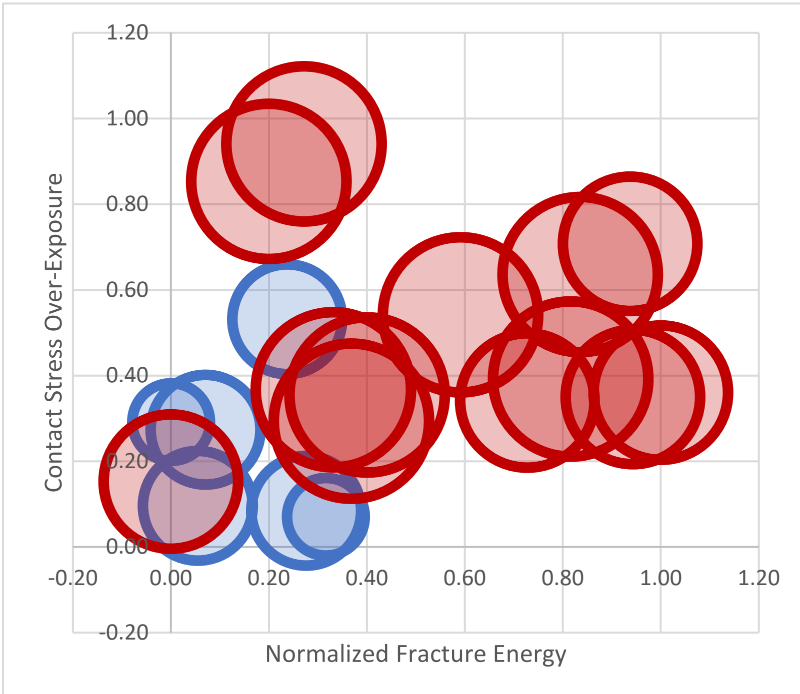

Figure 44. Normalized fracture energy is not correlated with contact stress over-exposure in fractures of the acetabulum. High levels of contact stress over-exposure and area-normalized fracture energy are associated with higher grades of radiographic arthritis (KL 0-1 are shown as small blue bubbles and KL 2-4 are shown as larger red bubbles).

Examining the relationships between the objective measures of injury severity and reduction accuracy, area-normalized fracture energy was plotted against contact stress over-exposure in Figure 44 and the combined severity metric from Figure 41d was plotted against the contact stress over-exposure above 1 MPa in Figure 45. Neither figure finds a strong correlation between the injury severity and the reduction accuracy in these cases. Noting the location of the small blue bubbles that indicate KL grades of 0 and 1 in relation to the large red bubbles indicating PTOA development of grades 2-4, cases that did not develop PTOA tended to have lower objective measures of injury severity and better reduction accuracy such that they were clustered in the lower left-hand corner. Conversely, cases found in the upper right of the plot area had poor reductions, high injury severity, and consequently, predictably progressed to PTOA.

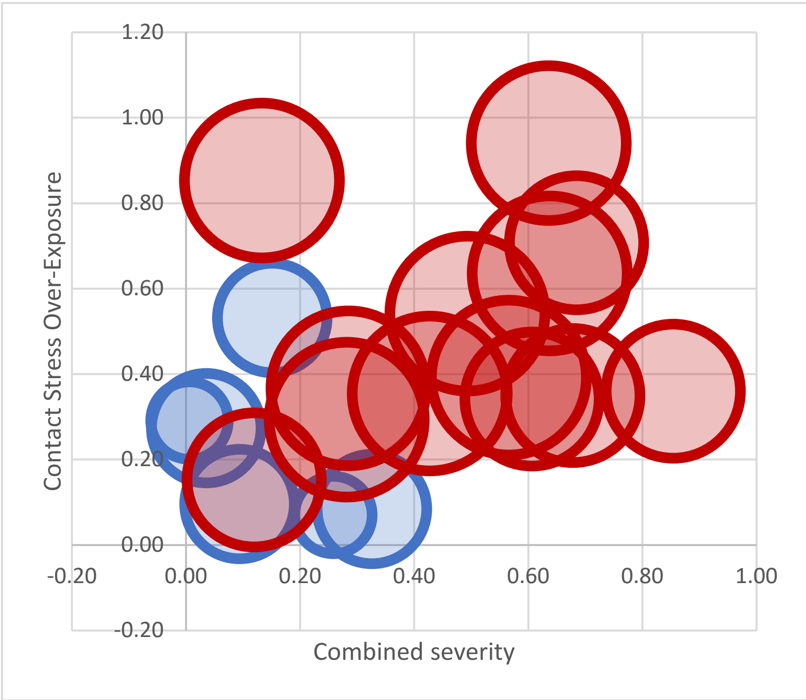

Figure 45. A combined metric to estimate the severity of articular injury is not correlated with contact stress over-exposure in the acetabulum. Low levels of contact stress over-exposure and injury severity are associated with forestallment of PTOA (small blue bubbles) while high levels of both either or both were associated with PTOA development (large red bubbles).

Table 14. Spearman Correlation Coefficients between mechanical predictors of PTOA and potential confounders.

Spearman Correlation Coefficients, N = 19									
	Contact Stress Exposure	Fracture Energy	Area norm energy	Articular comm	Injury Severity Composite	Stress& Severity	Age	Sex	Tonnis
Contact Stress Exposure	1.00000	0.40702 0.0837	0.37193 0.1169	0.37593 0.1127	**0.50175** **0.0286**	**1.00000** **<.0001**	0.12313 0.6155	-0.32998 0.1677	**0.67439** **0.0015**
Fracture Energy	0.40702 0.0837	1.00000	**0.92632** **<.0001**	**0.78173** **<.0001**	**0.91754** **<.0001**	0.40702 0.0837	-0.01671 0.9459	-0.21213 0.3833	0.43387 0.0635
Area norm energy	0.37193 0.1169	**0.92632** **<.0001**	1.00000	**0.69565** **0.0009**	**0.90877** **<.0001**	0.37193 0.1169	-0.05101 0.8357	-0.02357 0.9237	0.39131 0.0976
Articular comm	0.37593 0.1127	**0.78173** **<.0001**	**0.69565** **0.0009**	1.00000	**0.88450** **<.0001**	0.37593 0.1127	0.15103 0.5371	-0.05900 0.8104	0.44880 0.0539
Injury Severity Composite	**0.50175** **0.0286**	**0.91754** **<.0001**	**0.90877** **<.0001**	**0.88450** **<.0001**	1.00000	**0.50175** **0.0286**	0.00352 0.9886	-0.02357 0.9237	0.43294 0.0641
Stress& Severity	**1.00000** **<.0001**	0.40702 0.0837	0.37193 0.1169	0.37593 0.1127	**0.50175** **0.0286**	1.00000	0.12313 0.6155	-0.32998 0.1677	**0.67439** **0.0015**
Age	0.12313 0.6155	-0.01671 0.9459	-0.05101 0.8357	0.15103 0.5371	0.00352 0.9886	0.12313 0.6155	1.00000	0.02363 0.9235	0.22678 0.3505
Sex	-0.32998 0.1677	-0.21213 0.3833	-0.02357 0.9237	-0.05900 0.8104	-0.02357 0.9237	-0.32998 0.1677	0.02363 0.9235	1.00000	-0.16157 0.5087
Tonnis	**0.67439** **0.0015**	0.43387 0.0635	0.39131 0.0976	0.44880 0.0539	0.43294 0.0641	**0.67439** **0.0015**	0.22678 0.3505	-0.16157 0.5087	1.00000

The results of the Spearman's rank order correlations found significant correlations between some of the predictors and outcomes (Table 14). The two potential confounders, age and sex, were not significantly correlated to any of the predictors or outcomes. Fracture energy, area normalized fracture energy, and articular comminution were not significant predictors of the degree of arthritic development, but all trended toward significance, as was seen previously in the larger study of 71 acetabular fractures. Measures of contact stress exposure, and the combined measure of injury severity and contact stress exposure were significantly correlated with the degree of radiographic arthritis development indicated by the Tönnis grade.

CHAPTER 5 - DISCUSSION

Presently, clinical practice and research into optimal IAF treatment rely upon subjective measures of injury severity and reduction accuracy to control data and guide surgical management. However, such measures are inadequate to objectively characterize the degree of injury severity and to understand the accuracy of reduction required to optimally restore joint mechanics. Furthermore, due to this inability to fully understand the impact of injury severity on outcomes, the true effects of reduction are difficult to characterize. The only way to resolve these issues is through objective measurement of these pathomechanical factors within individual joints. The injury severity assessment and DEA contact stress models developed herein therefore hold great potential for improving research to better guide clinical practice.

Existing methods for objective measurement of injury severity and reduction accuracy after IAF had been developed in the tibial plafond. The plafond proved a useful model for establishing these objective methods due to its known tendency to degenerate quickly after injury and the relatively rare incidence of idiopathic PTOA development. Expansion of the severity and reduction analyses to include different joints in the body posed several challenges that were overcome in the course of the work described herein. Previously, the objective measures of injury severity had leveraged fracture energy and a measure of articular comminution to obtain estimates of severity. While these methods were expanded in earlier work to measure energy in other joints, they did not account for the significant differences in joint size and contact area through which the damage occurred across joints. Furthermore, development of a new articular comminution measure was also necessitated to better assess the damage to areas most critical for joint function. Finally, models of DEA in the calcaneus and acetabulum required development in order to assess reduction in the same cases where injury severity was measured and thereby provide a complete and objective assessment of the pathomechanical factors underlying PTOA development.

Normalized Fracture Severity

Expansion of the fracture severity measure to additional joints brought about consideration of the effects of the vastly different anatomies being injured. One of the most prominent differences was the size of the articular contact across which injurious energy was transferred. This study leveraged significant prior efforts investigating the variance in fracture energies across joints to establish the potential impact of differences in contact area normalized fracture energy on PTOA outcomes. There was a strong correlation between the fracture energy per unit contact area, obtained from pre-operative data, and PTOA rates across 5 different joints without controlling for any operative factors. This provided strong evidence that differences in energy per unit contact area may be more predictive of PTOA development and should be further investigated on a joint specific basis.

Though PTOA is a known sequela of acute IAF, the exact mechanism and the contributions of acute injury to its development have remained unclear. In 2011, Tochigi et al made two major discoveries. Upon examination of debrided fragments containing cartilage from calcaneal fractures, they found significantly lower chondrocyte viability near fracture edges. Interestingly, they also found that chondrocyte death propagated from these fracture sites over the next several days [9]. This discovery is important because it demonstrates that acute damage likely has a long-term effect on cartilage health through decellularization of the tissue and that the acute effects of the injury progress after surgical intervention. From these findings, one might expect joints with more fracture edges to report higher rates of injury severity, however, a 2017 study by Dibbern et al found the opposite. They found that tibial plateau fractures had significantly higher fracture edge lengths than plafond fractures, despite plateaus reporting PTOA rates half those found in plafonds[19]. To explain this finding, they suggested that differences in the impact tolerance of some joints could be due in part to differences in the size of the articular surface. Distributing the impact over a larger area would effectively lessen the magnitude of the injurious event per unit area, like contact stress is reduced by increasing contact area. For our study, to approximate this effect, the contact area was used to scale fracture energy by the area through which it could be transferred.

Fracture energy scaled by contact area is appealing in the context of assessing cartilage and joint damage. The distribution of the energy over that joint, now quantified by the scaled fracture energy, gives further insight into the severity of damage in a consistent and objective manner. The joints studied herein differ significantly in bony morphology, cartilage thickness, the surrounding anatomy, loading conditions, reconstruction difficulty, and injury patterns. However, the results suggest that 97% of variance in PTOA rates between them may be due to the acute fracture severity scaled simply by contact area.

This elucidates a potential reason for the disconnect between advances in fracture management and the lack of improvement observed in PTOA prevention. Acute biological damage caused by fracture is not meaningfully treated presently but appears to be a significant contributor to PTOA development. It likely manifests in a consistent manner across joints, but over an extended period of time as the effects of alterations in chondrocyte function after injurious impact lead to joint degeneration. The fact that the altered chondrocyte function arises over the course of over several days presents an exciting opportunity for intervention. As >97% of the variance in PTOA rates may be due to the initial severity, novel biological interventions may reduce PTOA development more substantially than previously estimated. It also suggests that less invasive surgical techniques may be preferred, especially when paired with interventions that can maintain chondrocyte viability in fractured joints.

Among the limitations of this study, the patients for whom fracture energies were computed were not all followed clinically. Therefore, rates of OA represent literature values derived from multiple patient populations. Similarly, PTOA was defined radiographically by the KL radiographic grade for studies that did not report OA development. However, the KL scale was not designed to consider symptoms when defining OA such that the relationships in this study represent radiographic, not necessarily symptomatic, OA. Finally, to be included in the study, CT scans had to be obtained during a standard of care protocol. As obtaining a CT scan does not necessarily fall under the standard of care for more minor fractures, it is possible the energy ranges are skewed toward the higher end and may not capture lower energy fractures.

Surface area-normalized fracture energy as a predictor of patient-specific PTOA development in individual joints

The purpose of this study was to improve our understanding of the influence of acute fracture severity on PTOA risk following IAFs across a variety of joints by implementing the contact area normalization within each joint. The primary hypothesis of this study was that normalized measures of acute severity would be predicted on a patient-by-patient basis was partially supported by the results. Two of the three joints examined, the tibial plafond in the ankle and the acetabulum in the hip, had significant correlations between fracture energy per unit joint surface area, obtained from pre-operative CT scans, and PTOA rates. The third joint, the calcaneus in the hindfoot, did not demonstrate these strong correlations between measures of acute severity and PTOA outcomes, but trended toward significance (p=0.06). A previous study by Rao et. al. using these data found no correlation between fracture energy and PTOA outcomes[37]. Therefore, it is notable that when accounting for joint surface area, a small to moderate correlation is found when neither fracture energy nor joint surface area demonstrate independent correlations with outcomes. Taken with the results of the tibial plafond and acetabulum and the overall correlation between all joints considered together, it confirms that a relationship exists between surface area-normalized fracture energy and PTOA development.

Logistic regressions were computed for all cases and within each joint to establish the extent to which acute severity is predictive on a patient-specific basis. For all cases, the results of the regression for both fracture energy and normalized fracture energy produced significant models with odds ratios greater than 1. For the overall models, each 1J increase in fracture energy is expected to increase the risk of PTOA development by 7.8% or 5% for each 0.1J/cm^2. However, these numbers are likely skewed by the observed lack of a significant correlation found for the calcaneus, as independent regression models of fracture energy and normalized fracture energy for both the tibial plafond and acetabulum were highly significant. The models predict a 6.6% and 10.6% increase in PTOA risk for each 1J increase in fracture energy in the acetabulum and plafond, respectively. Even greater differences were seen for the normalized fracture energy, where a 0.1J/cm^2 increase would predict a 16.2% increase in risk of PTOA development in the acetabulum and 16.6% increase in risk in the tibial plafond.

These results provide further evidence that area-normalized fracture energy as an objective measure of injury severity can explain previously unaccounted-for variance in PTOA rates. As delineated above, normalizing joints by average contact area revealed that up to 97% of the variance in PTOA rates across joints could be explained by these previously unaccounted-for differences in acute severity. This implied that there may be a consistent damage threshold across joints and led to a further hypothesis that there exists a unified damage threshold above which joints predictably progress to PTOA.

The results of this study, however, do not support that conclusion. It appears that even when controlling for the energy per unit area, joints have different impact tolerances. Despite each joint having relatively similar rates of PTOA development (for the cases included in our study this was 52-60%), joints had dissimilar average normalized fracture energies (acetabulum: 0.79 J/cm^2, tibial plafond: 1.84 J/cm^2, and calcaneus 2.42 J/cm^2). Additionally, average normalized fracture energies for the PTOA groups across joints were dissimilar (acetabulum: 0.87 J/cm^2, tibial plafond: 2.18 J/cm^2, and calcaneus 2.48 J/cm^2). Therefore, future studies are needed to establish thresholds of normalized fracture energies to best assess the contribution of initial severity to PTOA outcomes in each joint.

There are several limitations to this study. The surface areas measured may not be indicative of the areas through which energy is transferred. Contact areas through which the injurious forces are transferred will always be smaller than the surface area of the joints through which they are being transferred. Therefore, it is likely that the energy per unit area is underestimated in many cases leading to higher energies per unit area in joints with the large differences in contact versus surface area. Finally, to be included in the study, CT scans had to be obtained during standard of care protocol. It is possible then that the energy ranges are skewed toward higher energy fractures and may not capture the lower energy injuries.

PTOA development in the tibial plafond after IAF

The tibial plafond has served as the proving grounds for new objective measures of injury severity and reduction accuracy. It was therefore, used again to develop the new measures of articular comminution energy and area-normalized fracture energy as well as to compare them with the reduction. An additional seven cases were added to the nine that had both fracture severity and contact stresses reported previously. Highly significant differences were found in patients that developed PTOA from those that did not in fracture energy, normalized fracture energy, articular comminution, and contact stress over-exposure. Significant Spearman's rank order correlations were also found between all predictors and both KL graded degree of radiographic arthritis as well as OA status.

Articular comminution, in the preliminary studies on developing objective measures of injury severity, had been previously reported as the amount of surface area liberated within the first millimeter of the articular surface as a percentage of the intact area on the contralateral limb. The new measure of articular comminution was similar, but instead measured the energy absorbed within 1cm of the articular surface. The ability to measure energy without the constraint of needing an intact datum with which to compare enabled this measure to be directly applied to other joints as well. It is useful as it provides a direct measure of insult contained within the subchondral region.

The results of the new, normalized fracture energy measure appeared to modestly improve upon correlations with degree of PTOA development in the plafond when compared to the unnormalized energy (R^2=0.34 vs R^2 = 0.29). However, more significant improvements were noted when looking at the Spearman's correlations in the 71 patients reported earlier (ρ=0.52 vs ρ=0.26). On this basis, normalized fracture energy was selected as the measure to be combined with the measure of articular comminution to create a composite metric to more fully describe the severity of injury. This combined injury severity measure was more predictive of PTOA development than either of its constitutive components, indicating the necessity of studying both the articular insult and the damage to the entire bone when assessing severity in the tibial plafond.

The reduction accuracy, as measured by the contact stress over-exposure was also significantly correlated with rates of PTOA development. These findings are consistent with those reported on the smaller subset of 10 cases reported earlier. It is interesting to note that in these plafond fractures up to 61.7% of the variance in PTOA rates could be explained by this objective predictor alone compared to 70% for the combined model. It suggests the accuracy of reduction is more important than the initial injury severity in plafond injuries.

Having established the objective measures of the degree of initial injury and the degree to which loading characteristics have been altered, it is now possible to examine the true influence of reduction quality of PTOA risk in fractures of the tibial plafond. In order to better assess which predictor is most important and how they might be associated, bubble plots were created of severity and reduction with the color and size of the bubbles indicating the presence and degree of PTOA development, respectively. As might be expected of good predictors of PTOA development, the good outcomes are clustered in the lower left corner of the plot indicating low severity, excellent reduction fractures. Interestingly, the two fractures with low severity that developed PTOA had two of the highest contact stress over-exposures. This fits with one portion of the contradictory literature that reduction accuracy is important in the plafond. Similarly, several fractures with good reductions that developed PTOA had relatively higher combined severity scores. This fits with the other side of the literature where the study by Etter and Ganz suggested there may be other factors at play when good reductions result in poor outcomes with those factors now identified as the severity of injury.

The combined model demonstrated this improved understanding of PTOA development by identifying a threshold that has perfect sensitivity and specificity. It even demonstrates an highly significant correlation with the degree of PTOA severity ($\rho=0.80$, $p<0.001$). Therefore, in the plafond it appears likely that predicting PTOA development requires both assessment of injury severity and reduction accuracy. This refutes the hypothesis that acute severity more significantly contributes to PTOA in the plafond.

Examining these data in the context of our other hypothesis, that injury severity is correlated with reduction accuracy, they appear to support it. The most substantial corroborating data are the Spearman's correlations between contact stress over-exposure and measures of initial injury. Correlations between the contact stress over-exposure and each individual predictor of severity trended toward significance ($p=0.10$, $p=0.10$, $p=0.08$), while the combined measure was significantly correlated with reduction accuracy ($\rho=0.51$, $p=0.04$). However, from this limited dataset, it is difficult to determine conclusively whether the data are supportive of this hypothesis as none of the highest severity fractures achieved accurate enough reductions to have low contact stress over-exposures.

PTOA development in the calcaneus after IAF

Contrasting with the tibial plafond, PTOA development in the calcaneus is considered to result primarily from the severity of initial injury after IAF. The Sanders classification for displaced IAFs of the calcaneus is the present clinical gold standard for assessing injury severity and predicting outcomes. As prior studies have reported that up to 90% of Sanders class III fractures degenerate to PTOA despite 95% of cases having an anatomic reduction (0-1 mm), this claim is well supported in the present literature[38]. However, a previous study by Rao et al. found that a new measure of post-reduction step-off was correlated with Sanders classification[37]. This implicated surgical reduction as a potential contributor to PTOA development in IAFs of the calcaneus. The study by Rao also included a measure of fracture energy that was not found to be associated with radiographic evidence of PTOA. This finding was particularly noteworthy as it may further suggest that Sanders classification is merely indicative of how well joints are able to be reduced. It also offered the unique opportunity to study the new methods for articular comminution and area-normalization of fracture energy as improvements over the existing methods for measuring acute injury.

While the fracture energy was not significantly correlated with PTOA outcomes as discussed previously, the area-normalized fracture energy was significantly, albeit weakly, correlated with PTOA (ρ=.36, p=0.04). There were also significant differences in the area-normalized fracture energy. Area-normalized fracture energy was significantly higher for patients that developed PTOA than those that did not (2.54±0.40 MPa*s in the OA group vs 2.24±0.38 MPa*s in the no OA group, p=0.04). The articular comminution was even more significantly correlated with PTOA development (ρ=.48, p=0.004). The combined severity metric of articular comminution further improved upon the correlation between severity and outcomes. The articular comminution energy and combined metric were both more significantly correlated with PTOA outcomes than the present gold standard, Sanders classification and represent a substantial advancement in predicting the degree of PTOA development in these fractures.

In stark contrast to the literature findings of no association between reduction accuracy and PTOA development, the reduction accuracy, as measured by the contact stress over-exposure, was significantly correlated with rates of PTOA development. Furthermore, in this subset of cases, contact stress over-exposure was even more significantly related to patient outcomes than both Sanders classification and the objective measures of severity (ρ=.52, p=0.002). It is worth noting, however, that there was a relatively wide range of over-exposures and no clear threshold delineating cases that developed PTOA from those that did not. This suggests that while reduction accuracy is clearly an important factor in outcomes, the initial injury severity as well as other patient factors may contribute significantly to outcomes.

After establishing the importance of these new objective measures of injury severity and reduction accuracy, it is possible to examine their relative influence on PTOA risk in IAFs of the calcaneus. Again, bubble plots of severity and reduction were used with the color and size of the bubbles indicating the presence and degree of PTOA development, respectively. The clustering of good outcomes in the lower left corner of the plot shows that these cases involved low severity, excellent reduction fractures. Despite this, however, a number of these fractures in this region still progressed to PTOA, indicating that there remain unaccounted-for components of the PTOA development mechanism in the calcaneus. As indicated in the literature, we also found a number of cases in the lower right corner that despite excellent reduction, cases still progressed to PTOA. Interestingly, in the 33 cases we examined, none of the lowest severity injuries had poor reductions, while none of the lowest severity injuries had poor reductions, the worst reductions among them did all progress to PTOA.

The combined model of injury severity and reduction accuracy again provided the best prediction of cases that will progress to PTOA with a clear threshold above 0.4 indicating probable degeneration. It does not have the perfect sensitivity and specificity and specificity found in models of the plafond, however. It demonstrates a moderate correlation with the degree of PTOA severity (R^2=0.36), but is held back by four clear outliers. Therefore, it appears that predicting PTOA development in the calcaneus requires assessment of injury severity, reduction accuracy, and other unaccounted-for factors. Again, the clear, significant, contribution of reduction accuracy to PTOA development refutes the hypothesis that acute severity more significantly contributes to PTOA in IAFs of the calcaneus.

Finally, these data also appear to support the hypothesis that injury severity is correlated with reduction accuracy. Though fracture energy and area-normalized fracture energy are not associated with contact stress over-exposure, the articular comminution measure is highly correlated with it (ρ=.44, p=0.01). On the surface, this appears to be logical, as higher articular comminution energy fractures are more likely to have more fragments and be more difficult to reduce. However, the Sanders classification is a measure of the number of articular fragments and it was not associated with contact stress over-exposure or articular comminution energy. It is interesting to note that 3 of the 4 outliers mentioned previously were Sanders grade III fractures, suggesting that the objective measures of injury severity still lack some contextual information necessary to fully assess the injury. Therefore, while some key measures of injury severity are correlated with reduction accuracy, others are not, so the hypothesis can neither be refuted nor accepted. It is also worth noting that these fractures were all treated percutaneously at the University of Iowa. The percutaneous technique focuses on minimizing soft tissue damage, so surgery is performed through small incisions where the joint space is never visualized. Therefore, compared to extensile lateral approaches where a skin flap is created to fully visualize the joint in hopes of accurate restoration, the results may be skewed toward having poorer surgical outcomes which may make the initial injury have greater influence on and correlation with the reduction.

Contact stress over-exposure in the acetabulum after IAF

As a foil to the calcaneus, PTOA in the acetabulum is thought to result not from the severity of initial injury, but from the accuracy of surgical reduction. Many past studies have cited anatomic reductions of less than 1 mm as being a key factor in preventing PTOA in acetabulum fractures[29]. However, there is some evidence that certain fractures like posterior column and T-shaped fractures have negative impacts on outcomes[68].

These findings were confirmed previously in the larger series of 71 fractures where the fracture energy and area-normalized fracture energy were significantly predictive of PTOA development after IAF of the acetabulum ($p<0.001$). Higher articular comminution energy was also significantly predictive of PTOA development($p<0.001$). All measures of severity demonstrated moderate Spearman's correlations with outcomes, but these correlations were not significant (fracture energy $\rho=0.43$ $p=0.06$, normalized fracture energy $\rho=0.39$ $p=0.10$, articular comminution $\rho=0.43$ $p=0.054$). The combined severity metric improved upon the correlation between severity and outcomes ($R^2=0.36$ vs $R^2=0.23$, $R^2=0.20$, $R^2=0.21$).

Confirming literature findings of significant association between reduction accuracy and PTOA development, the reduction accuracy, as measured by the contact stress over-exposure, was also significantly correlated with the degree of PTOA development ($\rho=0.674$ $p=0.0015$). The association between PTOA outcomes and contact stress over-exposure, however, does not well delineate which cases will develop PTOA; two cases are misclassified and six fall within 5% of the optimal cutoff around 3.9MPa*s. This suggests that while reduction accuracy is clearly an important factor, the initial injury severity as well as other patient factors may contribute significantly to outcomes.

To examine the relative influence of injury severity and reduction accuracy on PTOA risk in IAFs of the acetabulum, bubble plots of severity and reduction were again used with the color and size of the bubbles indicating the presence and degree of PTOA development, respectively. The clustering of good outcomes in the lower left corner of the plot indicate these correspond to low severity, excellent reduction fractures. There are, however, two outliers to this trend: one developing PTOA while having low severity and an excellent reduction, while the other did not degenerate to PTOA despite having a poor reduction and high severity. The latter outlier is of note as it’s the only outlier with high contact stress over-exposure that did not degenerate to PTOA. This could potentially be explained by an error in our modeling assumptions or, if the data are real and can be confirmed in a larger study, may indicate that the acetabulum is more tolerant to incongruities than previously reported.

Once again, the combined model of injury severity and reduction accuracy provided the best prediction of cases that will progress to PTOA with a clear threshold above 0.25 indicating probable degeneration. It does not have perfect sensitivity and specificity as found in the plafond, however. It demonstrates a moderate correlation with the degree of PTOA severity (R^2=0.46) but also has the two aforementioned outliers. Therefore, in the acetabulum it again appears that predicting PTOA development requires assessment of injury severity, reduction accuracy, and other unaccounted for factors. Furthermore, significant correlation of reduction accuracy to PTOA development refutes the hypothesis that acute severity more significantly contributes to PTOA in IAFs of the acetabulum. Finally, more so than the distal tibia and calcaneus, these data clearly support the hypothesis that injury severity is correlated with reduction accuracy. Fracture energy, area-normalized fracture energy, and articular comminution are all associated with contact stress over-exposure, while the combined metric is significantly correlated (ρ=.50, p=0.03).

Limitations

There were several limitations to these studies. Perhaps the most important to note is that the PTOA outcomes data examined were exclusively radiographic. Both the Kellgren-Lawrence and Tonnis classification systems have been demonstrated to have problems with reproducibility, especially when measured from plain radiographs. Furthermore, these radiographic measures of PTOA development do not always correlate with patient reported pain and function outcomes. This is perhaps most evidenced in the calcaneus where ~90% of patients reported by Sanders developed radiographic PTOA while only ~30% were treated for late stage PTOA development[38]. In these studies, the reproducibility was addressed by having a consensus of multiple raters, but correlations with patient function and patient reported outcomes remain a confounding factor.

The severity metrics have several important limitations. The fracture energy is computed based on bone density derived from CT Hounsfield Units. However, bone density is known to decrease with age along with healing capacity. Therefore, older patients may have lower energy fractures in their lower density bone that end up being relatively more severe than comparable energy fractures in a younger population. Additionally, sex has also been demonstrated to influence PTOA development with women being slightly more likely to develop PTOA. To account for this, we examined correlations between all predictors and outcomes with age and sex. However, for our limited sample size, we did not find any significant correlations or differences between groups in the calcaneus and acetabulum, with the only significant association being an increased risk of PTOA in women with plafond fractures.

A further limitation of the fracture energy measure comes from fractures not loaded through the articular joint. Fractures where energy is not directed through the articulating surfaces may result in a breakdown of the logic involved in assessing severity as it is assumed that energy transferred through the articular surface causes damage to the cartilage, matrix, and subchondral bone leading to PTOA. In the plafond, common injury mechanisms are likely to produce this axial transfer as the talus hammers into the bottom of the tibia to produce fracture. It is, therefore, not surprising that the fracture energy measure performed best in this joint. In the calcaneus, however, the Achilles and contact with the ground can initiate fracture with an energy path that does not necessitate direct transfer through the joint. Accordingly, in this joint the fracture energy was found to be uncorrelated with PTOA development thereby evincing the limitations of this measure. Fortunately, the articular comminution metric can help to address this issue as it provides an estimate of the energy transferred through the articular surface. When the energy released within 1 cm of the subchondral bone was assessed, it was found to be significantly correlated with PTOA development in all joints. The articular comminution metric is itself limited, however, in that it does not capture all the energy transferred through the joint but rather is constrained to only the subchondral bone. Therefore, the combined measure of articular comminution and fracture energy is required to best account for both sets of limitations.

Finally, the DEA contact stress models also have significant limitations. Perhaps the most important limitation is that of stability. Often fractures are accompanied by increased ligamentous laxity from tears that occur during the injury. This increased laxity raises concerns for instability that can dramatically increases stresses when combined with incongruities[96-98].

The DEA models reported in this work did not account for any instabilities that may occur. A further limitation to the DEA models is that they did not account for differences in patient-specific gait nor did they account for variations in postoperative gait as the distal tibial, calcaneal, and acetabular models all relied upon gait obtained from sources other than IAF patients. As variations in gait have previously been demonstrated to have significant differences in contact stress distributions and magnitudes across surfaces, the modeled gait parameters may substantially impact results. Therefore, future work should ideally aim to use patient-specific gait parameters to best assess joint contact stresses.

CHAPTER 6 - CONCLUSIONS

Post-traumatic osteoarthritis is a complex disease with multiple elements contributing to its progression. It results from a combination of acute injury with surgical and biological factors. Presently, clinicians utilize subjective surrogates to assess acute and chronic mechanical damage when prognosticating PTOA development. Clinical tools like fracture classifications and step-off measures have presented challenges, however, given poor inter-observer reliability and difficulties in comparing categorical classifications with continuous predictors of PTOA development. Furthermore, such assessments do not account for the interaction between the acute injury and the chronic problems resulting from more difficult surgical reconstructions. This work has laid out significant advancements that address these issues. In particular, it details patient-specific assessment capabilities and leverages them toward unifying understanding of all mechanical aspects of PTOA development. Both fracture energy (preoperatively) and contact stress (postoperatively) proved powerful predictive tools and provided a means to begin objectively generating risk assessments on a patient-specific basis.

Acute mechanical damage, as measured by area-normalized fracture energy and articular comminution energy, was found to be a significant independent contributor to PTOA due to the chronic damage, as measured by contact stress over-exposure, associated with poor surgical reconstructions. This was the first line of work to be able to objectively control for both factors and establish their independence in three joints: the hindfoot, hip, and ankle. It is also the first to study mechanical damage thresholds across joints and identify differences between them. Specifically, when examining fracture energy in the calcaneus, distal tibia, proximal tibia, acetabulum, and distal radius, different ranges of acute damage and acute damage per unit area were found in different joints. These differences were highly correlated with the risk of PTOA development across joints, indicating that differences in PTOA rates seen across joints may be attributable to differences in initial injury. This would explain why, despite significant advances in surgical treatment, high PTOA rates persist.

There were not, however, consistent predictive thresholds of acute severity PTOA across joints. The calcaneal fracture energy was not significantly correlated with PTOA status while the tibial plafond and acetabulum's were albeit at different thresholds of area-normalized fracture energy. Taken together, these findings could imply the existence of inherent biological differences across joints in their ability to recover from initial trauma. Alternatively, some of these findings may be explained by differences in the subjective outcome measures. The Kellgren-Lawrence and Tönnis grades have well-documented challenges with reproducibility and only provide categorical information on patient outcomes. In the future, feature-rich weight-bearing CT's can provide a means through which continuous, objective measures of degeneration are obtained.

The ability to predict PTOA development is crucial to providing improved control for clinical studies. However, the utility of the measures studied herein could be greatly expanded if they were implemented to generate patient-specific risk models in a clinical setting. The greatest impediment to their implementation is the speed of CT segmentation. The fracture energy and contact stress computations that occur after segmentation take on the order of minutes or even seconds while extracting accurate geometries of bone fragments is a time-consuming task requiring up to four hours of manual editing per case. Future studies could leverage *a priori* data to minimize or even eliminate this component of analysis and thereby empower physicians and patients to make evidence-based decisions on these potentially devastating injuries.

REFERENCES

1. Thomas, T.P., et al., *Objective CT-based metrics of articular fracture severity to assess risk for posttraumatic osteoarthritis.* J Orthop Trauma, 2010. **24**(12): p. 764-9.
2. Bergmann, G., et al., *Hip contact forces and gait patterns from routine activities.* J Biomech, 2001. **34**(7): p. 859-71.
3. Giannoudis, P.V., et al., *Articular step-off and risk of post-traumatic osteoarthritis. Evidence today.* Injury, 2010. **41**(10): p. 986-95.
4. Macko, V.W., et al., *The joint-contact area of the ankle. The contribution of the posterior malleolus.* J Bone Joint Surg Am, 1991. **73**(3): p. 347-51.
5. Williams, T.M., et al., *Factors affecting outcome in tibial plafond fractures.* Clin Orthop Relat Res, 2004(423): p. 93-8.
6. Schenker, M.L., et al., *Pathogenesis and prevention of posttraumatic osteoarthritis after intra-articular fracture.* J Am Acad Orthop Surg, 2014. **22**(1): p. 20-8.
7. McKinley, T.O., et al., *Basic science of intra-articular fractures and posttraumatic osteoarthritis.* J Orthop Trauma, 2010. **24**(9): p. 567-70.
8. Brown, T.D., et al., *Posttraumatic osteoarthritis: a first estimate of incidence, prevalence, and burden of disease.* J Orthop Trauma, 2006. **20**(10): p. 739-44.
9. Tochigi, Y., et al., *Distribution and progression of chondrocyte damage in a whole-organ model of human ankle intra-articular fracture.* J Bone Joint Surg Am, 2011. **93**(6): p. 533-9.
10. Coleman, M.C., et al., *Differential Effects of Superoxide Dismutase Mimetics after Mechanical Overload of Articular Cartilage.* Antioxidants (Basel), 2017. **6**(4).
11. Coleman, M.C., et al., *Injurious Loading of Articular Cartilage Compromises Chondrocyte Respiratory Function.* Arthritis Rheumatol, 2016. **68**(3): p. 662-71.
12. Humphrey, C.A., D.R. Dirschl, and T.J. Ellis, *Interobserver reliability of a CT-based fracture classification system.* J Orthop Trauma, 2005. **19**(9): p. 616-22.
13. Swiontkowski, M.F., et al., *Interobserver variation in the AO/OTA fracture classification system for pilon fractures: is there a problem?* J Orthop Trauma, 1997. **11**(7): p. 467-70.
14. Anderson, D.D., et al., *Quantifying tibial plafond fracture severity: absorbed energy and fragment displacement agree with clinical rank ordering.* J Orthop Res, 2008. **26**(8): p. 1046-52.
15. Beardsley, C., J.L. Marsh, and T. Brown, *Quantifying comminution as a measurement of severity of articular injury.* Clin Orthop Relat Res, 2004(423): p. 74-8.
16. Beardsley, C.L., et al., *Interfragmentary surface area as an index of comminution severity in cortical bone impact.* J Orthop Res, 2005. **23**(3): p. 686-90.
17. Beardsley, C.L., et al., *Interfragmentary surface area as an index of comminution energy: proof of concept in a bone fracture surrogate.* J Biomech, 2002. **35**(3): p. 331-8.
18. Beardsley, C.L., et al., *High density polyetherurethane foam as a fragmentation and radiographic surrogate for cortical bone.* Iowa Orthop J, 2000. **20**: p. 24-30.
19. Dibbern, K., et al., *Fractures of the tibial plateau involve similar energies as the tibial pilon but greater articular surface involvement.* J Orthop Res, 2017. **35**(3): p. 618-624.
20. Thomas, T.P., et al., *A method for the estimation of normative bone surface area to aid in objective CT-based fracture severity assessment.* Iowa Orthop J, 2008. **28**: p. 9-13.

21. Bartlett CS, D.A.M., Weiner LS., *Fractures of the Tibial Pilon. In: Browner BD, Jupiter JB, Levine AM, Trafton PG.*, in *Skeletal trauma*. 1998, W.B. Saunders Company: Philadelphia, PA. p. 2295-2325.
22. Kempton, L.B., et al., *Objective Metric of Energy Absorbed in Tibial Plateau Fractures Corresponds Well to Clinician Assessment of Fracture Severity.* J Orthop Trauma, 2016. **30**(10): p. 551-6.
23. Anderson, D.D., et al., *Contact stress distributions in malreduced intraarticular distal radius fractures.* J Orthop Trauma, 1996. **10**(5): p. 331-7.
24. Anderson, D.D., et al., *Post-traumatic osteoarthritis: improved understanding and opportunities for early intervention.* J Orthop Res, 2011. **29**(6): p. 802-9.
25. Anderson, D.D., et al., *Is elevated contact stress predictive of post-traumatic osteoarthritis for imprecisely reduced tibial plafond fractures?* J Orthop Res, 2011. **29**(1): p. 33-9.
26. Archdeacon, M.T. and S.K. Dailey, *Efficacy of Routine Postoperative CT Scan After Open Reduction and Internal Fixation of the Acetabulum.* J Orthop Trauma, 2015. **29**(8): p. 354-8.
27. Tannast, M., S. Najibi, and J.M. Matta, *Two to twenty-year survivorship of the hip in 810 patients with operatively treated acetabular fractures.* J Bone Joint Surg Am, 2012. **94**(17): p. 1559-67.
28. Marsh, J.L., et al., *Articular fractures: does an anatomic reduction really change the result?* J Bone Joint Surg Am, 2002. **84-A**(7): p. 1259-71.
29. Matta, J.M., *Fractures of the acetabulum: accuracy of reduction and clinical results in patients managed operatively within three weeks after the injury.* J Bone Joint Surg Am, 1996. **78**(11): p. 1632-45.
30. Mayo, K.A., et al., *Surgical revision of malreduced acetabular fractures.* Clin Orthop Relat Res, 1994(305): p. 47-52.
31. Letournel, E.m., R. Judet, and R. Elson, *Fractures of the acetabulum*. 2nd ed. 1993, Berlin ; New York: Springer-Verlag. xxiii, 733 p.
32. Stevens, D.G., et al., *The long-term functional outcome of operatively treated tibial plateau fractures.* J Orthop Trauma, 2001. **15**(5): p. 312-20.
33. Kern, A.M. and D.D. Anderson, *Expedited patient-specific assessment of contact stress exposure in the ankle joint following definitive articular fracture reduction.* J Biomech, 2015. **48**(12): p. 3427-32.
34. Thomas-Aitken, H.D., M.C. Willey, and J.E. Goetz, *Joint contact stresses calculated for acetabular dysplasia patients using discrete element analysis are significantly influenced by the applied gait pattern.* J Biomech, 2018.
35. Coleman, M.C., et al., *Targeting mitochondrial responses to intra-articular fracture to prevent posttraumatic osteoarthritis.* Sci Transl Med, 2018. **10**(427).
36. Ibrahim, T., et al., *Displaced intra-articular calcaneal fractures: 15-year follow-up of a randomised controlled trial of conservative versus operative treatment.* Injury, 2007. **38**(7): p. 848-55.
37. Rao, K., et al., *Correlation of Fracture Energy with Sanders Classification and Post-Traumatic Osteoarthritis following Displaced Intra-Articular Calcaneus Fractures.* J Orthop Trauma, 2019.

38. Sanders, R., et al., *Operative treatment of displaced intraarticular calcaneal fractures: long-term (10-20 Years) results in 108 fractures using a prognostic CT classification.* J Orthop Trauma, 2014. **28**(10): p. 551-63.
39. Marsh, J.L., D.P. Weigel, and D.R. Dirschl, *Tibial plafond fractures. How do these ankles function over time?* J Bone Joint Surg Am, 2003. **85-A**(2): p. 287-95.
40. Ovadia, D.N. and R.K. Beals, *Fractures of the tibial plafond.* J Bone Joint Surg Am, 1986. **68**(4): p. 543-51.
41. Teeny, S.M. and D.A. Wiss, *Open reduction and internal fixation of tibial plafond fractures. Variables contributing to poor results and complications.* Clin Orthop Relat Res, 1993(292): p. 108-17.
42. Honkonen, S.E., *Degenerative arthritis after tibial plateau fractures.* J Orthop Trauma, 1995. **9**(4): p. 273-7.
43. Rademakers, M.V., et al., *Operative treatment of 109 tibial plateau fractures: five- to 27-year follow-up results.* J Orthop Trauma, 2007. **21**(1): p. 5-10.
44. Volpin, G., et al., *Degenerative arthritis after intra-articular fractures of the knee. Long-term results.* J Bone Joint Surg Br, 1990. **72**(4): p. 634-8.
45. Weigel, D.P. and J.L. Marsh, *High-energy fractures of the tibial plateau. Knee function after longer follow-up.* J Bone Joint Surg Am, 2002. **84-A**(9): p. 1541-51.
46. Letournel, E., *Acetabulum fractures: classification and management.* Clin Orthop Relat Res, 1980(151): p. 81-106.
47. Forward, D.P., T.R. Davis, and J.S. Sithole, *Do young patients with malunited fractures of the distal radius inevitably develop symptomatic post-traumatic osteoarthritis?* J Bone Joint Surg Br, 2008. **90**(5): p. 629-37.
48. Goldfarb, C.A., et al., *Fifteen-year outcome of displaced intra-articular fractures of the distal radius.* J Hand Surg Am, 2006. **31**(4): p. 633-9.
49. Lutz, M., et al., *Arthritis predicting factors in distal intraarticular radius fractures.* Arch Orthop Trauma Surg, 2011. **131**(8): p. 1121-6.
50. Crutchfield, E.H., et al., *Tibial pilon fractures: a comparative clinical study of management techniques and results.* Orthopedics, 1995. **18**(7): p. 613-7.
51. Wyrsch, B., et al., *Operative treatment of fractures of the tibial plafond. A randomized, prospective study*. J Bone Joint Surg Am, 1996. **78**(11): p. 1646-57.
52. Etter, C. and R. Ganz, *Long-term results of tibial plafond fractures treated with open reduction and internal fixation.* Arch Orthop Trauma Surg, 1991. **110**(6): p. 277-83.
53. Marsh, J.L., et al., *Use of an articulated external fixator for fractures of the tibial plafond.* J Bone Joint Surg Am, 1995. **77**(10): p. 1498-509.
54. Patterson, M.J. and J.D. Cole, *Two-staged delayed open reduction and internal fixation of severe pilon fractures.* J Orthop Trauma, 1999. **13**(2): p. 85-91.
55. DeCoster, T.A., et al., *Rank order analysis of tibial plafond fractures: does injury or reduction predict outcome?* Foot Ankle Int, 1999. **20**(1): p. 44-9.
56. Marsh J.L., W.T., Nepola J.V., DeCoster T., Hurwitz S., Dirschl D., *Tibial plafond fractures: does articular reduction and/or injury pattern predict outcome?* Orthop Trans., 1997. **21**: p. 563.
57. Kellgren, J.H. and J.S. Lawrence, *Radiological assessment of osteo-arthrosis.* Ann Rheum Dis, 1957. **16**(4): p. 494-502.
58. Busse, J., W. Gasteiger, and D. Tonnis, *[A new method for roentgenologic evaluation of the hip joint--the hip factor]*. Arch Orthop Unfallchir, 1972. **72**(1): p. 1-9.

59. Busse, J., W. Gasteiger, and D. Tonnis, *[Significance of the "summarized hip factor" in the diagnosis and prognosis deformed hip joints]*. Arch Orthop Unfallchir, 1972. **72**(3): p. 245-52.
60. Sanders, R., et al., *Operative treatment in 120 displaced intraarticular calcaneal fractures. Results using a prognostic computed tomography scan classification.* Clin Orthop Relat Res, 1993(290): p. 87-95.
61. Michelson, J.D., *Fractures about the ankle.* J Bone Joint Surg Am, 1995. **77**(1): p. 142-52.
62. Marsh, J.L., Buckwalter, J., Gelberman, R., Dirschl, D., Olson, S., Brown, T., Llinias, A. , *Articular Fractures: Does an Anatomic Reduction Really Change the Result?* JBJS, 2002: p. 1259.
63. Judet, R., J. Judet, and E. Letournel, *[Fractures of the Acetabulum]*. Acta Orthop Belg, 1964. **30**: p. 285-93.
64. Letournel, E., *[Surgical treatment of fractures of the acetabulum: results over a twenty-five year period (author's transl)]*. Chirurgie, 1981. **107**(3): p. 229-36.
65. Matta, J.M., D.K. Mehne, and R. Roffi, *Fractures of the acetabulum. Early results of a prospective study.* Clin Orthop Relat Res, 1986(205): p. 241-50.
66. Pantazopoulos, T. and C. Mousafiris, *Surgical treatment of central acetabular fractures.* Clin Orthop Relat Res, 1989(246): p. 57-64.
67. Kebaish, A.S., A. Roy, and W. Rennie, *Displaced acetabular fractures: long-term follow-up.* J Trauma, 1991. **31**(11): p. 1539-42.
68. Briffa, N., et al., *Outcomes of acetabular fracture fixation with ten years' follow-up.* J Bone Joint Surg Br, 2011. **93**(2): p. 229-36.
69. Hadley, N.A., T.D. Brown, and S.L. Weinstein, *The effects of contact pressure elevations and aseptic necrosis on the long-term outcome of congenital hip dislocation.* J Orthop Res, 1990. **8**(4): p. 504-13.
70. Maxian, T.A., T.D. Brown, and S.L. Weinstein, *Chronic stress tolerance levels for human articular cartilage: two nonuniform contact models applied to long-term follow-up of CDH.* J Biomech, 1995. **28**(2): p. 159-66.
71. Anderson, D.D., et al., *Intra-articular contact stress distributions at the ankle throughout stance phase-patient-specific finite element analysis as a metric of degeneration propensity.* Biomech Model Mechanobiol, 2006. **5**(2-3): p. 82-9.
72. Anderson DD, V.H.C., Marsh JL, Brown TD., *Is elevated contact stress predictive of post-traumatic osteoarthritis for imprecisely reduced tibial plafond fractures?* J Orthop Res, 2010. **29**: p. 33-39.
73. Anderson, D.D., et al., *Physical validation of a patient-specific contact finite element model of the ankle.* J Biomech, 2007. **40**(8): p. 1662-9.
74. Townsend, K.C., et al., *Discrete element analysis is a valid method for computing joint contact stress in the hip before and after acetabular fracture.* J Biomech, 2018. **67**: p. 9-17.
75. Thomas, T.P., et al., *ASB Clinical Biomechanics Award Paper 2010 Virtual pre-operative reconstruction planning for comminuted articular fractures.* Clin Biomech (Bristol, Avon), 2011. **26**(2): p. 109-15.
76. Snyder, S.M. and E. Schneider, *Estimation of mechanical properties of cortical bone by computed tomography.* J Orthop Res, 1991. **9**(3): p. 422-31.

77. Sangeorzan, B.J., et al., *Contact characteristics of the subtalar joint: the effect of talar neck misalignment.* J Orthop Res, 1992. **10**(4): p. 544-51.
78. Wagner, U.A., et al., *Contact characteristics of the subtalar joint: load distribution between the anterior and posterior facets.* J Orthop Res, 1992. **10**(4): p. 535-43.
79. Wang, C.L., et al., *Contact areas and pressure distributions in the subtalar joint.* J Biomech, 1995. **28**(3): p. 269-79.
80. Kura, H., et al., *Measurement of surface contact area of the ankle joint.* Clin Biomech (Bristol, Avon), 1998. **13**(4-5): p. 365-370.
81. Millington, S., et al., *A stereophotographic study of ankle joint contact area.* J Orthop Res, 2007. **25**(11): p. 1465-73.
82. Ramsey, P.L. and W. Hamilton, *Changes in tibiotalar area of contact caused by lateral talar shift.* J Bone Joint Surg Am, 1976. **58**(3): p. 356-7.
83. Fukubayashi, T. and H. Kurosawa, *The contact area and pressure distribution pattern of the knee. A study of normal and osteoarthrotic knee joints.* Acta Orthop Scand, 1980. **51**(6): p. 871-9.
84. Ihn, J.C., S.J. Kim, and I.H. Park, *In vitro study of contact area and pressure distribution in the human knee after partial and total meniscectomy.* Int Orthop, 1993. **17**(4): p. 214-8.
85. Giannoudis, P.V., et al., *Operative treatment of displaced fractures of the acetabulum. A meta-analysis.* J Bone Joint Surg Br, 2005. **87**(1): p. 2-9.
86. Greenwald, A.S. and D.W. Haynes, *Weight-bearing areas in the human hip joint.* J Bone Joint Surg Br, 1972. **54**(1): p. 157-63.
87. Wang, G., et al., *Three-dimensional finite analysis of acetabular contact pressure and contact area during normal walking.* Asian J Surg, 2017. **40**(6): p. 463-469.
88. Fischer, K.J., et al., *MRI-based modeling for radiocarpal joint mechanics: validation criteria and results for four specimen-specific models.* J Biomech Eng, 2011. **133**(10): p. 101004.
89. Wagner, W.F., Jr., et al., *Effects of intra-articular distal radius depression on wrist joint contact characteristics.* J Hand Surg Am, 1996. **21**(4): p. 554-60.
90. Li, W., et al., *Patient-specific finite element analysis of chronic contact stress exposure after intraarticular fracture of the tibial plafond.* J Orthop Res, 2008. **26**(8): p. 1039-45.
91. Akiyama, K., et al., *Three-dimensional distribution of articular cartilage thickness in the elderly talus and calcaneus analyzing the subchondral bone plate density.* Osteoarthritis Cartilage, 2012. **20**(4): p. 296-304.
92. Arndt, A., et al., *Ankle and subtalar kinematics measured with intracortical pins during the stance phase of walking.* Foot Ankle Int, 2004. **25**(5): p. 357-64.
93. Giddings, V.L., et al., *Calcaneal loading during walking and running.* Med Sci Sports Exerc, 2000. **32**(3): p. 627-34.
94. Stauffer, R.N., E.Y. Chao, and R.C. Brewster, *Force and motion analysis of the normal, diseased, and prosthetic ankle joint.* Clin Orthop Relat Res, 1977(127): p. 189-96.
95. Tonnis, D., *Normal values of the hip joint for the evaluation of X-rays in children and adults.* Clin Orthop Relat Res, 1976(119): p. 39-47.
96. McKinley, T.O., et al., *Incongruity versus instability in the etiology of posttraumatic arthritis.* Clin Orthop Relat Res, 2004(423): p. 44-51.
97. McKinley, T.O., et al., *Instability-associated changes in contact stress and contact stress rates near a step-off incongruity.* J Bone Joint Surg Am, 2008. **90**(2): p. 375-83.

98. Tochigi, Y., et al., *Correlation of dynamic cartilage contact stress aberrations with severity of instability in ankle incongruity*. J Orthop Res, 2008. **26**(9): p. 1186-93.

Toward a Unifying Understanding of the Influence of Acute Fracture Severity on PTOA Risk Following Intra-Articular Fractures

Kevin Dibbern[1], Todd O. McKinley[2], J. Lawrence Marsh[1], Donald D. Anderson[1]
[1]University of Iowa, Iowa City, IA; [2]Indiana University School of Medicine, Indianapolis, IN
kevin-dibbern@uiowa.edu

Disclosures: Kevin Dibbern (N), Todd. O. McKinley (N), J. Lawrence Marsh (N), Donald D. Anderson (N)

INTRODUCTION: Despite advances in surgical care over the past 50 years, the rates of post-traumatic osteoarthritis (PTOA) following intra-articular fractures (IAFs) have not substantially declined [1]. There are two broad theories regarding the mechanical origins of PTOA development. The first is that following surgical IAF reduction, residual incongruities lead to changes in the joint's mechanical environment that are deleterious to cartilage health. The second is that the initial fracturing event damages the joint beyond its capacity to recover. We hypothesize that it is the acute fracture severity, along with associated biological responses, that contributes most significantly to the risk of PTOA in these joints. The success of preventing PTOA after IAF is widely held to relate to the fracture type and its severity, even across different reconstruction techniques. However, clinical severity assessment relies upon categorical classifications that are joint-specific and have poor inter-observer reliability. To remedy these shortcomings, novel CT-based analysis methods have previously been developed to objectively quantify severity [2]. Over the past decade, these techniques have been further developed to enable larger-scale study of fracture severity in the clinical setting. The objective of the present study was to leverage new assessment capabilities toward a unifying understanding of the influence of acute fracture severity on PTOA risk following IAFs across a variety of articular joints.

METHODS: There were 262 patients having sustained IAFs in this IRB-approved multi-institutional level III diagnostic study. Patients were selected for having pre-operative CT scans available for IAFs of the distal radius, acetabulum, proximal tibia, distal tibia, or calcaneus. Fracture severity was analyzed for all fractures included in the study using previously validated, objective analysis methods working from pre-operative CT scans [2]. The analysis methods quantify the energy involved in creating a fracture (the fracture energy) using principles from fracture mechanics. When axial fracturing impacts are delivered to a joint, energy transfer across the joint is distributed over the articular surface through the contact area. To enable comparisons of the fracture energies across different joints, we normalized to characteristic joint-specific contact areas. We queries the published literature for generally accepted averages of the relevant contact areas. In lieu of appropriate duration longer-term clinical follow-up data for each of these patients, we again turned to the published literature to find average rates of PTOA development for each of the joints as a point of comparison. For consistency across the studies, we defined PTOA as being present in joints when the Kellgren-Lawrence radiographic grade [3] was greater than or equal to 2. To explore how acute fracture severity influences PTOA risk after IAF, we first examined correlations between the computed fracture energies and published PTOA rates. Then an additional data analysis step involved likewise examining correlations between contact area-normalized fracture energies and PTOA rates.

RESULTS: Fracture energies ranged from 0.9 to 38 J across all cases. Energies ranges were 14.2 to 26.2J (mean±SD = 19.3±3.1J) for calcaneal, 0.9 to 38J (15.3±7.3J) for distal tibial, 3.2 to 33.2J (13.1±6.5J) for proximal tibial, 4.6 to 32.8J (18.0±8.2J) for acetabular, and 2.8 to 9.0J (4.9±1.8J) for distal radial fractures. The contact area-normalized fracture energies ranged from 0.14 to 8.90 J/cm^2 for all cases. The range of contact area-normalized fracture energies was 4.80 to 8.90 (6.55±1.04) J/cm^2 for calcaneal, 0.21 to 4.66 (1.77±1.15) J/cm^2 for distal tibial, 0.28 to 2.92 (1.16±0.57) J/cm^2 for proximal tibial, 0.22 to 1.58 (0.87±0.39) J/cm^2 for acetabular, and 1.38 to 4.47 (2.41±0.87) J/cm^2 for distal radial fractures. The computed fracture energies showed no correlation whatsoever with the published rates of PTOA across the joints studied (Figure 1). However, there was a highly significant relationship between contact area-normalized fracture energies and the rates of PTOA (Figure 2).

DISCUSSION: This study sought to understand the influence of acute fracture severity on PTOA risk following IAFs across a variety of articular joints. The hypothesis that acute fracture severity contributes significantly to the risk of PTOA development was supported by these data. There was a strong correlation between the fracture energy per unit contact area, obtained from pre-operative data, and PTOA rates across 5 different joints without controlling for any operative factors. This elucidates a potential reason for the disconnect between advances in fracture management and the lack of improvement observed in PTOA prevention after IAFs. Acute biological damage caused by fracture is not effectively treated but appears to be a significant contributor to PTOA risk. As ~85% of the variance in PTOA rates appears to be due to the initial severity, novel biological interventions may reduce PTOA development substantially.

SIGNIFICANCE/CLINICAL RELEVANCE: This study is the first to objectively compare the contribution of acute injury severity across different joints throughout the body. The results suggest that acute fracture severity may, in large part, explain why high PTOA rates persist after intra-articular fractures.

REFERENCES: [1] McKinley et al. J Orthop Trauma, 2010. 24:567-70. [2] Thomas et al. J Orthop Trauma, 2010. 24:764-9. [3] Kellgren and Lawrence. Ann Rheum Dis. 1957. 16:494-502

ACKNOWLEDGEMENTS: Research supported by NIH/NIAMS (P50AR055533, R21AR061808) and the Department of Defense (W81XWH-15-2-0087).

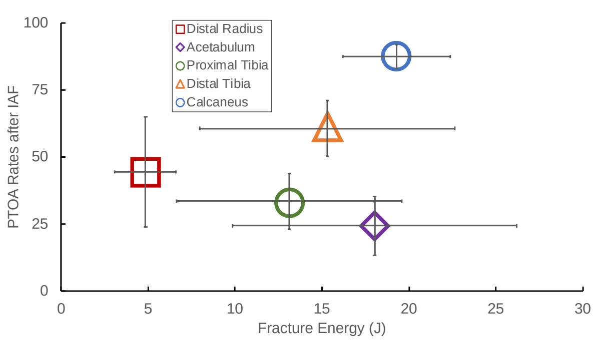

Figure 1: Poor agreement between fracture energy and rates of PTOA across different joint.

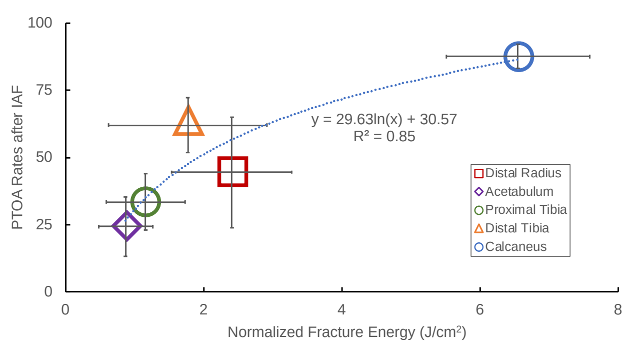

Figure 2: Contact area-normalized fracture energy is predictive of PTOA across joints

Objective Mechanical Measures Predict Post-traumatic OA Risk after Intra-articular Fracture of the Tibial Plafond

Kevin N. Dibbern, Michael C. Willey, J. Lawrence Marsh, Donald D. Anderson
University of Iowa, Iowa City, IA
Kevin-Dibbern@uiowa.edu

Disclosures: Kevin N. Dibbern (N), Michael C. Willey (N), J. Lawrence Marsh (N), Donald D. Anderson (N)

INTRODUCTION: Post-traumatic osteoarthritis (PTOA) after intra-articular fracture (IAF) of the tibial plafond commonly occurs within 2 years of injury. Contradictory clinical evidence has found both the severity of the initial injury and surgical reduction accuracy to be important determinants of this rapid progression to PTOA [1-3]. But, as Marsh et al. noted, "one of the biggest challenges for research on the effect of articular reduction is to disentangle the effect of injury to the articular surface from … the reduction" [4]. Recently, patient-specific techniques for objectively quantifying the fracture severity (using fracture energy) and the accuracy of surgical reduction (discrete element analysis (DEA) computed contact stress elevation) have been developed. The objective of this study was to use these measures to determine the relationships between the acute fracture severity, the accuracy of surgical reduction, and the PTOA risk after IAF of the tibial plafond.

METHODS: Sixteen patients with articular fractures of the tibial plafond were enrolled in this IRB-approved study. Patients were selected for having both pre- and post-operative CT imaging with a minimum of 24 months of radiographic follow-up. Kellgren-Lawrence grades were determined for each case with grades ≥2 considered as having PTOA. Distal tibia fracture fragment geometries were extracted from pre-op CT scans for injury severity analysis, while tibial and talar geometries were segmented from post-op CT scans for contact stress analysis. Fracture severity was analyzed using previously validated, objective analysis methods that involve quantifying the energy involved in creating a fracture (the fracture energy) by automatically identifying the fracture liberated surface area and scaling by density dependent energy release rates that can be estimated from pre-op CT scans. The amount of energy dispersed within 1cm of the joint surface and the area of the joint surface are also accounted for in the severity metric. Model generation for DEA was dependent upon estimation of the cartilage surface/thickness from CT. Cartilage surfaces were projected a uniform 1.7mm normal to each triangulated bone surfaces. DEA was performed using body weight-scaled forces and rotations to simulate the stance phase of gait with 13 quasi-static loading steps. DEA was used to compute deleterious contact stress exposure above a damage threshold of 3MPa (Figure 1). Both the combined injury severity metric and the contact stress over-exposure were used to predict PTOA outcomes, and their predictive capabilities were analyzed using receiver-operating characteristic (ROC) curves. Spearman's correlations were used to study inter-relationships of the objective mechanical measures with PTOA severity.

RESULTS: Acute fracture severity metrics and maximum contact stress over-exposures were both significantly correlated with the degree of PTOA severity ($\rho=0.82$, $p<0.001$ and $\rho=0.65$, $p=0.007$, respectively) for the 16 cases analyzed. The injury severity measure had an AUC of 0.93, the contact stress over-exposure measure had an AUC of 0.98 and a combined measure of the two had an AUC of 1.00 indicating a perfect delineation of cases that did / did not develop PTOA. Contact stress over-exposure was significantly correlated with the injury severity ($\rho=0.52$, $p=0.04$, Figure 2).

DISCUSSION: Presently, clinical practice and research into optimal IAF treatment rely upon subjective measures of injury severity and reduction accuracy to control data and guide surgical management. This was the largest study to objectively quantify both the severity of initial injury and the accuracy of surgical reduction in patients with intra-articular fractures of the tibial plafond. As found in the prior literature, both the surgical reduction accuracy and the fracture severity were strongly predictive of PTOA risk and severity. The contact stress over-exposures were more strongly correlated with PTOA, though a strong, significant correlation was also found with the fracture severity. This suggests that the accuracy of surgical reduction in these fractures remains paramount despite the inherent PTOA risk associated with the injury itself.

SIGNIFICANCE: The relative impact of injury severity and reduction accuracy has significant implications for clinical research and management of tibial plafond fractures. The results of this study demonstrate that both the severity of the initial injury and accuracy of surgical reduction must be accounted for to fully assess PTOA risk in these fractures.

REFERENCES: 1. Anderson, D.D., et al. *J Orthop Res*, 2011. 29(1): p. 33-9. 2. Etter, C. and R. Ganz. *Arch Orthop Trauma Surg*, 1991. 110(6): p. 277-83. 3. DeCoster, T.A., et al. *Foot Ankle Int*, 1999. 20(1): p. 44-9. 4. Marsh, J.L., et al. *JBJS*, 2002: p. 1259.

ACKNOWLEDGEMENTS: Research supported by NIH/NIAMS (P50AR055533, R21AR061808) and the Department of Defense (W81XWH-15-2-0087).

Figure 1. Contact stress over-exposure was significantly higher in cases that developed severe PTOA

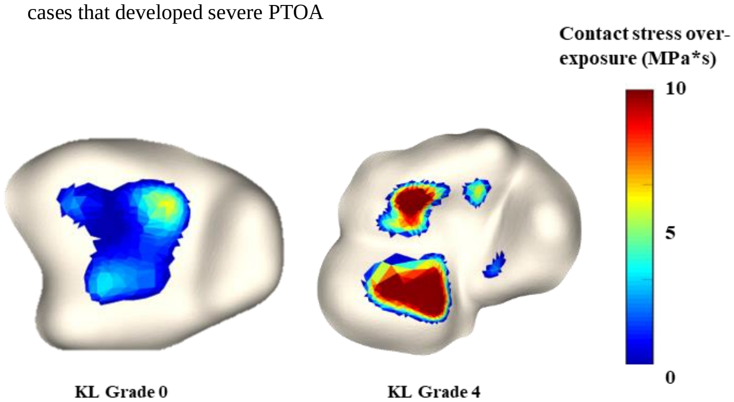

Figure 2. Fractures with lower severity and contact stress over-exposure had lesser degrees of PTOA (KL grades 0&1 shown as smaller blue bubbles and KL grades ≥2 as larger red bubbles).

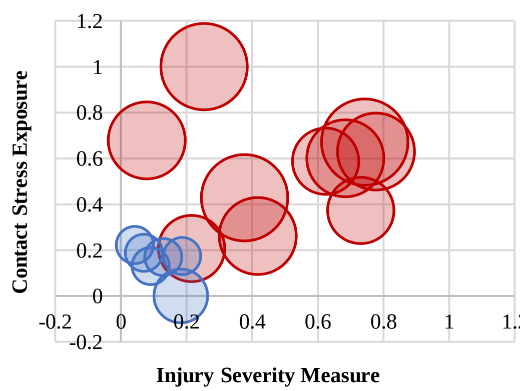

Objective Mechanical Measures Predict Post-traumatic OA Risk after Intra-articular Fracture of the Acetabulum

Kevin N. Dibbern, Matthew Engelken, Holly D. Thomas-Aitken, Tai Holland, Michael C. Willey, J. Lawrence Marsh, Donald D. Anderson
University of Iowa, Iowa City, IA
Kevin-Dibbern@uiowa.edu

Disclosures: Kevin N. Dibbern (N), Matthew Engelken (N), Holly D. Thomas-Aitken (N), Tai Holland (N), Michael C. Willey (N), J. Lawrence Marsh (N), Donald D. Anderson (N)

INTRODUCTION: Development of post-traumatic osteoarthritis (PTOA) after intra-articular fracture (IAF) of the acetabulum is thought to result primarily from the accuracy of surgical reduction. However, despite nearly 5 decades of advancements in fracture management, PTOA rates have remained constant [1]. The implication of this prior research is that there may be unaccounted for variation from the initial injury that causes certain cases to degenerate to PTOA. Recently, patient-specific techniques for objectively quantifying the fracture severity (using fracture energy) and the accuracy of surgical reduction (discrete element analysis (DEA) computed contact stress elevation) have been developed. These techniques enable the present study to determine the relationships between the acute fracture severity, the accuracy of surgical reduction, and the PTOA risk after IAF of the acetabulum.

METHODS: Nineteen patients with articular fractures of the acetabulum were enrolled in this IRB approved study. Patients were selected for having both pre- and post-operative CT imaging with a minimum of 12 months of radiographic follow-up. Tönnis grades were determined for each case by the adjudication of 3 experienced raters. Grades ≥2 were considered to have PTOA. Femoral and pelvic anatomy for each patient was segmented from pre- and post-operative CT scans to produce models for fracture severity and DEA analysis respectively [2]. Fracture severity was analyzed using previously validated, objective analysis methods that involve quantifying the energy involved in creating a fracture (the fracture energy) by automatically identifying the fracture liberated surface area and scaling by density dependent energy release rates that can be estimated from pre-op CT scans. The amount of energy dispersed within 1cm of the joint surface and the area of the joint surface are also accounted for in the severity metric. The models from post-operative scans for DEA analysis aligned to the coordinate system defined by Bergmann et al. [3]. The walking gait data obtained in that study of instrumented total hips was discretized into 13 evenly spaced time increments. Patient-specific forces were applied to each model based on body mass at the time of injury. DEA was used to compute deleterious contact stress exposure above a damage threshold of 3 MPa, defined as over-exposure, at each step in the gait cycle. Both the combined injury severity metric and the contact stress over-exposure were used to predict PTOA outcomes, and their predictive capabilities were analyzed using receiver-operating characteristic (ROC) curves. Spearman's correlations were used to study inter-relationships of the objective mechanical measures with PTOA severity.

RESULTS: Maximum contact stress over-exposures and the injury severity measures were both significantly correlated with the degree of PTOA severity (ρ=0.67, p=0.002 and ρ=0.45, p=0.05, respectively) for the 19 cases analyzed. The fracture severity measure had an AUC of 0.90, the contact stress over-exposure measure had an AUC of 0.87 and a combined measure of the two had an AUC of 0.91. Contact stress over-exposure was modestly correlated with the injury severity (ρ=0.50, p=0.03, Figure 2).

DISCUSSION: The relative impact of injury severity and reduction accuracy has significant clinical implications for the treatment of acetabular fractures. This was the first study to objectively quantify both the severity of initial injury and the accuracy of surgical reduction in patients with intra-articular fractures of the acetabulum. The results of this study confirm literature findings that surgical reduction, as measured by contact stress over-exposure, is predictive of PTOA risk. However, they also find that, in addition to the surgical reduction, the severity of the initial injury also plays a critical role in assessing of PTOA risk. This elucidates a potential reason for the disconnect between advances in surgical care and the lack of improvement observed in PTOA prevention after IAFs of the acetabulum. Acute biological damage caused by fracture is not effectively treated but appears to be a significant contributor to PTOA risk. Therefore, to improve management of these challenging injuries, novel biological interventions may be needed in addition to improvements in mechanical restoration of the articular surface to substantially reduce PTOA risk.

SIGNIFICANCE: The relative impact of injury severity and reduction accuracy has significant clinical implications in the treatment of acetabular fractures. The results of this study help to elucidate the combined risk presented by acute and chronic mechanical factors toward development of PTOA.

REFERENCES: [1] McKinley et al. J Orthop Trauma, 2010. 24:567-70. [2] Townsend, et al. J Biomech. 67:9-17, 2018. [3] Bergmann, et al. J Biomech. 34:859-71, 2001

ACKNOWLEDGEMENTS: Research supported by NIH/NIAMS (P50AR055533, R21AR061808) and the Department of Defense (W81XWH-15-2-0087).

IMAGES AND TABLES:

Figure 1. Contact stress over-exposure was significantly higher in cases that developed severe PTOA

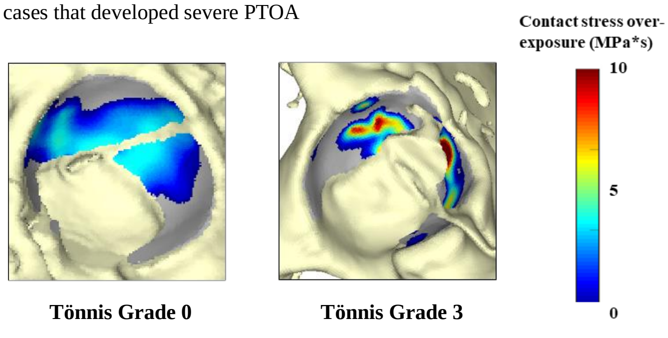

Figure 2. Cases that have low severity and contact stress over-exposures demonstrate lesser degrees of radiographic arthritis (KL grades 0&1 demonstrated by smaller blue bubbles while PTOA demonstrated by KL grades ≥2 are shown as increasingly large red bubbles).

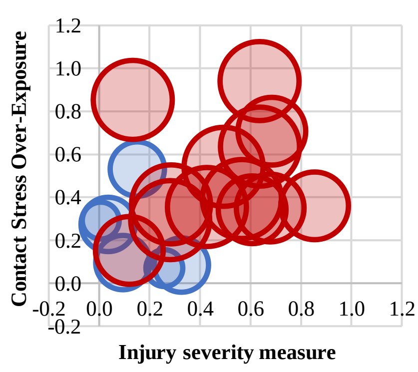

Objective Mechanical Measures Predict Post-traumatic OA Risk after Intra-articular Fracture of the Calcaneus

Kevin N. Dibbern, Karan Rao, Molly Day, J. Lawrence Marsh, Donald D. Anderson
University of Iowa, Iowa City, IA
Kevin-Dibbern@uiowa.edu

Disclosures: Kevin N. Dibbern (N), Karan Rao (N), Molly Day (N), J. Lawrence Marsh (N), Donald D. Anderson (N)

INTRODUCTION: PTOA risk after intra-articular fracture (IAF) of the calcaneus has been reported to highly correlate with the severity of the acute injury. Up to 90% of Sanders class III fractures developed PTOA, despite 95% having an anatomic (0-1 mm) reduction [1]. However, Rao et al. found that a new objective measure of post-reduction step-off magnitude correlated with Sanders classification [2]. This implies that surgical reduction as a significant contributor to PTOA development in IAFs of the calcaneus. Recently, patient-specific techniques for objectively quantifying the fracture severity (using fracture energy) and the accuracy of surgical reduction (discrete element analysis (DEA) computed contact stress elevation) have been developed. The objective of this study was to use these measures to determine the relationships between the acute fracture severity, the accuracy of surgical reduction, and the PTOA risk after IAF of the calcaneus.

METHODS: Thirty-three patients with articular fractures of the calcaneus were enrolled in this IRB-approved study. Patients were selected for having both pre- and post-operative CT imaging with a minimum of 18 months of radiographic follow-up. Kellgren-Lawrence grades were determined for each case by adjudication of 3 experienced raters. KL grades ≥2 were considered to have PTOA. Calcaneal fracture fragment geometries were extracted from pre-op CT scans for fracture severity analysis, while calcaneal and talar geometries were segmented from post-op CT scans for contact stress analysis. Fracture severity was analyzed using previously validated, objective analysis methods that involve quantifying the energy involved in creating a fracture (the fracture energy) by automatically identifying the fracture liberated surface area and scaling by density dependent energy release rates that can be estimated from pre-op CT scans. The amount of energy dispersed within 1cm of the joint surface and the area of the joint surface are also accounted for in the severity metric. Model generation for DEA was dependent upon estimation of the cartilage surface/thickness from CT. Cartilage surfaces were first projected a uniform 1mm normal to each triangulated bone surface. To simulate natural thinning at the periphery of the articular surface, cartilage boundaries were tapered toward zero thickness at the outermost boundary. Weight-bearing CT scans of fracture reconstructed patients were used to obtain initial weight bearing alignments. Forces and rotations associated with the stance phase of gait were discretized into 13 evenly spaced pairings. DEA was used to compute deleterious contact stress exposure above a damage threshold of 3MPa (Figure 1). Both the combined injury severity metric and the contact stress over-exposure were used to predict PTOA outcomes, and their predictive capabilities were analyzed using receiver-operating characteristic (ROC) curves. Spearman's correlations were used to study inter-relationships of the objective mechanical measures and the Sanders classification with PTOA severity.

RESULTS SECTION: Both the acute fracture severities and maximum contact stress over-exposures significantly correlated with the PTOA severity (ρ=0.52, p=0.002 and ρ=0.48, p=0.004, respectively) for the 33 cases analyzed. The Sanders classification was also significantly correlated with PTOA severity, although the relationship was less strong (ρ=0.41, p=0.02). The acute fracture severity metric had an AUC of 0.83, the contact stress over-exposure measure had an AUC of 0.82 and a combined measure of the two had an AUC of 0.88. Contact stress over-exposure was modestly correlated with the injury severity (ρ=0.35, p=0.05, Figure 2).

DISCUSSION: Presently, clinical practice and research into optimal IAF treatment rely upon subjective measures of fracture severity and reduction accuracy to guide surgical management. This was the first study to objectively quantify both the acute fracture severity and the chronic elevated contact stress in patients with IAFs of the calcaneus. In contrast to prior strong associations reported between initial severity and PTOA risk, the reduction accuracy, as measured by the contact stress over-exposure, was also significantly correlated with PTOA risk. In fact, contact stress over-exposure was more strongly correlated with PTOA risk than either the Sanders classification or the objective fracture severity. However, there was a relatively wide range of over-exposures and no clear threshold delineating cases that developed PTOA from those that did not. This suggests that while reduction accuracy is clearly an important factor in outcomes, the acute fracture severity as well as other patient factors also contribute significantly to PTOA risk.

SIGNIFICANCE: The results of this study suggest that contrary to prior research, the accuracy of reduction plays a significant independent role in dictating PTOA risk after IAF of the calcaneus. Better understanding of the relative impact of fracture severity and reduction accuracy on PTOA risk has significant clinical implications for the treatment of calcaneal fractures.

REFERENCES: [1]. Sanders R et al. J Orthop Trauma, 2014. 28(10):551-63. [2]. Rao K et al. J Orthop Trauma, 2019. 33(5):261-6.

ACKNOWLEDGEMENTS: Research supported by NIH/NIAMS (P50AR055533, R21AR061808) and the Department of Defense (W81XWH-15-2-0087).

Figure 1. Contact stress over-exposure was significantly higher in cases that developed severe PTOA.

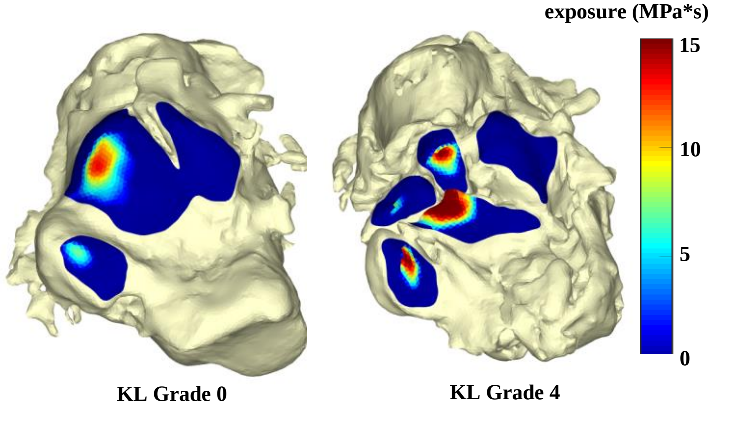

Figure 2. Fractures with lower severity and contact stress over-exposure had lesser degrees of PTOA (KL grades 0&1 shown as smaller blue bubbles and KL grades ≥2 as larger red bubbles).